SYNTHESIS OF NEW PORPHYRINOID CONJUGATES AND PORPHYRINOID NANOPARTICLES FOR PHOTODYNAMIC THERAPY APPLICATIONS

by

DIANA SAMAROO

A dissertation submitted to the Graduate Faculty in Biochemistry in partial fulfillment of the requirements for the degree of Doctor of Philosophy,

The City University of New York

2007

ProQuest Information and Learning Company
300 North Zeeb Road
P.O. Box 1346
Ann Arbor, MI 48106-1346

This manuscript has been read and accepted for the
Graduate Faculty in Biochemistry in satisfaction of the dissertation
requirement for the degree of Doctor of Philosophy.

Dr. Charles Michael Drain

January 23, 2007 _____
Chair of Examining Committee

Dr. Lesley Davenport

January 23, 2007 _____
Executive Officer

Dr. Derrick Brazill
Dr. Thomas Haines
Dr. Catarina E. Hioe
Dr. Akira Kawamura
Supervisory Committee

THE CITY UNIVERSITY OF NEW YORK

Abstract

Synthesis of New Porphyrinoid Conjugates and Porphyrinoid Nanoparticles for Photodynamic Therapy Applications

by

Diana Samaroo

Adviser: Professor Charles Michael Drain

Photodynamic therapy (PDT) has become a feasible modality for the treatment of numerous cancers using a combination of a photosensitizer, light (600-800nm range) and molecular oxygen. To date, Photofrin® is the only porphyrin-based photosensitizer approved by the FDA for cancer therapy. However due to its poor selectivity, the development of novel porphyrin conjugates is a primary goal in research. Therefore cell recognition and/or selectivity by chromophores are key issues in PDT research. It has been shown that the chemical attachment of polyethylene glycol (PEG) and polyamines to peptides, proteins and other drugs have numerous advantages. Pegylation improves drug solubility, greatly increases its retention time in the circulation system (thereby reducing dosing frequency), improves stability and decreases immunogenicity. Whereas polyamine have been shown to target some cancer cells.

Therefore, in the search for new PDT candidates, the attachment of PEGs and/or polyamine derivatives to the porphyrin should increase the relative uptake and

phototoxicity toward a given cancer cell line. Therefore, a series of protected PEG and amino acid porphyrin conjugates have been synthesized. Synthesis begins with 5,10,15,20-tetrakis(pentafluorophenyl)porphyrin, due to the high reactivity of the fluoro group at the *para* position in nucleophilic substitution reactions. The synthesis and characterization of various porphyrin derivatives, and small solution phase combinatorial libraries of these macrocycles, are reported herein. Binding studies based both on fluorescence microscopy and photodynamic activities quantify the extent that these porphyrin conjugates are selectively taken up into cancer cells. A new method to select winning compounds from the solution phase porphyrin libraries based on mass spectrometric analysis of extracts of cells treated with the library is also reported. One major finding is that porphyrins bearing amphipathic motifs spontaneously form 5-50 nm nanoparticles in the cell culture media and that these are taken up into MDA-231 (a human breast cancer cell line). Strategies to induce disaggregation once inside the cell and the photodynamic activity of these systems indicate that upon disaggregation these porphyrins are highly active PDT agents. Reduction of a pyrrole double bond to yield the chlorin analogues, which have a strong absorption in the red region of the spectra where biofluids are more transparent, results in highly fluorescent molecules, but reduced triplet quantum yields.

Preface

In this dissertation, porphyrinoid materials are explored for their use as photodynamic agents for their potential use as anti-cancer agents. The first chapter provides a detailed introduction into porphyrin and other related macrocycles, as well as the mechanism of action in terms of photodynamic therapy (PDT). Applications of porphyrins to related diseases are also discussed. The second chapter deals with the synthesis and characterization of three amine-linked porphyrinoid compounds using microwave heating. The third chapter explores the use of the porphyrinoid compounds as nanoparticles for PDT. Chapter four examines the use of porphyrin and corroles in solution phase combinatorial libraries, as well as the discovery of active photodynamic agents from the porphyrin library[1]. Chapter five is devoted to several projects that represent and can lead to exciting future directions in this area of research. It explores the many aspects of other porphyrin-type compounds, such as chlorins, in terms of their synthesis and application to cancer therapy. This chapter also looks at the bioactivity of several porphyrins across several cancer cell lines and tissue types. In addition to this, the anti-HIV properties of a few selected porphyrins are also examined.

---

1 In an effort to combine previous results obtained from studies of a tetraglycosylated porphyrin (Por-Glu_4) as a PDT agent [1], with earlier results from the Drain lab on the activity of porphyrins bearing two amphipathic and two charged methylpyridinium moieties selected from a combinatorial library [2], Dr. Xin Chen synthesized a series of $TPPF_{20}$ porphyrin derivatives with two thioglucose and two 4-thio-pyridal groups (Glu/Glu/SPy/SPy) using a "combinatorial approach." After incubating MDA-MB-231 cells with these derivatives, the initial conclusion from fluorescence microscopy was that they did not enter the cells to the same extent as the Por-Glu_4. Fortuitously however, these slides were re-examined a week later and found that indeed the Glu/Glu/SPy/SPy molecule was significantly taken up by this cell line. Further preliminary studies suggested that the porphyrins were aggregated in the cell culture solution and likely enter the cells as aggregates. The fluorescence of dye aggregates is known to be significantly quenched, so the increased fluorescence after a few days must arise from the disaggregation of the porphyrins inside the cells. These initial, but quite preliminary results lead to the investigations described in chapters three and four.

(1) Chen, X.; Hui, L.; Foster, D. A.; Drain, C. M. *Biochemistry* **2004**, *43*, 10918-10929. (2) Gong, X.; Milic, T.; Xu, C.; Batteas, J. D.; Drain, C. M. *J. Am. Chem. Soc.* **2002**, *124*, 14290-14291.

Acknowledgments

The encouragement and support of many people have contributed to this dissertation.

First and foremost, I would like to extend thanks and appreciation to my adviser, Dr. Charles Michael Drain for his generous time and commitment. I am fortunate that he has stimulated me to develop independent thinking and research skills.

I extend many thanks to my colleagues and friends, Ms. Gabriela Smeureanu for her help with the AFM measurements, Mr. Giorgio Bazzan, Mr. Alexander Falber, Ms. Ivana Radivojevic and Dr. Mikki Vinodu for providing the compounds mentioned in Chapter 4, in particular, the 21-member solution-phase combinatorial library.

I owe special thanks to my exceptional doctoral committee: Drs. Thomas Haines, Derrick Brazill, Akira Kawamura and Catarina E. Hioe for their time and input over the years. Dr. Hioe, thanks for the brief time I spent in your lab carrying out the anti-HIV experiments.

Many people on the faculty of City University of New York assisted and encouraged me in various ways during my trek to this degree. The administrative staff of CASI at City College, specifically Dr. Daniel L. Akins, for allowing me to be part of the IGERT initiative. Thank you for the financial support. I generously thank Dr. David Foster for allowing me to work in his group and providing me with lab space to conduct the molecular and cell biology studies. I also wish to thank Dr. Louis Todaro for the effort that he put forth in elucidating the X-ray structure of one of my porphyrins. Dr. Clifford

E. Soll for being a solid mass spec support and “jack of all trades” is thanked very much. I also would like to thank Dr. Michael Blumenstein for help with NMR. Thanks is extended to Dr. Horst Schulz, Dr. Lesley Davenport and Ms. Judy Li, for keeping tabs on all the paperwork that needed to be done at the Graduate Center. Thanks to Dr. Claude Braithwaite and Dr. Gail Smith who helped fund this research by providing research fellowships via Louis Stokes Alliance for Minority Participation (LS-AMP) program and MAGNET program, respectively over the years.

Special thanks needs to be extended to Dr. Karen E. Phillips, whom I always thought of as a friend. Thanks for the encouragement and support from the start of my graduate studies. It was truly a great experience being a teaching assistant under your guidance.

Lastly, I would also like to thank my family, especially my parents, Urmeela and Roopchand, whose hard work, determination, and encouragements have been central in getting me to this point. I am grateful to my best friends, Denise Nicole and Diandra for being free spirits, and showing some enthusiasm for science. I am especially grateful to my husband Nathan, who has been an instrumental part of my life in so many ways, and without whose programming skills to code FLim and Instruview, my data analysis and management would have been quite tedious. Although, his suggestions were not always welcomed, without him, this dissertation would not have been completed. Thank you for your patience and for keeping my life in proper perspective and balance. And finally, my biggest accomplishment in life, Dylan Sam, who came to me early. Thank you little one! Thank you for teaching me how to prioritize, focus and showing me what's truly important in life.

Dedicated to my parents who taught me that

with an education, you can achieve anything.

Table of Contents

List of Tables

List of Schemes

List of Figures

List of Appendices

List of Abbreviations

$^1O_2$..... singlet oxygen

AFM..... atomic force microscopy

API..... atmospheric photo ionization

BCS..... bovine calf serum

DEA.....diethylamine

DLS.....dynamic light scattering

DME..... ethylene glycol dimethyl ether

DMEM.....Dulbecco's modified eagle medium

DNA.....deoxyribonucleic acid

ELISA..... enzyme linked immunosorbent assay

ESI-MS..... electrospray ionization mass spectrometry

FDA.....Food & Drug Administration

Fe(III)PEG.....Iron(III)pegylated porphyrin

G1/G0/G2/M.....cell cycle: gap1/gap0 (growth arrest)/gap2/mitosis

gp120.....glycoprotein of molecular weight 120,000 daltons

gp160.....glycoprotein of molecular weight 160,000 daltons

gp41.....glycoprotein of molecular weight 41,000 daltons

HIV.....human immunodeficiency virus

HR-MS.....high resolution mass spectrometry

LDL.....low density lipoprotein

NMR..... nuclear magnetic resonance

mAbs.....monoclonal antibodies

MALDI..... matrix assisted laser desorption ionization

MW.....microwave irradiation

PARP..... poly(ADP-ribose) polymerase

PBS..... phosphate buffered saline

PDT..... photodynamic therapy (therapeutics)

Q-bands.....quasi-bands

RT.....room temperature

sCD4..... soluble CD4

TCPP.....tetracarboxyphenyl porphyrin

TPP..... 5,10,15,20-tetrakis(phenyl)porphyrin

$TPPF_{20}$.....5,10,15,20-tetrakis(pentafluorophenyl)porphyrin

$TPPS_4$..... 5,10,15,20-tetrakis(sulfonatedphenyl)porphyrin

UV-vis..... ultraviolet-visible

CHAPTER 1: Introduction

1.1 Photodynamic Therapy

Photodynamic therapy (PDT) relies on several concepts: (a) preferential localization of the photosensitizer (b) activation of photosensitizer by light to sensitize the generation of singlet oxygen ($^1O_2$), which results in free radicals (·OH, HO·$_2$) and

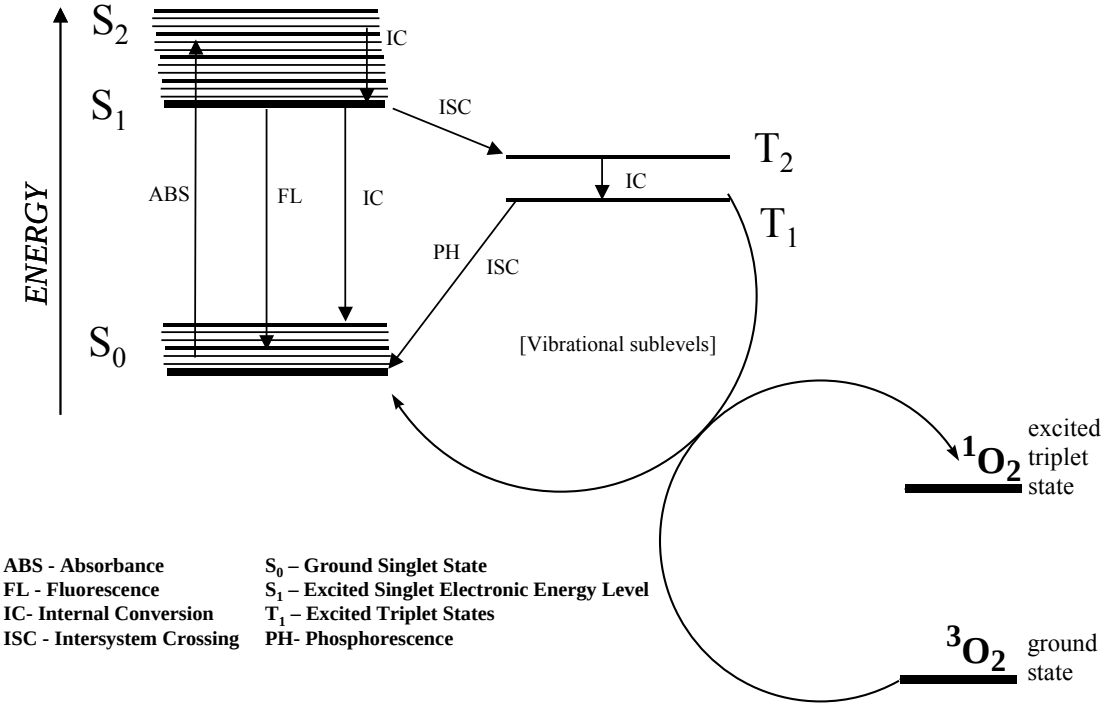

Figure 1.1: Jablonski diagram. Porphyrins have a singlet electronic ground state, absorb light energy and become electronically excited to produce a singlet excited state of the porphyrin S_2. If the porphyrin returns to the ground state radiatively, it fluoresces. The electron can also change its spin by ISC to form a triplet state. Energy transfer from the porphyrin triplet state to ground state molecular oxygen, generates the excited singlet oxygen [81].

radicals ions (·O$^-_2$) [1-3]. Varying the delivery system of the photosensitizers by liposome incorporation [2], nanoparticles [4,5], or binding to host molecules such as

cyclodextrins [6] can strengthen the localization. The activating light is specifically chosen to be within 600-900 nm, because (a) hemoglobin/blood, strongly absorbs light under 600 nm, so (b) longer wavelengths allow for deeper penetration into tissue (c) photons in the visible region of the spectrum alone are inadequate to produce $^1O_2$, the excited state of oxygen [3,7].

Photochemically generated excited triplet states can undergo electron transfer reactions with substrate to form radicals/ions, or can transfer energy to molecular oxygen to produce singlet oxygen ($^1O_2$, lifetime is 0.6 μs in biological environment, 4 μs in H_2O, 10 – 100 μs in organic solvents, 50 – 100 μs in lipids) (Figure 1.1) [8]. The excitation to form $^1O_2$ requires as a minimum of 20 kcal/mole, which puts limits on the absorption wavelength of the photosensitizer [3]. These reactions involving $^1O_2$ require that the photosensitizer and target are close in terms of distance, since $^1O_2$ travels ~20 nm in cells,

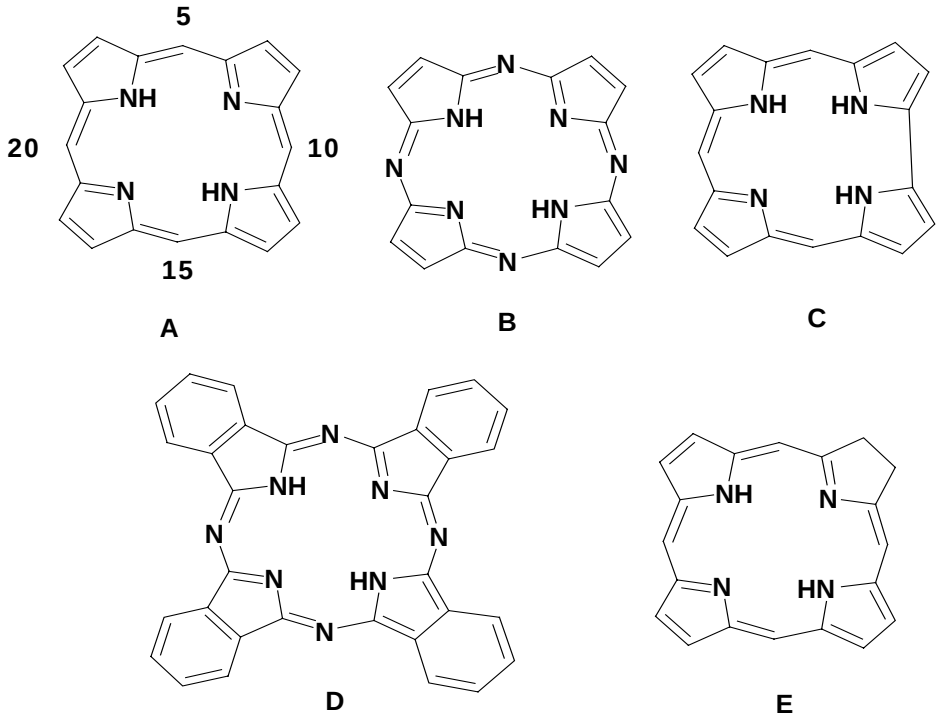

Figure 1.2: Porphyrin and porphyrin-related macrocycles. A: porphyrin, B: porphyrazine, C: corrole, D: phthalocyanine, E: chlorin

due to quenching/reactivity in cellular environments [3,9]. Because $^1O_2$ is so reactive, PDT induces oxidative damage to cell membranes, proteins (aromatic amino acids), lipids (double bonds), and DNA damage (bases and phosphate backbone); which are localized to areas no greater in diameter than the cell membrane thickness (bilayers 6 – 10 nm, human tissue cell ~ 20 microns) [10,11]. Some limitations of PDT include target accessibility to illuminating light, dosimetry (related to tissue depth), and also "photobleaching" or self-destruction of the photosensitizer, which also complicates light dose [3]. In general terms, in order for a photosensitizer to be effective, using 630 nm irradiation, a tumor must be less than ~ 2 – 3 mm within biological tissues. If it is to be effective at a depth of 5 – 6 mm, 700 – 800 nm would be required [3,8,12]. These effective depths are determined by a variety of factors including triplet quantum yield, optical cross section of the dye at the given wavelengths, and efficiency of sensitization of singlet oxygen. Changing the structure of the photosensitizer affords a means to optimize PDT activity and increasing the effective treatment depth – such as the optical cross section at the irradiating wavelength.

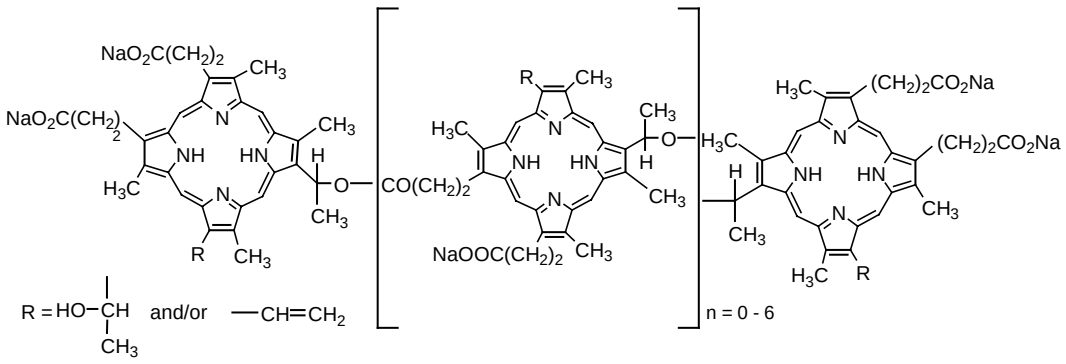

Figure 1.3: Structure of Photofrin [19]

Most photosensitizers (dating back to 1913 by Meyer-Betz [3]) are based on porphyrinoid-type compounds (Figure 1.2), which exhibit a high affinity towards cancerous cells in vitro and solid tumors in vivo [13,14]. Most photosensitizers are hydrophobic (lipophilic) and tend to accumulate in membranes of organelles such as mitochondria and lysosomes [11]. Porphyrins have a strong absorption band ~ 400 nm (Soret band). Since blue light or UVA does not deeply penetrate tissues, the Q-bands (600 – 800 nm) are used for therapeutic purposes [10].

1.2 Porphyrins as anti-cancer agents

PDT-induced cell death can occur as apoptosis or necrosis. The former appears to be the most prevalent route [9,10]. While there are multiple paths to the apoptotic process, PDT seems to elicit the pathway triggered by cytochrome c release from the mitochondrial intermembrane space into the cytosol. This results in the initiation and activation of downstream apoptotic signaling events such as caspase-3, one of the key 'executioner' proteases in apoptosis [15]. Other characteristics of apoptosis are cell shrinkage, expression of surface antigens like Fas, release of soluble apoptosis-inducing factor and formation of apoptotic bodies [11,16].

The reasons for photosensitizer uptake and/or retention in tumorigenic cells are not well understood, but it may involve their structure, charge and solubility [9]. Porphyrin aggregates are engulfed by phagocytosis, whereas hydrophobic porphyrin photosensitizers – incorporated into lipid-based formulations (e.g. liposomes, polyoxyethyleneglycol (PEG) triricinoleate, Tween 80 (polyoxyethylenesorbitan monoleate), nanoparticles and γ-cyclodextrin either go enter cells via fusion with the plasma membrane or endocytosis [6]. Cationic photosensitizers build up in the

mitochondria, because of the steeper negative electrochemical gradient across the inner mitochondria membrane in tumor cells than in normal cells. The PDT effect of porphyrins, is mainly attributed to destroying the tumor vasculature, as opposed to the hypothesis that positively charged macrocyles are cellularly localized molecules and "act at the tumor cell level" [3,6,10]. The binding affinity of porphyrins for mitochondrial benzodiazepine receptors can also explain this localization [6]. In addition to porphyrin aggregates, low-density lipoproteins (LDLs)-mediated uptake of porphyrins, and anionic photosensitizers diffuse through the plasma membrane better than cationic species, and localize in lysosomes [6]. Many photosensitizers have an affinity for lipoproteins, particularly LDLs. Since proliferating cells (normal or cancerous) have more LDL receptors than quiescent cells do, the photosensitizer piggybacks onto LDL, which then binds to its receptor [3,12]. Proliferating cells/tumors are predominantly in the G2/M cell phase, making them radiosensitive in vivo, whereas the quiescent cell (and G0/G1 phase) population are radioresistant. Therefore the target for PDT can be the G0/G1 and G2/M cell populations [17]. The proposed pH hypothesis for the uptake of therapeutics is based on the lower extracellular pH found in tumors compared to the pH surrounding normal tissues. The low pH due to poor microvasculature, increased metabolism and proliferation leads to increased lipophilicity of acidic photosensitizers as they gain entry into the extracellular part of tumors. Increasing the lipophilicity leads to increased cellular uptake with decreasing pH [18]. The primary means of uptake are passive and active transport. Passive transport/diffusion of the photosensitizer is driven by an electrochemical potential present across the plasma membrane, resulting from the negative interior with respect to the exterior. This difference opposes the entry of anionic

species, but allows cationic ones into the cells. Additionally, nearly all cell membranes contain negatively charged lipids and the electrostatics of the ion and dipoles in the membrane result in a negative exterior and positive interior [19]. For an uncharged, non-polar photosensitizer, its concentration gradient is the determining force for diffusive

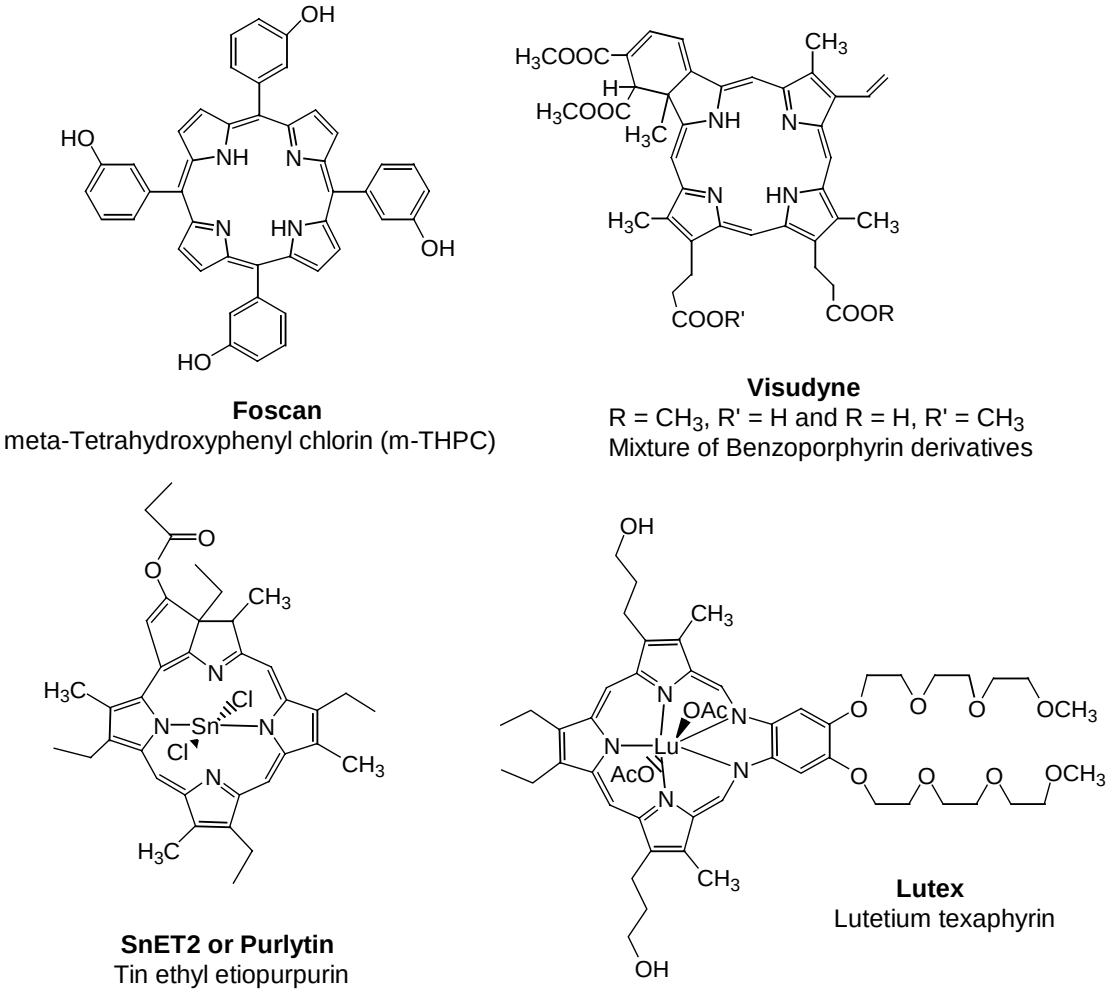

Figure 1.4: Second generation porphyrinoid photosensitizers in clinical trials

uptake. Active transport is a result of endocytosis (e.g. receptor/non-receptor-mediated endocytosis, pinocytosis, phagocytosis), where the photosensitizers adsorb to the cell surface without invading the plasma membrane. These are ingested and transported to

lysosomes (low internal pH) by clathrin-coated pits (vesicles). This form of cellular uptake may be pH dependent, particularly for amphiphilic photosensitizers [18]. Uptake also depends on the presence or absence of serum, since 80 – 90 % of photosensitizers bind to the various proteins present in serum [18].

Currently there is one FDA approved drug, porfimer sodium (Photofrin, Figure 1.3), which is approved and known to cause photodamage in various types of cancers (esophageal, lung, bladder, cervical) [12]. Several others are in various phases of clinical trials. Benzoporphyrin derivative (Verteporfin®, $\lambda_{abs} \cong 692$ nm) is a liposomal formulation used for the treatment of age-related macular generation and choroidal melanoma [19]. Lutetium texaphyrin (Lutex, Lutrin™, $\lambda_{abs} \cong 732$ nm) is a water-soluble photosensitizer that is used for the treatment of cardiovascular disease and certain skin lesions [19,20]. meta(Tetra-hydroxyphenyl)chlorin (mTHPC, Foscan®, $\lambda_{abs} \cong 652$ nm) is used in PDT for head and neck cancers, whereas mono-L-aspartyl chlorin e6 (NPe6; $\lambda_{abs} \cong 664$ nm) is used for skin and nasopharynx cancer [21]. Tin ethyl etiopurpurin (SnET2 or Purlytin®, $\lambda_{abs} \cong 664$ nm) is being used for breast and prostate cancer, Kaposi's sarcoma associated with AIDS, and for age-related macular degeneration [22].

Photofrin, which is lipophilic, is not a single compound, but rather a mixture of ester and ether oligomers. The fact that it is a heterogeneous mixture may be the reason as to why it is effective in cancer treatments [6,12]. However, poor chemical characterization and low absorption in the 600 – 900 nm regions, limits its use to the treatment of easily accessible tumors. These determinants and the increased clinical aspects of PDT have motivated research in the investigation of novel, non-Photofrin based photosensitizers [3]. Thus there is need for compounds, which absorb red light

(700 – 800 nm), which have greater effectiveness in PDT. Along with porphyrins, phthalocyanines and porphyrazines are also likely candidates, with the latter exhibiting strong absorption bands between 710 and 800 nm [7]. Since Photofrin has proven to be an effective heterogeneous mixture, it is logical to design compounds in that fashion. Solution-phase combinatorial chemistry enables for the synthesis of small-directed mixtures, termed libraries [23,24]. Libraries may yield a number of compounds with similar binding affinities for different parts of a tumor/cell. When these compounds are activated, they cooperatively act to bring about an additive effect that would efficiently destroy a tumor/cell.

Many infectious diseases have similar abnormal rapid cell division as cancer cells. Porphyrin accumulation in these cells evokes the potentiality of treating infectious diseases as well as cancer [1]. Gram-negative bacteria, which have a sturdy cell wall, bar porphyrin uptake, unless the porphyrin is attached to a polymer such as polylysine. The polymer fractures the lipid structure, allowing the porphyrins to enter the cell. This type of modified porphyrin had antimicrobial activity against a variety of gram-negative and gram-positive bacteria [1]. Large quantities of some photosensitizers are taken up by activated immune cells compared to their quiescent counterpart or red blood cells. Experiments with HIV-infected immune cells are shown to take up porphyrins, which makes them susceptible to light (PDT) treatment [1]. In HIV-infected patients, “the light could be applied either by withdrawing blood, illuminating it and transfusing it back into the body (extracorporeal phototherapy) or by shining it onto the skin (transdermal phototherapy)”. It remains to be seen if this technique will be effective enough to abolish infectious diseases [1].

1.3 Porphyrins as anti-HIV agents

Human immunodeficiency virus type 1 (HIV-1) entry into host cells (Figure 4) is mediated by viral envelope glycoproteins---gp120 and gp41, CD4 binding and coreceptor (CCR5 or CXCR4) [25-27]. These glycoproteins are synthesized as a gp160 precursor, which becomes proteolytically cleaved in the Golgi into a surface gp120 molecule, noncovalently tethered to a transmembrane gp41 [28,29]. Each spike on a virion or infected cell surface is composed of three gp120 and three gp41 molecules $(gp120\text{-}gp41)_3$, held together in a trimer, by factors present in gp41 (Figure 1.5) [29]. The external gp41 amino (N-) terminus (residues 1-29) contains two α-helices, bridged by a disulfide loop region, and the "hydrophobic, glycine rich fusion peptide" which is crucial for viral and host cell membrane fusion [28]. The gp120 glycoprotein is visible to host antibodies and comprises five variable loops (V1-V5) which may aid replicating viruses in evading neutralization by antibodies. These loops are distributed among more conserved regions (C1-C5). In comparison to gp120, gp41 is more conserved [29]. The

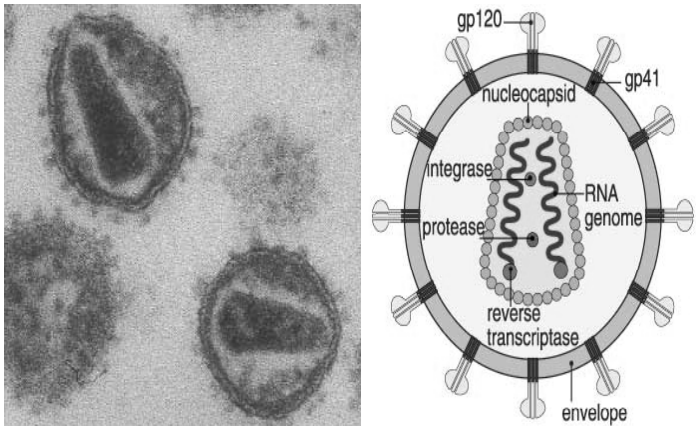

Figure 1.5: The HIV particle: spikes on the exterior of the enveloped virus composed of gp120 and gp41. The nucleocapsid encloses RNA and viral enzymes. Source: http://post.queensu.ca/~forsdyke/hiv01.htm#Reciprocal%20Relationship%

crystal structure elucidated by Kwong and others, of gp120 show that the V1, V2 and V3 loops (without the C- and N- termini) is composed of an outer and inner domain, and a mini-domain called the bridging sheet [25-27]. The outer domain shows a heavily glycosylated surface [28]. The inner domain accommodates the C- and N- termini of gp120, which are involved in gp41 interaction and is the likely site of trimer assembly. The bridging sheet has four antiparallel β-sheets projecting from the distal ends of both domains. Together with the base of the V1/V2 loop, it forms the conserved chemokine coreceptor-binding site [28]. Due to their absence from the gp120 crystal structure, the spatial relationship of how the V1/V2 and V3 loops relate to each other and to the CD4 and CCR5 or CXCR4 binding sites is unclear [30]. But more importantly, it is the V3 loop that determines coreceptor usage depending on whether HIV-1 binds to CCR5 (R5 virus) or CXCR4 (X4 virus). A single amino acid mutation (D329R) in the V3 sequence, converts a R5 virus into a X4 virus [28,30,31].

The CD4 (T4, 55kDa) antigen is the primary receptor for HIV. Each monomer of gp120 contains a CD4 binding site, which is highly conserved (among all primate lentiviruses) [29,32]. The surface area of the binding pocket is larger than that occupied by an antibody-protein interaction. The interface shows a hydrophilic pocket lacking depth that may play a role in immune evasion. The site on CD4 (part of the CDR2-like region) that contacts gp120 (C3 and C4 domains) “forms a charged ridge on the N-terminus domain” most distal from the cell membrane [29]. A phenylalanine (F43) side chain creates a cavity on gp120, forming various contacts with negatively charged residues (D368, E370, and hydrophobic W427). Residues 40-48 on CD4 make about 63% of CD4-gp120 contacts but it is the backbone of the gp120 peptide chain, rather than

the side chains that contact CD4 [29]. Recruitment of a single CD4 molecule by one gp120 molecule is enough to bring about conformational changes in all three gp120 monomers of the trimer [29]. Although CD4 is expressed mainly on helper T-lymphocytes, it is also expressed in minute amounts, on cell types not expressing a T-cell receptor (TCR), e.g. macrophages, monocytes, and dendritic cells, all of which can be infected by HIV. It is postulated that HIV may attach without CD4 binding to these cells by interacting with sugar groups on gp120 or lectin-like domains on cell surface receptors, e.g. the mannose-specific macrophage endocytosis receptor [29].

CD4 undergoes several conformational changes upon gp120 binding due to its flexible regions (between D2-D3 and D4 and membrane). The D1-D2 domain does not undergo any changes. However upon gp120 binding there is a loss of epitopes on D3 and D4 domains, concordant with rearrangements far from the gp120-binding site. Both

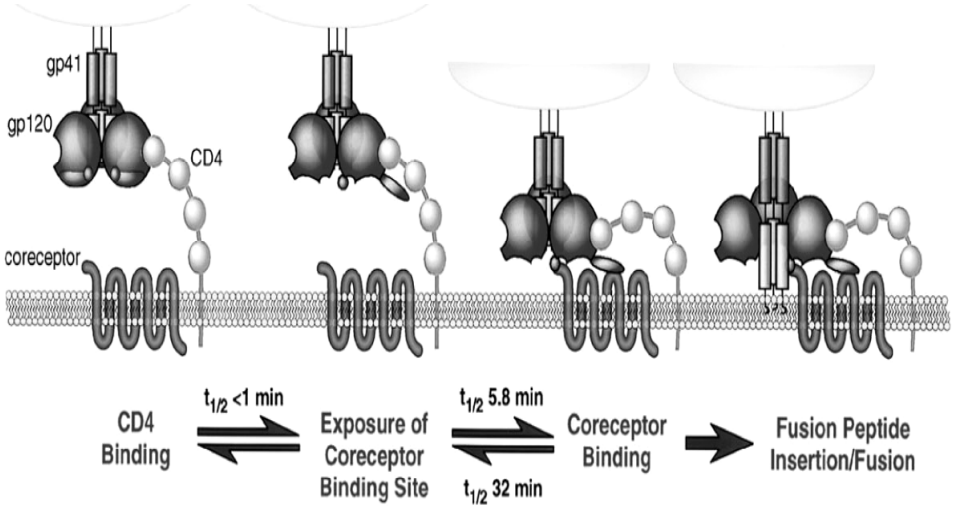

Figure 1.6: Steps in HIV-1 Viral Entry (1) The viral gp120 domains bind to CD4 on host cells (2,3) This binding triggers conformational changes and exposure of coreceptor sites (i.e. CCR5), which leads to binding (4)Upon complex formation, gp41 contacts the cell surface; inserts fusion peptide into membrane, which allows HIV-1 and host cell membrane to fuse and transfer viral RNA (courtesy T. Dragic, Albert Einstein College of Medicine, NY).

flexible regions are key for HIV infection. Antibodies to D2-D3 loop inhibit HIV infection but not CD4-gp120. Deletions in the flexible region of D4 postpone infection and diminish V3 loop unmasking, which suggests that conformational alterations in gp120 cannot occur without CD4 flexibility [29].

While the crystal structure provided important information regarding the CD4-gp120 complex, biophysical studies provide an understanding of the properties that drive complex formation. Myszka et al [33] examined the energetics of soluble CD4 (sCD4) binding to soluble recombinant gp120 proteins and found that gp120-CD4 binding results in a large bonding energy. This formation has a favorable binding enthalpy ($\Delta H° = -63$ kcal/mol, $-T\Delta S° = 52$ kcal/mol) [33].

Despite HIV attachment to cells by a number of interactions, fusion/infection will not occur until sufficient CD4 and coreceptor molecules are engaged to trigger formation of a fusion pore [29]. The V1, V2 loops obscure both CD4 and coreceptor binding sites in the mature gp120 oligomer. Therefore upon multivalent binding of a CD4 cluster to the gp120 oligomer, conformational changes displace the V1, V2 and V3 loops and reveal the coreceptor-binding site [28]. The flexibility of CD4 causes it to come into contact with gp120 laterally and to align the coreceptor towards the cell surface, bringing the viral and host cell membranes close [28]. Upon coreceptor binding, subsequent conformational changes cause rearrangements in gp41, triggering the insertion of the fusion peptide into the host membrane; leading to gp120 dissociation; membrane fusion, and the release of the nucleocapsid (RNA) into the host cell [28]. The crystal structures of the extracellular gp41 domains show a rod-like structure with a six-helix bundle at its core. This six-helix bundle is created when three α-helices close to the viral cell

membrane interact in an anti-parallel manner with a coiled-coil structure comprised of three leucine zipper domains (one from each oligomer in the trimer) projecting up towards the fusion domain [34]. Some glycoprotein spikes assembly to form a ring to induce the formation of a fusion pore [29].

Neurath, Debnath, Song and Vzorov have shown that certain porphyrins---protoporphyrin, hemin, natural and metallo-porphyrins among others, exhibited antiviral activity against HIV infection in inhibition assays measuring viral replication, most likely by binding to gp120, which prevents CD4 mediated membrane fusion [35-38]. Three possible mechanisms exist for the inhibitory effects of porphyrins, however the exact mode of action and at what stage in the virus life cycle it takes place, is not well defined. The first and second mechanisms involve reverse transcriptase (RT) and HIV protease inhibition, respectively [35-38]. The third mode of action deals with the binding of porphyrins to a sequence in the V3 loop of gp120, the envelope glycoprotein. As stated before, the V3 loop is the primary antigenic factor of the external domain of gp120 and functions in viral attachment and penetration. Highly conserved positively charged residues (K305, I307, R313, F315) and several hydrophobic ones led to the hypothesis that porphyrins containing ionic substituents may interact via hydrophobic and electrostatic forces with these sites, inducing conformational changes in gp120, which ultimately inhibits viral entry [35-38].

1.4 Polyethylene Glycol Linked Porphyrinoids

In addition to the use of porphyrinoids in fields such as PDT of anti-cancer, anti-viral, anti-fungal and anti-bacterial [39-43] agents, use as sensors, receptors, nanoparticles for catalysts, photonics, and self-assembled electronics are among other

applications [44-46]. Although, PDT is a promising therapy for diseased tissues, only few agents are FDA approved. Therefore, the development for next generation porphyrinoid-based PDT agents has received great attention in this area of research. Potential routes are the use of pegylated (polyethylene glycol, PEG), peptidic, amino acids and polyamine-linked porphyrinoid. The advantages of these groups has been well established [47-50]. Amine-linked porphyrinoid can preferentially accumulate in tumor tissues due to the acidic environment. Since receptors for amines (such as spermine) are present on cellular membrane, these biologically significant groups can bind to membrane and be actively endocytosis. The amphipathic nature of amine-linked porphyrinoid can also facilitate incorporation into membrane features [51]. It has been demonstrated that polyethylene groups can facilitate uptake of drugs into cells and are relevant to drug design and delivery [48,52,53]. Both amino acid and polyamine derivatives are known to impart selectivity toward cancer cells [51,54-57], and the latter promotes cell permeability [49,50,58-60].

Polyethylene glycol conjugated porphyrinoids pose many advantages. PEG with a large molecular weight can be exploited to enhance the permeability of tumor microvasculature and thus facilitate site-specific accumulation of the porphyrinoid [61]. Pegylation has been demonstrated the reduce aggregation and increase solubility of porphyrinoid because of the amphiphilic nature of the PEG chains [52]. Aggregated porphyrinoids tend to have reduced photoactivity and fluorescence, and since less go into the triplet state, the yield of singlet oxygen production is reduced [52].

7,8-dihydro-5,10,15,20-tetrakis(3-hydroxyphenyl)-21-23-[H]-porphyrin (m-THPC), a second-generation PDT agent, induces skin photosensitivity that lasts 2 – 4

weeks after administration. m-THPC conjugates with different PEG chain lengths are reported in literature, and these studies show that the varying chain lengths affect drug kinetics [61]. The advantages of using PEG-porphyrinoid conjugates results in reduced skin photosensitivity and increased water solubility or hydrophilicity [61].

The first pegylated photosensitizer, tetrakis-(m-methoxypolyethylene glycol) derivative of m-THPC, (PEG-m-THPC), was prepared using four long hydroxyl (PEG 2000) side chains connected to m-THPC by a triazine group [14,62]. This chlorin exhibited high tumor selectivity and retention up to 8 days following administration. This drug was cleared from normal tissues before 5 days [14].

The covalent pegylation of poly-L-lysine chlorin$_{e6}$ (Figure 1.7) has been shown to increase the targeting of the porphyrinoid to ovarian cancer (OVCAR-5), resulting in high tumor: normal tissue ratios in nude mice bearing OVCAR-5 tumors. Moreover,

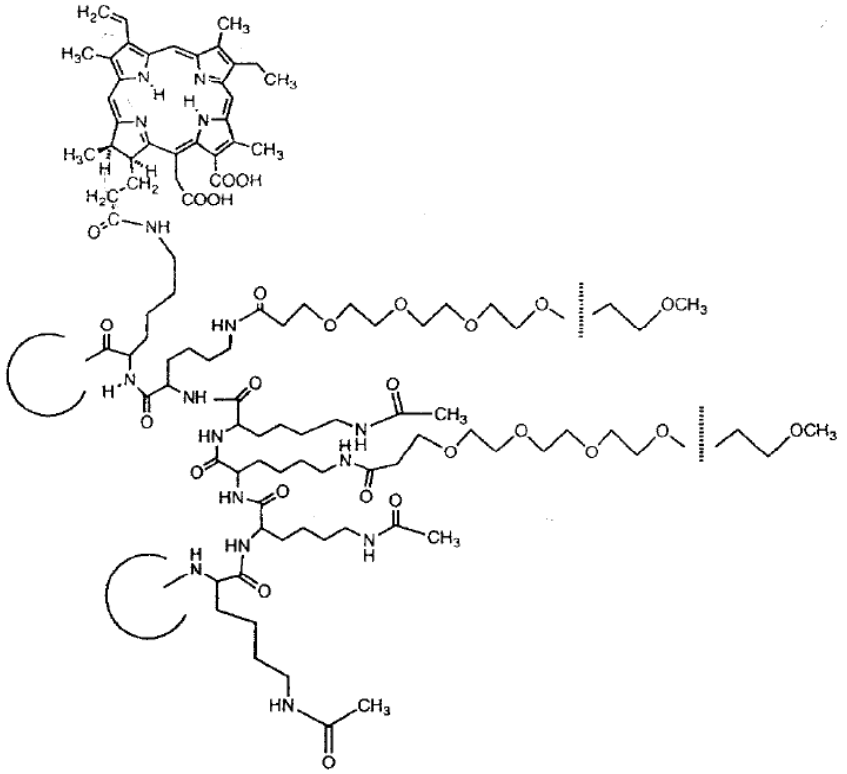

Figure 1.7: Structure of PEG-poly-L-lysine chlorin$_{e6}$ [51]

pegylation increased the depth of chlorin$_{e6}$ penetration into the peritoneal wall, as well as, resulted in more mitochondrial localization and higher phototoxicity over the non-pegylated chlorin [52,53].

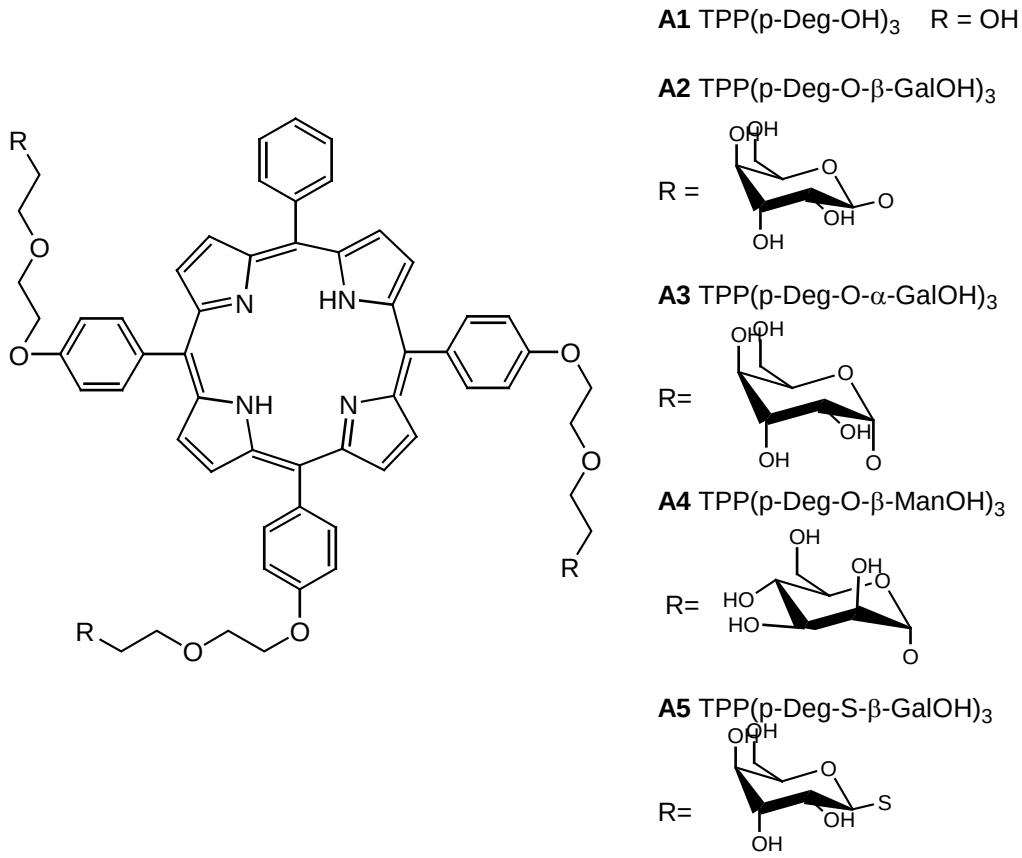

Figure 1.8: Structure of PEG-glycoconjugated porphyrinoid [62]

PEG-glycoconjugated porphyrins, use a PEG to link a sugar to a porphyrin, as in the case of diethylene glycol (Deg)-linked O- and S-galacto/mannoconjugated TPP (Figure 1.8). These systems were synthesized and examined against a human retinoblastoma (intraocular tumor) cell line (Y79) for PDT activity [63]. The diethylene glycol TPP (TPP-(p-Deg-OH)$_3$) was prepared by Williamson type condensation of TPP-(p-OH)$_3$. The unconjugated derivative (A1, Figure 1.8) was poorly internalized by Y79

cells compared to the pegylated glycoconjugated derivatives. Increasing the length of the PEG spacer between the sugar and the porphyrinoid resulted in greater uptake as well, specifically for compounds A2, A4 and A5 (Figure 1.8). These studies also demonstrated that triglycoconjugated porphyrinoids are more phototoxic than the symmetrical tetraglycoconjugated conjugates [63].

Pegylation of porphyrinoids also positively alters pharmacokinetics and biodistribution, as in the case of a porphyrin-platinum system [64,65]. In addition, the PDT effect is increased. J82 bladder cancer cells are more sensitive to PEG-HPPt (diammine{7,12-bis[1-(polyethyleneglycol-750-monomethylether-1-yl)ethyl]-3,8,13,17-tetramethylporphyrin-2,18-dipropionato}platinum(II)) (Figure 1.9) than normal urothelial cells [64-66]. This combines the effect of one of the most widely used chemotherapeutics ─ cisplatin with the porphyrin.

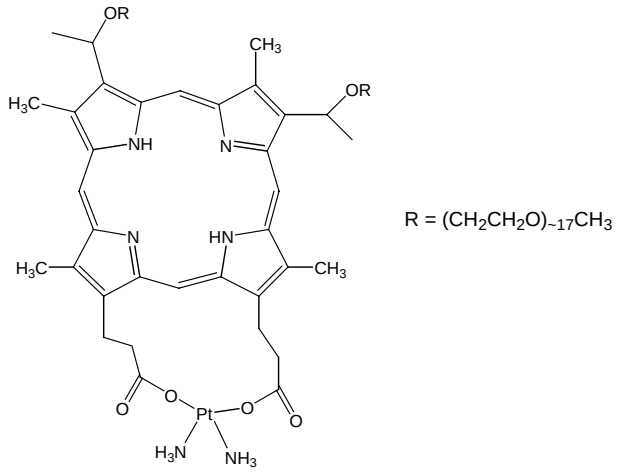

Figure 1.9: PEG-HPPt [63]

1.5 Polyamine and Peptidic Glycosylated Porphyrinoids

Peptidic glycosylated porphyrinoids have two important cell recognition targets, a saccharide and a peptide. It has been demonstrated that Arg-Gly-Asp and Asn-Gly-Arg

peptides linked to the drug, doxorubicin, improved the targeting of the drug to tumor cells, enhanced its efficacy and reduced the toxicity. Furthermore, glycopeptides and glycoproteins have been involved in transport and cell recognition [67]. It has been established that the free R-amino group of alanine improves targeting to cancer cells [67].

From this perspective, TPP containing amino acids were synthesized by the Lindsey method. Reduction of NO_2 groups yields the amines, which were coupled to N-Fmoc-L-alanine. Additionally, reduction of mono(nitrophenyl) tritolylporphyrins yields the corresponding amino-linked porphyrins, which were subsequently coupled to N-Fmoc-L-serine substituted tetra-acetyl-glucose [67-69]. The PDT activity of the three glycosylated aminoporphyrins (Figure 1.10) was examined against human chronic myelogenous leukemia (K562) cells. Porphyrins B1 and B2 (Figure 1.10) generated limited necrosis initially, however increased cell death resulted over a 24 hour period. Compound B3 showed a diminished effect.

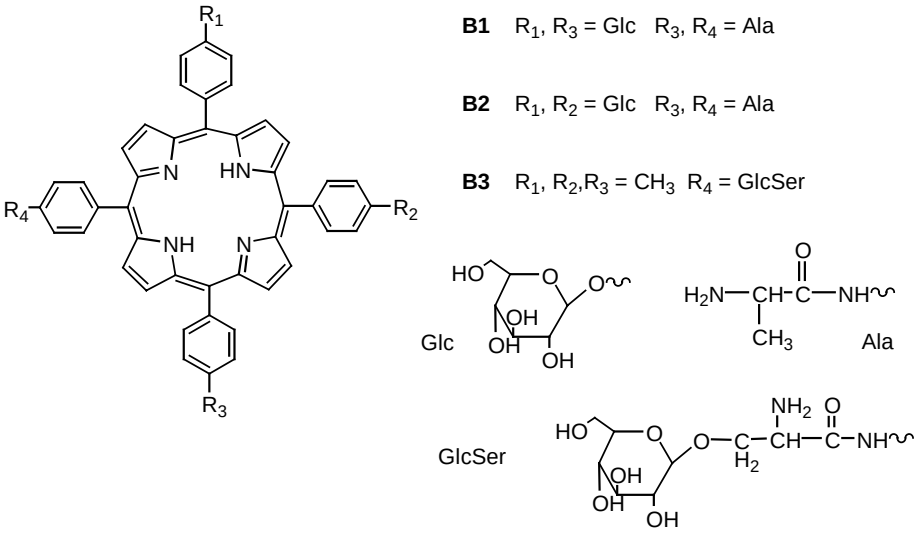

Figure 1.10: Glycosylated amino acids porphyrins [66-68]

The use of monoclonal antibody-porphyrinoid conjugates has also been explored, however these bear major disadvantages for instance poor tissue penetration, preparative difficulties and potential immunogenicity [52,70,71]. As mentioned before porphyrins are known to be effective against HIV. As a matter of fact, anti-hemin (porphyrin) monoclonal antibody (1D3 antibody) is well established [72]. The sequence and chemical feature, such as binding of the porphyrin to the heavy chain of CDR-2 (complementary determining region) in the antibody has been elucidated [72].

The attachment of an arginine-glycine-aspartate (RGD) tripeptide to tris(para-glucosylphenyl) porphyrin, by solid-phase synthesis has been reported [73]. Integrins mediate cell adhesion between cells and the extracellular matrix, by binding to ligands with an RGD sequence. The glycosylated tripeptide porphyrin (2 μM) was compared to Photofrin® (1.2 μg/mL) and evaluated against the K562 cell line. The conclusion drawn from these studies indicated that peptidic porphyrins were comparable with Photofrin®[73].

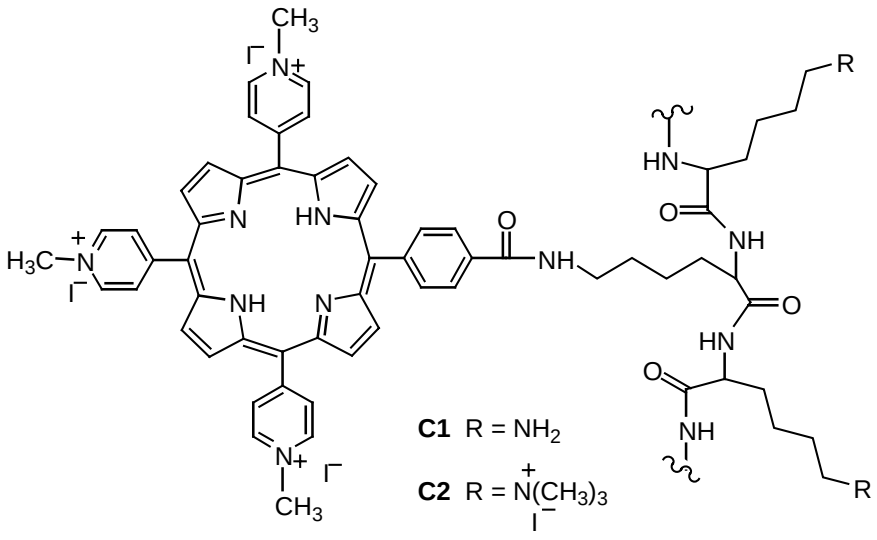

Figure 1.11: Poly-S-lysine conjugated porphyrin [42]

5,10,15,20-tetrakis(aminophenyl)porphyrin (TAPP) was aminoacylated with L-Boc-Asp(OBn)-OH and further coupled to Boc-Arg-OH. This study focused on the chemistry of combinatorial libraries as no compounds synthesized were evaluated for PDT activity [74]. L-Proline was linked to TAPP [75] and used as a catalyst in the epoxidation of alkenes.

Poly-lysine conjugated to a cationic porphyrin, compounds C1 and C2 (Figure 1.11) were used to photoinactivate Gram (-) *E. coli* and Gram (+) *S. aureus* bacteria. The neutral counterparts of these porphyrins were able to photoinactivate *S. aureus*, but not *E. coli*. This study also indicates that only positively charged porphyrins lead to the photoinactivation of *E. coli* and that polylysine enhances the activity of the porphyrinoid [39,43].

Derivatives of 4-carboxyphenylporphyrin were synthesized, where folic acid was linked to the porphyrin by either 1,6-diaminohexane or a small PEG, 2,2'-

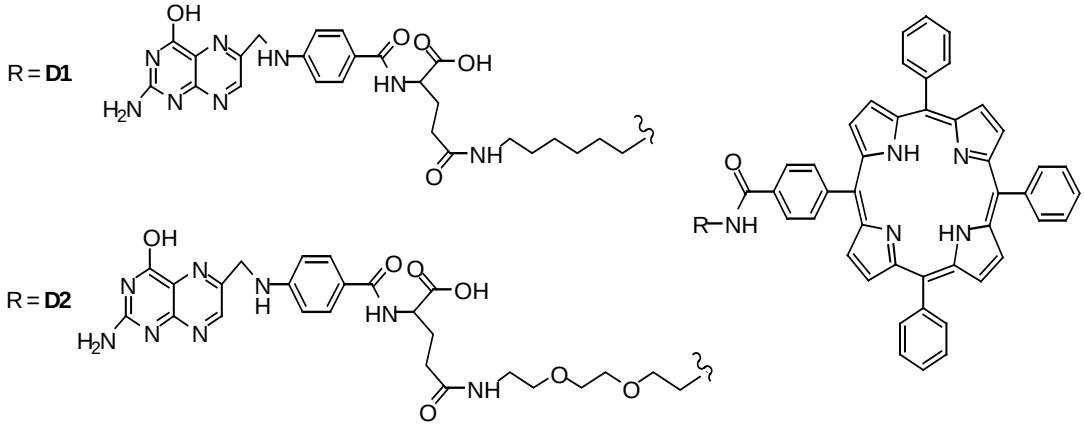

Figure 1.12: Three component folic acid-conjugated porphyrins. D1: folic acid/1,6-diaminohexane/4-carboxyphenylporphyrin, D2: folic acid/2,2'-(ethylenedioxy)-bis-(ethylamine)/4-carboxyphenylporphyrin [70]

(ethylenedioxy)-bis-(ethylamine) (Figure 1.12). The photodynamic activity towards KB nasopharyngeal cells overexpressing folate receptors of these compounds (D1 and D2) compared to TPP showed photocytotoxicity with 50% growth inhibition using light doses of 22.6 J cm^{-2} and 6.7 J cm^{-2} respectively [71]. In addition to amino acids, nucleosides and nucleotides have also been appended to porphyrinoid compounds [76].

Besides the advantages stated earlier, polyamines are needed for cell growth and high levels are present in rapidly dividing cancer cells [49,50,59]. Furthermore, since tumors have an active polyamine uptake, appending polyamines to porphyrinoid should enhance the uptake.

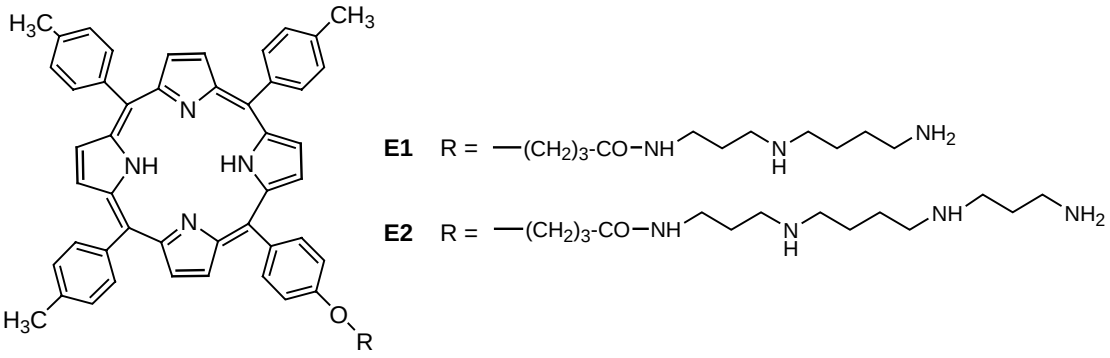

Figure 1.13: Polyamine-conjugated porphyrins. E1 represents the spermidine-porphyrin conjugate, whereas E2 is the spermine-porphyrin conjugate [58]

Spermine and spermidine, two polyamines found in nature, can bind DNA via electrostatic interactions. This binding interferes with protein synthesis, replication, transcription and membrane stabilization [59,77]. 5-hydroxyphenyl-10,15,20-tritolylporphyrin bearing spermine and spermidine were synthesized and the photocytotoxicities evaluated against K562 cells and compared to Photofrin®. Compounds E1 and E2 (Figure 1.13) were less active than Photofrin® (1.2 μg/mL), but did produce a dose-dependent cell death at 2 μM, which increased after 24 hour [59]. In

addition, these polyamines were conjugated to chlorin$_{e6}$ and to TCPP, which was reduced with di-imide to the chlorin [77].

Amino- and PEG- linked porphyrinoids have drawn attention in recent years for use in PDT [71,78-80]. This basis of this research relies on the fact that amino acids, peptides, PEG and glycopeptides are targetable moieties that may assist porphyrinoid absorption into malignant cells. Although the research on polyamines, amino acids and PEG moieties attached to porphyrinoids presented is limited, this area looks promising.

1.6 References

(1) Lane, N. *Scientific American* **2003**, *288*, 38-44.

(2) Rosenkranz, A. A.; Jans, D. A.; Sobolev, A. S. *Immunol. Cell Biol.* **2000**, *78*, 452-464.

(3) Hasan, T.; Moor, A. C. E.; Ortel, B. In *Cancer Medicine*; 5th ed.; Holland, J. F., Frei III, E., Bast Jr., R. C., Kufe, D. W., Morton, D. L., Weichselbaum, R. R., Eds.; B.C. Decker Inc.: Hamilton, Ontario (Canada), 2000.

(4) Ahmad, K. *The Lancet: Oncology* **2002**, *3*, 451.

(5) Konan, Y. N.; Berton, M.; Gurny, R.; Allemann, E. *Eur. J. Pharmaceutical Sciences* **2003**, *18*, 241-249.

(6) Osterloh, J.; Vicente, M. G. H. *J. Porphyrins Phthalocyanines* **2002**, *6*, 305-324.

(7) Morgan, A. R.; Petousis, N. H.; van Lier, J. E. *Eur. J. Med. Chem.* **1997**, *32*, 21-26.

(8) Henderson, B. W.; Dougherty, T. J. *Photochem. Photobiol.* **1992**, *55*, 145-157.

(9) Noodt, B. B.; Berg, K.; Stokke, T.; Peng, Q.; Nesland, J. M. *British J. Cancer* **1999**, *79*, 72-81.

(10) MacDonald, I. J.; Dougherty, T. J. *J. Porphyrins Phthalocyanines* **2001**, *5*, 105-126.

(11) Lam, M.; Oleinick, N. L.; Nieminen, A.-L. *J. Biol. Chem.* **2001**, *276*, 47379-47386.

(12) Rouhi, A. M. *C&E News* **1998**, *76*, 22-27.

(13) Aviezer, D.; Cotton, S.; David, M.; Segev, A.; Khaselev, N.; Galili, N.; Gross, Z.; Yayon, A. *Cancer Res.* **2000**, *60*, 2973-2980.

(14) Hornung, R.; Fehr, M. K.; Monti-Frayne, J.; Krasieva, T. B.; Tromberg, B. J.; Berns, M. W.; Tadir, Y. *Photochem. Photobiol.* **1999**, *70*, 624-629.

(15) Kessel, D.; Luo, Y. *J. Porphyrins Phthalocyanines* **2001**, *5*, 181-184.

(16) Yslas, I.; Alvarez, M. G.; Marty, C.; Mori, G.; Durantini, E. N.; Rivarola, V. *Toxicology* **2000**, *149*, 69-74.

(17) Shibata, Y.; Matsumura, A.; Yoshida, F.; Yamamoto, T.; Nakai, K.; Nose, T.; Sakata, I.; Nakajima, S. *Cancer Lett.* **1998**, *129*, 77-85.

(18) Friberg, E. G.; Cunderlikova, B.; Pettersen, E. O.; Moan, J. *Cancer Lett.* **2003**, *195*, 73-80.

(19) Chen, X.; Drain, C. M. *Drug Design Rev.* **2004**, *1*, 215-234.

(20) Woodburn, K.; Fan, Q.; Kessel, D.; Luo, Y.; Young, S. *J. Invest. Dermatol.* **1998**, *110*, 746-751.

(21) Taber, S.; Fingar, V.; Coots, C.; Wieman, T. *Clin Cancer Res* **1998**, *4*, 2741-2746.

(22) Razum, N.; Snyder, A.; Doiron, D. *Proceedings of SPIE (Society for Photo-optical International Engineering),* **1996**, *2675*, 43-46.

(23) Berlin, K.; Jain, R. K.; Richert, C. *Biotechnol. Bioeng. Comb. Chem.* **1998**, *61*, 107-118.

(24) Drain, C. M.; Gong, X.; Ruta, V.; Soll, C. E.; Chicoineau, P. F. *J. Comb. Chem.* **1999**, *1*, 286-290.

(25) Kwong, P. D.; Wyatt, R.; Majeed, S.; Robinson, J.; Sweet, R. W.; Sodroski, J.; Hendrickson, W. A. *Structure* **2000**, *8*, 1329-1339.

(26) Moulard, M.; Phogat, S. K.; Shu, Y.; Labrijn, A. F.; Xiao, X.; Binley, J. M.; Zhang, M.-Y.; Sidorov, I. A.; Broder, C. C.; Robinson, J.; Parren, P. W. H. I.; Burton, D. R.; Dimitrov, D. S. *Proc. Natl. Acad. Sci.* **2002**, *99*, 6913-6918.

(27) Kwong, P. D.; Wyatt, R.; Robinson, J.; Sweet, R. W.; Sodroski, J.; Hendrickson, W. A. *Nature* **1998**, *393*, 648-659.

(28) Labrijn, A. F.; Parren, P. W. H. I. **1999**.

(29) Clapham, P. R.; McKnight, A. *J. Gen. Virol.* **2002**, *83*, 1809-1829.

(30) Zwick, M. B.; Kelleher, R.; Jensen, R.; Labrijn, A. F.; Wang, M.; Quinnan, G. V.; Parren, P. W. H. I.; Burton, D. R. *J. Virol.* **2003**, *77*, 6965-6978.

(31) Sharon, M.; Kessler, N.; Levy, R.; Zolla-Pazner, S.; Gorlach, M.; Anglister, J. *Structure* **2003**, *11*, 225-236.

(32) Pantophlet, R.; Wilson, I. A.; Burton, D. R. *J. Virol.* **2003**, *77*, 5889-5901.

(33) Myszka, D. G.; Sweet, R. W.; Hensley, P.; Brigham-Burke, M.; Kwong, P. D.; Hendrickson, W. A.; Wyatt, R.; Sodroski, J.; Doyle, M. L. *Proc. Natl. Acad. Sci.* **2000**, *97*, 9026-9031.

(34) Gallo, S. A.; Finnegan, C. M.; Viard, M.; Raviv, Y.; Dimitrov, A.; Rawat, S. S.; Puri, A.; Durell, S.; Blumenthal, R. *Biochim. Biophys. Acta - Biomembranes* **2003**, *1614*, 36-50.

(35) Neurath, A. R.; Strick, N.; Haberfield, P.; Jiang, S. *Antivir. Chem. Chemother.* **1992**, *3*, 55-63.

(36) Debnath, A. K.; Jiang, S.; Strick, N.; Lin, K.; Kahl, S. B.; Neurath, A. R. *Med. Chem. Res.* **1999**, *9*, 267-275.

(37) Song, R.; Witvrouw, M.; Schols, D.; Robert, A.; Balzarini, J.; De Clercq, E.; Bernadou, J.; Meunier, B. *Antivir. Chem. Chemother.* **1997**, *8*, 85-97.

(38) Vzorov, A. N.; Dixon, D. W.; Trommel, J. S.; Marzilli, L. G.; Compans, R. W. *Antimicrob. Agents Chemother.* **2002**, *46*, 3917-3925.

(39) Valduga, G.; Breda, B.; Giacometti, G. M.; Jori, G.; Reddi, E. *Biochem. Biophys. Res. Commun.* **1999**, *256*, 84-88.

(40) Malik, Z.; Ladan, H.; Nitzan, Y.; Smetana, Z. Photodynamic therapy of cancer, Budapest, Hungary, 1994; p 305-312.

(41) Nitzan, Y.; Gutterman, M.; Malik, Z.; Ehrenberg, B. *Photochem. Photobiol.* **1992**, *55*, 89-96.

(42) Nitzan, Y.; Dror, R.; Ladan, H.; Malik, Z.; Kimel, S.; Gottfried, V. *Photochem. Photobiol.* **1995**, *62*, 342-347.

(43) Tome, J. P. C.; Neves, M. G. P. M. S.; Tome, A. C.; Cavaleiro, J. A. S.; Soncin, M.; Magaraggia, M.; Ferro, S.; Jori, G. *J. Med. Chem.* **2004**, *47*, 6649-6652.

(44) Mizutani, T.; Wada, K.; Kitagawa, S. *J. Am. Chem. Soc.* **1999**, *121*, 11425-11431.

(45) Bouy-Debec, D.; Brigaud, O.; Leduc, P.; Battioni, P.; Mansuy, D. *Gazz. Chim. Ital.* **1996**, *126*, 233-237.

(46) Samaroo, D.; Soll, C. E.; Todaro, L. J.; Drain, C. M. *Org. Lett.* **2006**, *8*, 4985-4988.

(47) Greenwald, R. B.; Choe, Y. H.; McGuire, J.; Conover, C. D. *Adv. Drug Delivery Rev.* **2003**, *55*, 217-250.

(48) Molineux, G. *Pharmacotherapy* **2003**, *23*, 3S-8S.

(49) Blagbrough, I. S.; Geall, A. J.; Neal, A. P. *Biochem. Soc. Trans.* **2003**, *31*, 397-406.

(50) Frydman, B.; Valasinas, A. *Exp. Opin. Ther. Patents* **1999**, *9*, 1055-1068.

(51) Venkatesh, B.; Jayakumar, R.; Pandian, R. P.; Manoharan, P. T. *Biochem. Biophys. Res. Commun.* **1996**, *223*, 390-396.

(52) Hamblin, M. R.; Miller, J. L.; Rizvi, I.; Ortel, B.; Maytin, E. V.; Hasan, T. *Cancer Res.* **2001**, *61*, 7155-62.

(53) Hamblin, M. R.; Miller, J. L.; Loew, H. G.; Hasan, T. *British J. Cancer* **2003**, *89*, 937-943.

(54) Barrett, G. C.; Elmore, D. T. In *Amino acids and peptides*; Cambridge University Press: Cambridge, UK, 1998.

(55) Biron, E.; Voyer, N. *Chem. Commun.* **2005**, 4652-4654.

(56) Dixon, D. W.; Kim, M. S.; Kumar, V.; Obara, G.; Marzilli, L. G.; Schinazi, R. F. *Antivir. Chem. Chemother.* **1992**, *3*, 279-282.

(57) Mizutani, T.; Wada, K.; Kitagawa, S. *J. Org. Chem.* **2000**, *65*, 6097-6106.

(58) Blagbrough, I. S.; Geall, A. J. *Tet. Lett.* **1998**, *39*, 439-442.

(59) Lamarche, F.; Sol, V.; Huang, Y. M.; Granet, R.; Guilloton, M.; Krausz, P. *J. Porphyrins Phthalocyanines* **2002**, *6*, 130-134.

(60) Valasinas, A.; Reddy, V. K.; Blokhin, A. V.; Basu, H. S.; Bhattacharya, S.; Sarkar, A.; Marton, L. J.; Frydman, B. *Bioorg. Med. Chem.* **2003**, *11*, 4121-4131.

(61) Rovers, J. P.; Saarnak, A. E.; de Jode, M.; Sterenborg, H. J. C. M.; Terpstra, O. T.; Grahn, M. F. *Photochem. Photobiol.* **2000**, *71*, 210-217.

(62) Hornung, R.; Fehr, M. K.; Walt, H.; Wyss, P.; Berns, M. W.; Tadir, Y. *Photochem. Photobiol.* **2000**, *72*, 696-700.

(63) Laville, I.; Pigaglio, S.; Blais, J.-C.; Doz, F.; Loock, B.; Maillard, P.; Grierson, D. S.; Blais, J. *J. Med. Chem.* **2006**, *49*, 2558-2567.

(64) Lottner, C.; Knuechel, R.; Bernhardt, G.; Brunner, H. *Cancer Lett.* **2004**, *215*, 167-177.

(65) Lottner, C.; Knuechel, R.; Bernhardt, G.; Brunner, H. *Cancer Lett.* **2004**, *203*, 171-180.

(66) Rietveld, I. B.; Kim, E.; Vinogradov, S. A. *Tet.* **2003**, *59*, 3821-3831.

(67) Sol, V.; Blais, J. C.; Granet, R.; Guilloton, M.; Spiro, M.; Krausz, P. *J. Org. Chem.* **1999**, *64*, 4431-4444.

(68) Sol, V.; Blais, J. C.; Bolbach, G.; Carre, V.; Granet, R.; Guilloton, M.; Spiro, M.; Krausz, P. *Tet. Lett.* **1997**, *38*, 6391-6394.

(69) Sol, V.; Branland, P.; Granet, R.; Kaldapa, C.; Verneuil, B.; Krausz, P. *Bioorg. Med. Chem. Lett.* **1998**, *8*, 3007-3010.

(70) Flessner, M. F.; Dedrick, R. L. *Cancer Res* **1994**, *54*, 4376-4384.

(71) Schneider, R.; Schmitt, R.; Frochot, C.; Fort, Y.; Lourette, N.; Guillemin, F.; Muller, J.-F.; Barberi-Heyob, M. *Bioorg. Med. Chem.* **2005**, *13*, 2799-2808.

(72) Hifumi, E.; Sakata, H.; Nango, M.; Uda, T. *J. Mol. Cat. A: Chem.* **2000**, *155*, 209-218.

(73) Chaleix, V.; Sol, V.; Huang, Y.-M.; Guilloton, M.; Granet, R.; Blais, J. C.; Krausz, P. *Eur. J. Org. Chem.* **2003**, 1486-1493.

(74) Dombi, K. L.; Richert, C. *Molecules* **2000**, *5*, 1265–1280.

(75) Boitrel, B.; Baveux-Chambenoit, V.; Richard, P. *Eur. J. Org. Chem.* **2001**, 4213-4221.

(76) Li, H.; Czuchajowski, L. *Heterocyclic Chem.* **1999**, *6*, 57-77.

(77) Garcia, G.; Sol, V.; Lamarche, F.; Granet, R.; Guilloton, M.; Champavier, Y.; Krausz, P. *Bioorganic & Medicinal Chemistry Letters* **2006**, *16*, 3188-3192.

(78) Hirohara, S.; Obata, M.; Saito, A.; Ogata, S.; Ohtsuki, C.; Higashida, S.; Ogura, S.; Okura, I.; Sugai, Y.; Mikata, Y.; Tanihara, M.; Yano, S. *Photochem. Photobiol.* **2004**, *80*, 301-308.

(79) Tome, J. P. C.; Neves, M. G. P. M. S.; Tome, A. C.; Cavaleiro, J. A. S.; Mendonca, A. F.; Pegado, I. N.; Duarte, R.; Valdeira, M. L. *Bioorg. Med. Chem.* **2005**, *13*, 3878-3888.

(80) Haylett, A. K.; Forbes, E.; MacLennan, A.; Truscott, T. G.; Moore, J. V. *Cancer Lett.* **1996**, *105*, 187-193.

(81) Lakowicz, J. R. *Principles of fluorescence spectroscopy; 2nd Ed.* Kluwer Academic/Plenum Publishers: New York, 1999.

Chapter 2: Efficient Microwave-assisted Synthesis of Amine Substituted Tetrakis(pentafluorophenyl)porphyrin

Abstract

An efficient and rapid means for the synthesis of tetrakis(pentafluorophenyl)porphyrin ($TPPF_{20}$) derivatives by microwave irradiation in an environmentally acceptable solvent is reported. The selective displacement of the para-fluorine groups in $TPPF_{20}$ by primary amines occurs in yields between 70 and 95 %. The derivatives are characterized by absorption and emission spectroscopies, MALDI, high-resolution mass spectrometry and NMR. In addition, the X-ray crystal of one of the derivative is elucidated. This method demonstrates that $TPPF_{20}$ is an ideal platform for the rapid formation of porphyrin conjugates for therapeutic, catalytic, and other applications.

2.1 Introduction

Applications of porphyrin derivatives range from catalysts [1], materials, and devices [2] to photodynamic therapeutic agents (PDT) [3] because of their rich photochemistry and redox chemistry. However, most applications require modification of the porphyrin macrocycle to allow attachment of additional substituents with various other functionalities.

Microwave-assisted reactions have become increasingly important in chemical synthesis in the last 20 years due to the advantages they provide over conventional heating methods [4]. Significant reduction in reaction times, side reactions, increased yields, ease of purification, and minimization of the amount of solvent used are only a few of these desirable qualities [5]. Shorter reaction times (usually <15 min) allow rapid investigation into new methodologies and reaction optimization. Microwave-assisted reactions are believed to facilitate polarization of the substrates thereby promoting the reactions [6].

Drain's group previously demonstrated a solvent-free [7] porphyrin synthesis, and solid-supported reactions that minimize the amount of subsequent purification [8]. In view of the significant need for rapid synthesis of porphyrin derivatives-especially for therapeutic applications, methods for the facile preparation of porphyrin derivatives around a core platform of 5,10,15,20-tetrakis(2,3,4,5,6-pentafluorophenyl)porphyrin ($TPPF_{20}$) are presented. As a demonstration of the method, a variety of amphipathic moieties are grafted onto the core for evaluation as photodynamic therapeutic (PDT) agents.

2.2 Experimental Procedures

Material & Methods

UV-Vis spectra were recorded on a Varian Bio3 spectrophotometer. Steady-state fluorescence (emission) spectra were measured with a Fluorolog τ3, Jobin-SPEX Instruments S.A., Inc. Flash column chromatography was performed using 230-400 mesh ASTM Merck silica gel-60. ESI-MS spectrometric analyses were performed at the Mass Spectrometry Facility of the Department of Chemistry, Hunter College using an Aligent Technologies HP-1100 LC/MSD instrument. ^{1}H NMR was run in CD_3OD on a Bruker Avance 500 MHz spectrometer. Chemical shifts are reported in parts per million (ppm). X-ray structure for Por-EDA_4 was obtained from a Bruker-Nonius KappaCCD X-ray diffractometer at 100K. High Resolution Mass Spectrometry (HRMS) was preformed at CUNY Mass Spectrometry Facility at Hunter College. All reagents were obtained from commercial sources and used without further purification.

General Synthetic Procedures

Preparation of EDA Derivative of $TPPF_{20}$ by Microwave Irradiation

Into a 3.4 mL vial, 5 mg of 5,10,15,20-tetrakis(pentafluorophenyl)porphyrin (5.1 μmol) and 10 equivalents of mono-N-t-boc EDA (Quanta BioDesign) in NMP (0.1 mL) were added. The closed vial was irradiated using a domestic microwave oven (1100 W, Samsung MW4250W) at 2 min intervals until no starting material was visualized by TLC (10 min). After the vial was cooled, the solvent (NMP) was removed in vacuo. The reaction mixture was purified on a silica gel prep TLC plate (hexane: ethyl acetate: methanol, 2:1.5:0.5). The porphyrin was re-dissolved in methanol and evaporated under reduced pressure to afford >90 % yield. Alternatively, the Por-EDA_4 derivative was

crystallized from a hexane-toluene mixture over several weeks. This derivative can also be precipitated using from methanol, dichloromethane and hexane as solvents. **EDA porphyrin** (Por-EDA$_4$): ^{1}H NMR (CD_3OD, 500 MHz) δ 9.18 (br, pyrrole βH, 8H), 3.77 (t, amine or amide CH_2, 8H), 3.52 (t, amine or amide CH_2, 8H), 1.54 (s, tboc, 36H). HRMS (ESI): calculated for $C_{72}H_{70}F_{16}N_{12}O_8$ (M+H)+ 1535.52568, found (M+H)+ 1535.52566, Δ 0.02 ppm.

Preparation of Lys Derivative of TPPF$_{20}$ by Microwave Irradiation

Into a 3.4 mL vial, 5 mg of 5,10,15,20-tetrakis(pentafluorophenyl)porphyrin (5.1 μmol) and 10 equivalents of Nα-acetyl-L-lysine-methyl ester hydrochloride salt (Aldrich) and sodium bicarbonate (10equiv) in NMP (0.1 mL) were added. The closed vial was irradiated using a domestic microwave oven (1100 W, Samsung MW4250W) at 2 min intervals until no starting material was visualized by TLC (30 min). After the vial was cooled, the solvent (NMP) was removed in vacuo. The reaction mixture was purified on a silica gel prep TLC plate (hexane: ethyl acetate: methanol, 2: 1.5: 0.5). The porphyrin was re-dissolved in methanol and evaporated under reduced pressure to afford >70 % yield. Alternatively, the Por-Lys$_4$ derivative was further purified by precipitation using dichloromethane and hexane as solvents. **Lysine porphyrin** (Por-Lys$_4$): ^{1}H NMR (CD_3OD, 500 MHz) δ 9.11 (br, pyrrole βH, 8H), 4.54 (m, amine or amide CH, 4H), 3.79 (s, $COOCH_3$, 12H), 3.70 (m, amine or amide CH_2, 8H), 2.06 (s, OCH_3, 12H), 2.00 (m, CH_2, 8H), 1.90 (m, CH_2, 8H), 1.68 (m, CH_2, 8H). HRMS (ESI): calculated for $C_{80}H_{78}F_{16}N_{12}O_{12}$ (M+H)+ 1703.56794, found (M+H)+ 1703.56946, Δ 0.89 ppm.

Preparation of PEG Derivative of $TPPF_{20}$ by Microwave Irradiation

Into a 3.4 mL vial, 5 mg of 5,10,15,20-tetrakis(pentafluorophenyl)porphyrin (5.1 μmol) and 10 equivalents of mono-N-t-boc amido-dPEG amine (Quanta BioDesign) in NMP (0.1 mL) were added. The closed vial was irradiated using a domestic microwave oven (1100 W, Samsung MW4250W) at 2 min intervals until no starting material was visualized by TLC (12 min). After the vial was cooled, the solvent (NMP) was removed in vacuo. The crude reaction product was purified via silica gel chromatography using hexane/ethyl acetate/methanol solvent systems to afford >90 % yield. **PEG porphyrin** (Por-PEG_4): ^{1}H NMR (CD_3OD, 500 MHz) δ 9.15 (br s, pyrrole βH, 8H), 3.85-3.60 (m, CH_2O, 6 methylene groups next to O, 48H), 3.54 (t, amine or amide CH_2, 8H), 3.14 (t, amine or amide CH_2, 8H), 2.13 (t, CH_2, 8H), 1.74 (t, CH_2, 8H), 1.38 (s, tboc, 36H). HRMS (ESI): calculated for $C_{104}H_{134}F_{16}N_{12}O_{20}$ (M+H)+ 2175.96546, found (M+H)+ 2175.96280, Δ 1.22ppm.

Deprotection of the Porphyrin Derivatives

For the Por-PEG_4 and Por-EDA_4, the t-boc group was cleaved using 3N HCl in methanol, stirring the reaction in the dark at RT for 24 hr. Each mixture was neutralized using $NaOCH_3$ in methanol and extracted several times using a complex mixture of water/ethyl acetate/toluene. The deprotected Por-PEG_4 and Por-EDA_4 derivatives were analyzed by ESI-MS. For the deprotection of Por-Lys_4, both the acetamide and methyl ester groups were cleaved using 6N HCl. The results were analyzed by MALDI.

2.3 Results & Discussion

Previously reported $TPPF_{20}$ derivatives were typically synthesized in refluxing DMF with a large excess of the amine or thiol reagents [9]; however, the yields were

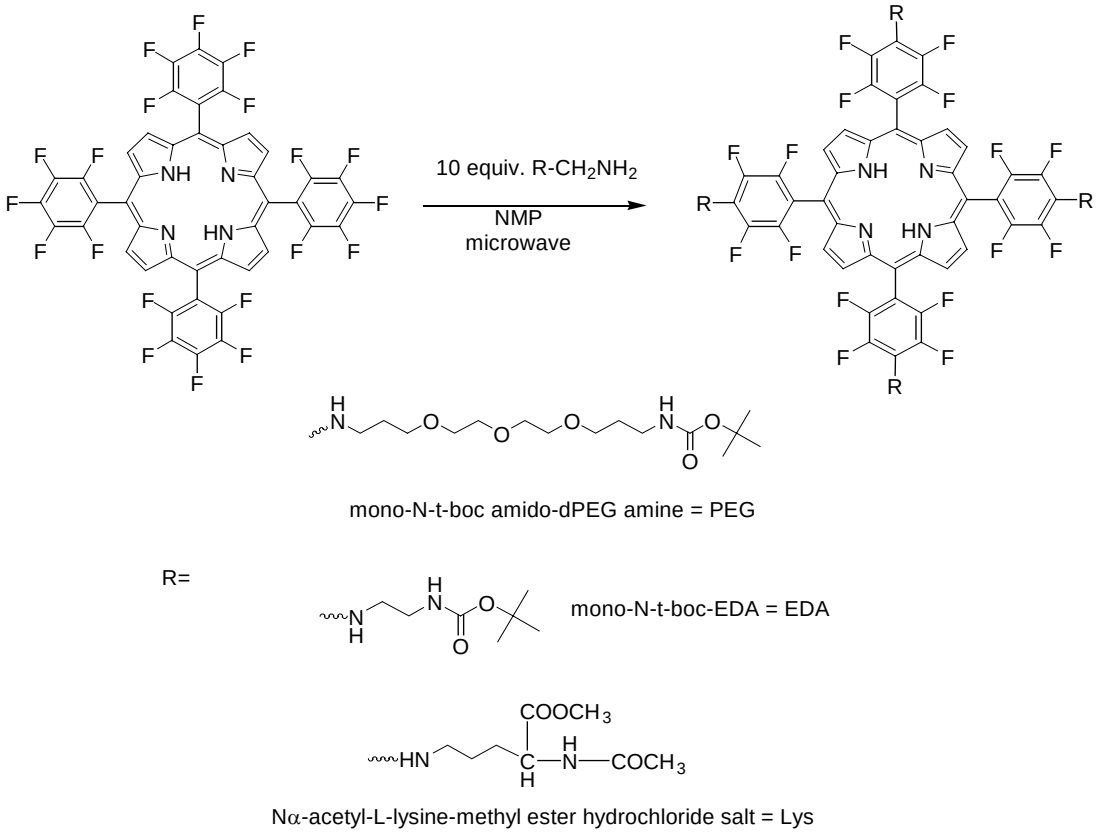

Figure 2.1: Microwave reaction scheme

relatively poor, and the substitution was sometimes incomplete. Better yields, ~90%, are obtained by using thiol reagents and stirring for ~12 h at room temperature in DMF with a stoichiometric amount of dialkylamine [3a,c]. To decrease the reaction time, improve yields, and employ a greener solvent, the development of a synthetic method using microwave irradiation (MW) in *N*-methylpyrrolidone was used (Figure 2.1). A diverse array of primary amines were chosen to demonstrate the method: poly(ethylene glycol)s (PEGs) are relevant to drug design and delivery as they enable the facile uptake of drugs

into cells [10]; polylysine derivatives because these moieties are known to impart selectivity toward cancer cells; and polyamines because these impart both cancer cell selectivity and cell permeability. The functional groups other than the intended amine are *t*-boc protected. Reaction of 5-10 mg (5.1 or 10.2 μmol) of $TPPF_{20}$ with 10 equiv of a primary amine in 1-2 mL of *N*-methylpyrrolidone (NMP) at 60-70 ºC overnight leads to mixture of six different $TPPF_{20}$ derivatives, representing the possible incomplete reaction products. However, the same amounts of porphyrin and amine in 100 μL of NMP and 10 min MW irradiation yields only the tetra-substituted products. The reaction time was dramatically reduced (Table 2.1). The nucleophilic aromatic substitution of the *para*-fluoro group by primary amines takes 10-30 min in this procedure compared to 1-2 days with conventional heating [9c]. A significant added advantage for the MW reaction is that it tolerates functional groups that can decompose under extended heating.

The improved yields of the tetra-substituted derivatives are concomitant with the reduced amounts of incompletely reacted products. Also, prolonged heating in DMF results in the fragmenting of the PEG moieties (data not shown). A 95% yield of the Por-PEG_4 product indicates that each reaction on the porphyrin proceeds with ~99% efficiency. In general, the protected acids are used because these are more soluble in NMP and are found to result in greater yields. The deprotection of these groups is readily accomplished using literature procedures. For the EDA and the PEG, the amide esters are cleaved using HCl in MeOH. For the Lys derivative, 6 N HCl is used to cleave both the acetamide and methyl ester groups.

These conditions are specific for *para*-fluoride substitution by primary amines because under similar reaction conditions secondary amines exhibit no reactivity.

Table 2.1. Comparison of conventional versus microwave heating in the synthesis of protected porphyrin derivatives[a]

porphyrin derivative	solvent	conventional heating[b]	yield	microwave irradiation	yield
R= 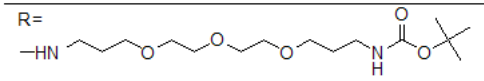 Por-PEG $_4$	NMP	2 days	~50%	12 min	94 + 1%
R= 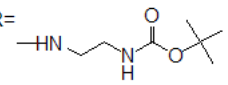 Por-EDA$_4$	NMP	1 day	~50%	10 min	94 ± 2%
R= 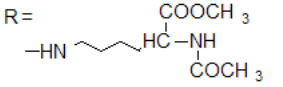 Por-Lys $_4$	NMP	20 h	72%	30 min	77 ± 5%

[a] Reaction conditions: 5.1 μmol of $TPPF_{20}$, 10 equivalent of amine in 100 μL of N-methylpyrrolidone were irradiated for the times indicated at 2 min intervals. The solvent was removed in vacuo; the residue was purified by silica gel column chromatography. [b] In an oil bath maintained at 60-70 ºC.

Refluxing of $TPPF_{20}$ in DMF is known to yield dimethylamino substitution on the para position, thus previous methods require temperatures <60 ºC and extended reaction times [9c]. When 5 mg of $TPPF_{20}$ in DMF is heated in the microwave for 10 min, several dimethylamino derivatives are observed. Procedures in other solvents, such as toluene, DMSO, and morpholine, generally result in low reactivity or significantly diminished yields compared to NMP.

All porphyrins were characterized by electrospray ionization mass spectrometry and high-resolution mass spectrometry (ESI-MS and HR-MS). For all porphyrins, the parent [$M + H^+$] was seen and in some cases the sodium adducts was seen (Figure 2.2 – 2.4). Figures 2.5 – 2.7 present high-resolution mass spectrometry data confirming the molecular formula for the prepared porphyrin derivatives. The ESI-MS for the deprotected Por-(PEG-NH_2)$_4$ and Por-(EDA-NH_2)$_4$ which are now free amines, are presented in Figures 2.8 – 2.9. Figure 2.10 shows the MALDI spectrum of the deprotected Por-(Lys-NH_2)$_4$ derivative. Each protected porphyrin compound was also characterized by ^{1}H NMR. A singlet for the pyrrole H in the ^{1}H NMR indicates the presence of the four *para* substituents, whereas incomplete substitution results in multiplets for these protons. The ^{1}H NMR for each porphyrin derivative is presented in Figures 2.11 – 2.15. The electronic absorption spectra of the porphyrins were characterized at 1 μM concentrations in methanol and were found to be typical for nonaggregated porphyrins. Substitution of the electron-withdrawing fluorine with the electron-donating amine results in a 7-9 nm red shift in the Soret. Table 2.2 summarizes the UV-visible spectra of these porphyrins in methanol. All the derivatives show similar

spectra, including the B band or Soret band at 417-419 nm and the Q-band at 508-509 nm together with three vibronic bands at 543-545, 585-587, and 643-649 nm.

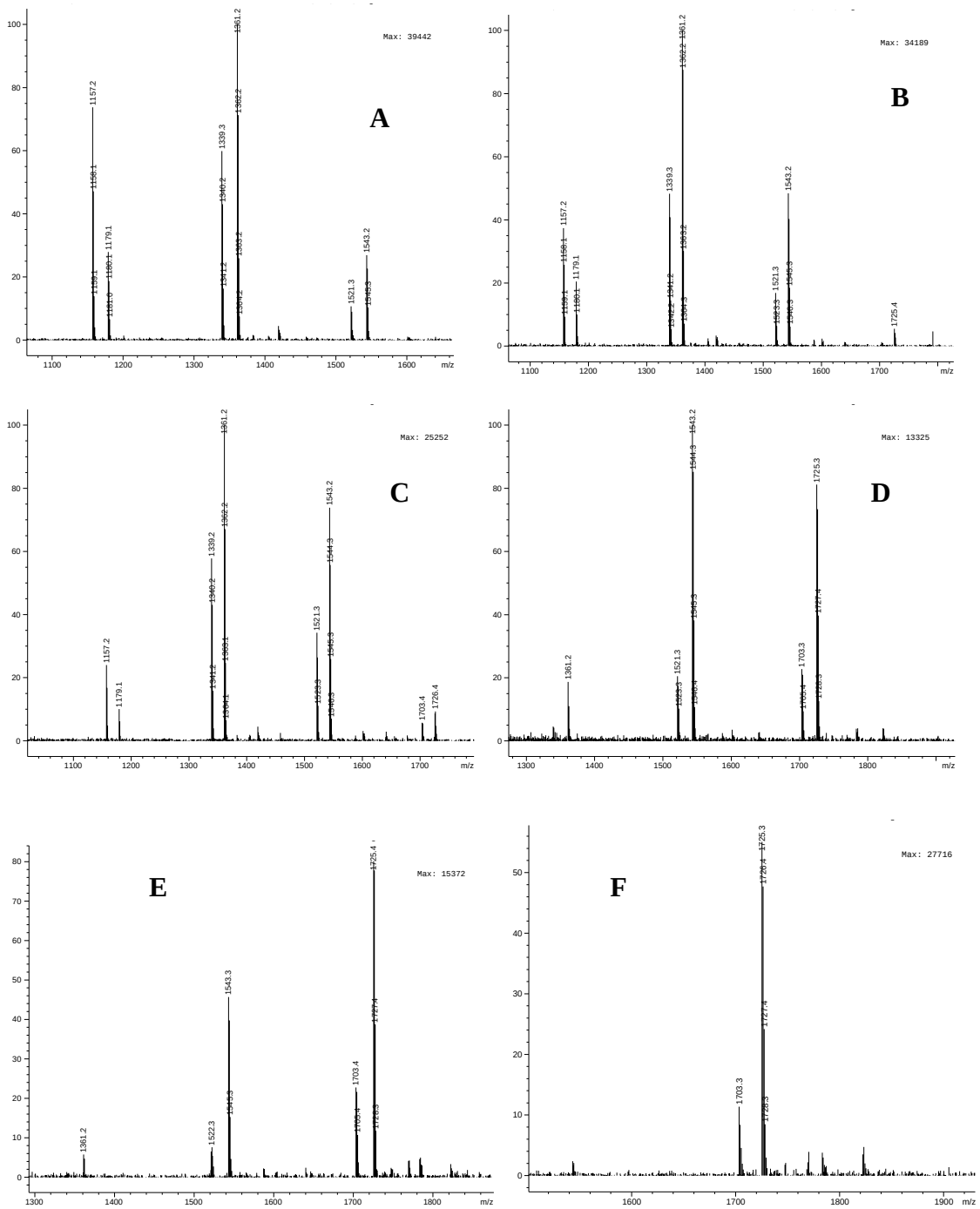

Figure 2.2: Monitoring the Por-Lys$_4$ reaction every 5 minutes via ESI-MS (API, positive ion mode) shows reaction progression to the tetra Por-Lys$_4$ product only. **[A]** shows the mono-substituent (H^+ 1157 and Na^+ adduct 1179), di-substituent (H^+ 1339 and Na^+ adduct 1361), tri-substituent (H^+ 1521 and Na^+ adduct 1543). **[B, C]** shows all four substituents as well as the tetra-substituent $M+H^+$ at 1703 (Na^+ adduct 1725). **[D, E]** shows the di-, tri-, and tetra-substituent. Going from **D** to **E** it is noticeable that the tri-substituent is decreased and the tetra-substituent is increased. [**F]** shows the tetra-substituent only.

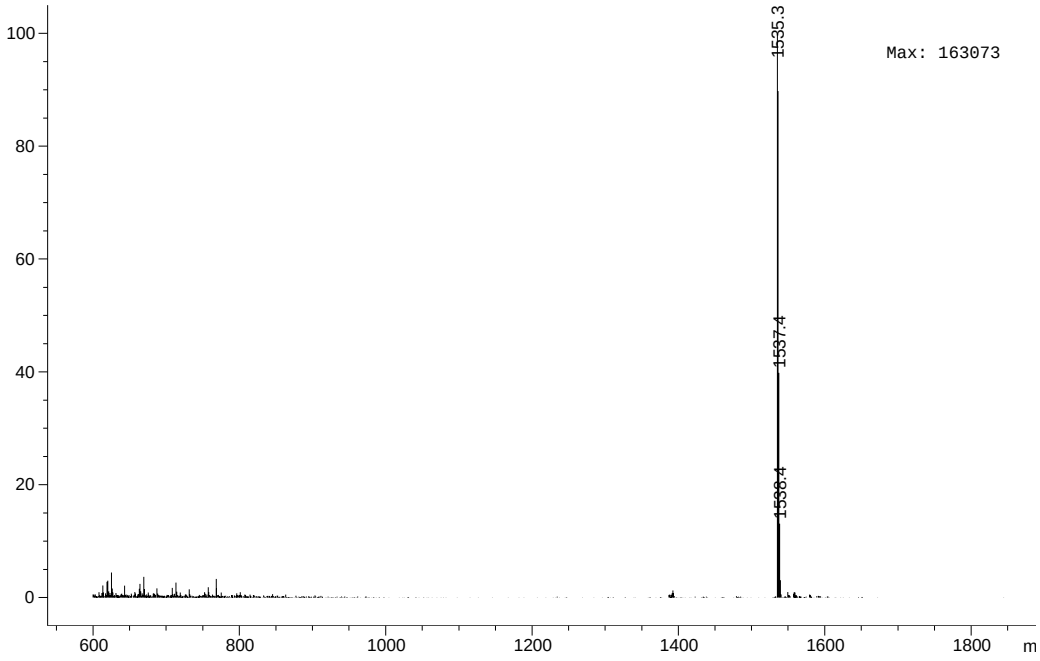

Figure 2.3: ESI-MS (API, positive ion mode) of Por-EDA_4 ($M+H^+$ peak at 1535)

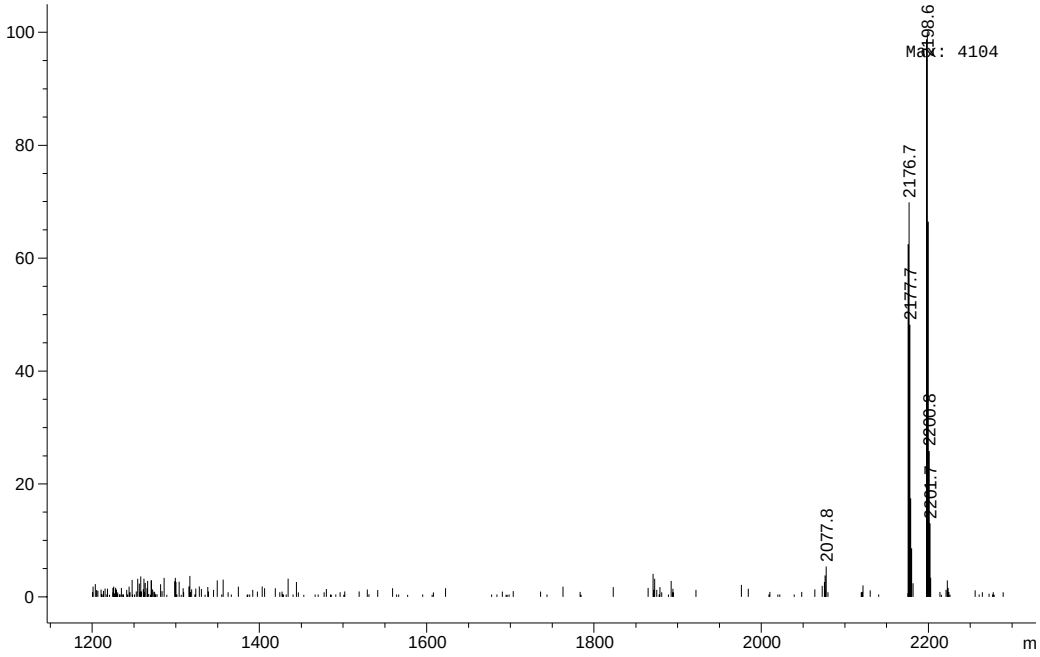

Figure 2.4: ESI-MS (API, positive ion mode) of Por-PEG_4 (parent $M+H^+$ peak at 2176 and Na^+ adduct 2198)

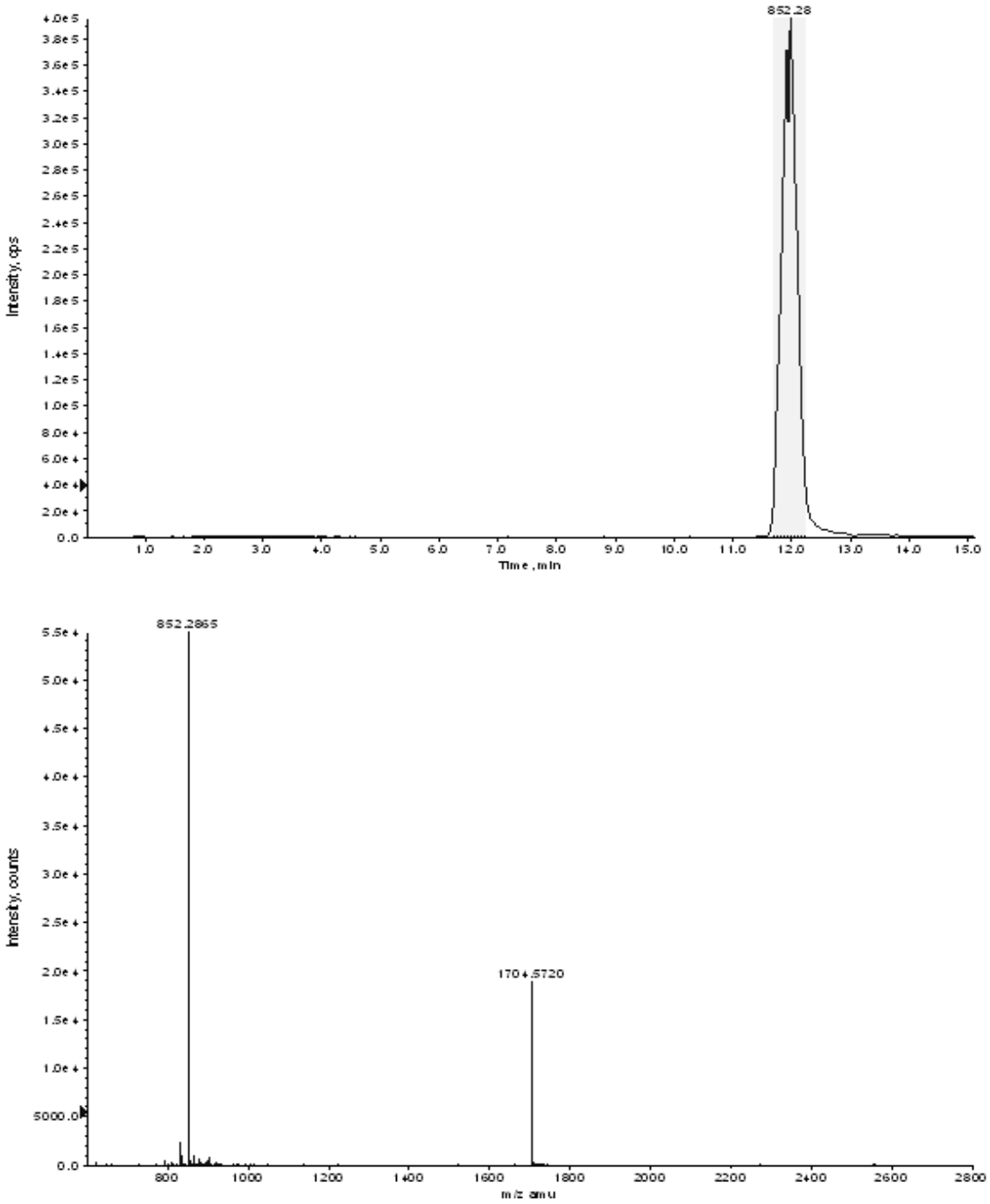

Formula	Compound Name	Mass	Peak RT (min)	Peak area	Description
C80H78F16N12O12	Por-Lys$_4$	1702.56067	11.98	7.12310E6	--

Species	Abundance (counts)	Ion Mass	Measured Mass	Error (mDa)	Error (ppm)	Ret. Time Error (min)
[M+2H]2+	55378.73	852.28761	852.28645	-1.15526	-1.36	--
[M+H]+	15609.15	1703.56794	1703.56946	1.51285	0.89	--

Figure 2.5: Empirical Formula Confirmation of Por-Lys$_4$ by High Resolution Mass Spectrometry

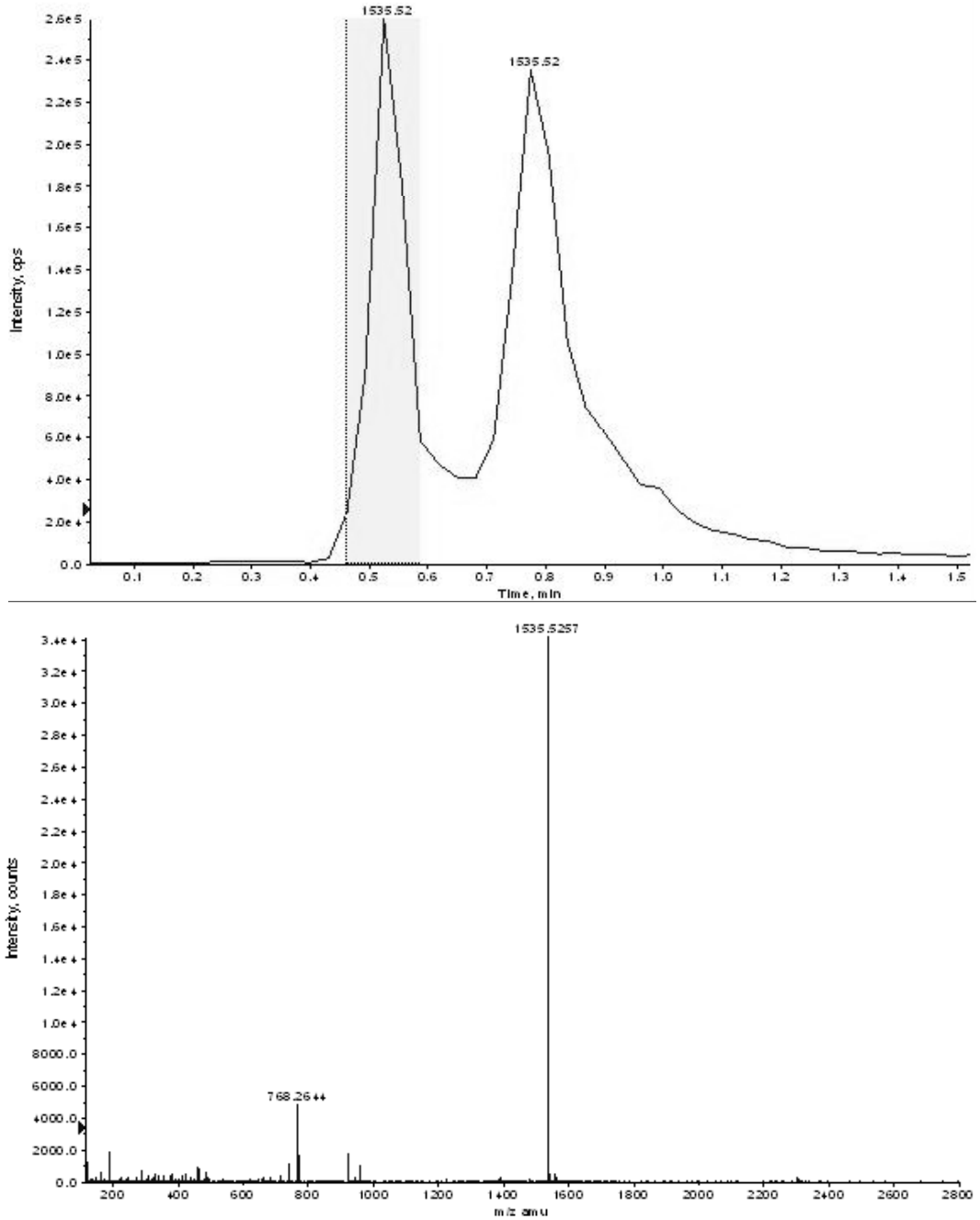

Formula	Compound Name	Mass	Peak RT (min)	Peak area	Description
C72H70F16N12O8	Por-EDA$_4$	1534.51841	0.53	1.32892E6	--

Species	Abundance (counts)	Ion Mass	Measured Mass	Error (mDa)	Error (ppm)	Ret. Time Error (min)
[M+2H]2+	4974.21	768.26648	768.26643	-2.04712	-2.66	--
[M+H]+	34263.36	1535.52568	1535.52566	-0.02866	-0.02	--

Figure 2.6: Empirical Formula Confirmation of Por-EDA$_4$ by High Resolution Mass Spectrometry

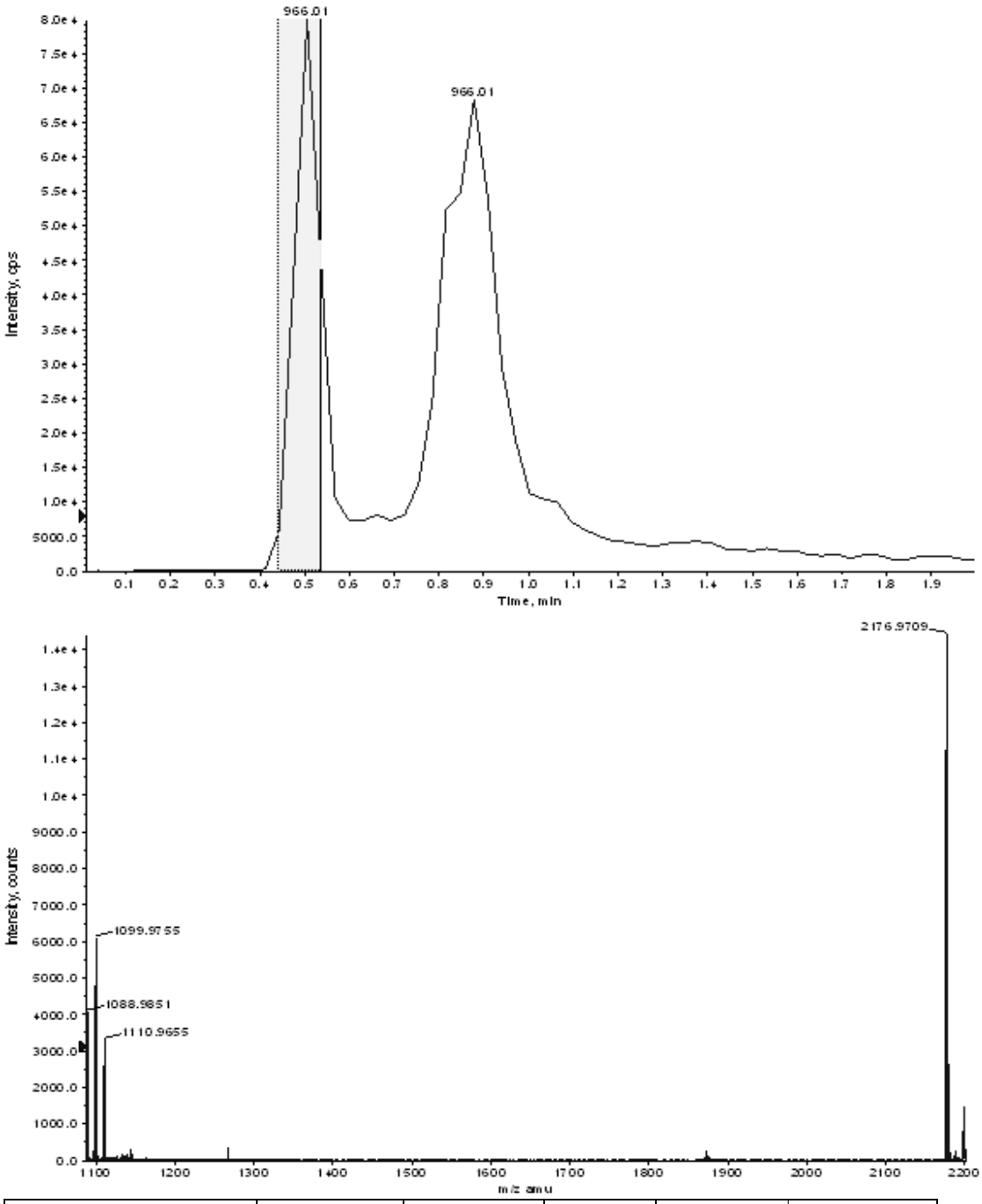

Formula	Compound Name	Mass	Peak RT (min)	Peak area	Description
C104H134F16N12O20	**Por-PEG$_4$**	**2174.95819**	**0.51**	**3.53648E5**	**--**

Species	Abundance (counts)	Ion Mass	Measured Mass	Error (mDa)	Error (ppm)	Ret. Time Error (min)
[M+2H]2+	**3275.03**	**1088.48637**	**1088.48229**	**-4.07498**	**-3.74**	**--**
[M+H]+	**11267.31**	**2175.96546**	**2175.96743**	**1.97073**	**0.91**	**--**

Figure 2.7: Empirical Formula Confirmation of Por-PEG$_4$ by High Resolution Mass Spectrometry

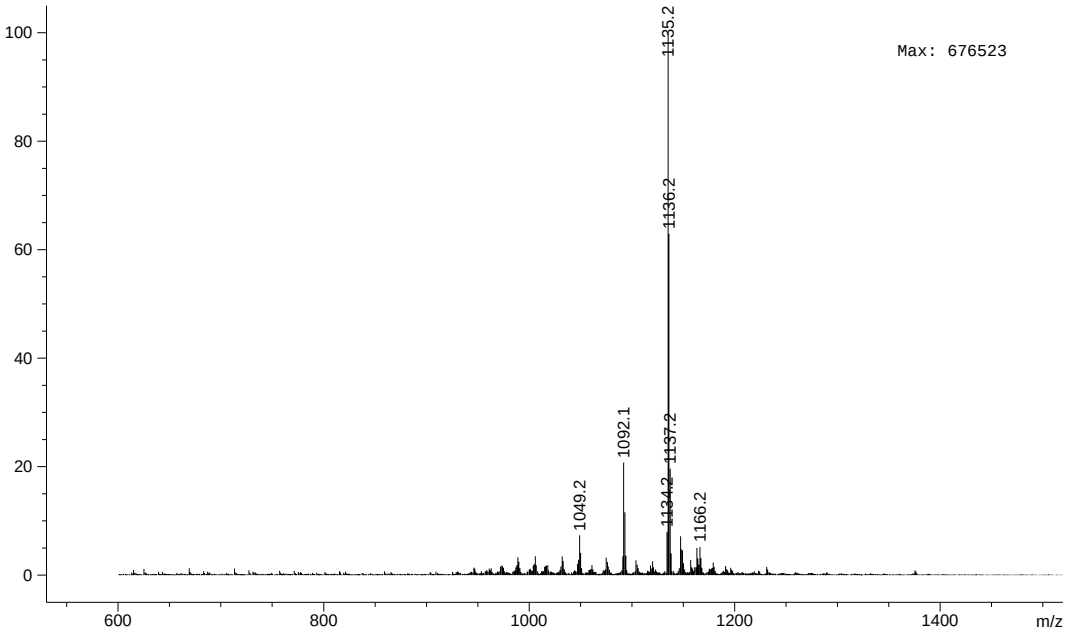

Figure 2.8: ESI-MS (API, positive ion mode) of deprotected Por–$(EDA\text{-}NH_2)_4$, showing the expected $M+H^+$ peak at 1135

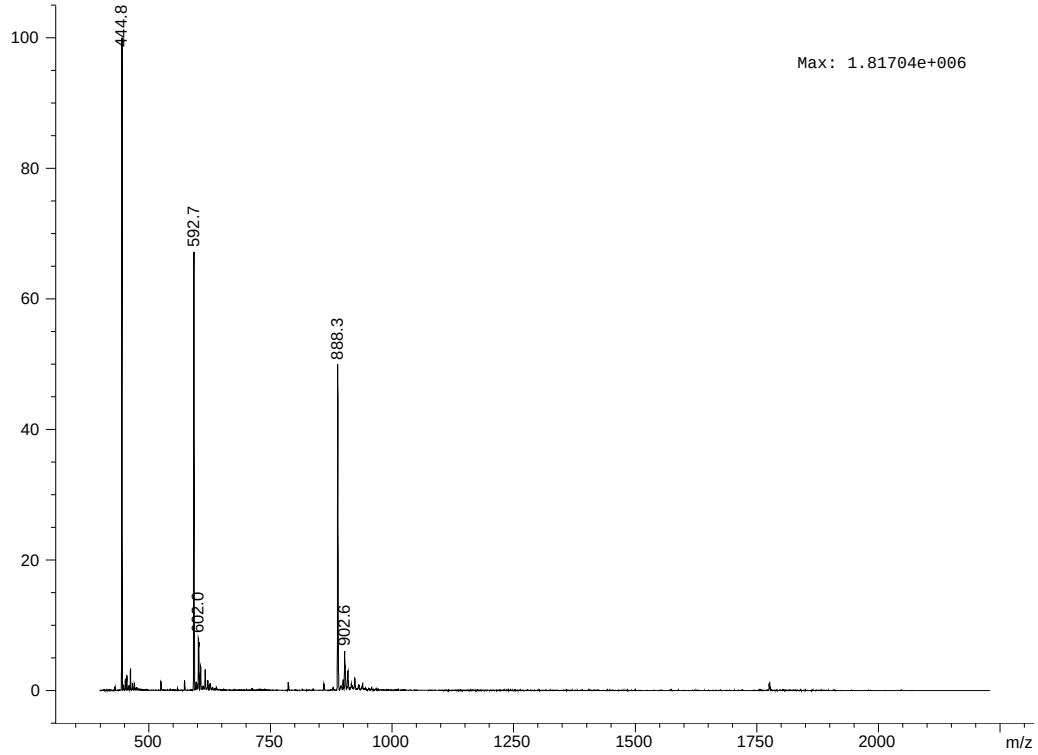

Figure 2.9: ESI-MS (API, positive ion mode) of deprotected Por–$(PEG\text{-}NH_2)_4$, does not have the expected $M+H^+$ peak at 1774, but rather the doubly (888), triply (592), and quadruply (444) charged species, $M+2H^+$, $M+3H^+$, $M+4H^+$

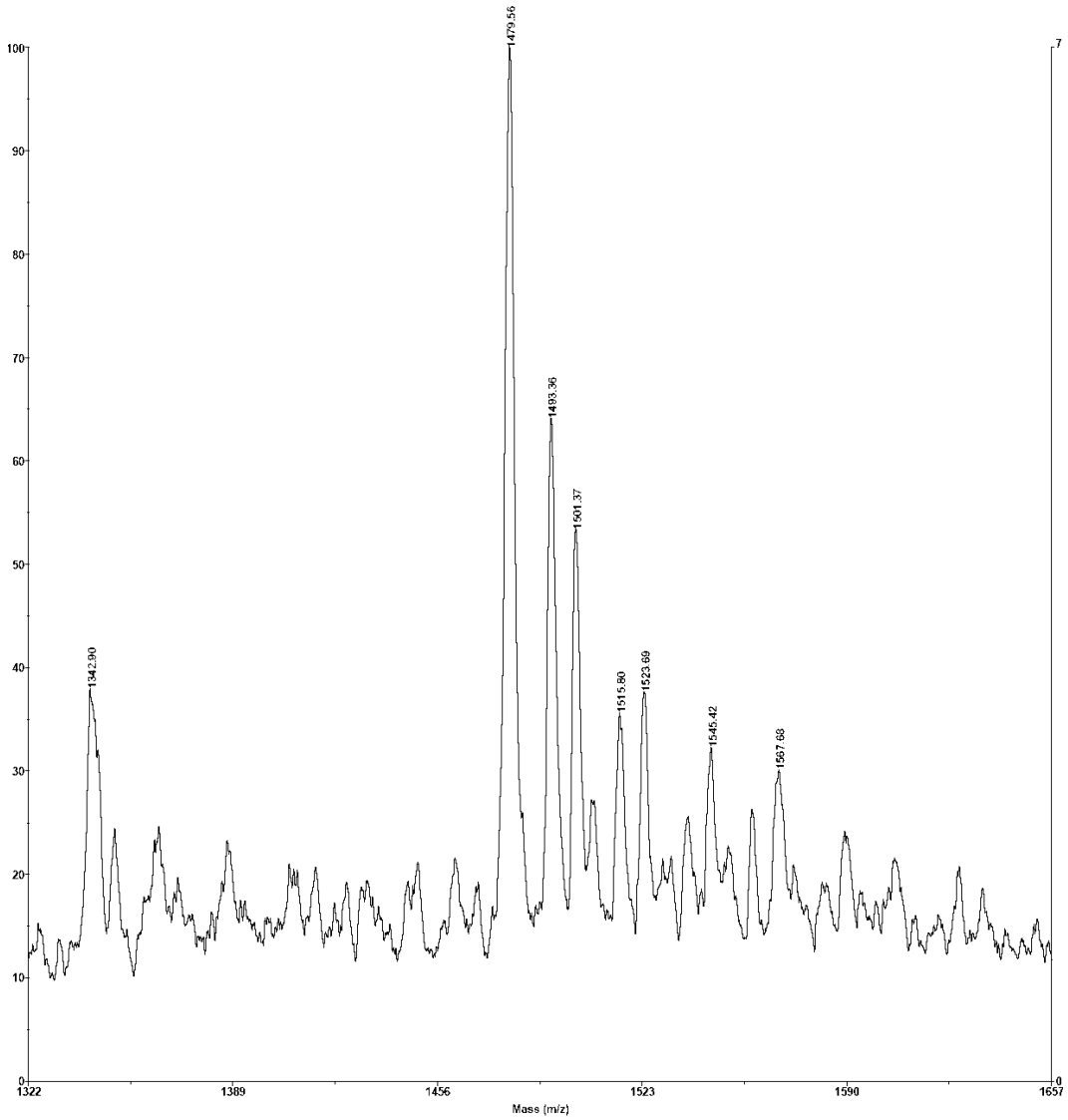

Figure 2.10: MALDI of the deprotected Por–$(Lys\text{-}NH_2)_4$, showing the expected $M+H^+$ ion peak at 1479

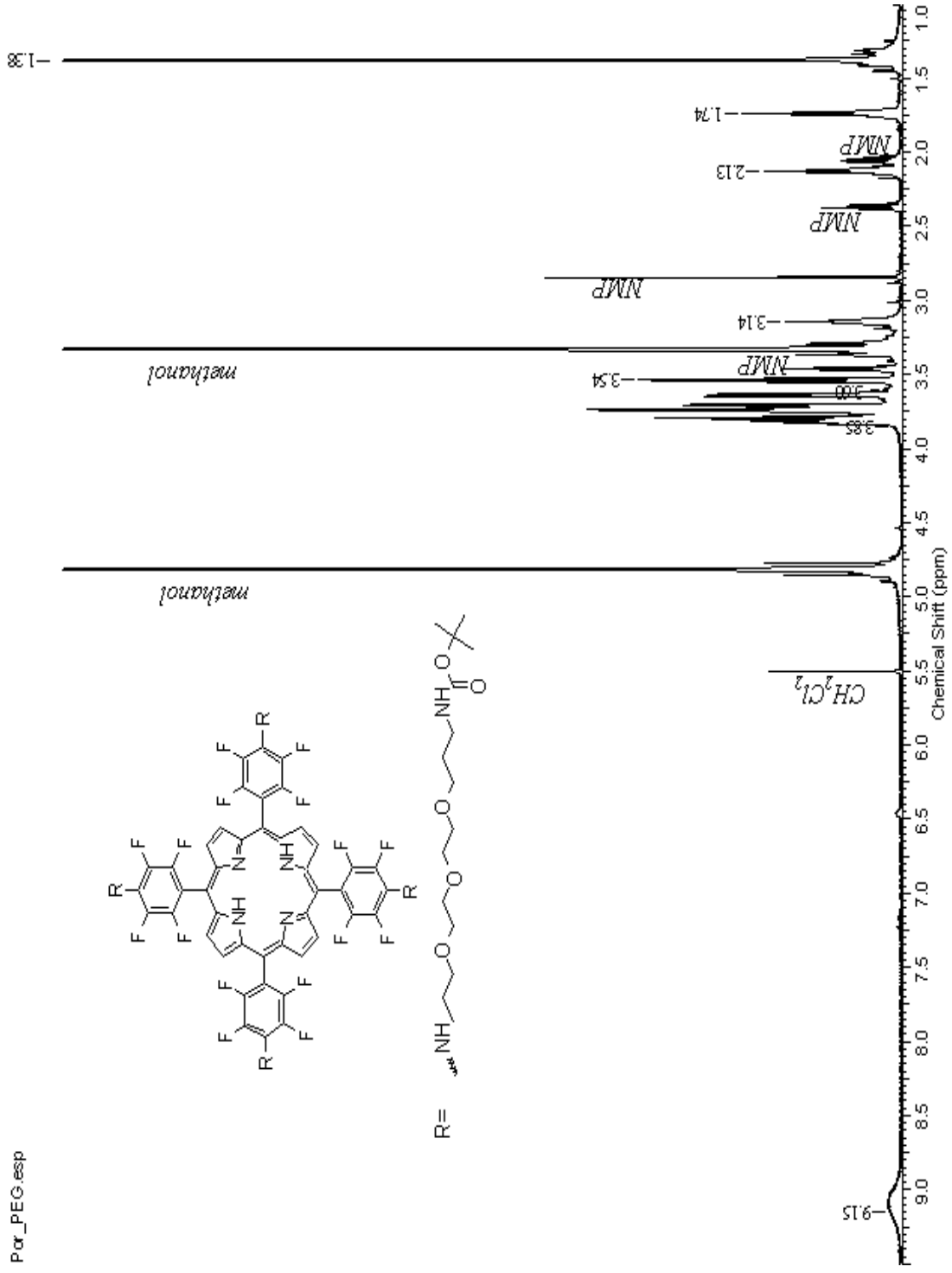

Figure 2.11: 500 MHz ^{1}H NMR (CD_3OD) of Por-PEG_4

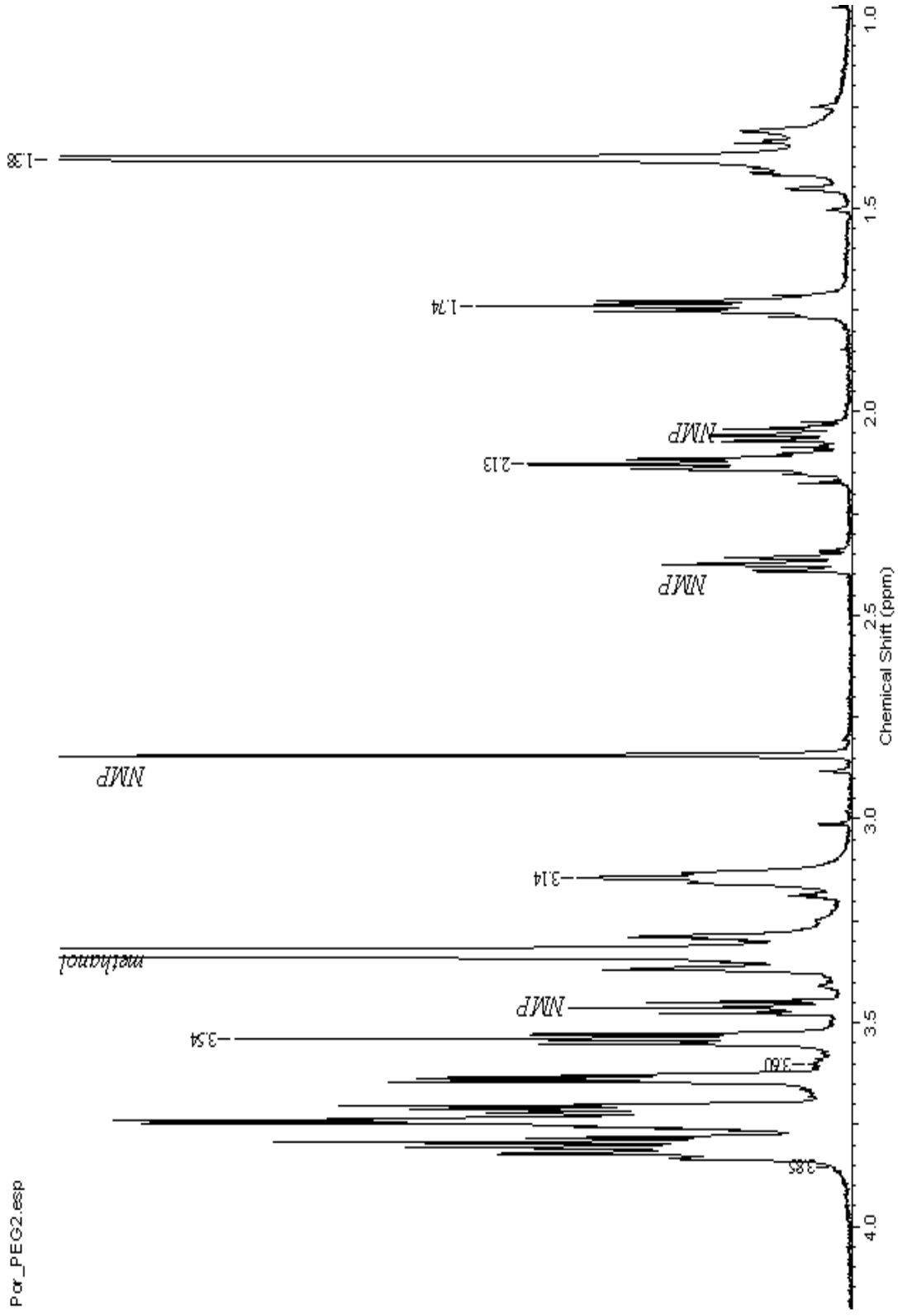

Figure 2.12: Enlarged region between 4 ppm – 1 ppm for ^{1}H NMR of Por-PEG$_4$

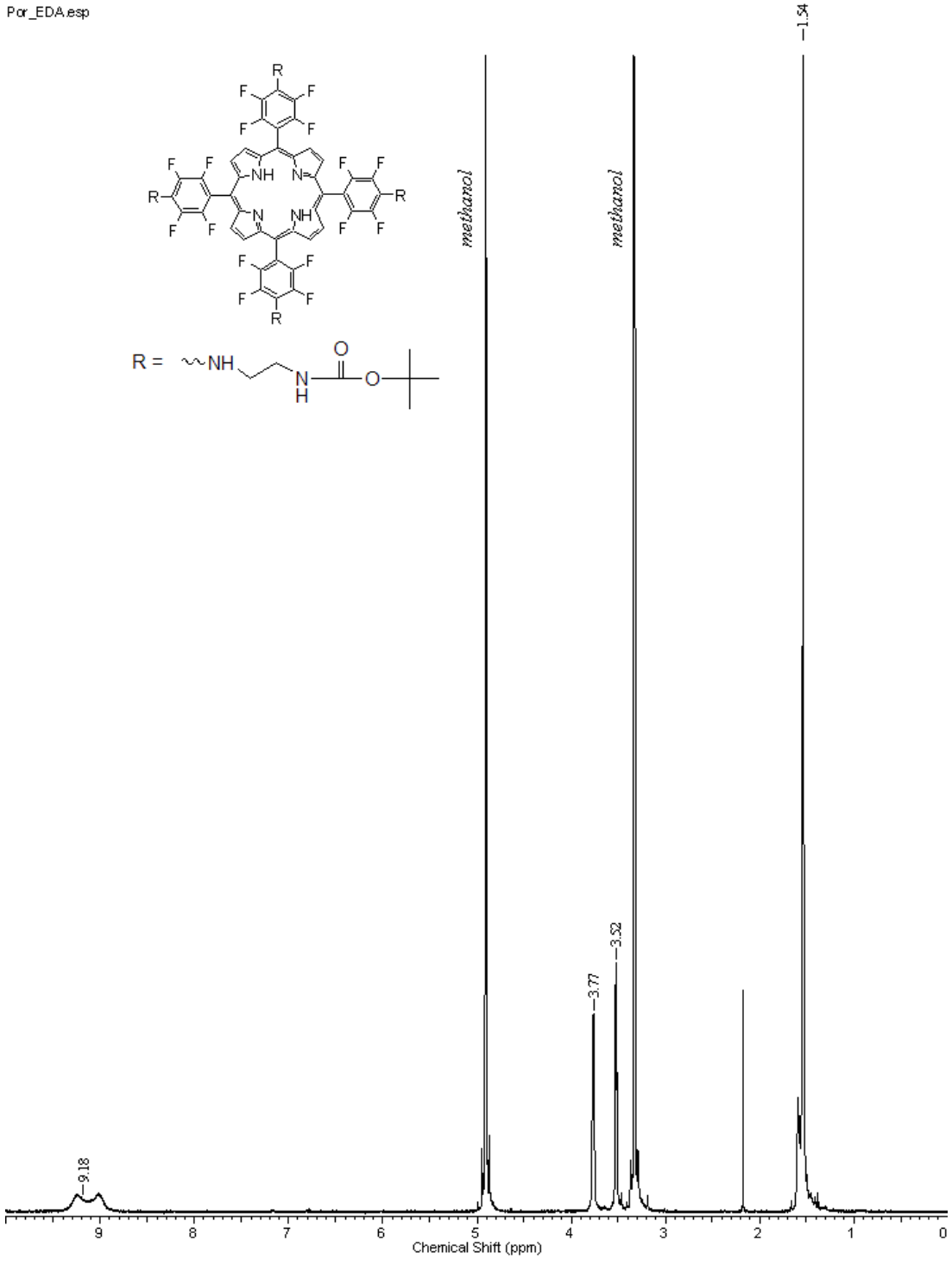

Figure 2.13: 500 MHz ^{1}H NMR (CD_3OD) of Por-EDA_4

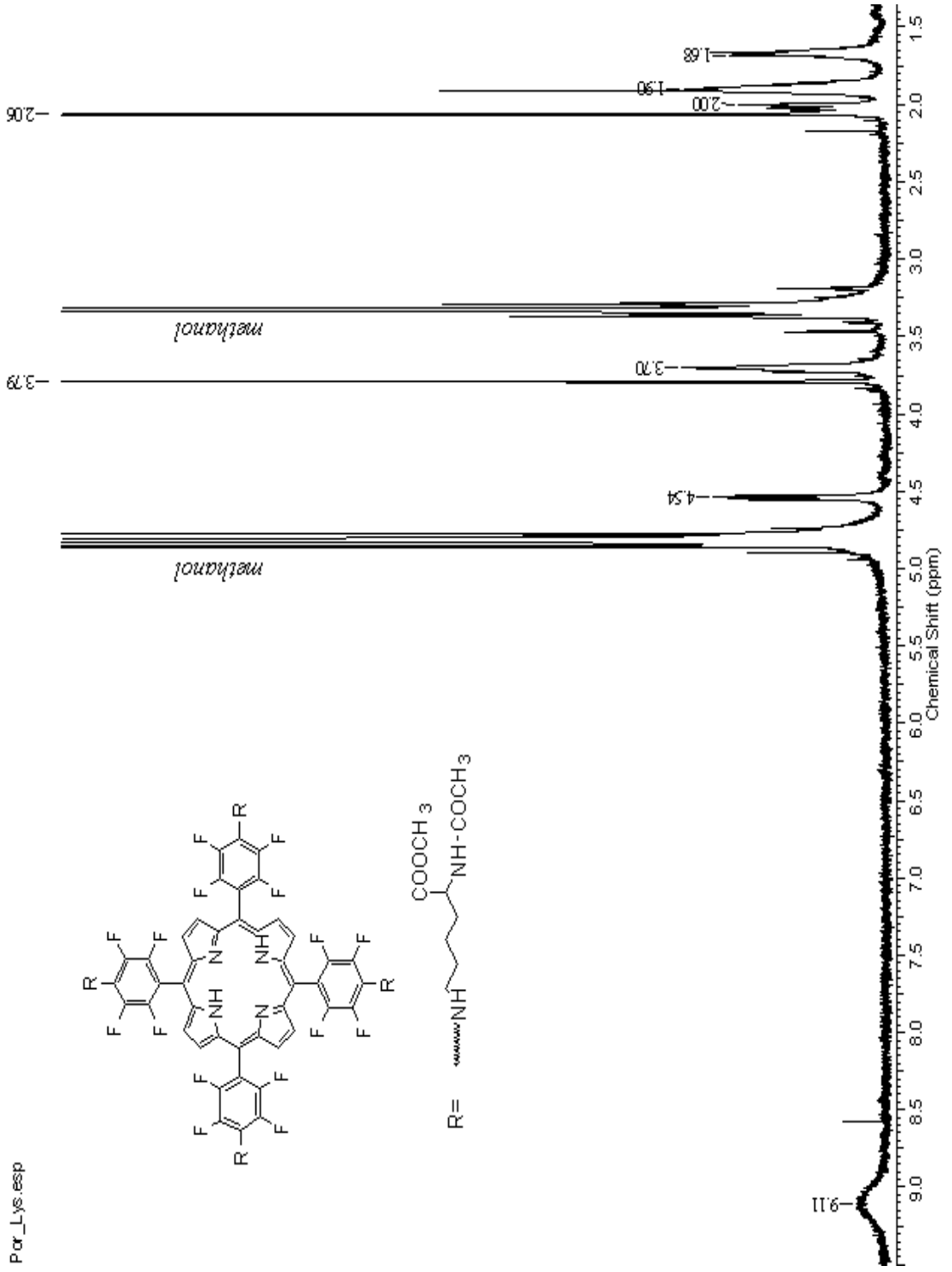

Figure 2.14: 500 MHz ^{1}H NMR (CD_3OD) of Por-Lys_4

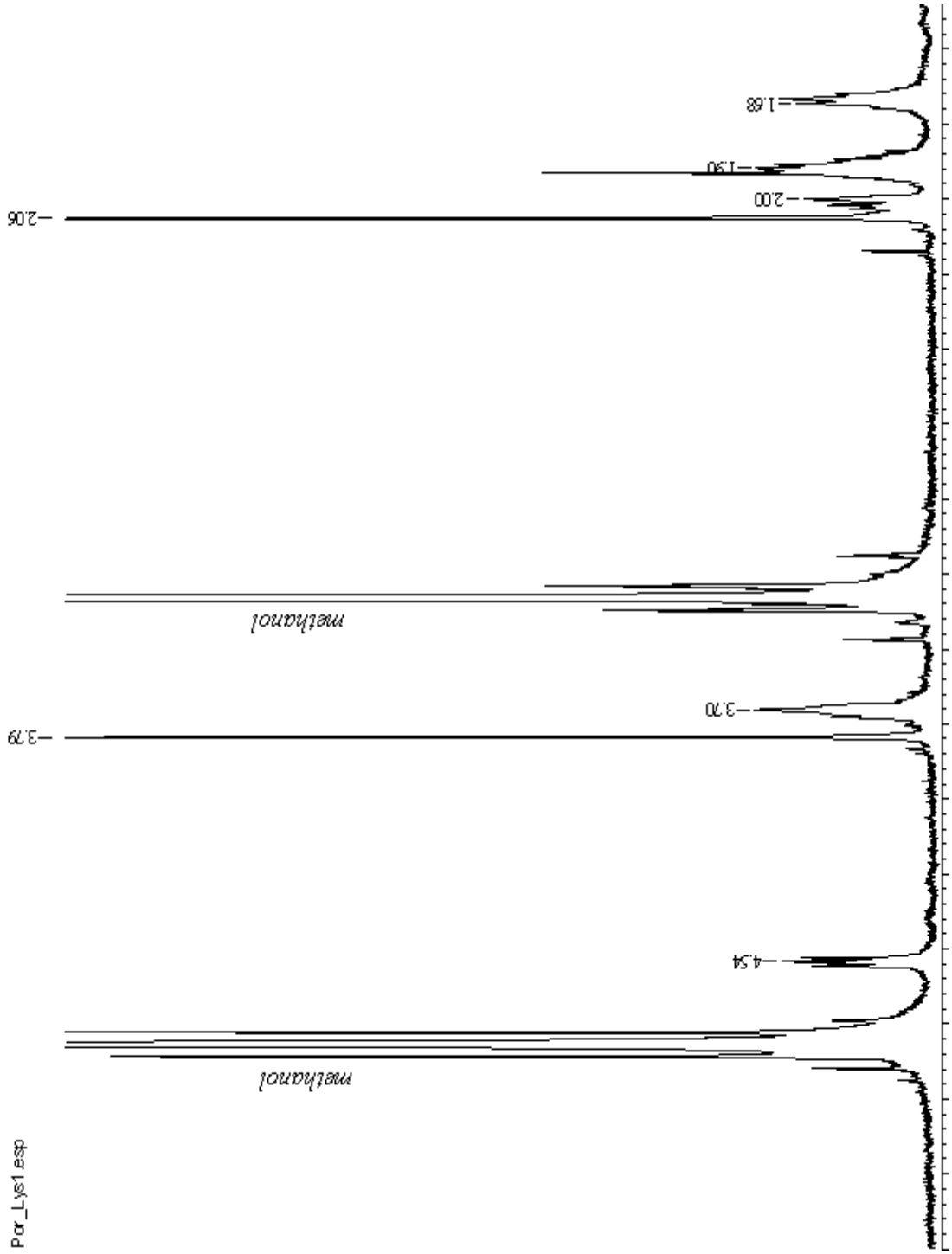

Figure 2.15: Enlarged region between 5 ppm – 1.5 ppm for ^{1}H NMR of Por-Lys_4

The X-ray crystal structure of the t-boc protected Por-EDA$_4$ derivative was elucidated (Figures 2.16 – 2.17). This derivative was crystallized from layered hexane over toluene at room temperature over several weeks. There are two different EDA conformations, bent and extended; the bent conformation is organized by an intramolecular H-bond. The occupancy of the NH protons is 25% (2H) and 75% (2H), not 50:50. The symmetry as suggested by the unit cell (Figure 2.16) is P1, triclinic. The most interesting aspect of the structure is that it forms a two-dimensional lattice (Figure 2.18) organized by intermolecular N-H···O=C hydrogen bonds. The bent EDA moieties form a cyclic structure mediated by intramolecular hydrogen bonds. The extended EDA moieties on opposite sides of the porphyrin H-bond to the bent EDA moieties on adjacent porphyrins. (See packing diagram Figures 2.18 – 2.19). There is a surprising lack of porphyrin π-stacking in the crystal structure, and the layers are organized by dispersion and packing forces.

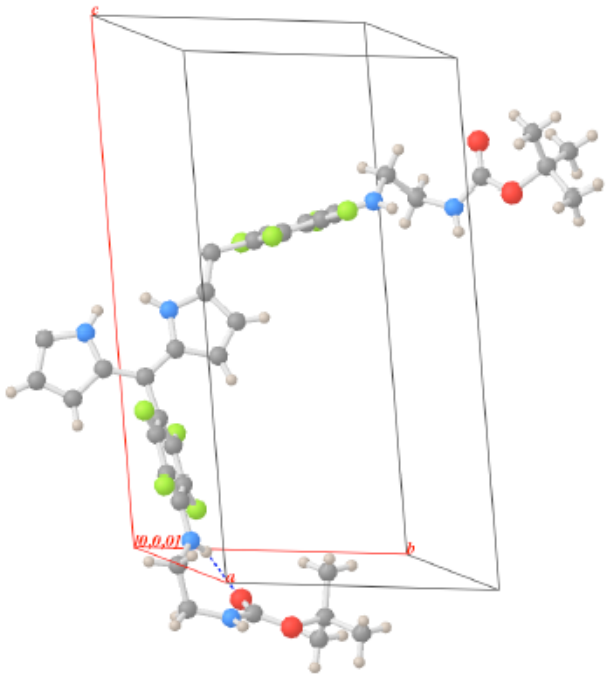

Figure 2.16: Unit Cell (H white; C grey; N blue; O red; F green)

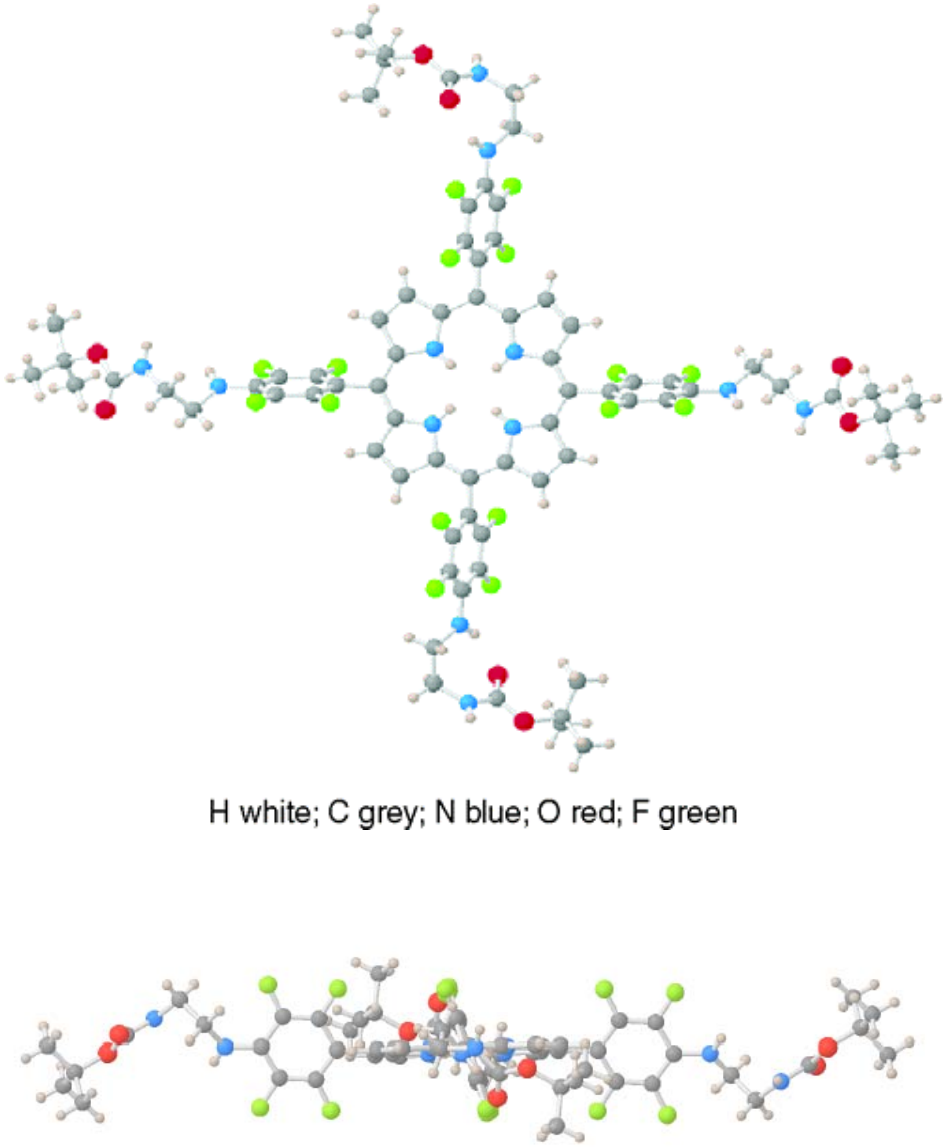

Figure 2.17: X-ray crystal structure of t-boc protected Por-EDA_4

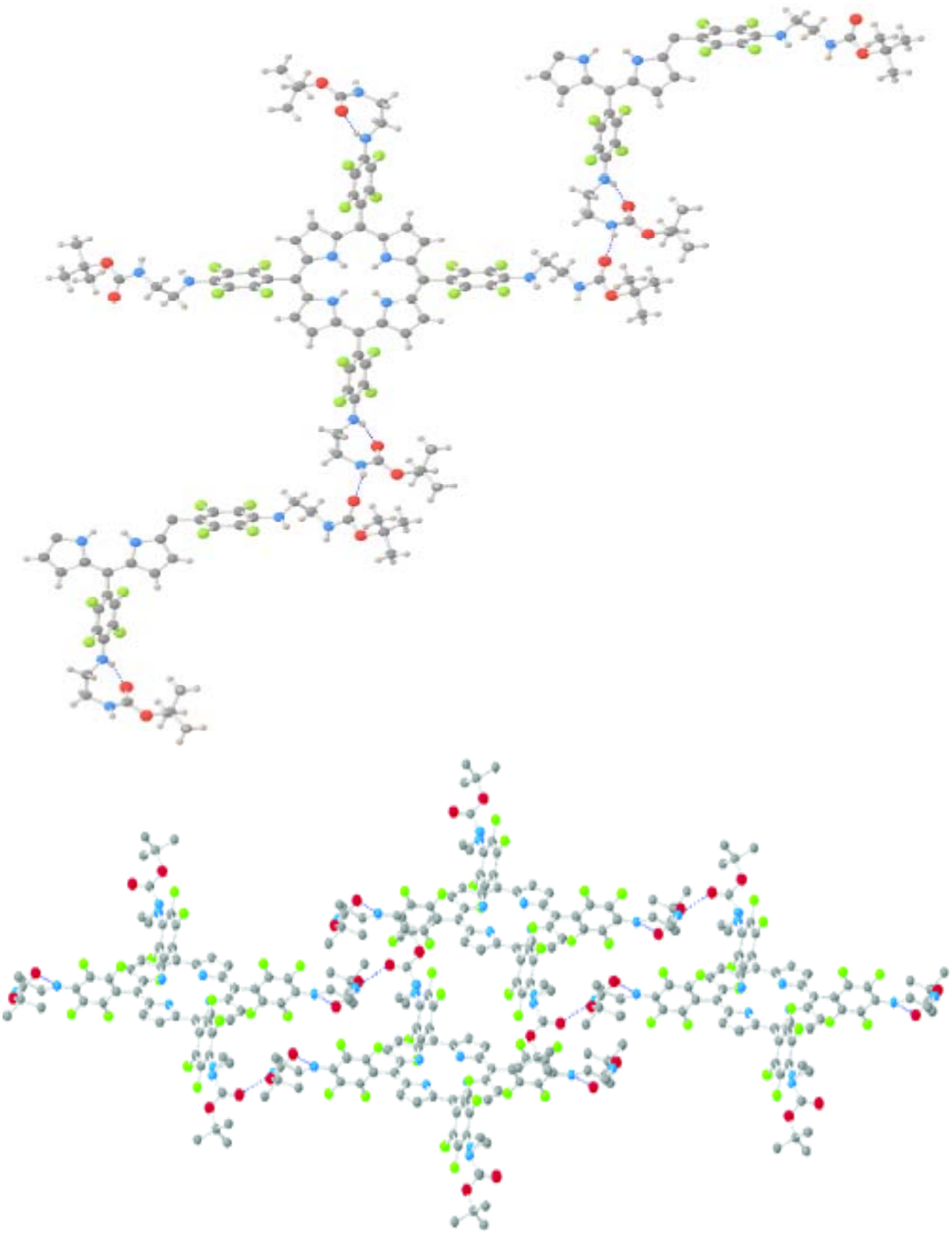

Figure 2.18: X-ray crystal packing structure of t-boc protected Por-EDA$_4$ illustrating the inter- and intramolecular H-bonding. (H white; C grey; N blue; O red; F green)

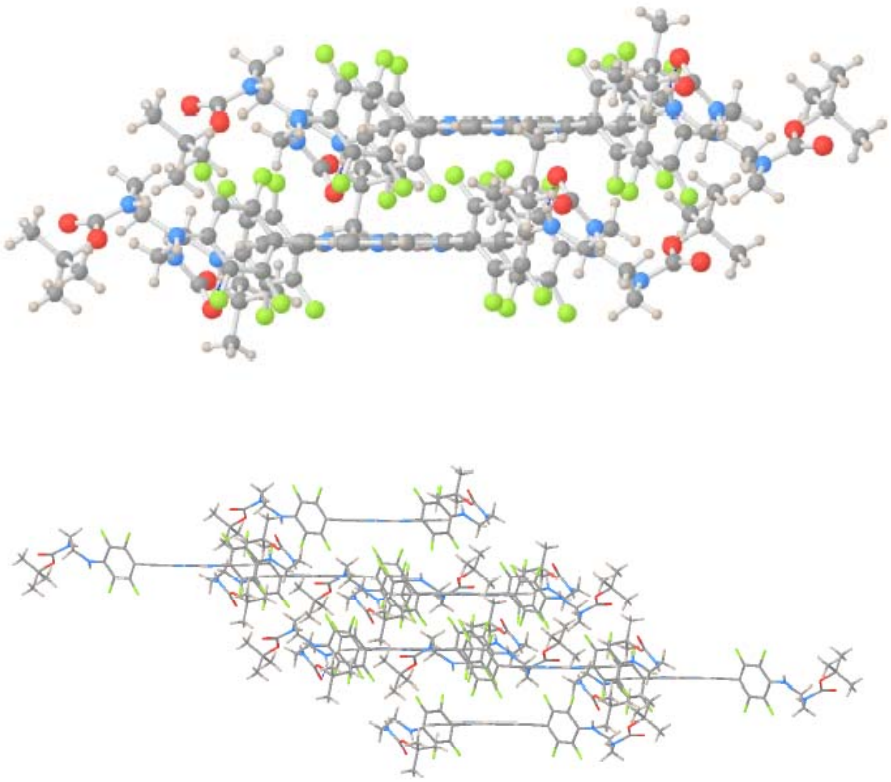

Figure 2.19: Alternative views for the X-ray crystal packing structure of t-boc protected Por-EDA_4 illustrating the inter- and intramolecular H-bonding

The intramolecular and intermolecular hydrogen-bonding motifs were not expected but may explain the aggregation of these compounds at unexpectedly low concentrations.

One of the goals for these porphyrin derivatives is to evaluate their uptake into cancer cells. In addition to hydrophilic derivatives, amphipathic and lipophilic porphyrins are also known to be taken up by cancer cells [3d]. Thus it was decided to assess both the protected and deprotected derivatives. The solubility of these protected derivatives in an aqueous cell culture medium (Dulbecco's modified eagle medium without phenol red or phosphate-buffered saline) must be considered. The absorption

spectra of the t-boc protected Por-EDA_4 in this medium show a red shift from 417 nm to 431 nm and substantial broadening of the Soret band; (discussed in Chapter 3) and similar spectral changes are observed for the other derivatives. These changes in the electronic spectra are indicative of aggregate formation [11].

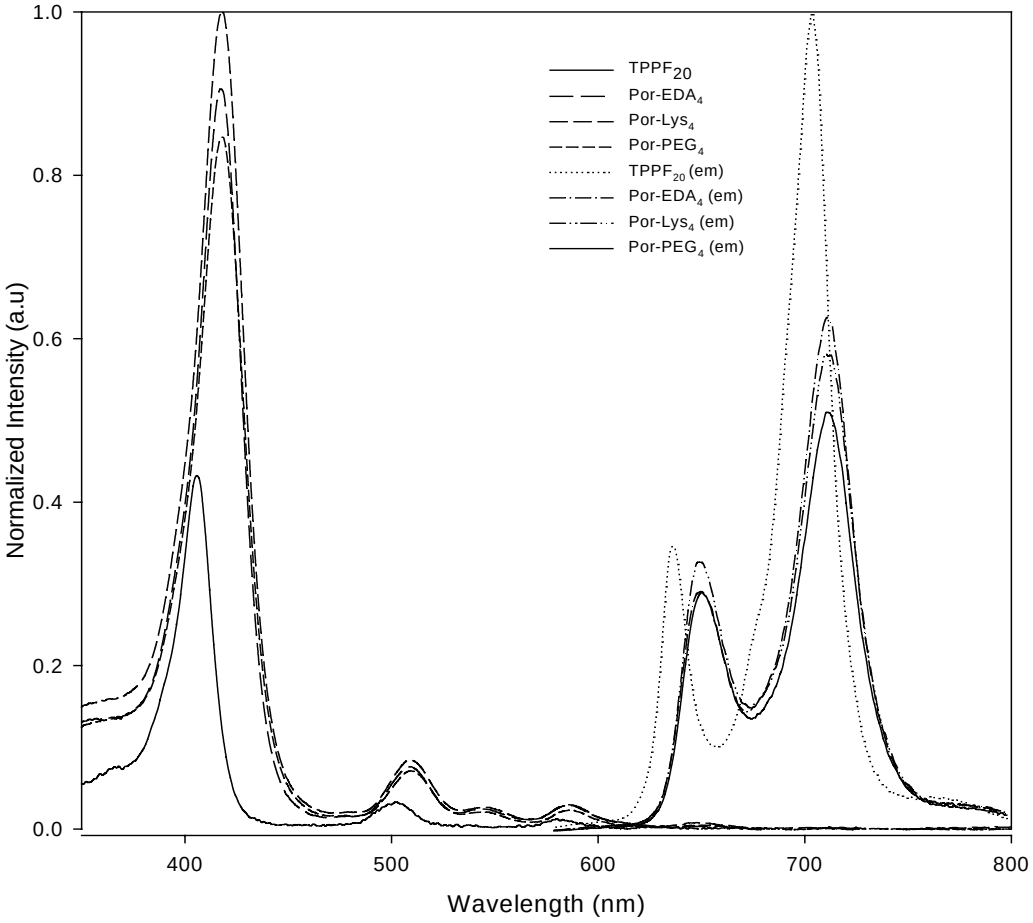

Figure 2.20: Absorption and emission of the parent porphyrin ($TPPF_{20}$) and the protected derivatives (Por-EDA_4, Por-Lys_4, Por-PEG_4) in MeOH. The solubility of $TPPF_{20}$ is < 1 μM in methanol and its fluorescence yield is greater.

The fluorescence emission of these protected derivatives in methanol was also recorded (Figure 2.20). For Por-EDA_4 in methanol, excitation at 417 nm in the Soret band resulted in a strong fluorescence emission at 647-652 nm with a Stokes shift of 7-12 nm, which is typical of porphyrins. In the cell culture medium, the ground-state spectra

are red shifted by 6-10 nm, and there is a similar red shift in the emission bands (Table 2.2).

Table 2.2: ESI-MS, UV-vis and emission data of protected porphyrin derivatives

derivative	mass[a]	UV-vis[b]	emission[b]
$TPPF_{20}$	975	406, 502 (536, sh), 580 (634, sh)	640, 707
Por-PEG_4	2176	418, 509, 545, 586, 643	652, 714
Por-EDA_4	1535	417, 508, 543, 585, 644	647, 713
Por-Lys_4	1703	419, 509, 545 587, 649	652, 711

[a] observed $[M+H]^+$ [b] Absorption and emission in methanol.

On the basis of the above reactivity of primary amines, it is reasonable to hypothesize that combinatorial libraries of porphyrins can be created by this method as long as the individual reagents react with the $TPPF_{20}$ with similar rates and efficiencies. Chapter 4 explores the use of the core $TPPF_{20}$ as a building block of combinatorial libraries. As a proof-of-principle experiment, a 1:1:1 ratio of the three-amine reagents was used in a solution-phase combinatorial reaction. The total amount of the three primary amines was present in the reaction at the same 10:1 ratio with the porphyrin as used above. Statistically, this should yield 21 compounds, but ESI-MS analysis indicated incomplete reactivity as a significant number of compounds with one or more unsubstituted fluorines were observed. Sequential addition of the less reactive amine followed by the more reactive amines also yields inconsistent results.

2.4 Conclusion

In summary, protected amine conjugates of tetrakis(pentafluorophenyl)porphyrin with poly(ethylene glycol), ethylenediamine, and lysine groups were synthesized by microwave irradiation. The protocol described allows for significant reduction in reaction times yet results in high yields and limits byproduct formation compared to earlier reports. The procedure uses commercially available reagents at ca. 10-fold greater concentrations in an environmentally friendly solvent. In general, the MW method works for primary nucleophiles significantly better than secondary and better for amines than for sulfides.

The prepared protected and deprotected porphyrin conjugates will be assessed for their photodynamic efficiency using MDA-MB-231 cancer cells. The crystal structure indicates that these types of porphyrins may self-organize into photonic materials.

2.5 References

(1) (a) Benaglia, M.; Danelli, T.; Fabris, F.; Sperandio, D.; Pozzi, G. *Org. Lett.* **2002**, *4*, 4229. (b) Yang, J.; Weinberg, R.; Breslow, R. *Chem. Commun.* **2000**, 531.

(2) Drain, C. M.; Hupp, J. T.; Suslick, K. S.; Wasielewski, M. R.; Chen, X. *J. Porphyrins Phthalocyanines* **2002**, *6*, 243.

(3) (a) Chen, X.; Hui, L.; Foster, D. A.; Drain, C. M. *Biochemistry* **2004**, *43*, 10918. (b) Sylvain, I.; Zerrouki, R.; Granet, R.; Huang, Y. M.; Lagorce, J.-F.; Guilloton, M.; Blais, J.-C.; Krausz, P. *Bioorg. Med. Chem.* **2002**, *10*, 57. (c) Pasetto, P.; Chen, X.; Drain, C. M.; Franck, R. W. *Chem. Commun.* **2001**, 82. (d) Chen, X.; Drain, C. M. *Drug Design Rev.* **2004**, *1*, 215.

(4) Sauer, D. R.; Kalvin, D.; Phelan, K. M. *Org. Lett.* **2003**, *5*, 4721.

(5) Yoon, D. S.; Han, Y.; Stark, T. M.; Haber, J. C.; Gregg, B. T.; Stankovich, S. B. *Org. Lett.* **2004**, *6*, 4775.

(6) (a) Liu, M. O.; Tai, C.-H.; Wang, W.-Y.; Chen, J.-R.; Hu, A. T.; Wei, T.-H. *J. Organomet. Chem.* **2004**, *689*, 1078. (b) Liu, M. O.; Hu, A. T. *J. Organomet. Chem.* **2004**, *689*, 2450. (c) Boufatah, N.; Gellis, A.; Maldonado, J.; Vanelle, P. *Tetrahedon* **2004**, *60*, 9131.

(7) Drain, C. M.; Gong, X. *Chem. Commun.* **1997**, 2117.

(8) (a) Chaouchi, M.; Loupy, A.; Marque, S.; Petit, A. *Eur. J. Org. Chem.* **2002**, 1278. (b) Mojtahedi, M. M.; Saidi, M. R.; Shirzi, J. S.; Bolourtchian, M. *Synth. Commun.* **2002**, *32*, 851.

(9) (a) Shaw, S. J.; Elgie, K. J.; Edwards, C.; Boyle, R. W. *Tetrahedron Lett.* **1999**, *40*, 1595. (b) Suzuki, M.; Shimizu, S.; Shin, J.-Y.; Osuka, A. *Tetrahedron Lett.* **2003**, *44*,

4597. (c) Battioni, P.; Brigaud, O.; Desvaux, H.; Mansuy, D.; Traylor, T. G. *Tetrahedron Lett.* **1991**, *32*, 2893.

(10) (a) Molineux, G. *Pharmacotherapy* **2003**, *23*, 3S. (b) Hamblin, M. R.; Miller, J. L.; Rizvi, I.; Ortel, B.; Maytin, E. V.; Hasan, T. *Cancer Res.* **2001**, *61*, 7155.

(11) (a) Castriciano, M. A.; Romeo, A.; Scolaro, L. M. *J. Porphyrins Phthalocyanines* **2002**, *6*, 431. (b) Gandini, S. C. M.; Borissevitch, I. E.; Perussi, J. R.; Imasato, H.; Tabak, M. J. *Luminescence* **1998**, *78*, 53.

Chapter 3: Porphyrinic Nanoparticles for Photodynamic Treatment of Cancer: Preparation, Characterization, Cell Uptake, and Cell Death

Abstract

Porphyrins bearing four amphipathic motifs such as amino triethyleneglycol (PEG), lysine (Lys), and ethylenediamine (EDA) can be synthesized in high yields by nucleophilic displacement of the 4-fluoro moiety of 5,10,15,20-tetrakis(2,3,4,5,6-pentafluorophenyl)porphyrin in N-methylpyrrolidone. These amphipathic porphyrins form stable 8 – 50 nm nanoscaled aggregates in cell culture media without the need for an auxiliary PEG stabilizer. Fluorescence microscopy reveals that these nanoparticles are taken up by MDA-MB-231 breast cancer cells and that the nanoparticles slowly disaggregate with time. Thus the amphipathic moieties on the porphyrin serve two functions: (1) a means to make nanoparticles, and (2) cell targeting. While the nanoparticles of the chromophores are inactive as photodynamic agents, illumination of cells containing disaggregated chromophores with low power white light results in cell death. Notably, the disaggregated porphyrinic material is partitioned from mother to daughter cells. The amphipathic porphyrins are effective PDT agents even though they are delivered as inactive nanoparticles. Treating cells with lower concentrations of some of these chromophores (e.g. a tetraglucose derivative) were there is less aggregation and/or smaller nanoparticles, can result in greater killing efficiencies.

3.1 Introduction

Nanotechnology is based on sub-micron sized structures. The use of nanoparticles for a variety of applications such as drug and gene delivery [3,4], pharmaceutical formulations [5], therapeutic imaging and biosensing is currently being exploited [4]. This is an emerging field of research and studies to determine optimal size and shape of nanoparticles for cellular uptake are underway. Toxicity is also a key issue in question [6]. Several groups report that 50 nm diameter particles can be taken up by HeLa cells whereas smaller (14 nm, 30 nm) or larger (74 nm, 100 nm) sized particles generally are not taken up [4,7]. However most studies focus on gold nanoparticles, nanoparticles coated or stabilized with surfactants such as CTAB or poly(D,L-lactic acid), silica, or ceramic based nanoparticles [3]. For example, the reported synthesis and evaluation of silica nanoparticles targeted to bind and release intact plasmid DNA showed that the DNA is protected from degradation by nucleases [3,8], thus has potential for gene delivery. Shape also dictates the uptake of nanoparticles into cells; spheres are preferred over rod or pyramid-shaped particles [4].

In addition to size and shape, the toxicity of nanoparticles is important to biomedical applications [9,10]. There is lack of information in terms of toxicity when it comes to the cellular exposure to nanoparticles [6]. The mode of entry of nanoparticles into cells has been hypothesized to be by endocytosis or receptor-mediated endocytosis. For gold nanoparticles possessing a negative surface charge, it is perplexing to understand the mechanism of uptake [11], since cellular membranes, which are negatively charged, generally do not bind anionic molecules efficiently [12,13]. For example, cell membranes generally bind cationic or neutral molecules preferentially, and it would be expected that electrostatic repulsion would inhibit gold nanoparticles with

anionic groups from cellular uptake. Hence lysine-rich macromolecules and positively charged liposomes are commonly used for cell transfection [4]. Proteins, such as transferrin, generally enter cells via receptor-mediated endocytosis. Because a diverse array of serum proteins (i.e. α- and β-globulin) may non-specifically adsorb onto nanoparticle surfaces, these may mediate nanoparticle entrance into cells through the

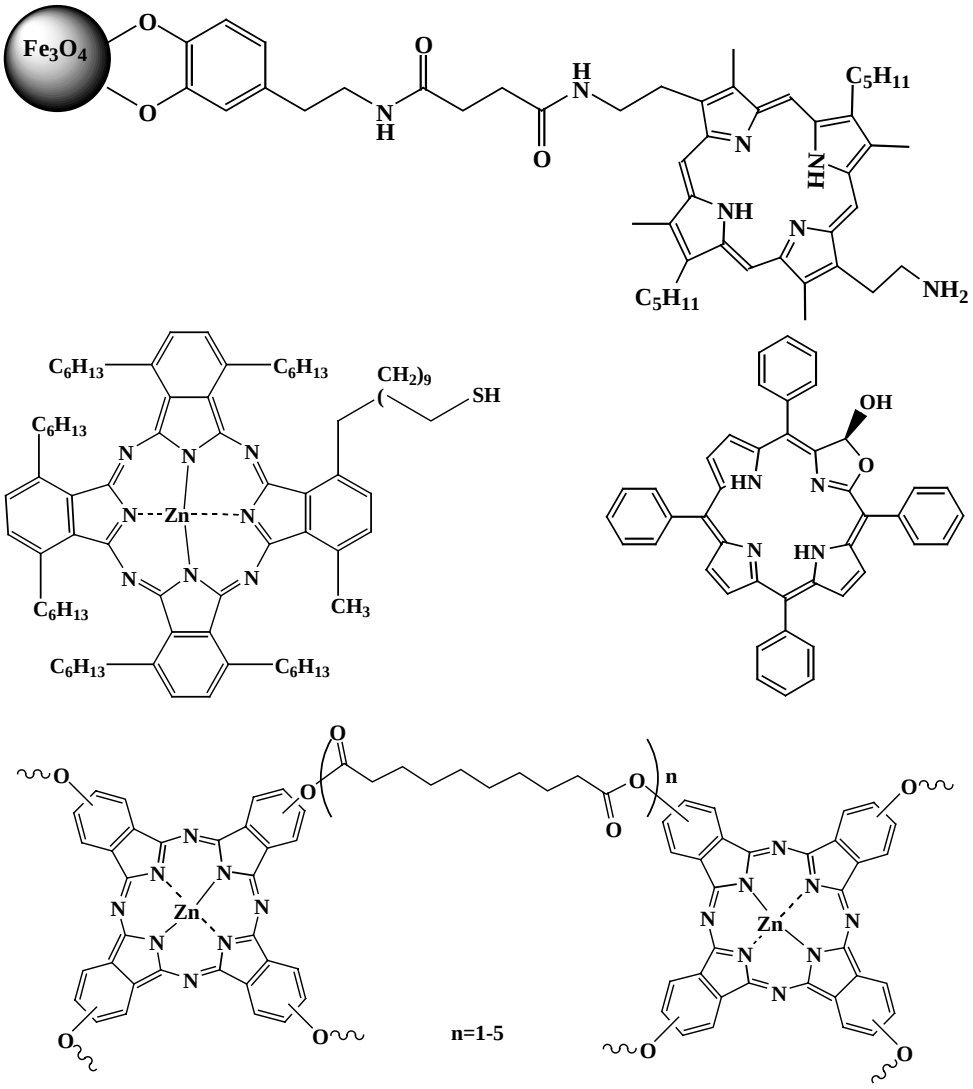

Figure 3.1: Structures of various porphyrinoids used in nanoparticle formation (Fe_3O_4-porphyrin nanoparticle [4]; Zn-phthalocyanine with thiolalkyl linkage [5]; *meso*-tetraphenylporpholactol [6]; Zn-phthalocyanine copolymers [7].

various receptors, similar to transferrin [4]. Another possibility of cellular uptake could be non-specific endocytosis.

There are several reports on the attachment of porphyrinoids to nanoparticles [5,14-22] but a paucity of these or similar systems have been evaluated as potential photodynamic therapeutics (PDT). PDT agents or formulations should have a high affinity to cancer cells or tissues. The cellular uptake of 6 - 50 nm iron oxide nanoparticles decorated with porphyrins with has been reported [19]. The observation that these nanoparticle-porphyrin adducts (Figure 3.1) were taken up by HeLa cells and located in the cytoplasm rather than absorbed outside the cellular membrane was interpreted to be "consistent with the intracellular location of other soluble porphyrin derivatives that are used as PDT agents" [19], but this is likely an oversimplification. One of the inherent problems associated with the use of phthalocyanines as PDT agents is that these macrocycles have a high propensity for aggregation – especially in aqueous media. The aggregation of porphyrinoids significantly enhances the deactivation of the excited state via non-radiative internal conversion, and concomitant large decrease in the triplet lifetime. The resulting significant reduction of the triplet quantum yield dramatically reduces the efficiency of photosensitization by this pathway [23]. Coating phthalocyanines with surfactants decreases aggregation due to the micelle-like environment created, resulting in high photoactivity, but these systems are not stable and have poor specificities to cancer cells [23]. For this reason modifying the surface of particles, with poly(ethylene oxide), poly(ethylene glycols) or other agents can improve the distribution of these particles in vitro.

Attachment of Zn-Phthalocyanine bearing a C_{11} thiolalkyl tether (Figure 3.1) to 2-4 nm diameter gold nanoparticles associated with TOAB (tetraoctylammonium bromide)

results in a system that can produce singlet oxygen with 65% quantum yields [11,23]. In terms of PDT applications, the 695 nm absorption band of the phthalocyanine on these small nanoparticles is considered more suitable than shorter wavelength absorption bands because of the increased depth of skin penetration of [11,23]. Wu et al, have shown that Zn-phthalocyanine modified sebacic anhydride polymers (Figure 3.1) form ~166 nm nanoparticles when added to water [23]. These polymers hydrolyze over time in water to release the phthalocyanine, which was followed by an increase of the fluorescence spectral intensity over time [23].

The encapsulation of TPP, TCPP, pheophorbide-a and chlorin e_6 in nanoparticles composed of poly(D,L-lactic acid) as a formulation for treatment of age-related macular degeneration is also being explored. PDT using verteporfin or Visudyne®, the first approved PDT drug for use in ophthalmology, results in photothrombic activity on the choroidal neovascularization (CNV) [5]. This investigation found that compounds with more hydrophobic/lipophilic character such as TPP and pheophorbide-a were encapsulated more efficiently as well as exhibited greater vascular damage compared to less hydrophobic TCPP and chlorin e_6 [5]. This effect is due to the "limited water solubility" of the hydrophobic porphyrin.

Water-insoluble HPPH (2-devinyl-2-(1-hexyloxyethyl)pyropheophorbide) which is in phase I/II clinical trials was absorbed onto 30 nm diameter spherical silica-based nanoparticles [20]. These inorganic nanoparticle-porphyrin adducts are actively taken up by HeLa and UCI-107 cancer cells. HPPH were embedded inside the nanoparticle, and upon irradiation, the generation of singlet oxygen resulted in killing of these cancer cells [20]. Furthermore, chlorins such as *meso*-tetraphenylporpholactol (Figure 3.1) in nanoparticles prepared using PLGA (poly(lactic-*co*-glycolic acid) showed that the

excited state of the chromophoric nanoparticles are quenched. However upon internalization into the cell, the fluorescence is recovered presumably by the release of the porphyrin upon hydrolysis of the polymer. The disaggregated porphyrinoid compound can then be used as a PDT agent [18].

Unlike the aforementioned systems wherein the chromophores are attached to, or encapsulated into, inorganic and polymeric nanoparticles, the Drain group reported the means to create and stabilize nanoscaled aggregates of porphyrinoids [2]. For example, nanoparticles of hydrophobic porphyrins and their metal complexes are made by dissolving the dye into a minimal amount of a host solvent that is miscible with water. To this solution is added ca. 20 times the volume of water containing ca. 3% of a polyethylene glycol. Conversely nanoparticles of water-soluble porphyrins and their metal complexes can be made dissolving them in water with the PEG and adding the organic solvent. The size, stability and properties of these porphyrinic nanoparticles depends on a variety of factors including concentration, vigorousness of mixing and the complex array of intermolecular interactions between the solute, solvents and stabilizer. The photonic and catalytic properties of these nanoparticle systems arise from the component chromophores, yet are different from either the molecules or the bulk solid materials [24]. Preparations of these nanoparticle suspensions can be stable for a year without precipitation or substantial changes in particle size. But since these nanoparticles are self-organized by supramolecular chemistry, changes in the environment can result in disaggregation to yield the solvated component molecules or precipitation to yield amorphous solids.

We report herein that tetraarylporphyrins bearing four amphipathic motifs such as amino triethyleneglycol, lysine, and ethylenediamine (Por-PEG_4, Por-Lys_4, Por-EDA_4,

Figure 3.2) form stable 8 – 50 nm nanoscaled aggregates in cell culture media without the need for a PEG stabilizer. Fluorescence microscopy reveals that these nanoparticles are taken up by MDA-MB-231 breast cancer cells and that the nanoparticles slowly disaggregate with time. Additionally, the disaggregated porphyrinic material is partitioned from mother to daughter cells. Illumination of the cells containing non-aggregated chromophores with low power white light induces cell death, thus indicating that the amphipathic porphyrins are effective PDT agents even though the cells were treated with nano-aggregates of the dye.

3.2 Experimental Procedures

Materials

All chemicals were purchased from Sigma-Aldrich. Dulbecco's Modified Eagle Medium (DMEM), trypsin-EDTA and antimycotic for cell culture were obtained from GibcoBRL. Hanks' balanced salt solution was obtained from Cellgro (Mediatech). Bovine calf serum was obtained from HyClone. PBS (136 mM NaCl, 2.6 mM KCl, 1.4 mM KH_2PO_4, 4.2 mM Na_2HPO_4) was obtained from Invitrogen. The 13W fluorescent bulb was from Sanco. A Brightline hemacytometer (Sigma) was used.

Instrumentation

UV-vis spectra were collected on a Varian Bio3 spectrophotometer. Steady-state fluorescence spectra were taken of the porphyrin in methanol and in PBS, with excitation at the maximum UV-vis absorbance (Soret band), and recorded on a Fluorolog τ3, Jobin-SPEX Instruments S. A., Inc. All fluorescence spectra are corrected for instrument response. Dynamic light scattering (DLS) data was collected on Precision Detectors

PD2000DLS^{PLUS}. Atomic force microscopy measurements were obtained on a Veeco Digital Instrument (Molecular Imaging).

Atomic force microscopy

AFM measurements were performed on glass substrates, either uncleaned or ozone cleaned as specified. Measurements were obtained in either tapping or contact mode using silicon cantilevers. Images were analyzed and saved as jpeg file format.

Dynamic light scattering

DLS measurements were obtained from 10 μM porphyrin nanoparticle dispersions. Samples were run on Precision DLS detector in 1x1 mm cuvettes using the "solid particle" normalization (n=3) to determine nanoparticle size and distribution.

Tumor cell lines

Human breast cancer cell line, MDA-MB-231 was obtained from Dr. David Foster (Hunter College, NY). Cells were cultured in Dulbecco's modified Eagle medium (DMEM) supplemented with 10% bovine calf serum (BCS), and 1% antimycotic at 37°C in a humidified atmosphere containing 95% air and 5% carbon dioxide. Cells were maintained near confluence in Petri dishes and then subcultured every 4 days by dissociating with trypsin-EDTA solution. The immortalized cells were used between passages 10 and 20. 3Y1 rat fibroblasts, v-Src-transformed 3Y1 cells, and 3Y1 cells overexpressing c-Src were maintained in DMEM supplemented with 10% bovine calf serum (HyClone).

Cell culture

Typically for dosing with porphyrin nanoparticles, MDA-MB-231 cells were seeded in 60 x 15 mm cell culture plates at a density suitable for confluency exposures by 24 – 48 hours. For cell uptake assays, after the monolayer of cells became confluent the

cells were treated with the appropriate concentration of colloidal porphyrinic nanoparticles for 20 hours prior to the photodynamic experiments. Prior to light irradiation, the cells were first washed with either PBS buffer or DMEM four to five times, to remove any residual or unbound porphyrinic material (confirmed by fluorescence microscopy, which indicates no unbound porphyrin remains).

Porphyrins and nanoparticles

The porphyrins were prepared as previously described [25]. 2.4 – 3.7 mM stock solutions of the porphyrins were made by dissolving the porphyrin in methanol. An appropriate volume of this solution (8 µL to 15 µL) was diluted into 3 mL of the cell culture medium (ca. 10 µM, see below) to make the desired concentration for incubation with the breast cancer cells. The final concentration of methanol in the cell culture medium never exceeded 0.5%. Dilution of the amphipathic porphyrins into the cell culture medium results in nanoparticle formation.

Phototoxicity assays

After treating the cells with various concentrations of the porphyrin nanoparticles and varying light power, the viability of the cells were assayed were evaluated by trypan blue exclusion staining assay. Briefly, cells were harvested using trypsin-EDTA, and a 0.4% w/v trypan blue solution was added to the cells. Following 5 min room temperature incubation, cells that had taken up trypan blue were counted with a hemacytometer and considered as dead.

Western blot

MDA-MB-231 cells were treated with nanoparticles for 20 hours, rinsed and irradiated as described above. After a period of time appropriate for the given experiment, cells were washed with cold PBS twice before lysis using RIPA buffer (65

mM Tris-HCl, 1% IGEPAL, 0.25% Na-deoxycholate, 154 mM NaCl, 1 mM EDTA, 1 mM PMSF, 1 μg/mL aprotinin, leupeptin, and pepstatin each, 1 mM Na_3VO_4, and NaF). The cell lysates were rotated at 4 °C for 25 minutes and centrifuged at maximum speed for 10 minutes. After protein quantification, the supernatant were applied to a Western blot. Equal amounts of protein were adjusted into gel-loading buffer (50 mM Tris-HCl, pH 6.8, 100 mM dithiothreitol, 2% SDS, 0.1% bromophenol blue, 10% glycerol), and heated for 5 minutes at 100 °C prior to separation by SDS-polyacrylamide (4 – 20 %) gel electrophoresis. After transferring to nitrocellulose membrane (Osmonics), the membrane filters were blocked overnight at 4 °C with 5% non-fat dry milk in PBS with 0.05% Tween-20 (Bio-Rad). The nitrocellulose membrane was washed three times for 5 minutes in PBS -Tween-20 at room temperature, before incubation with PARP rabbit polyclonal antibody overnight at 4 °C. The membrane was washing three times for 10 minutes in PBS-Tween-20 at room temperature, followed by incubation in anti-rabbit PARP as a secondary antibody. The bands were visualized using an enhanced chemiluminescent detection system (Pierce Biotechnology). For loading comparison, actin was also probed. The steps are the same as above, except actin-rabbit was used as the primary antibody (incubated for one hour at room temperature) and anti-rabbit as the secondary antibody (incubated for one hour at room temperature). Pierce reagent was used as the detection system.

Fluorescence Microscopy

For all experiments, cells were cultured under identical conditions. Cells were plated onto coverslips in cell culture dishes. Porphyrin nanoparticles were added to the cultures to a final concentration of 10 μM. After incubation for 20 hours the cells were washed 4-5 times with PBS and fixed with a 4% paraformaldehyde solution for 15 min at

room temperature. The cells were then washed with PBS 3 times. The coverslips were mounted in Dako fluorescence mounting medium, and visualized using a Nikon Optiphot 2 fluorescence microscope, where images were captured as high quality JPEG and TIFF files. Fluorescence microscopy of cells treated with porphyrin nanoparticles used a 505-565 nm excitation band pass filter and emission was detected between 565-685 nm using a dichroic mirror. JPEG images captured using phase contrast light microscope were used for comparison with fluorescence images and also as a means to document cell morphology. For all experiments, fluorescence images were taken under identical microscopic conditions. Each fluorescent experiment was performed at least three times.

FLim program

FLim is a Java-based program for handling FLuorescence images of cells that have been tagged with some kind of fluorescence probe. It allows for the relative fluorescence intensity between images to be compared by assessing the red (R), green (G), and blue (B) vectors (intensities) of an area of pixels in one or more images. One of the basic functions that it performs is background subtraction. Relative intensities are computed using a pixel sampling method that uses the weighted average of the most intense pixels (based on the RGB values) within a specific range. The program checks statistical significance, and if these criteria are not met an "under sampled" error message indicates that not enough pixels were sampled. This can be solved by either reducing the pixels to sample, or adjusting the range. The distribution of intensities also shows which image has the areas with the most intense fluorescence. Another important point is that the program scans an entire image, rather than a selected region(s) of that image. This latter feature allows a large number of areas in an image – in this case a large number of cells – to be evaluated in a single process, thus eliminating user prejudices and generally

facilitating the comparison of a large number of cells, which lead to more accurate intensity calculations. This program and detailed instructions are available on the web for free at:http://casilab10.sci.ccny.cuny.edu/~nathan/projects/FLim/index.html

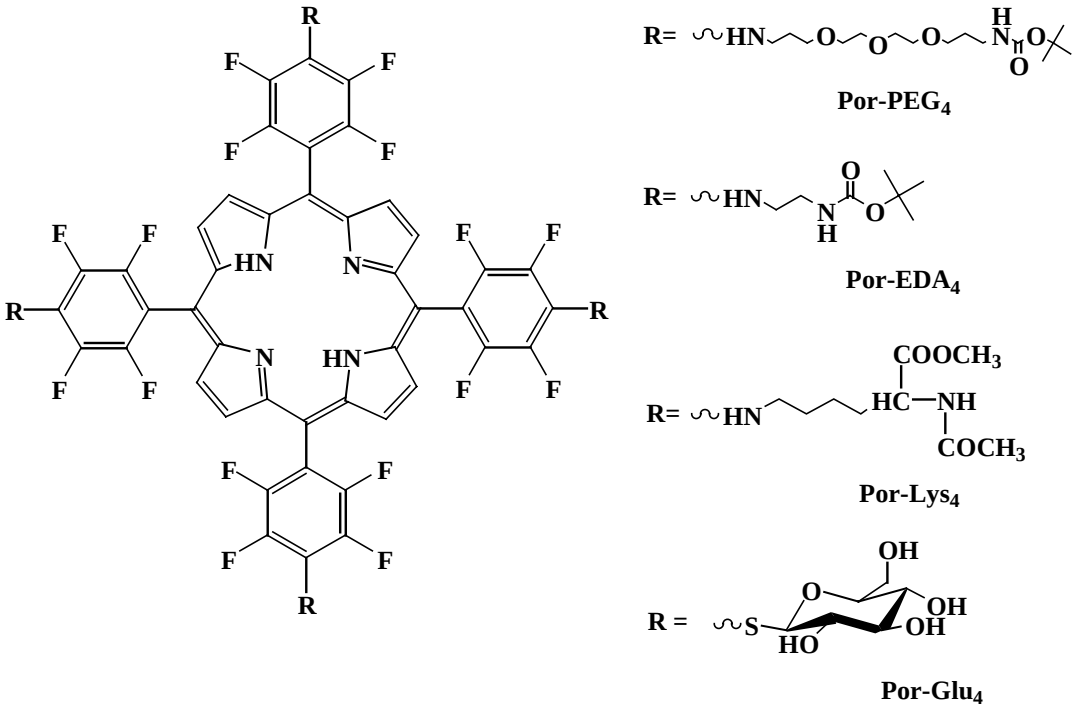

Figure 3.2: Structures of porphyrins used in colloidal nanoparticles preparation, Por-PEG_4, Por-EDA_4, and Por-Lys_4. The affinity and PDT activity of Por-Glu_4 is published [1] and used for comparison.

3.3 Results & Discussion

The microwave synthesis of protected porphyrin derivatives using $TPPF_{20}$ has been previously reported [25] and is briefly described. The synthesis uses 5,10,15,20-tetrakis(2,3,4,5,6-pentafluorophenyl)porphyrin ($TPPF_{20}$) since the 4-fluoro group is known to be reactive towards nucleophilic substitution reactions R-SH > $R-NH_2$ > R-OH [1,25,26]. The facile and efficient substitution of this group on the porphyrin can be exploited as an ideal platform for the rapid synthesis of a plethora of derivatives. The protected amphipathic groups on the porphyrins are used in this study (Por-Lys_4, Por-EDA_4, Por-PEG_4 and Por-Glu_4 see Figure 3.2). This study focuses on the uptake of these dyes into MDA-MB-231 cells and photodynamic induced cell death as indicators of the potential application of these derivatives as photodynamic agents.

The initial report on the methods used to formulate porphyrin into nanoparticles, involved the addition of water (guest solvent) to a porphyrin solution dissolved in a water-miscible organic solvent such as dimethylsulfoxide, tetrahydrofuran, and dimethyformamide (host solvent) while vigorously mixing [24]. A key feature of this procedure is the use of a stabilizer such as tri(ethylene glycol) monomethyl ether (PEG) to prevent eventual agglomeration of the porphyrin nanoparticles and precipitation (Scheme 3.1, Method 1). It was also shown that the presence of four PEGs covalently attached to the porphyrin macrocycle also allows the formation of stable nanoparticles without the need for an auxiliary PEG stabilizer (Scheme 3.1, Method 2) [2]. In the present case for the Por-EDA_4, Por-Lys_4, and the Por-PEG_4 the sizes obtained from the host/guest solvent Method 1 with 1.8 % tri(ethylene glycol) monomethyl ether ranged from 2 – 5 nm in diameter as determined by DLS.

Since many drug formulations use PEG or append PEG moieties onto the drug itself [27-35], it might be expected that porphyrin nanoparticles containing auxiliary PEGs may be taken up by cells. Although 2 – 5 nm diameter nanoparticles of the three

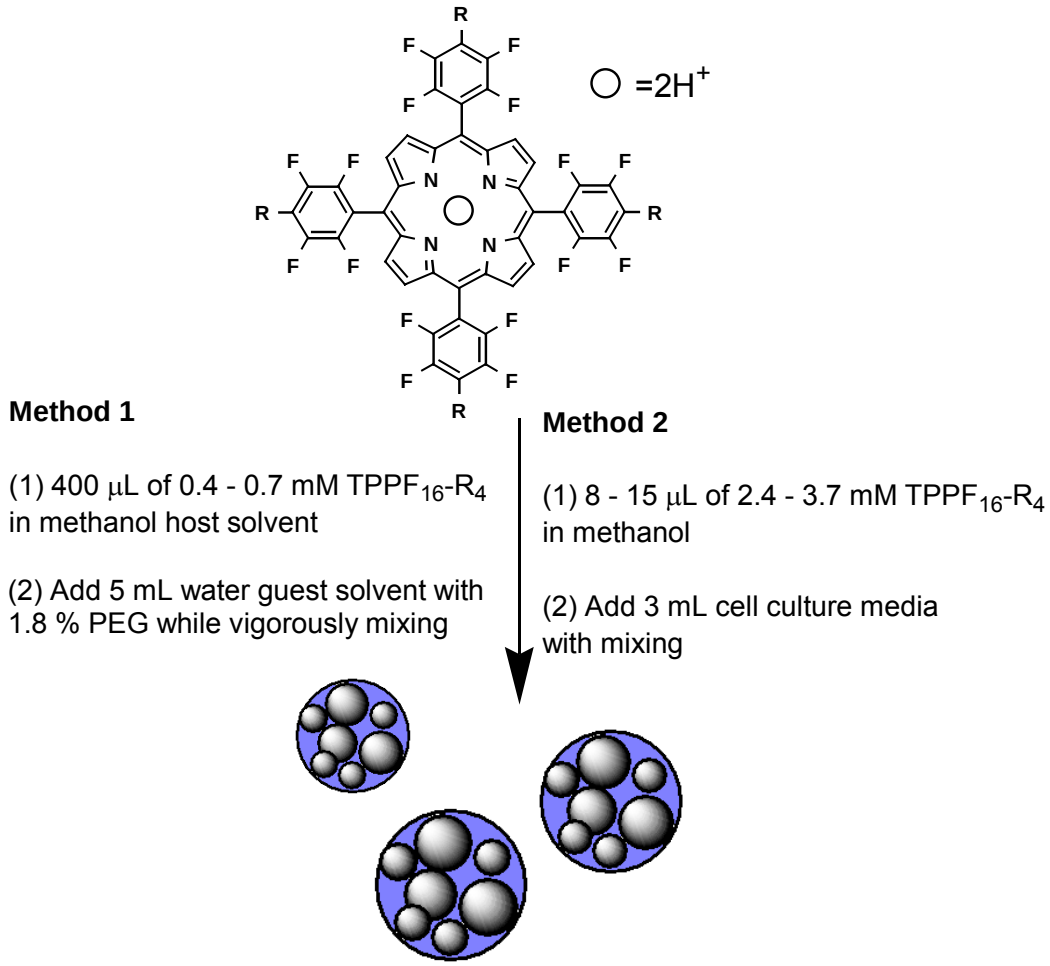

Scheme 3.1. There are two strategies to make aqueous solutions of porphyrin nanoparticle: (Method 1) uses an amphipathic polyethylene glycol as an auxiliary stabilizer in the guest solvent, and (Method 2) appends the amphipathic motif to the porphyrin macrocycle -- in each case mixing is necessary [2].

porphyrin derivatives made by method 1, have PEG, these proved to be ineffective as PDT agents under the conditions assayed (data not shown). Whether this is due to poor

uptake by the cells or the inability of the nanoparticles to disaggregate once inside the cell is not known.

Though the terminal amines on Por-PEG_4 and Por-EDA_4 are protected with hydrophilic t-boc groups and Por-Lsy_4 bears methyl protecting groups, these are amphipathic porphyrin derivatives. Thus when a methanol solution of any of the three porphyrin derivatives is added to the aqueous cell culture solution they tend to aggregate into surprisingly small 8 – 50 nm diameter nanoparticles depending on the specific derivative (Scheme 3.1 Method 2) and these three porphyrin derivatives do not precipitate under ambient conditions or at 4 °C. These nanoparticles are of a size that has been demonstrated to be appropriate for cell uptake [4,7,36]. This is consistent with the previous reports [2]. In this case the Lys, PEG and EDA moieties not only serve as amphipathic groups for nanoparticle formation, but poly-lysines, PEGs, and poly-amines have known affinities to cancer cells [28,29,37,38]. The remarkable ease of preparation of these nanoparticles in this aqueous environment, without the use of auxiliary stabilizers, is a distinct advantage of this system

Spectral Properties of Porphyrin Nanoparticles

The optical absorption spectra of the Por-Lys_4, Por-EDA_4, and Por-PEG_4 nanoparticle solutions in phosphate buffered saline (PBS) made by Method 2 were compared to those in methanol (Appendix, Figure 3A.2). The former solution is used because the nanoparticles behave in the same way as they do in the culture medium, Dulbecco's modified eagle medium (DMEM), but eliminates the absorption from the riboflavin and the phenol red present in DMEM. In the aqueous environment the Soret bands, the absorption maxima at ca. 430 nm, are red-shifted compared to the

corresponding porphyrin solutions in methanol. In addition, the observed broadening in PBS is due to the aggregation and formation of the nanoparticles. Briefly, aggregates can be classified as "J-" (monomer transition moments are parallel or edge-to-edge) or "H-" (monomer transition moments are perpendicular or face-to-face) types with resulting absorption band that are to the red or blue of the solvated molecule, respectively. There are several descriptions of the exciton theory that explains the relative energy shifts of the absorption bands of the aggregates [39].

The steady state emission spectra of both the porphyrin solutions and the nanoparticles were recorded (Appendix, Figure 3A.2). The solution spectra were taken at 1 μM in methanol and the nanoparticle spectra at 1 μM porphyrin. The porphyrins are quite fluorescent in methanol, while in the PBS solution there is a drastic decrease in fluorescence intensity. There are diverse reasons for the substantially reduced fluorescence in the nanoparticles such as: solvent polarity, energy transfer, shading, dynamics and the associated branching pathways of deactivation [40]. For therapeutic applications that rely on the formation of singlet dioxygen, any factor that results in a decrease in the porphyrin triplet quantum yield is deleterious. Also, the shading of porphyrin units within the nanoparticle from the irradiating light results in an inefficient use of the dye.

As mentioned above, 2 – 5 nm diameter nanoparticles of the three protected porphyrins (Por-PEG_4, Por-EDA_4, Por-Lys_4) formed by Method 1 were ineffective as PDT agents. The reasons for this inactivity include: (1) lack of adhesion to the cells, (2) lack of endocytosis, (3) lack of nanoparticle disaggregation once inside the cell. There may also be a time dependent disaggregation process once inside the cell.

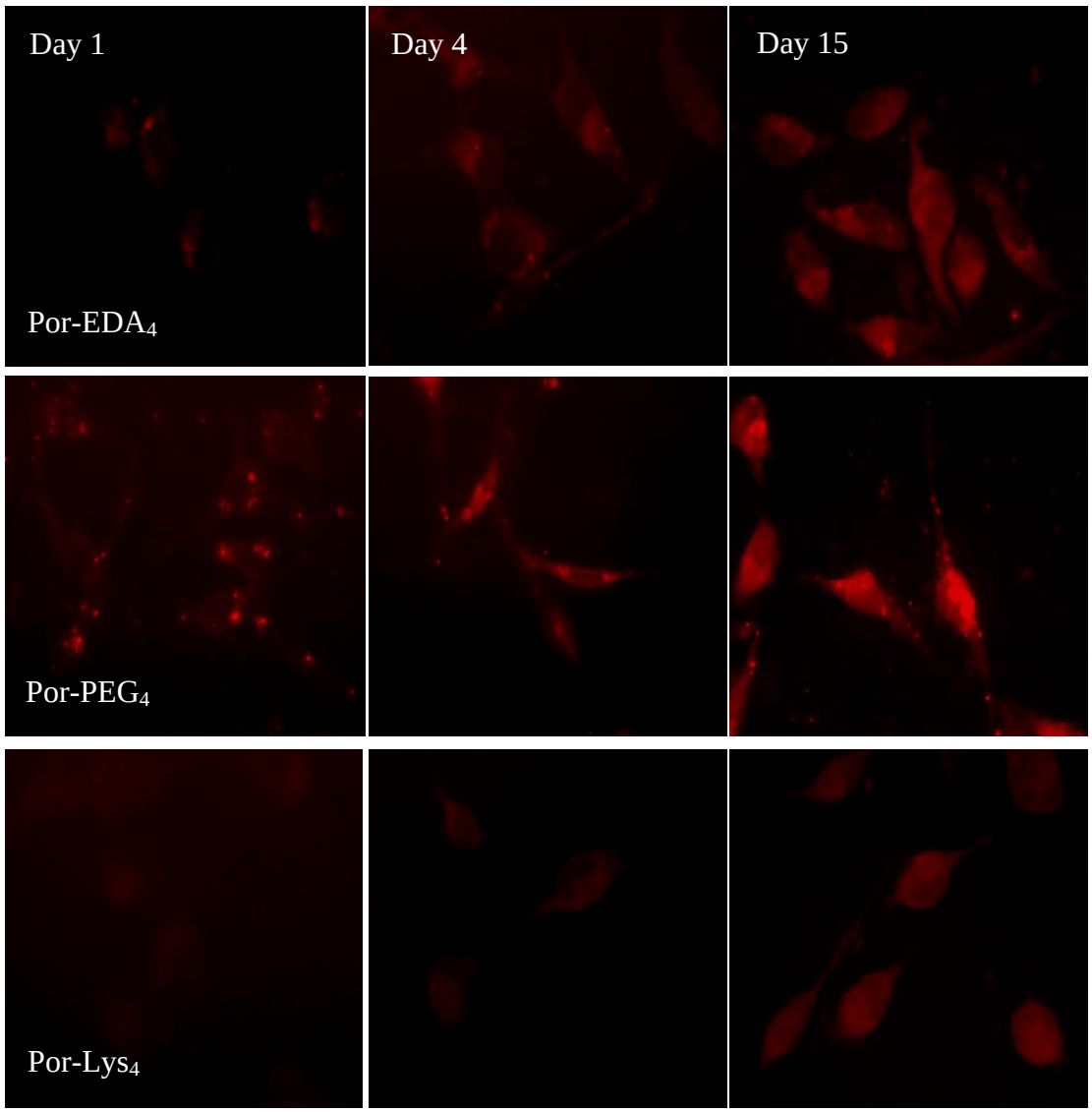

Figure 3.3: Fluorescence images showing the time-dependent increase in fluorescence intensity of the cells treated with nanoparticles of the three protected porphyrins formed by Method 2 at 10 μM. These are of fixed, dead cell post incubation and rinsing to remove all unbound porphyrinic material. Row 1, Por-EDA_4; Row 2, Por-PEG_4; Row 3, Por-Lys_4 (from left to right, day 1, 4 and 15, respectively). Magnification 60X.

Studies using 8 – 50 nm nanoparticles of the three protected porphyrins with no auxiliary PEG (Method 2) showed that they required days to disaggregate, as suggested by the increase in fluorescence intensity with time (Figure 3.3). These micrographs image the same slide(s) of the dead, fixed cells kept in the dark at room temperature, but taken on different days under the same microscopic conditions. Several factors influence

the rate of nanoparticle disaggregation: (1) elevated temperatures can weaken the intermolecular forces holding the nanoparticle together (cells are incubated at 37 ºC in 5% CO_2), (2) nanoparticle interactions with hydrophobic and amphipathic cellular components can induce disaggregation, (3) light irradiation may facilitate disaggregation process by the heat generated by deactivation of the excited state by internal conversion (vibration pathway).

The DLS size distributions of 10 μM solutions of the nanoparticles formed by Method 2 without auxiliary PEG (the same concentration used to treat the cells) at 22 ºC and 37 ºC was determined to be ~50 nm for the Por-Lys_4, ~8 nm for Por-EDA_4, and ~30 nm for Por-PEG_4 nanoparticles. The DLS data revealed very little change in the distribution of sizes (Appendix, Figure 3A.3 – 3A.5), which indicates no significant changes in particle size at the higher temperature. This conclusion is supported by the lack of significant changes in the half-widths of the Soret bands of these porphyrin nanoparticles between spectra taken at 22 ºC and 37 ºC.

An optimally packed 20 nm diameter porphyrin nanoparticle can contain greater than ~20,000 porphyrin units, but there are likely much fewer macrocycles in the nanoparticles [24]. The exact organization of the porphyrin units within these nanoparticles is unclear and will depend on a variety of factors arising from the intermolecular interactions between the porphyrin units and the solvents [24]. For the present three porphyrin derivatives, dipolar and hydrogen bonding likely play a key role in the organization of the macrocycles within the nanoparticles, e.g. the crystal structure of Por-EDA_4 reveals a network of hydrogen bonds [25].

AFM studies corroborate the DLS size distribution for the nanoparticles made by Method 2 were prepared on ozone-cleaned glass substrates. Briefly, 10 μM nanoparticle

solutions were drop-cast onto ozone-cleaned glass substrate and allowed to air-dry before scanning and results in distributions consistent with the DLS experiments (Appendix, Figure 3A.3 – 3A.5). The porphyrin nanoparticles remain suspended in an aqueous environment when they are incubated with the cancer cell cultures.

Nanoparticles Selectivity of Cellular Uptake

To determine if these particular porphyrin nanoparticles will be relevant agents for the inactivation of cancer cells by PDT, in vitro studies used MDA-MB-231, which is a well known and representative cancer cell line for mammary adenocarcinoma. The cellular uptake of the colloidal porphyrinic nanoparticles was evaluated by fluorescence microscopy. Our working hypothesis is that the mode of entry of the nanoparticles into cells is via endocytosis [3,4,6-8,36,41-43]. Porphyrin nanoparticles at a low concentration of 10 μM were incubated with these cells for 20 hours. After washing off the unbound materials from the cells and fixed to glass slide, fluorescence images of the cells were taken under identical conditions. For MDA-MB-231 cell treated with the nanoparticles made by Method 2 an increase in fluorescence intensity with time is observed (Figure 3.4). Nevertheless, the disaggregation in the cells is slow. A possible means to accelerate the break-up the nanoparticles uses light irradiation and the heat generated by the porphyrin relaxation to the ground state by vibrational processes.

The micrographs clearly show that the nanoparticles made by Method 2 bind to MDA-MB-231 breast cancer cells, but these cells appear to take up more of the protected Por-Lys_4 nanoparticles than protected Por-PEG_4 or Por-EDA_4 nanoparticles (Figure 3.4). A primary characteristic of cancer cells is the increased metabolism of nutrients and substances present in the culture media. Thus nanoparticle uptake most likely can be

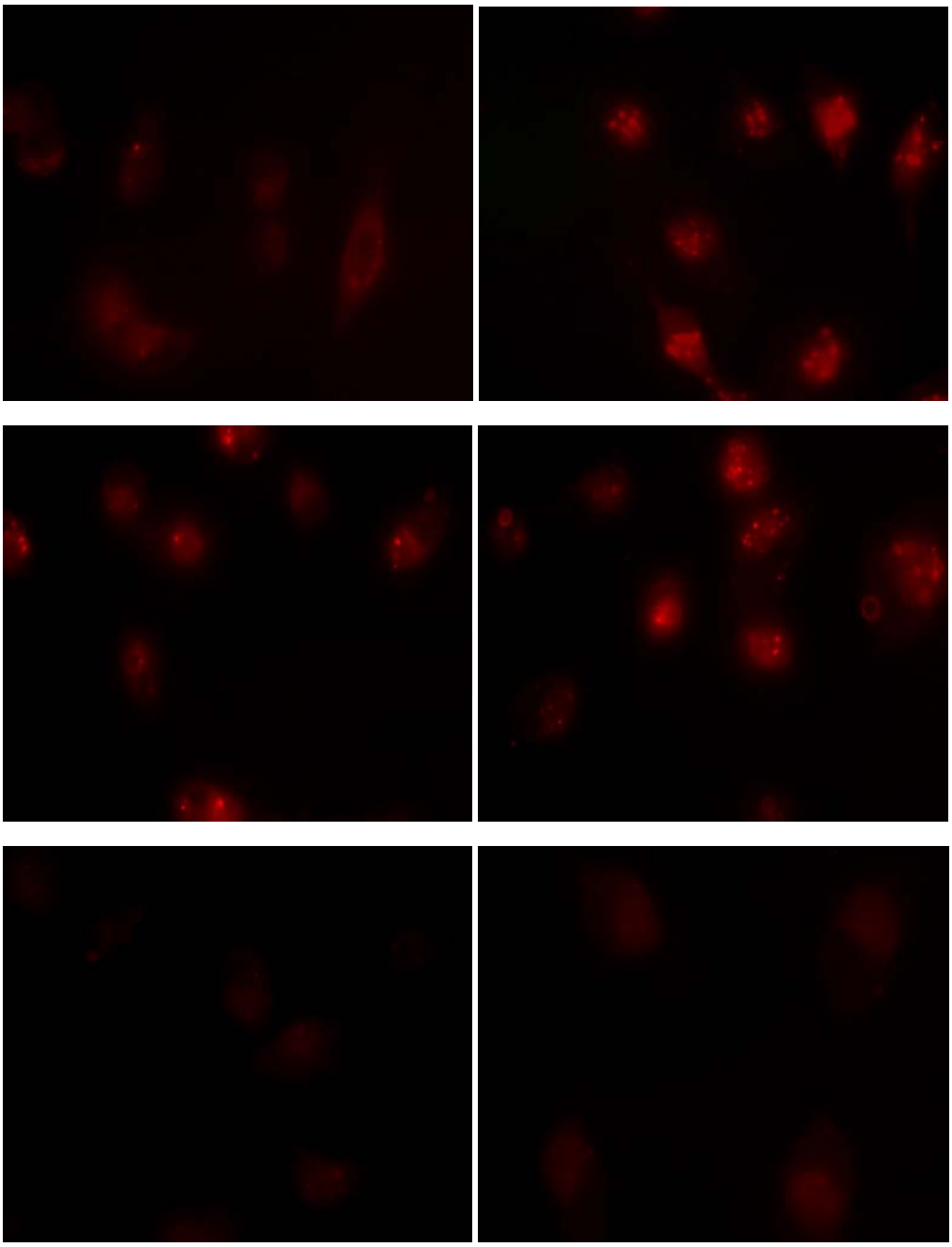

Figure 3.4: Fluorescence microscopy showing the difference between disaggregation in the dark (left column), and light-aided disaggregation (right column). Cells were treated with 10 μM Por-Lys_4 (top), Por-PEG_4 (middle) and Por-EDA_4 (bottom) nanoparticles made by Method 2 for 20 hr, and washed. The samples on the right were then irradiated for 10 minutes (4.13 kJ/m^2) with white light. The cells were then fixed with a 4% paraformaldehyde solution. Fluorescence images were taken immediately after fixing the cells under identical conditions. 60X magnification. Micrographs are not enhanced.

attributed to the increased active transport [1]. Figure 3.4 shows that the rate of

fluorescence intensity increases when the porphyrin nanoparticle containing cells are treated with 4.13 kJ m^{-2} white light. For the cells with Por-Lys_4 and Por-PEG_4 nanoparticles, there is ca. 3 fold increase in fluorescence intensity following a brief exposure to white light, whereas for the Por-EDA_4, there is less than a 1.5 fold increase. (Computed using the FLim program, see Experimental Procedures).

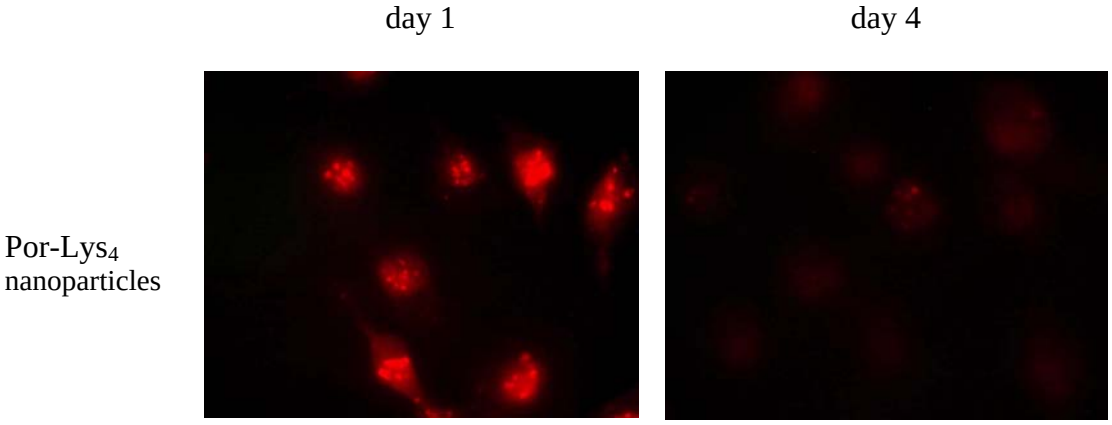

Figure 3.5: Fluorescence microscopy showing initial uptake and distribution of Por-Lys_4 nanoparticles made by Method 2 in MDA-MB-231 cells. Two sets of cells were treated with 10 μM Por-Lys_4 nanoparticles for 20 hr, washed, and then irradiated for 10 minutes (4.13 kJ m^{-2}) with white light. One set was fixed with a 4% paraformaldehyde solution and imaged. The second set of cells was allowed to culture for four days before being fixed and imaged to show the distribution of the porphyrins from the nanoparticles to the third generation of daughter cells. Fluorescence images were taken under identical conditions. 60X magnification. The contrast of micrographs is enhanced by a scale factor of 1.7 using FLim.

The nanoparticles made by Method 2 may be taken up into the cells or merely adhere onto to the cell surfaces. To distinguish between these two possibilities, fluorescence micrographs were taken after allowing cell growth for three generations (Figure 3.5). Porphyrin fluorescence, albeit diminished, was observed in the cells after each cell cycle. This is a strong indication that as cellular division takes place, the porphyrinic material is distributed or passed on to the daughter cells. In this experiment

the cells are exposed to a low dose (4.13 kJ/m^2) of white light to accelerate nanoparticle disaggregation. The effect of the low dose light on cell viability is negligible; see discussion on the PDT activity of these nanoparticles. Therefore, with a starting concentration of 10 μM and assuming a maximum of 90 % uptake, there is approximately 2.25 μM porphyrin nanoparticles available after two cell generations and 1.125 μM after three generations. Though a lower concentration of the porphyrin is available for PDT after the third generation, these concentrations are within an acceptable range for modest effectiveness [1].

To assess whether these nanoparticles were selectively taken up by cancer cells and not taken up into normal cells, three cell lines varying in the expression of tyrosine kinase (TK) were used. Overexpression of TK due to mutations has been implicated in numerous cancers. 3Y1 cells are normal non-transformed rat fibroblast, however overexpression of c-Src leads to partial transformation when treated with "tumor-promoting phorbal esters" [44,45]. Overexpressed v-Src leads to fully transformed 3Y1 cells [44]. Therefore, using non-transformed (3Y1), partially transformed ($3Y1^{c\text{-}Src}$) and fully transformed ($3Y1^{v\text{-}Src}$) cells to gauge the binding of nanoparticles, in particular Por-Lys_4 and Por-EDA_4, (Por-PEG_4 was not used in these experiments because it is taken up the least) will determine the specificity of towards cancerous versus normal cell types.

After incubation for 20 hours with the Por-EDA_4 or Por-Lys_4 nanoparticles made by method 2, rinsing, and fixing onto slides, the 3Y1, $3Y1^{c\text{-}Src}$ and $3Y1^{v\text{-}Src}$ cells were evaluated by fluorescence microscopy (Figure 3.6). The observed fluorescence intensity is considered proportional to the amount of porphyrin taken up by these cells. This relative intensity is computed using FLim program. These results show that Por-Lys_4 nanoparticles are taken up by the fully transformed $3Y1^{v\text{-}Src}$ cells more than the Por-

EDA_4 nanoparticles. Notably, neither of the nanoparticles is absorbed by normal 3Y1 rat fibroblasts, as indicated by the near zero fluorescence observed in the micrographs. The partially transformed $3Y1^{c\text{-}Src}$ cells show an intermediate uptake for the nanoparticles, which indicates that these porphyrin nanoparticles are selective toward cancerous cells over normal cells. Figure 3.6 illustrates that the uptake of Por-Lys_4 nanoparticles increases in the order of 3Y1 (non-transformed) < $3Y1^{c\text{-}Src}$ (partially transformed) < $3Y1^{v\text{-}Src}$ (fully transformed) rat fibroblast. The relative affinities of Por-Lys_4 to 3Y1, $3Y1^{c\text{-}Src}$ and $3Y1^{v\text{-}Src}$, determined by fluorescence intensities, are 1:25:33. Similar results were obtained for the Por-EDA_4 nanoparticles, where the relative fluorescence intensities are 1:20:21 for 3Y1, $3Y1^{c\text{-}Src}$ and $3Y1^{v\text{-}Src}$.

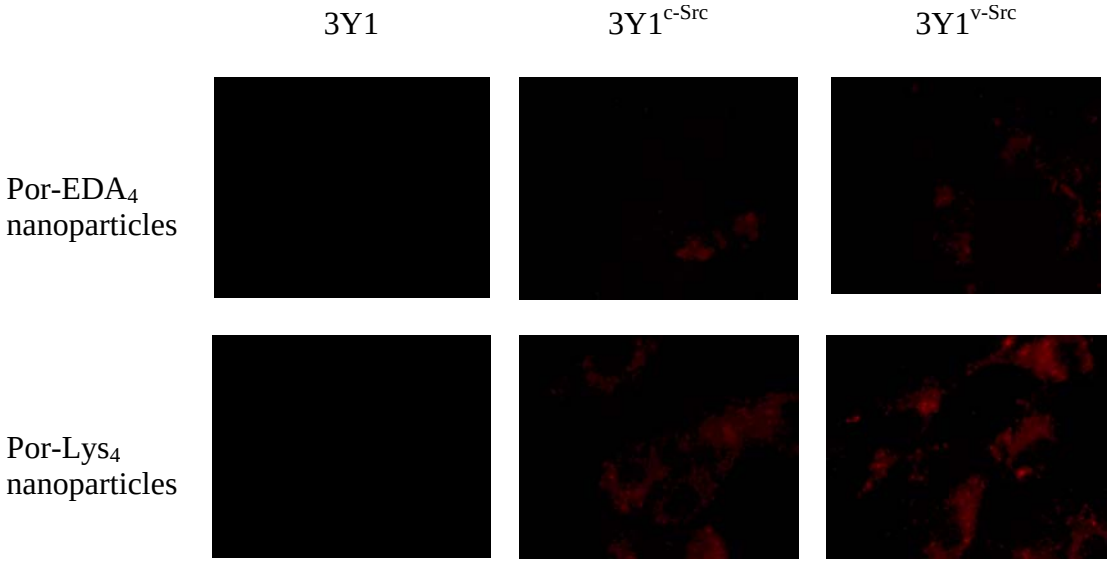

Figure 3.6: Fluorescence microscopy showing the uptake of porphyrin nanoparticles in 3Y1 cell lines. Cells were treated with 10 μM Por-Lys_4 and Por-EDA_4 nanoparticles for 20 hr, washed, then irradiated for a brief time with white light then finally fixed with a 4% paraformaldehyde solution. Fluorescence images were taken under identical conditions immediately after fixing. 60X magnification. The contrast of micrographs is enhanced by a scale factor of six using FLim. The relative fluorescence intensities of cells treated with Por-EDA_4 nanoparticles is 1:20:21, whereas for Por-Lys_4 1:25:33 for the 3Y1, $3Y1^{c\text{-}Src}$, $3Y1^{v\text{-}Src}$, respectively.

Photocytotoxicity

The evaluation of the effectiveness of photodynamicly rendering the cells non-viable by the Por-Lys_4, Por-PEG_4, and Por-EDA_4 nanoparticles included several assays. MDA-MB-231 cells were incubated with 10 μM porphyrin nanoparticles for 20 hours, the growth media was then exchanged to remove unbound nanoparticles, followed by a low light dose (0.69 mW/cm^2 white light for 10 min) to disperse the nanoparticles and finally the "active" light dose (0.69 mW/cm^2 for 20 min) to irradiate the cancer cells (total of 30 min, 12.4 kJ m^{-2}). The results from these studies indicate that just after irradiation ca. 27% of the cells have undergone necrosis for all three systems, but this increase to ca. 80% over the next over 24 hrs (Figures 3.7, 3.8, 3.9). There is less than 20 % cell death associated with dark toxicity over 24 hrs for all porphyrin nanoparticles tested. These results are similar with those of a water-soluble tetra glucose derivative (Por-Glu_4) where initial cell necrosis is 20-30% and this increases to near 100% over the next 24 hours [1]. The maximum cell necrosis obtained from using 10 μM nanoparticles was ~ 80 %, which likely indicates that a population of the porphyrins remains aggregated under these conditions; therefore are ineffective as photosensitizes.

To test the assumption that some of the porphyrin remains aggregated, a second assay was carried out wherein the cells were allowed to grow for two generations following the initial low light dose to initiate the disaggregation the porphyrin nanoparticles (see Figure 3.5). After the cancer cells are irradiated with the "active" light dose (20 minutes). The results of the control experiments are similar. In this case 90 – 98 % of the cells treated with the Por-Lys_4 nanoparticles were necrotic after 24 hours (Figure 3.10). This indicates that once the porphyrins are freed from the nanoparticle they are effective PDT agents.

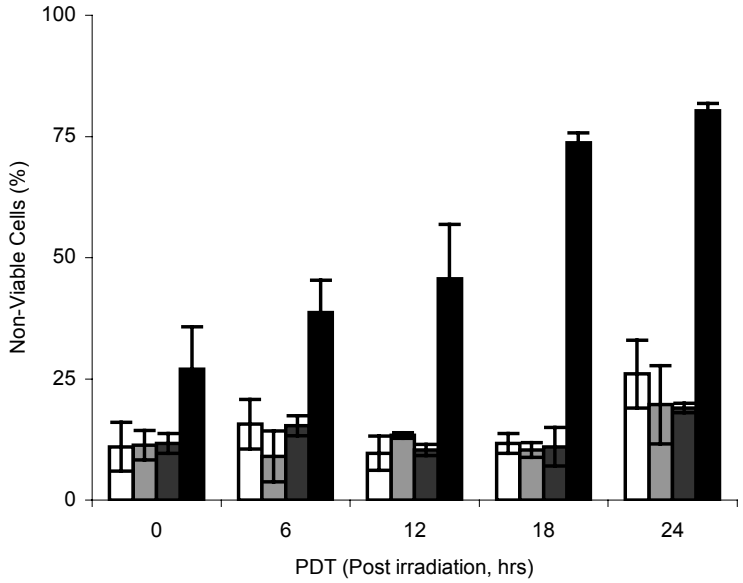

Figure 3.7: Photocytotoxicity of Por-Lys$_4$ nanoparticles on human mammary adenocarcinoma MDA-MB-231 cells. Nonviable cells were counted with hemacytometer after staining with 0.4% w/v trypan blue. Cells were treated with 10 μM Por-Lys$_4$ nanoparticles for 20 hr, washed by exchanging the growth medium, and irradiated under a white 13 W fluorescent light (0.69 mW cm^{-2} for 30 min; 12.4 kJ m^{-2}). The nonviable cells were counted at various lengths of time after photodynamic irradiation. Control experiments in the absence of nanoparticles with (□) or without (■) light show that MDA-MB-231 cells remain viable. Por-Lys$_4$ nanoparticles in the absence (■, dark control) or presence (■) of light. Each data point represents an average ± 1 SD from at least three independent measurements.

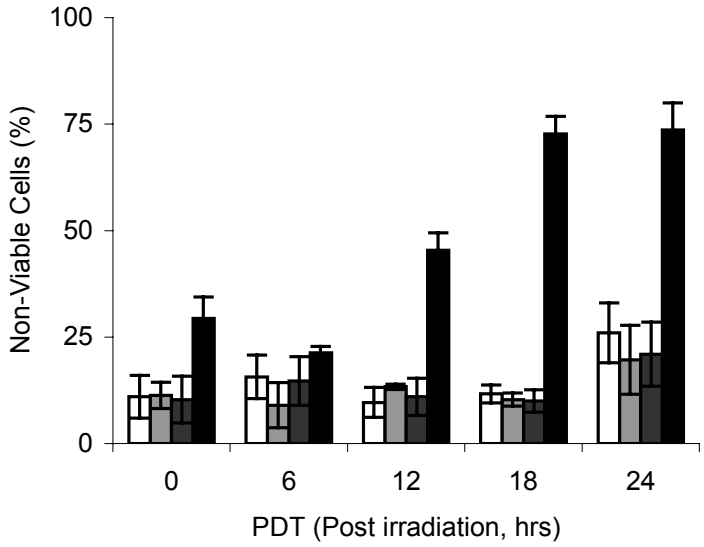

Figure 3.8: Photocytotoxicity of Por-EDA_4 nanoparticles on human mammary adenocarcinoma MDA-MB-231 cells. Nonviable cells were counted with hemacytometer after staining with 0.4% w/v trypan blue. Cells were treated with 10 μM Por-EDA_4 nanoparticles for 20 hr, washed by exchanging the growth medium, and irradiated under a white 13 W fluorescent light (0.69 mW cm^{-2} for 30 min; 12.4 kJ m^{-2}). The nonviable cells were counted at various intervals of time after photodynamic irradiation. Control experiments in the absence of nanoparticles with (□) or without (■) light show that MDA-MB-231 cells remain viable. Por-EDA_4 nanoparticles in the absence (■, dark control) or presence (■) of light. Each data point represents an average ± 1 SD from at least three independent measurements.

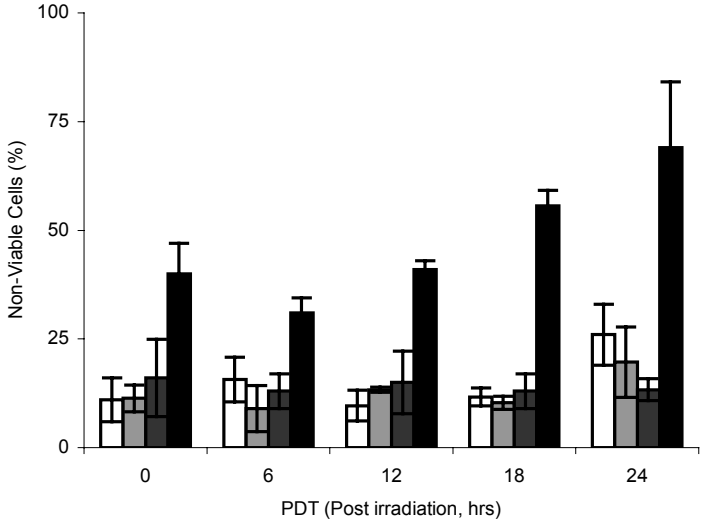

Figure 3.9: Photocytotoxicity of Por-PEG_4 nanoparticles on human mammary adenocarcinoma MDA-MB-231 cells. Nonviable cells were counted with hemacytometer after staining with 0.4% w/v trypan blue. Cells were treated with 10 μM Por-PEG_4 nanoparticles for 20 hr, washed by exchanging the growth medium, and irradiated under a white 13 W fluorescent light (0.69 mW cm^{-2} for 30 min; 12.4 kJ m^{-2}). The nonviable cells were counted at various lengths of time after photodynamic irradiation. Control experiments in the absence of nanoparticles with (□) or without (■) light show that MDA-MB-231 cells remain viable. Por-PEG_4 nanoparticles in the absence (■, dark control) or presence (■) of light. Each data point represents an average ± 1 SD from at least three independent measurements.

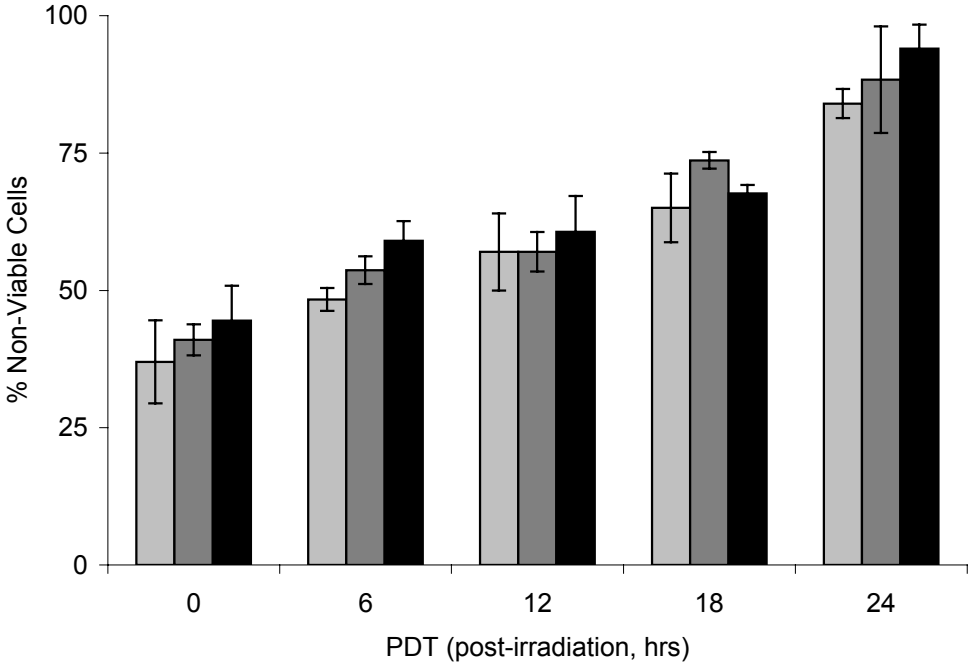

Figure 3.10: Photocytotoxicity of Por-EDA_4 (▒), Por-PEG_4 (■) and Por-Lys_4 (■) nanoparticles on MDA-MB-231 breast cancer cells. MDA-MB-231 cells were treated with 10 μM porphyrin nanoparticles for 20 hr, washed by exchanging the growth medium, and irradiated under a white 13 W fluorescent light (0.69 mW cm^{-2} for 10 min; 4.13 kJ m^{-2}). Cells were allowed to grow for two cell generations over 48 hours. Cells were then irradiated under a white 13 W fluorescent light (0.69 mW cm^{-2} for 20 min; 8.28 kJ m^{-2}). The nonviable cells were counted with hemacytometer after staining with 0.4% w/v trypan blue at various time intervals following photodynamic irradiation. Each data point represents an average ± 1 SD from at least three independent measurements. Control experiments with no light or no porphyrin never resulted in less than 20% necrotic cells.

Porphyrin nanoparticles	% necrotic after 24 hr	% necrotic after 48 hr	% necrotic after 72 hr
Por-EDA_4[a]	24.33 ±2.31	19.67±4.16	36±5.46
Por-EDA_4[b]	37±7.55	55.50±3.54	68.50±14.85
Por-PEG_4[a]	19±4.36	31.67±2.89	25.50±0.71
Por-PEG_4[b]	41±2.83	46±1.41	66.50±9.19
Por-Lys_4[a]	28.50±4.95	25±9.54	37±5.66
Por-Lys_4[b]	44.50±6.36	49.50±10.61	73±8.49
Por-Glu_4[a]	24.50±0.71	30±7.94	38.67±2.31
Por-Glu_4[b]	38.67±15.31	64±18.38	71±16.97

[a] single irradiation with no secondary irradiation and % cell necrosis counted after the specified time. [b] second irradiation occurs after the specified time and % cell death counted immediately

Table 3.1: Photocytotoxicity of colloidal Por-EDA4, Por-PEG4, Por-Lys4 nanoparticles compared to Por-Glu4 on MDA-MB-231 cells. (a) Cells were treated with 10 mM porphyrin nanoparticles for 20 hr, washed by exchanging the growth medium, and irradiated under a white 13 W fluorescent light (0.69 mW cm-2 for 10 min; 4.13 kJ m-2) and counted after the specified time. A second set of cells (b) was allowed to grow for one, two, and three cell generations (doubling time is ca. 24 hours) after the same initial irradiation as used experiment (a). After the specified time interval, the cells were then irradiated a second time (0.69 mW cm-2 for 20 min; 8.28 kJ m-2). The nonviable cells were counted immediately after white light irradiation. Nonviable cells were counted with hemacytometer after staining with 0.4% w/v trypan blue. Each data point represents an average ± 1 SD from at least three independent measurements. The cell density, as an indicator of the ability of the cells to propagate, increases as expected.

Figures 3.7 – 3.9 reveal that there are small differences in the PDT assays that parallel the fluorescence microscopy, e.g. the percentage of necrotic cells after 24 hours Por-Lys_4 > Por-EDA_4 > Por-PEG_4 mirrors the relative fluorescence intensities. Although in addition to this, the bio-distribution or localization of these porphyrins and nanoparticles to cellular structures such as organelles may be different.

Figure 3.10 and Table 3.1 compares the activities of the porphyrin nanoparticle over the course of three generations. After treating the cells with nanoparticles of one of the three porphyrins for 20 hours, rinsing, and irradiating with 10 minutes of white light, ca. 25 % cell are not viable even after two more generations (Table 3.1). Figure 10 shows that the porphyrins are divided between mother and daughter cells from one generation to the next. Despite the reduced concentrations, the disaggregation of the nanoparticles to yield the free porphyrins as the cells grow and divide make the chromophores more effective at causing immediate necrosis after a second dose of light. Though the data in Table 3.1 were obtained immediately after a second irradiation, it is likely that the percentage of necrotic cells will increase over the course of 24 hours after the light dosage as shown above for these porphyrins (Figure 3.7 – 3.9) and for the Por-Glu_4 [1]. Therefore these results indicate that the second and third generation of cells may be effectively treated with the initial dose of porphyrin.

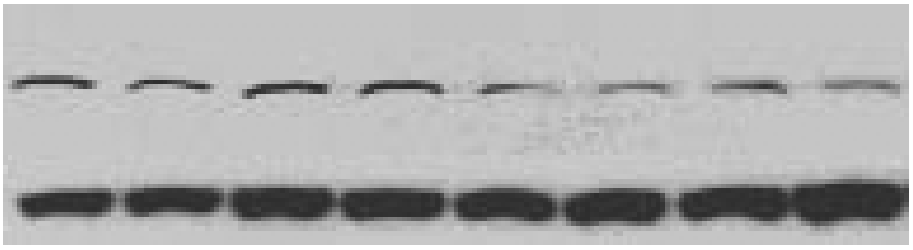

Figure 3.11: Western blot analysis specifically probing for cleaved poly(ADP-ribose) polymerase (PARP) in MDA-MB-231 cells as an indication of apoptosis. MDA-MB-231 cells were treated with 10 μM Por-EDA_4, Por-PEG_4 or Por-Lys_4 porphyrin nanoparticles as well as Por-Glu_4 for 20 hours, washed by exchanging the growth medium, and irradiated under a 13 W fluorescent light (0.69 mW cm^{-2} for 10 min; 4.13 kJ m^{-2}). Cells were allowed to grow for two cell generations during 48 hours. Cells were then irradiated at 0.69 mW cm^{-2} for 20 min; 8.28 kJ m^{-2}. Cells were collected six hours after irradiation. The supernatant of the cell lysates were applied to western blot to detect PARP cleavage. Samples were run in duplicates. Lane 1,2: with irradiation and Por-Glu_4; Lane 3,4: with irradiation and Por-Lys_4; Lane 5,6: with irradiation and Por-PEG_4; Lane 7,8: Por-EDA_4 and irradiation. The top band is the PARP cleavage product and the bottom band actin control.

The photocytotoxicity of all three types of nanoparticles initially leads to ca. 25% necrosis and this increases to greater than 80 % after a 24-hour period. In all the cases described above, our hypothesis is that the continued mortality of the cells following light irradiation is due to the induction of apoptosis. One of the hallmarks of apoptosis is the proteolytic cleavage of full length poly(ADP-ribose) polymerase (PARP) [46-50]. PARP, which is a DNA repair enzyme [47], is cleaved during this process from a 113 kDa functional form into 89 kDa and 24 kDa polypeptide fragments. PARP is one target of activated caspase and is a common marker of executioner caspases such as caspase-3 in cell death by apoptosis [49]. Western blot assays of PARP cleavage indicates that apoptosis was induced in MDA-MB-231 cells by photodynamic treatment with Por-EDA_4, Por-PEG_4 and Por-Lys_4 porphyrin nanoparticles as well as Por-Glu_4 (Figure 3.11). This assay, which specifically probes for cleaved PARP rather than total PARP, reveals

that the 89-kDa band is present for each cell culture treated with both nanoparticles and light irradiation. These observations are consistent with previous reports on PDT and PARP induction [48,49,51]. (See appendix for controls, Figure 3A.1)

As shown in Figure 3.10, a low light dose to break up the nanoparticles followed

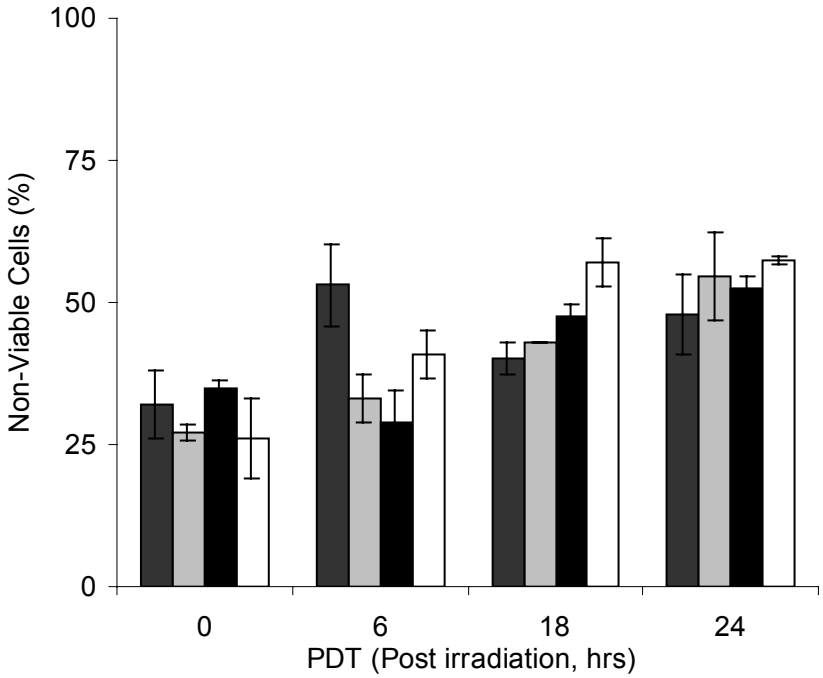

Figure 3.12: Photocytotoxicity of Por-EDA_4 (▒), Por-PEG_4 (■), Por-Lys_4 (■) and Por-Glu_4 (□) nanoparticles on MDA-MB-231 breast cancer cells. MDA-MB-231 cells were treated with 1 μM porphyrin nanoparticles for 20 hr, washed by exchanging the growth medium, and irradiated under a white 13 W fluorescent light (0.69 mW cm^{-2} for 30 min; 12.41 kJ m^{-2}). The nonviable cells were counted with hemacytometer after staining with 0.4% w/v trypan blue at various time intervals following photodynamic irradiation. Each data point represents an average ± 1 SD from at least three independent measurements.

by cell growth for 2 generations and then a secondary irradiation results in efficient cell death. The concentration at the final stage is at most 1.25 μM. This led us to ascertain if the incubation of the breast cancer cell line with 1 μM was as effective as 10 μM. Figure

3.12 shows a PDT assay using 1 μM porphyrin nanoparticles of the three derivatives and the standard Por-Glu_4 and one-30 min irradiation. The results show a maximum of ca. 50% cell death achieved under these conditions. Note that increased time and a secondary irradiation should significantly improve these results as illustrated above. In addition to free, solvated porphyrins, a population is likely aggregated at 1 μM concentrations (UV-visible spectra are less broad, DLS at this low concentration could not be obtained).

3.4 Conclusion

$TPPF_{16}$ bearing four protected but amphiphilic PEG, Lys, and EDA groups, which are known to direct small molecules to cancer cells, can be made into nanoparticles without auxiliary stabilizers to prevent agglomeration and precipitation. Fluorescence micrographs of MDA-MB-231 human mammary carcinoma cells incubated with these nanoparticles show an increase in fluorescence intensity with time indicating the slow disaggregation of the nanoparticle to the constituent dyes. Significantly, the fact that normal 3Y1 rat fibroblasts do not take up the porphyrin nanoparticles and the fully transformed $3Y1^{v\text{-}Src}$ cells do take them up indicates a degree of discrimination between healthy and malignant cells. Photodynamically induced cell death using these porphyrin nanoparticles depends on several factors including (1) the irradiating light dose, (2) the degree of disaggregation of the nanoparticles inside the cancer cells. Disaggregation of the porphyrin nanoparticles to release the photodynamically active macrocycle occurs slowly over the course of several cell cycles, but the rate of disaggregation of the porphyrin nanoparticles can be accelerated by light [52,53]. The approach that uses two doses of light irradiation yields greater than 85% cell death for all nanoparticles tested

and may be applicable to other photodynamic therapeutic protocols to enhance the efficacy of treatment. The fate of the protecting groups once inside the cell, i.e. are they cleaved or remain on the porphyrin, is not known at this time and will be the subject of future investigations.

There are several other points that should be noted: (1) the tetraglucose porphyrin aggregates above ca. 5 μM in PBS, thus a double light dose or waiting an extra amount of time to disaggregate these improves the PDT results. Also, lower concentrations, which are not as aggregated can, elicit a better PDT response. (2) Aggregates of hydrophobic porphyrins do not disaggregate either with a short irradiation or with time in these cells, so are ineffective as PDT agents. Thus there is a careful balance in the stability of the aggregated nanoparticle in PBS (i.e. intermolecular interactions) versus the disaggregation in the cell. (3) Lastly, this strategy does not use an inorganic core which may have long term toxicity issues as these are not biodegradable.

3.5 References

(1) Chen, X.; Hui, L.; Foster, D. A.; Drain, C. M. *Biochem.* **2004**, *43*, 10918-10929.

(2) Gong, X.; Milic, T.; Xu, C.; Batteas, J. D.; Drain, C. M. *J. Am. Chem. Soc.* **2002**, *124*, 14290-14291.

(3) Kneuer, C.; Sameti, M.; Haltner, E. G.; Schiestel, T.; Schirra, H.; Schmidt, H.; Lehr, C.-M. *Int. J. Pharm.* **2000**, *196*, 257-261.

(4) Chithrani, B. D.; Ghazani, A. A.; Chan, W. C. W. *Nano Lett.* **2006**, *6*, 662-668.

(5) Pegaz, B.; Debefve, E.; Borle, F.; Ballini, J.-P.; van de Bergh, H.; Konan-Kouakou, Y. N. *J. Photochem. Photobiol. B: Biol.* **2005**, *80*, 19-27.

(6) Hussain, S. M.; Hess, K. L.; Gearhart, J. M.; Geiss, K. T.; Schlager, J. J. *Toxicology in Vitro*

Thirteenth International Workshop on In Vitro Toxicology **2005**, *19*, 975-983.

(7) Popielarski, S. R.; Hu-Lieskovan, S.; French, S. W.; Triche, T. J.; Davis, M. E. *Bioconjugate Chem.* **2005**, *16*, 1071-1080.

(8) Cui, Z.; Mumper, R. J. *Bioconjugate Chem.* **2002**, *13*, 1319-1327.

(9) Berry, C. C.; Curtis, A. S. G. *J. Phys. D: Appl. Phys.* **2003**, *36*, R198-R206.

(10) Berry, C. C. *J. Mater. Chem.* **2005**, *15*, 543-547.

(11) Hone, D. C.; Walker, P. I.; Evans-Gowing, R.; FitzGerald, S.; Beeby, A.; Chambrier, I.; Cook, M. J.; Russell, D. A. *Langmuir* **2002**, *18*, 2985-2987.

(12) Mauzerall, D.; Drain, C. M. *Biophys. J.* **1992**, *63*, 1544-1555.

(13) Drain, C. M.; Mauzerall, D. *Biophys. J.* **1992**, *63*, 1556-1563.

(14) Vargas, A.; Pegaz, B.; Debefve, E.; Konan-Kouakou, Y.; Lange, N.; Ballini, J.-P.; van de Bergh, H.; Gurny, R.; Delie, F. *Int. J. Pharm.* **2004**, *286*, 131-145.

(15) Konan, Y. N.; Berton, M.; Gurny, R.; Allemann, E. *Eur. J. Pharmaceutical Sciences* **2003**, *18*, 241-249.

(16) Konan, Y. N.; Cerny, R.; Favet, J.; Berton, M.; Gurny, R.; Allemann, E. *Eur. J. Pharmaceutics Biopharmaceutics* **2003**, *55*, 115-124.

(17) Wieder, M. E.; Hone, D. C.; Cook, M. J.; Handsley, M. M.; Gavrilovic, J.; Russell, D. A. *Photochem. Photobiol. Sci.* **2006**, *5*, 727-734.

(18) McCarthy, J. R.; Perez, J. M.; Bruckner, C.; Weissleder, R. *Nano Lett.* **2005**, *5*, 2552-2556.

(19) Gu, H.; Xu, K.; Yang, Z.; Chang, C. K.; Xu, B. *Chem. Commun.* **2005**, *34*, 4270 - 4272.

(20) Roy, I.; Ohulchanskyy, T. Y.; Pudavar, H. E.; Bergey, E. J.; Oseroff, A. R.; Morgan, J.; Dougherty, T. J.; Prasad, P. N. *J. Am. Chem. Soc.* **2003**, *125*, 7860-7865.

(21) Yan, F.; Kopelman, R. *Photochem. Photobiol.* **2003**, *78*, 587–591.

(22) Brasseur, N.; Ouellet, R.; La Madeleine, C.; van Lier, J. E. *British J. Cancer* **1999**, *80*, 1533-1541.

(23) Fu, J.; Li, X.; Ng, D. K. P.; Wu, C. *Langmuir* **2002**, *18*, 3843-3847.

(24) Drain, C. M.; Smeureanu, G.; Patel, S.; Gong, X.; Garno, J.; Arijeloye, J. *New J. Chem.* **2006**, *12*, 1834-1843.

(25) Samaroo, D.; Soll, C. E.; Todaro, L. J.; Drain, C. M. *Org. Lett.* **2006**, *8*, 4985-4988.

(26) Battioni, P.; Brigaud, O.; Desvaux, H.; Mansuy, D.; Traylor, T. G. *Tet. Lett.* **1991**, *32*, 2893-2896.

(27) Greenwald, R. B.; Choe, Y. H.; McGuire, J.; Conover, C. D. *Adv. Drug Delivery Rev.* **2003**, *55*, 217-250.

(28) Hamblin, M. R.; Miller, J. L.; Rizvi, I.; Ortel, B.; Maytin, E. V.; Hasan, T. *Cancer Res.* **2001**, *61*, 7155-62.

(29) Hamblin, M. R.; Miller, J. L.; Loew, H. G.; Hasan, T. *British J. Cancer* **2003**, *89*, 937-943.

(30) Hornung, R.; Fehr, M. K.; Monti-Frayne, J.; Krasieva, T. B.; Tromberg, B. J.; Berns, M. W.; Tadir, Y. *Photochem. Photobiol.* **1999**, *70*, 624-629.

(31) Hornung, R.; Fehr, M. K.; Walt, H.; Wyss, P.; Berns, M. W.; Tadir, Y. *Photochem. Photobiol.* **2000**, *72*, 696-700.

(32) Ris, H.-B.; Krueger, T.; Giger, A.; Lim, C. K.; Stewart, J. C. M.; Althaus, U.; Altermatt, H. J. *British J. Cancer* **1999**, *79*, 1061-1066.

(33) Rovers, J. P.; Saarnak, A. E.; de Jode, M.; Sterenborg, H. J. C. M.; Terpstra, O. T.; Grahn, M. F. *Photochem. Photobiol.* **2000**, *71*, 210-217.

(34) Benaglia, M.; Danelli, T.; Fabris, F.; Sperandio, D.; Pozzi, G. *Org. Lett.* **2002**, *4*, 4229-4232.

(35) Benaglia, M.; Danelli, T.; Pozzi, G. *Org. Biomol. Chem.* **2003**, *1*, 454-456.

(36) Gao, H.; Shi, W.; Freund, L. B. *Proc. Natl. Acad. Sci.* **2005**, *102*, 9469-9474.

(37) Lamarche, F.; Sol, V.; Huang, Y. M.; Granet, R.; Guilloton, M.; Krausz, P. *J. Porphyrins Phthalocyanines* **2002**, *6*, 130-134.

(38) Molineux, G. *Pharmacotherapy* **2003**, *23*, 3S-8S.

(39) Kim, Y. K.; Jeong, D. H.; Kim, D.; Jeoung, S. C.; Cho, H. S.; Kim, S. K.; Aratani, N.; Osuka, A. *J. Am. Chem. Soc.* **2001**, *123*, 76-86.

(40) Lakowicz, J. R. *Principles of fluorescence spectroscopy*; 2nd. ed.; Kluwer Academic/Plenum Publishers: New York, 1999.

(41) Aoyama, Y.; Kanamori, T.; Nakai, T.; Sasaki, T.; Horiuchi, S.; Sando, S.; Niidome, T. *J. Am. Chem. Soc.* **2003**, *125*, 3455-3457.

(42) Mao, H.-Q.; Roy, K.; Troung-Le, V. L.; Janes, K. A.; Lin, K. Y.; Wang, Y.; August, J. T.; Leong, K. W. *Journal of Controlled Release* **2001**, *70*, 399-421.

(43) Nakai, T.; Kanamori, T.; Sando, S.; Aoyama, Y. *J. Am. Chem. Soc.* **2003**, *125*, 8465-8475.

(44) Zhong, M.; Shen, Y.; Zheng, Y.; Joseph, T.; Jackson, D.; Foster, D. A. *Biochem. Biophys. Res. Commun.* **2003**, *302*, 615-619.

(45) Zhong, M.; Lu, Z.; Foster, D. A. *Oncogene* **2002**, *21*, 1071-1078.

(46) Ame, J.-C.; Spenlehauer, C.; de Murcia, G. *BioEssays* **2004**, *26*, 882-893.

(47) Yu, S.-W.; Wang, H.; Poitras, M. F.; Coombs, C.; Bowers, W. J.; Federoff, H. J.; Poirier, G. G.; Dawson, T. M.; Dawson, V. L. *Science* **2002**, *297*, 259-263.

(48) Lam, M.; Oleinick, N. L.; Nieminen, A.-L. *J. Biol. Chem.* **2001**, *276*, 47379-47386.

(49) Oleinick, N. L.; Morris, R. L.; Belichenko, I. *Photochem. Photobiol. Sci.* **2002**, *1*, 1-21.

(50) de Murcia, G.; de Murcia, J. M. *Trends Biochem. Sci.* **1994**, *19*, 172-173.

(51) Noodt, B. B.; Berg, K.; Stokke, T.; Peng, Q.; Nesland, J. M. *British J. Cancer* **1999**, *79*, 72-81.

(52) Sharoni, Y.; Bosin, E.; Miinster, A.; Levy, J.; Schally, A. V. *Proc. Natl. Acad. Sci.* **1989**, *86*, 1648-1651.

(53) Jessani, N.; Niessen, S.; Mueller, B. M.; Cravatt, B. F. *Cell Cycle* **2005**, *4*, 253-255.

Chapter 3 Appendix

FLim program

FLim is a Java-based program for handling FLuorescence images of cells that have been tagged with some kind of fluorescence probe. It allows for the relative fluorescence intensity between images to be compared by assessing the red (R), green (B), and blue (B) vectors (intensities) of an area of pixels in one or more images. The program is compatible with images in jpg, png, or gif format, but only saves in jpg format. One of the basic functions that it performs is background subtraction. After selecting a rectangular background region, pressing “BG Color” to save it, followed by “Run” to calculate the average background intensity by averaging the RGB vectors in the selected region. Relative intensities are computed using a pixel sampling method, which uses the weighted average of the most intense pixels (based on the RGB values) within a specific range. If no errors occurred during the calculation process, then an error label displays “none.” The program checks statistical significance, and if these criteria are not met an "under sampled" error message indicates that not enough pixels were sampled. This can be solved by either reducing the pixels to sample, or adjusting the range. The program automatically generates a distribution of pixels. A good distribution is one in which the minimum intensity is greater than the lower limit of the range, and the maximum is less than the upper limit of the range. The distribution of intensities also shows which image has the areas with the most intense fluorescence. When comparing images, it is important that the same range of parameters such as the number of pixels sampled be used for all images. Another important point is that the program scans an entire image, rather than look at a selected section/region of that image. This latter feature allows a large number of areas in an image – in this case a large number of cells –

to be evaluated in a single process, thus eliminating user prejudices and generally facilitating the comparison of a large number of cells, which lead to more accurate intensity calculations. This program and detailed instructions are available on the web for free at:http://casilab10.sci.ccny.cuny.edu/~nathan/projects/FLim/index.html

Controls

All three types of porphyrin nanoparticles displayed no dark toxicity up to a concentration of 20 μM (data not shown). Greater concentrations were not used, since one of the aims of this study was to reduce the effective concentration. Furthermore, control experiments show there is no significant effect without both irradiating light and Por-Lys_4, Por-EDA_4 or Por-PEG_4 nanoparticles (Figures 3.7-3.9).

Continued Cell Death after Light Irradiation

To verify, that the MDA-MB-231 cells were undergoing apoptosis and PARP was cleaved upon exposure to the porphyrin nanoparticles and light, various negative controls were used. Nanoparticles of Por-EDA_4, Por-PEG_4, Por-Lys_4 and Por-Glu_4 were incubated with the breast cancer cells for 20 hours and kept in the dark. MDA-MB-231 cells without porphyrin nanoparticles were irradiated for 30 min at 0.69 mW cm^{-2} (12.41 kJ m^{-2}). This control was used to show that light had no apoptotic effect on the cells. As a positive control, Por-Glu_4 with irradiating light was used, since this has previously shown to induce apoptosis [1]. The results in Figure 3A.1 show that there is no PARP cleavage present in the dark controls (lanes 1-4). These nanoparticles in the absence of light do not induce apoptosis, and this observation confirms that as a requirement for PDT, light must be present. The indication of PARP cleavage occurs in the presence of light (lane 5) and Por-Glu_4. Lane 6 in Figure 3A.1 shows no PARP cleavage for cells

exposed to doses of light. This shows that porphyrin nanoparticles and light are needed to induce apoptosis as displayed by PARP cleavage products.

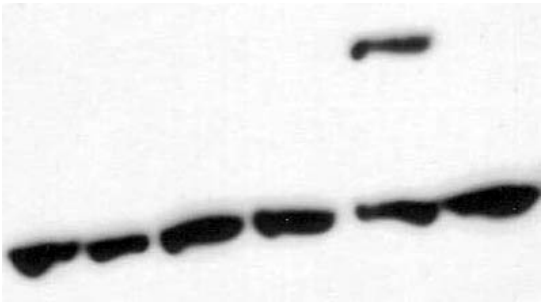

Figure 3A.1: Western blot analysis of control samples that were kept in the dark, probing for cleaved poly(ADP-ribose) polymerase (PARP) in MDA-MB-231 cells. Cells were treated with 10 μM Por-EDA_4, Por-PEG_4 and Por-Lys_4 porphyrin nanoparticles as well as Por-Glu_4 light for 20 hr. After exchanging the growth medium, cells were collected six hours later. Supernatant of the cell lysates were applied to western blot to detect PARP cleavage. From left to right: Lane 1: Por-EDA_4, no irradiation; Lane 2: Por-PEG_4, no irradiation; Lane 3: Por-Lys_4, no irradiation; Lane 4: Por-Glu_4, no irradiation; Lane 5: Por-Glu_4 with irradiation (showing 89 kDa cleaved PARP band); Lane 6: MDA-MB-231 cells with no porphyrin and 20 minute white light irradiation. Bottom lanes are the standard actin control used as a marker.

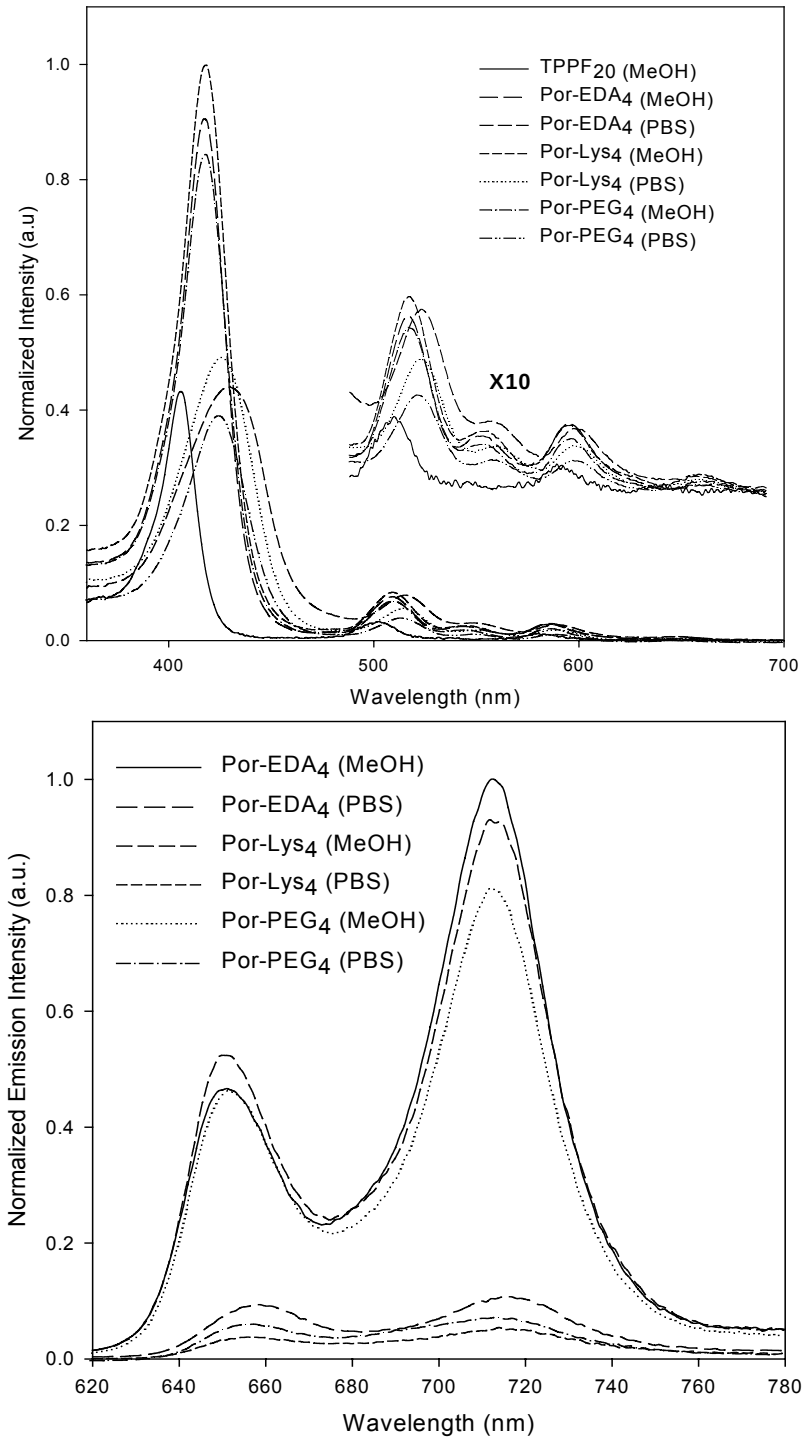

Figure 3A.2: (Top) The concentration normalized 1μM UV-Vis spectrum of Por-Lys_4, Por-PEG_4 and Por-EDA_4 in methanol and PBS, where the inset is Q-band region x 10. $TPPF_{20}$ is partially soluble in MeOH. (Bottom) The concentration normalized fluorescence emission spectra of Por-Lys_4, Por-PEG_4 and Por-EDA_4 in methanol and PBS. Spectra in DMEM are similar to those in PBS. The excitation wavelength is at same optical density for each of the solutions.

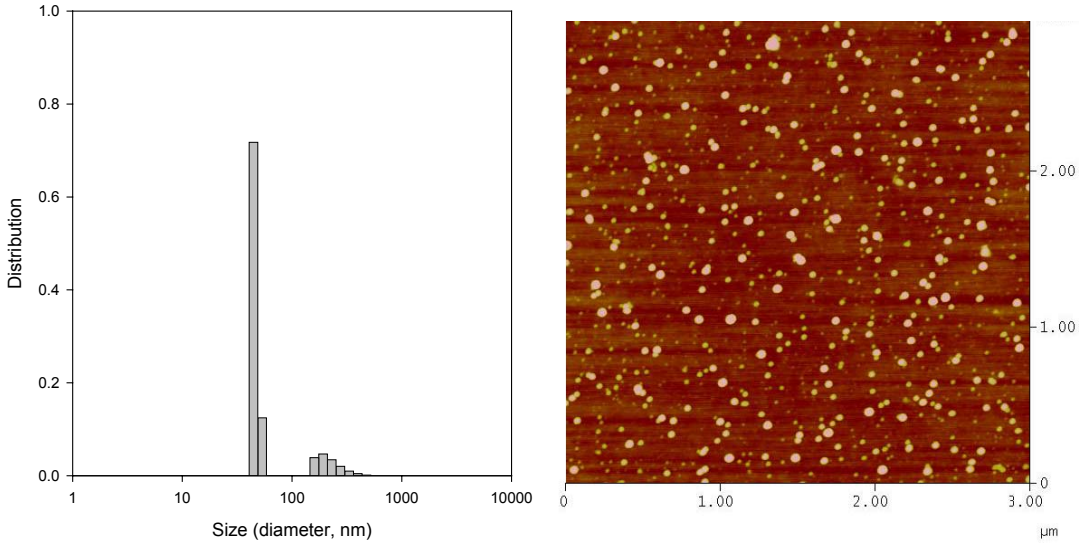

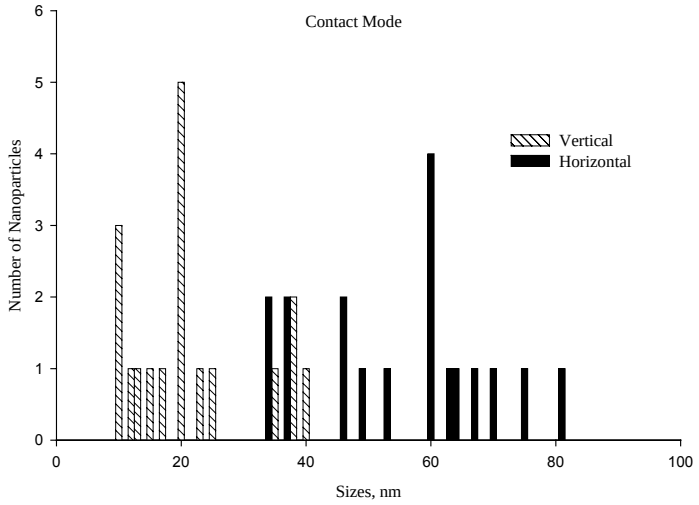

Figure 3A.3: Dynamic light scattering and Atomic Force Microscopy (3x3 µm scan, tapping mode) showing the size distribution of the Por-Lys_4 nanoparticles in solution (at 37 °C) and on ozone cleaned glass substrate, respectively. The histogram represents the distribution of particles in contact mode AFM.

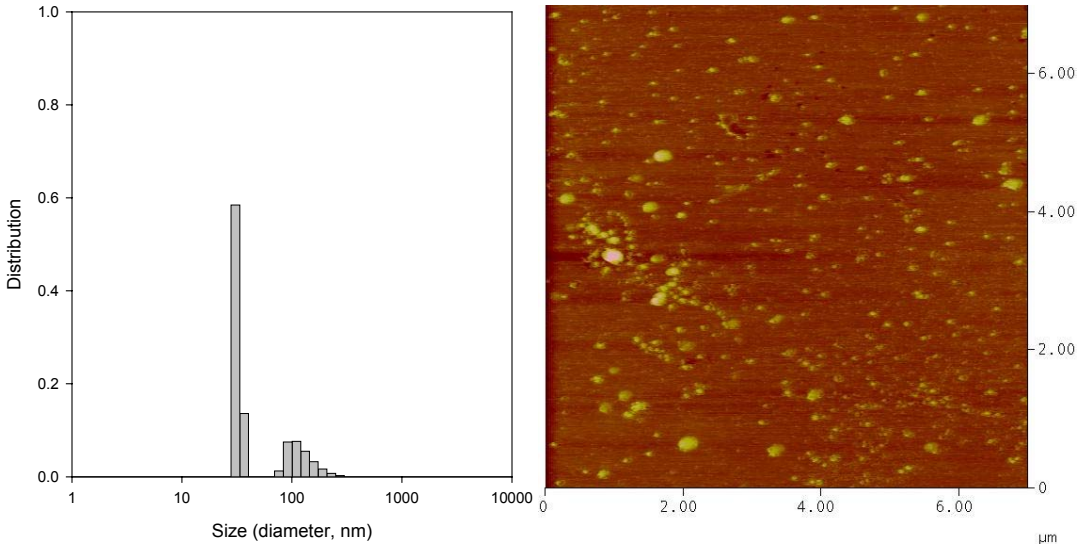

Figure 3A.4: DLS and AFM (7x7μm scan, contact mode) showing the size distribution of colloidal Por-PEG_4 nanoparticles in solution (at 37 °C) and on ozone cleaned glass substrate, respectively. The average height in the AFM is 20 – 23 nm.

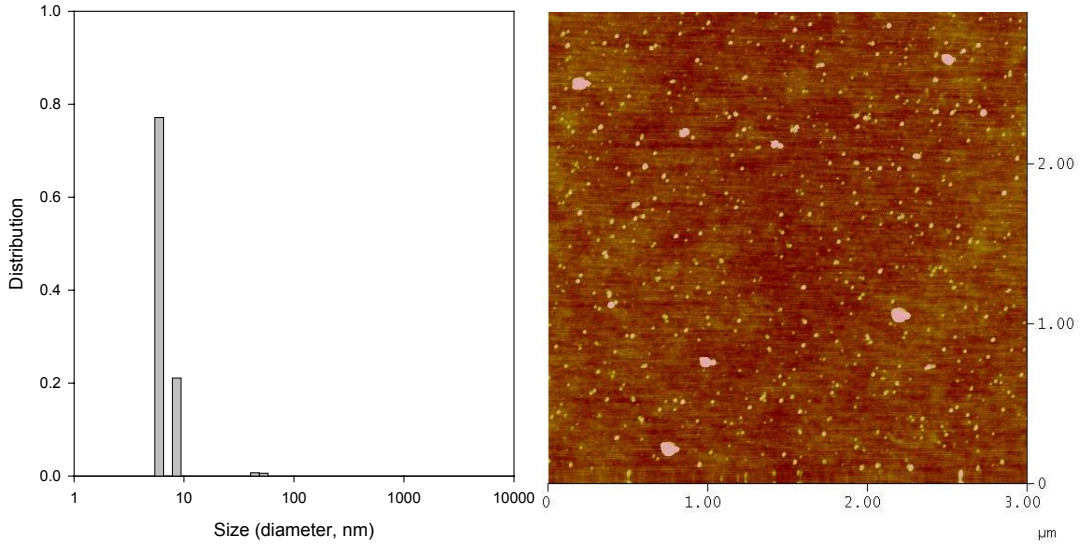

Figure 3A.5: DLS and AFM (3x3μm scan, tapping mode) showing the size distribution of colloidal Por-EDA_4 nanoparticles in solution (at 37 °C) and on ozone cleaned glass substrate, respectively. The average height in the AFM is 6 – 8 nm.

Chapter 4: Using Meso-tetrakis(pentafluorophenyl)porphyrin as an Efficient Platform for Combinatorial Synthesis and the Discovery of New Photodynamic Therapeutics

4.1 Introduction

Peripheral substituents on the porphyrin core can be used both to modulate the photophysical properties and impart desired chemical characteristics to the macrocycle. For example these substituents can: direct the self-assembly or self-organization of the molecules into solid state materials [1-3], target the chromophore to various biological materials [4,5], modulate the electronic properties such as absorption and emission [6,7], serve as recognition motifs for small molecules [8], and serve as a scaffold for further chemical modifications [9]. Porphyrinic systems coordinating redox active metals are can be used as oxidation catalysts [10-12], and metalloporphyrins have wide applications as selective and cross-reactive sensors [13,14].

There are several therapeutic applications of porphyrins [4,5,15-18]. In terms of photodynamic therapeutics (PDT), the applications of porphyrins and related macrocycles to the treatment of cancers and as potential antibacterial or antiviral compounds arise from the high triplet quantum yields of the free bases and some metalloporphyrins. The main mechanism for the therapeutic activity of these compounds is that the triplet state of the chromophore acts as a photosensitizer in the formation of singlet oxygen. Singlet oxygen then reacts with near diffusion-limited kinetics with a variety of biomolecules, such as those containing double bonds, aromatic moieties, sugars, and phosphate esters. There are other potential therapeutic applications of porphyrins including treatment of

stroke by iron porphyrins acting as superoxide dismutases, and as potential agents that prevent the misfolding of the prion proteins that cause scrapies and Jacob-Creutzfeldt syndrome [19-23].

A complex mixture of monomers and oligomers of free base hematoporphyrin, Photofrin, is widely used in the treatments of variety of cancers, and other applications are in the pipeline [15-18]. Because of the huge market as an anti-cancer treatment and the numerous other possible therapeutic applications, there are numerous academic and industrial labs exploring the design and efficacy of new porphyrinic derivatives for PDT applications. One widely claimed rationale for this research is that a major disadvantage of Photofrin is that it is a mixture, however its efficacy as an anti-cancer treatment may be due to the fact that it is a mixture. In this scenario the various Photofrin components partition into different parts of the diseased tissues and bind to different cellular components (e.g. cell walls, mitochondria and other organelles). When cell death is the intended outcome, this multi-pronged attack reduces the ability of the cell machinery to simultaneously repair the damage caused by singlet oxygen-induced oxidative stress at multiple sites. Secondly, the broad range of cancers that are effectively treated with Photofrin may be a result of the partitioning of different components into different cancer tissues and cancer cells. Thus, it is unlikely that one pure compound will be as broadly applicable to as wide a variety of diseased tissues and as effective as Photofrin. However, pure compounds that can be synthesized in high yields, that are directed towards or selective to cancer cells or other diseased tissues, have significant advantages over the currently used mixtures. These advantages include less cross reactivity to non-cancerous cells and lower dosages. This necessitates discovery of specific cell

recognition or targeting motifs, perhaps coupled with non-specific motifs that modulate hydrophobic properties as substituents on the porphyrinoid core.

A previous report on a single molecule approach that targets cancer cells is illustrated. Appending sugars onto porphyrins can direct them to cancer cells because of the significantly increase metabolic needs of these cells and the increased number of sugar transporters found on cancer cells. A simple, high-yield procedure for making non-hydrolysable thio- glycosylated porphyrins based on the $TPPF_{20}$ core was reported [5,24]. It was shown that a glucose derivative of $TPPF_{20}$ was 2 – 5 times more active as a PDT agent than a $TPPF_{20}$-galactose derivative on a breast cancer cell line known to express glucose transporters, MDA-MB-231 [5].

Depending on the intended application and the modality of use, some of the goals of the current research on the therapeutic applications of porphyrinoids are, broadly, to make compounds that: (a) are more selective to target cells or tissues, (b) have greater triplet quantum yields, (c) are good two-photon absorbers, (d) have increased optical density in the 650 – 850 nm region where bio-fluids absorb light less, (e) cross the blood brain-barrier and (f) selectively bind to target bacteria, viruses, or infected cells. There is vigorous research on other applications of porphyrins and metalloporphyrins as sensors, catalysts, electronic, and luminescent materials. The vast majority of this research focuses on the design and synthesis of the peripheral substituents on the porphyrin to affect the desired chemical or materials properties.

In contrast to appending porphyrins with one or more substituents designed to meet a given criterion for a given application, a combinatorial approach can be used to rapidly discover new substituents, combinations of substituents, and isomers for this

application. Previously, it was demonstrated that large solution phase combinatorial libraries of porphyrins can be screened for DNA binding by running the library down a chromatography column of DNA adsorbed onto glass fibers [9]. From a library of 1540 compounds, 4-6 members were selected as the best binders to DNA. A significant finding was that amphipathic molecules with two polar groups and two positively charged groups, each on the same side of the macrocycle, have substantially greater affinity to DNA than the widely studied tetra cationic tetrakis(4-N-methylpyridinium)porphyrin. Photo-induced cleavage assays using plasmid DNA further indicated the activity of the winning compounds [9].

This chapter presents work done on solution phase combinatorial libraries of porphyrins that uses $TPPF_{20}$ as a core platform. A significant advantage is that $TPPF_{20}$ is commercially available and can be made in large 100 g batches in the laboratory. By appending substituents to $TPPF_{20}$, this approach eliminates the need to remove the tarry side products of the typical porphyrin synthesis, and obviates the need for many protecting groups because substitution of the 4-fluoro groups proceeds R-SH> R-NH_2 >> R-OH. The chemistry is demonstrated by forming focused solution phase libraries of this porphyrin bearing functionalities known to be important for PDT, e.g. sugars, cationic groups, and moieties that impart amphipathic solubility properties. The reagents used herein are also commercially available and can be made in large quantities. As a proof-of-concept selection assay, these solution phase libraries were screened for binding to the MDA-MB-231 breast cancer cells by incubating the cells, washing away the unbound materials, and identifying the absorbed porphyrins in cell extracts by MALDI mass spectrometry. The winning compounds were made by directed synthesis. Fluorescence

microscopy based cell binding assays of the winning compounds made from the $TPPF_{20}$ platform and from the original solution phase libraries were compared to the tetra(thioglucose) derivative ($TPPF_{16}$-Glu_4) standard and confirm the selection criteria.

4.2 Experimental Procedures

General

UV-visible spectra were recorded with a Cary spectrophotometer system. Absorptions are given in nanometers (solutions in methanol, unless otherwise indicated). Electrospray ionization mass spectra (ESI-MS) were recorded on an Agilent 1100 LC/MSD equipped with a diode array detector. Results are given as m/z + H+ (relative intensity). Baker-flex (J. T. Baker) silica gel IB2 pre-coated sheets (2.5cm x 7.5cm) were used for analytical thin layer chromatography (TLC) and silica gel 60Å supplied by Sorbent Technologies, Inc. was used for column chromatography. Basic alumina (J. T. Baker) was also used. Preparative TLC was carried out using EM Science (Merck) silica gel 60Å. All solvents (Fischer Scientific) were used without further purification. 5,10,15-tris-pentafluorophenylcorrole ($TPF_{15}C$) was purchased from Frontier Scientific. 5,10,15,20-tetrakis(pentafluorophenyl)porphyrin ($TPPF_{20}$) was either purchased from Aldrich or Frontier Scientific.

Synthesis

The porphyrins bearing different *meso* aryl groups were synthesized by the usual mixed aldehyde condensation method with pyrrole in propionic acid: 5,10-di-(pentafluorophenyl)-15,20-di-(pyridin-4-yl)porphyrin (**F/F/Py/Py**), 5,15-di-(pentafluorophenyl)-10,20-di-(pyridin-4-yl)porphyrin (**F/Py/F/Py**), 5,10,15-tri-

(pentafluorophenyl)-20-(pyridin-4-yl)porphyrin (**F/F/F/Py**) and 5-(pentafluorophenyl)-10,15,20-tri-(pyridin-4-yl)porphyrin (**F/Py/Py/Py**). All products had satisfactory UV-Visible and mass spectra. The NMR of the compounds bearing the protected sugars was taken in chloroform, because NMR spectra of the free glycosylated porphyrins are poorly resolved. Deprotection of the sugars used 1 equivalent of $NaOCH_3$ for each acetate group at RT in 9:1 v/v solution of methanol/dichloromethane for 1 hour. The detailed characterization of the compounds used herein will be reported elsewhere.

Synthetic methods to couple thio sugars/reagents to $TPPF_{20}$

5,10-di-[4-(1'-thio-2',3',4',6'-O-acetyl-glucosyl)-2,3,5,6-tetrafluorophenyl]-15,20-di-(pyridin-4-yl)porphyrin (GluAc/GluAc/Py/Py). A mixture of **F/F/Py/Py** (20 mg, 25.1 μmol), 2,3,4,6-tetra-O-acetyl-glucosylthioacetate (41 mg, 100.9 μmol) and diethyl amine (40 μL, 387.4 μmol) were stirred in a solvent mixture of DMF, chloroform and methanol (4: 4:1 v/v, 3 mL), for 24 h at RT in the dark under nitrogen. The crude product was purified by flash column chromatography using dichloromethane/methanol, 97:3 v/v. UV-Vis ($CHCl_3$): 416, 511, 543, 586. ESI-MS: 1485 ($M+H^+$)

5,15-di-[4-(1'-thio-2',3',4',6'-O-acetyl-glucosyl)-2,3,5,6-tetrafluorophenyl]-10,20-di-(pyridin-4-yl)porphyrin (GluAc/Py/GluAc/Py). A mixture of **F/Py/F/Py** (20 mg, 25.1 μmol), 2,3,4,6-tetra-O-acetyl-glucosylthioacetate (41 mg, 100.9 μmol and diethyl amine (40 μL, 387.4 μmol) were stirred in DMF/chloroform/methanol (4:4:1 v/v, 3 mL) for 24 h at RT in the dark under nitrogen. The eluent used for column chromatography was dichloromethane/methanol, 97:3 v/v. UV-Vis ($CHCl_3$): 415, 509, 542, 584 and 641. ESI-MS: 1485 ($M+H^+$) and 1507 ($M+Na^+$).

5-[4-(1'-thio-2',3',4',6'-O-acetyl-glucosyl)-2,3,5,6-tetrafluorophenyl]-10,15,20-tri(pyridin-4-yl)porphyrin (GluAc/Py/Py/Py). A mixture of **F/Py/Py/Py** (21 mg, 29.7 μmol), 2,3,4,6-tetra-O-acetyl-glucosylthioacetate (25 mg, 61.5 μmol and diethyl amine (30 μL, 290 μmol) were stirred in a mixture of DMF, chloroform and methanol (4:4:1 v/v, 3mL) at RT in the dark under nitrogen. The eluent for column chromatography was dichloromethane/methanol, (97:3 v/v) mixture.

5,10,15-tri-[4-(1'-thio-2',3',4',6'-O-acetyl-glucosyl)-2,3,5,6-tetrafluorophenyl]- 20- (pyridin-4-yl)porphyrin (GluAc/GluAc/GluAc/Py). A mixture of **F/F/F/Py** (20 mg, 22.5 μmol), 2,3,4,6-tetra-O-acetyl-glucosylthioacetate (55 mg, 135 μmol and diethyl amine (30 μL, 290 μmol) were stirred in a mixture of DMF, chloroform and methanol (4:4:1 v/v, 3 mL). The eluent for column chromatography was dichloromethane/methanol, (97:3 v/v) mixture.

Synthesis of 21-membered porphyrin library

A mixture of $TPPF_{20}$ (30 mg, 30.8 μmol), 2,3,4,6-tetra-O-acetylglucosylthioacetate (17.1 mg, 42.1 μmol), 2,3,4-tri-O-acetyl-xylosylthioacetate (14.1 mg, 42.1 μmol), 4-mercaptopyridine (4.7 mg, 42.1 μmol) and diethylamine (63.6 μL, 616 μmol) were stirred in DMF in the dark under nitrogen at RT for 24 h. Solvent was evaporated and the library was subjected to ESI-MS without purification. In order to deprotect the acetate groups on the protect thiosugars, the library (5 mg, 2.87 μmol) was stirred with sodium methoxide (53.5 μL of 0.5 M in CH_3OH, 2.87 μmol) in dry CH_3OH/CH_2Cl_2 (10 mL, 9:1) for 1 hour, followed by neutralization with a pH 7.2 ammonium acetate buffer. The solvents were evaporated and the library was subjected to MALDI-MS with no further purification.

Synthesis of winning compounds from 21-membered library

5,15-di-[4-(1'-thio-glucosyl)-2',3',5',6'-tetrafluorophenyl]-10,20-di-[4-(4'-thiopyridyl) -2,3,5,6-tetrafluorophenyl]porphyrin (Glu/SPy/Glu/SPy) and 5,10-di-[4-(1'-thio-glucosl)-2',3',5',6'-tetrafluorophenyl]-15,20-di-[4(-4'-thiopyridyl)-2,3,5,6-tetrafluorophenyl]porphyrin (Glu/Glu/SPy/SPy).

A mixture of $TPPF_{20}$ (30 mg, 30.8 μmol), 2,3,4,6-tetra-O-acetyl-glucosylthioacetate (25.0 mg, 61.6 μmol), 4-mercaptopyridine (6.8 mg, 61.6 μmol) and diethylamine (63.6 μL, 616 μmol) were stirred in DMF, in the dark under N_2 at RT for 24h. The resulting mixture was subjected to a flash silica gel column using 0 – 3% gradient of methanol in dichloromethane as eluent, followed by preparatory thin layer chromatography using 5% methanol in dichloromethane as eluent to obtain the acetate protected glucose 5,15-glycosyl and 5,10-glycosyl $TPPF_{16}$ isomers with yields of 6.9 % and 10.0%, respectively. 5,15-glycosyl isomer: UV-Vis (CH_2Cl_2) λ_{max}, nm: 415, 508, 542, 584, 638. ESI-MS: 1845 ($M + H^+$). 5,10-glycosyl isomer: UV-Vis (CH_2Cl_2) λ_{max}, nm: 415, 508, 541, 584, 638. ESI-MS: 1845 ($M + H^+$). The isomers (5mg, 2.7 μmol) were then treated with 8 equivalents $NaOCH_3$ at RT in 9:1 v/v solution of methanol/dichloromethane for 1 h to give the deprotected derivatives in quantitative yields. The products were neutralized by pH 7.2 ammonium acetate buffer. UV-Vis (CH_3OH) λmax, nm: 412, 505, 537, 582, 637. ESI-MS: 1510 ($M + H^+$) (5,15- isomer). UV-Vis (CH_3OH) λmax, nm: 412, 505, 538, 582, 635. ESI-MS: 1510 ($M + H^+$) (5,10-isomer)

Synthetic methods to couple primary amino reagents to $TPPF_{20}$ and creation of 6-member libraries based on this chemistry

For amine substitution of $TPPF_{20}$, 5mg (5.1 μmol) $TPPF_{20}$ ($C_{44}H_{10}F_{20}N_4$, 974g/mol) was dissolved in 2 ml of N-methylpyrrolidone (NMP), which was passed through a basic alumina pipette column to remove any water present. 20 total equivalents of two primary amines (histamine and 1-aminopentane) were added, and the solution was stirred in the dark at room temperature overnight, at which time TLC showed all starting porphyrin material completely reacted. Complete substitution of the 4-fluoro groups would yield a library with six members, while incomplete substitution can yield a "library" with 21 members. After removal of the solvent under reduced pressure with heating, the sample was re-dissolved in methanol and analyzed by ESI-MS. Since the pentylamine has a low boiling point, this reaction was unsuccessful using microwave irradiation. A second method for coupling amines to the $TPPF_{20}$ platform uses microwave heating of the reagents in NMP [25].

Synthesis of solution phase combinatorial library using $triPCF_{15}$ corrole

A mixture of $triPCF_{15}$ (5 mg, 6.3 μmol), 2,3,4,6-tetra-O-acetylglucosylthioacetate (7.7 mg, 18.9 μmol), 2,3,4-tri-O-acetyl-xylosylthioacetate (6.3 mg, 18.9 μmol), 4-mercaptopyridine (2.1 mg, 18.9 μmol) and diethylamine (13 μL, 126 μmol) in NMP were subjected to a stream of nitrogen for 10 min. The vial was seal and stirred in the dark at room temperature for 24 h. Solvent was evaporated and the library was subjected to ESI-MS without further purification.

Extraction of 21-membered library from MDA-MB-231 cells

The 21-membered library (6.74 mM) dissolved in 144 μL CH_3OH was added to 10 mL culture medium in a 100 mm cell culture dish to make a final concentration of 100 μM in total porphyrin concentration (1-5 μM per member). 24 hours later, the cells were rinsed with cell culture medium to wash off any unbound porphyrins and collected in an Eppendorf tube with a rubber policeman in 0.5 mL distilled water. 1.5 mL 2-chloroethanol was added to the mixture and sonicated for 1.5 minute with pulses on ice. Solvents were evaporated and 300 μL of CH_3OH was added. The mixture was centrifuged and the supernatant was collected. The solvent was evaporated again and 100 μL of CH_3OH was added. The mixture was centrifuged again; the combined supernatant was collected and submitted for MALDI-MS analysis.

Fluorescence imaging of cells

Cells maintained in DMEM, 10% BCS, 1% antimycotic at 37ºC and in 5% CO_2 atmosphere were plated onto coverslips in cell culture dishes. Porphyrins (dissolved in methanol) were added to the cultures to a final concentration of 2, 5 or 10 μM. After 24 h incubation, cells were washed with PBS and fixed in 4% paraformaldehyde solution for 10 min at RT. The cells were then washed with PBS 3 times. The coverslips were mounted onto glass slides in Dako fluorescent mounting medium, and then visualized using a Nikon Optiphot 2 fluorescence microscope. Images were captured as JPEG or TIFF files at 60X magnification, with excitation: 505 – 565 nm and emission: 565 – 685 nm. For each set of experiments, cells were cultured and the fluorescence images were taken under identical culture and microscopic conditions. For quantitative studies, the image intensities of the cells in the fluorescence micrographs were calculated by FLim program (coded by Dr. Nathan Stevens, see Chapter 3).

Quantum Yield Calculations

From the normalized absorption and corrected emission spectra, the quantum yield for radiative decay can be indirectly obtained using the following equation from George et al [26]:

$$Q = Q_R \frac{I}{I_R} \frac{OD_R}{OD} \frac{n^2}{n_R^2}$$

In this equation, Q is the quantum yield of the unknown sample; Q_R is the quantum yield of the standard sample, I_R and I are the integrated intensity for the standard and unknown samples, respectively. OD represents the optical density and η is the refractive index of the solvent used. The standard or reference sample used for the quantum yield determination was cresyl violet dissolved in methanol. This dye has a quantum yield of 0.54 in the spectral range 600 – 650 nm [27].

4.3 Results and Discussion

4.3.1: Libraries based on a core $TPPF_{20}$ platform

Nucleophilic substitution reactions of the four para fluoro groups on $TPPF_{20}$ are well documented [5,24,25,28]. The reactivity of the para fluoro group on the pentafluorophenyl moiety varies significantly with the specific primary nucleophile used, where softer nucleophiles are more reactive than harder nucleophiles, $HS\text{-}CH_2R > H_2N\text{-}CH_2R >> HO\text{-}CH_2R$. As expected, secondary nucleophiles are much less reactive than similar primary derivatives. For example, primary amine derivatives are efficiently synthesized in N-methylpyrrolidone and microwave heating for about 12 minutes [25], and thiol derivatives are made in DMF under an inert atmosphere at room temperature for

8-24 hours [24]. The yields of both of these reactions can exceed 90%, and are tolerant of other functional groups such as alcohols. This research surveyed a variety of primary thiols to probe the versatility of the reaction.

Synthesis and selection from 21-member $TPPF_{20}$ porphyrin combinatorial library

Although there are many potential therapeutic applications of porphyrinoids, at present the primary clinical use is for the photodynamic treatment of macular degeneration and of cancer. For the treatment of cancer, the goal is to kill or eliminate cells by any means that target diseased cells and tissues. There are a variety of cellular processes and components that can be targeted, but since most crucial cellular processes have various repair mechanisms, it may be preferable to target more than one, or even many, parts of the cell or tissue to maximize the probability of killing it. Rather than specifically targeting a particular cellular component, or specific cellular process, or evaluating solubility properties, by designing a molecule or a class of molecules and individually testing them for PDT efficacy, one can hypothesize that the cells themselves may indicate which molecules bind or are taken up most efficiently. Thus an assay was developed wherein viable human breast cancer cells (MDA-MB-231) were treated with focused solution phase libraries to allow the cells to select the members of the library that are best taken up. This strategy assumes that compounds with high affinities and uptake into the cells will have the greatest PDT activities.

The efficiency of the nucleophilic substitution of the 4-fluoro groups by various thio compounds indicated that $TPPF_{20}$ would be a good platform for the formation of core-centered combinatorial libraries. Based on the PDT activity of the aforementioned thioglycosylated derivatives [5] and the amphipathic solubility of pyridyl moieties, small 21-member libraries focusing on different thiosugars and pyridine were synthesized and

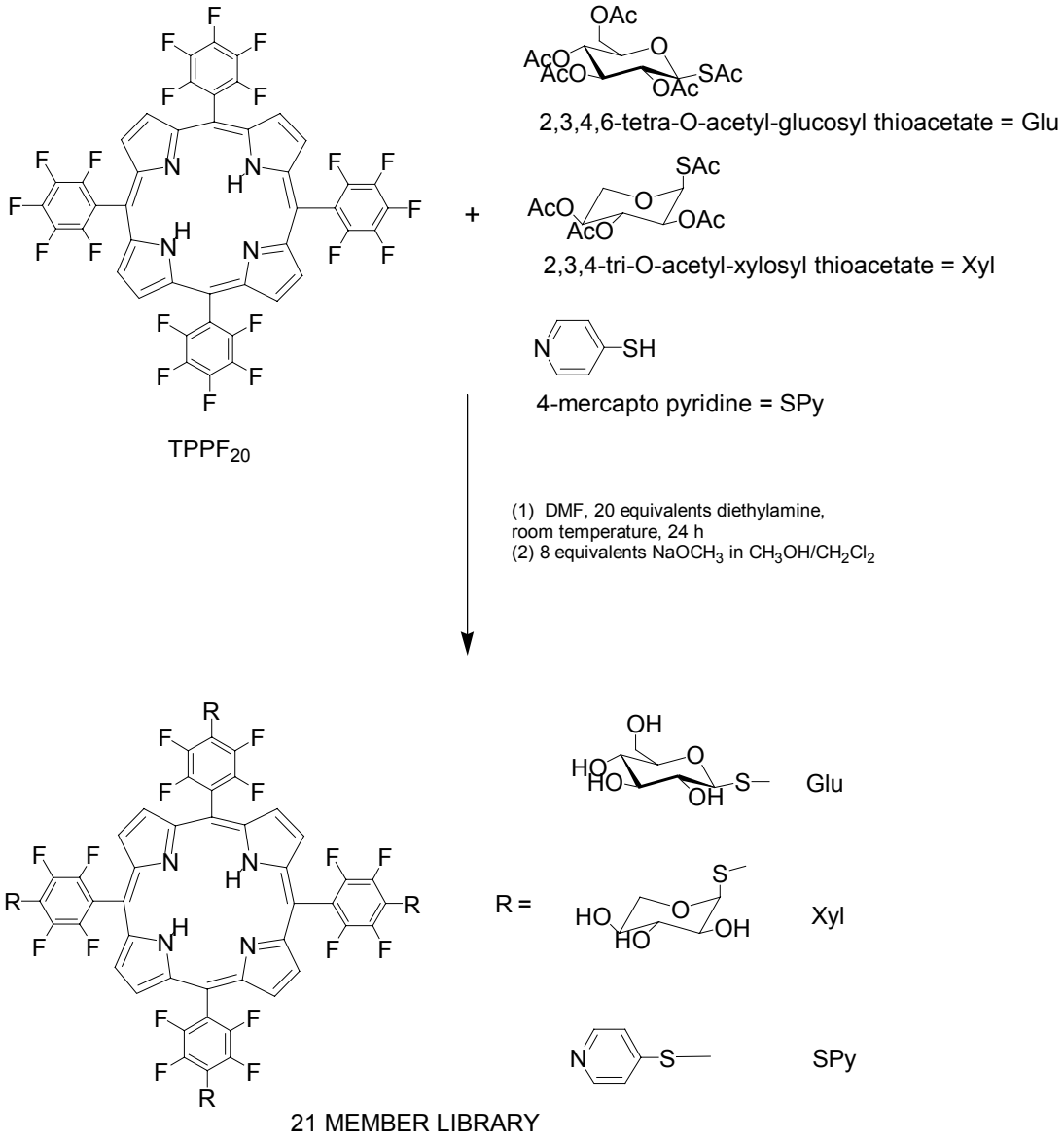

Figure 4.1: Synthesis of a 21-member library, L-1, using $TPPF_{20}$ as a core platform.

characterized to assure this strategy results in a statistical distribution of products. When one equivalent of $TPPF_{20}$ is stirred with 1.4 equivalents of each of the three thiols (2,3,4,6-tetra-O-acetyl-glucosylthioacetate, 2,3,4-tri-O-acetylxylosylthioacetate and 4-mercaptopyridine; a 1:4.2 ratio of $TPPF_{20}$ to thiol, or about 1:1.03 per 4-fluoro group) and 20 equivalents of diethylamine (DEA) at room temperature in DMF for 24 hours, a statistical mixture of 21 compounds is formed (Figure 4.1). Core-centered libraries based on this chemistry have positional isomers (e.g. two copies of a substituent on adjacent versus opposite sides of the porphyrin), such that the statistical reaction of three auxiliaries to the four side of the porphyrin results in 15 isobaric compounds that can be observed by mass spectrometry. Isobaric peaks arise both from isomers and from coincidental m/e overlap at standard MS resolution. The ESI-MS spectrum of the reaction mixture indicates all 15 compounds are present [29]. Quantitative deprotection of the sugars is accomplished using an equal molar ratio of NaOMe to the acetate protecting groups to form the active library, L-1.

We chose the Glu and SPy^{+} motifs because they have demonstrated affinity for cancer cells and biomolecules [4,5], and the xylose because it has a different molar mass, which aids in characterization of the libraries by mass spectrometry. For these proof-of-principle experiments, a small library was used to both identify lead compounds and to simplify the identification of the selected porphyrins from the cell extracts. Briefly, after incubation of the cells with library L-1 for 24 hours, the cells were washed to remove unbound porphyrins and collected. The cells were treated with 2-chloroethanol, sonicated and the solvents removed. The porphyrins taken up by the cancer cells were extracted from the lysates by sonicating in 2-chloroethanol for 1.5 minute with pulses on

ice and the solvents removed. 300 μL methanol was added, followed by centrifugation to remove insoluble materials. This was repeated until no porphyrin fluorescence was observed in the methanol. The methanol was concentrated to ca. 100 μL and assayed by MALDI-MS. Two major parent ion peaks corresponding to members of the library were identified [29]; each can be one of two isomers: (1) Glu/Glu/SPy/SPy, Glu/SPy/Glu/SPy, and (2) Xyl/Glu/SPy/SPy, Xyl/SPy/Glu/SPy. Additionally, two minor peaks were

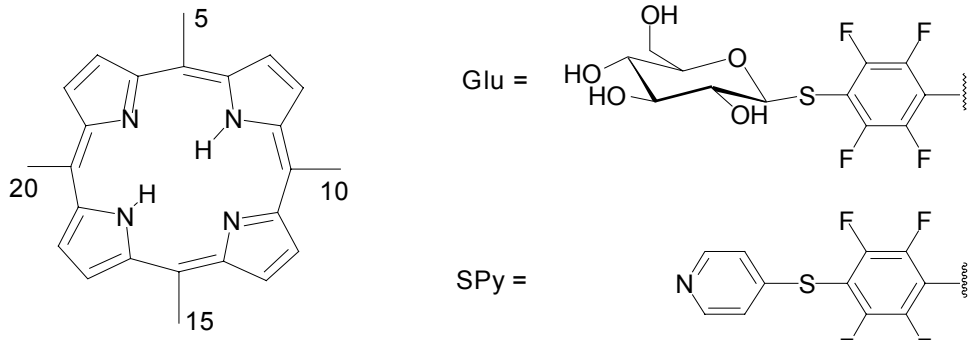

	5	10	15	20
A	Glu	Glu	SPy	SPy
B	Glu	SPy	Glu	SPy
C	Glu	Glu	Glu	SPy
D	Glu	Glu	SPy^+	SPy^+
E	Glu	SPy^+	Glu	SPy^+
F	Glu	Glu	Glu	Glu

Figure 4.2: The two major porphyrin compounds (A,B) that were indicated in the cell-selection assays if Xyl is considered a surrogate for Glu, which were subsequently synthesized directly and tested for PDT activity using MDA-MB-231 cells [30]. A third was indicated as a minor component by the cell selection assay (C). Because of the known affinity of pyridinium porphyrins to negatively charged biomolecular structures such as DNA, the N-methylpyridinium compounds were also made (D, E). Results were compared to the previously reported tetraglucosyl compound (F).

identified; each can be one of two isomers: (3) Glu/Glu/Xyl/SPy, Glu/Xyl/Glu/SPy, and (4) Xyl/Xyl/Glu/SPy, Xyl/Glu/Xyl/SPy. Thus, there are eight potential winning

compounds. If one considers the Xyl as a surrogate for Glu, then these eight possible compounds distill into the three indicated in Figure 4.2 At this stage of the research program, we do not know if there are any bio-conjugated porphyrins present which would manifest themselves as species with unknown molar mass, also no attempt was made to identify the small peaks with low signal/noise in the mass spectra. Since some porphyrinic isomers are known to have greater affinity to cancer cell membranes and other cellular components than other isomers [4], the identification of the selected isomer was accomplished by cell binding assays of the individual compounds.

The compounds initially identified from L-1 (Figure 4.2, L-1 A, B, C) had polar pyridyl groups, but cationic N-methyl pyridinium groups on porphyrins have known affinities for DNA, RNA, [30,31] and anionic membranes [30]. Thus, it was decided to further this work by investigating compounds bearing the cationic species.

Cell-selected compounds — affinity towards cancer cells

Of the compounds selected from the 21-membered library L-1 by the MDA-MB-231 cells (Figure 4.2) only the two Glu/Glu/SPy/SPy and Glu/SPy/Glu/SPy compounds were made, since most cells do not specifically take up xylose. In addition to this the cationic derivatives, Glu/Glu/SPy^+/SPy^+ and Glu/SPy^+/Glu/SPy^+, were prepared. Figure 4.3 shows the electronic spectra of Glu/Glu/SPy/SPy, which indicates that this porphyrin is aggregated in cell culture media. Conversely, the pyridinium derivative, Glu/Glu/SPy^+/SPy^+ exhibits less aggregation. Fluorescence microscopy was used to investigate the affinity of these compounds to MDA-MB-231 cells, and compared to the well-studied Glu/Glu/Glu/Glu (tetraGlu) derivative, which was also a member of the library.

Figure 4.4 shows the fluorescence microscopy of MDA-MB-231 cells treated with 2.5 and 10 μM of three porphyrin derivatives for 24 hours under identical conditions. After rinsing the unbound compounds from the cells on the cover slips and fixing, fluorescence images of the cells were taken on the same day and one week later. The observed fluorescence intensity was taken to be proportional to the quantity of porphyrin bound to the cells, and was quantified by FLim (Chapter 3, Experimental Procedures). When cells are treated with either the uncharged or the cationic 5,10 isomer Glu/Glu/SPy/SPy, Glu/Glu/SPy^+/SPy^+ or the Glu/Glu/Glu/Glu standard for 24 hours, the low intensity of the fluorescence observed by fluorescence microscopy seems to indicate that little of these porphyrins is taken up by the cells just after fixing the cells (Figure 4.4, day 1). This result is misleading because the same cells examined one week later exhibit

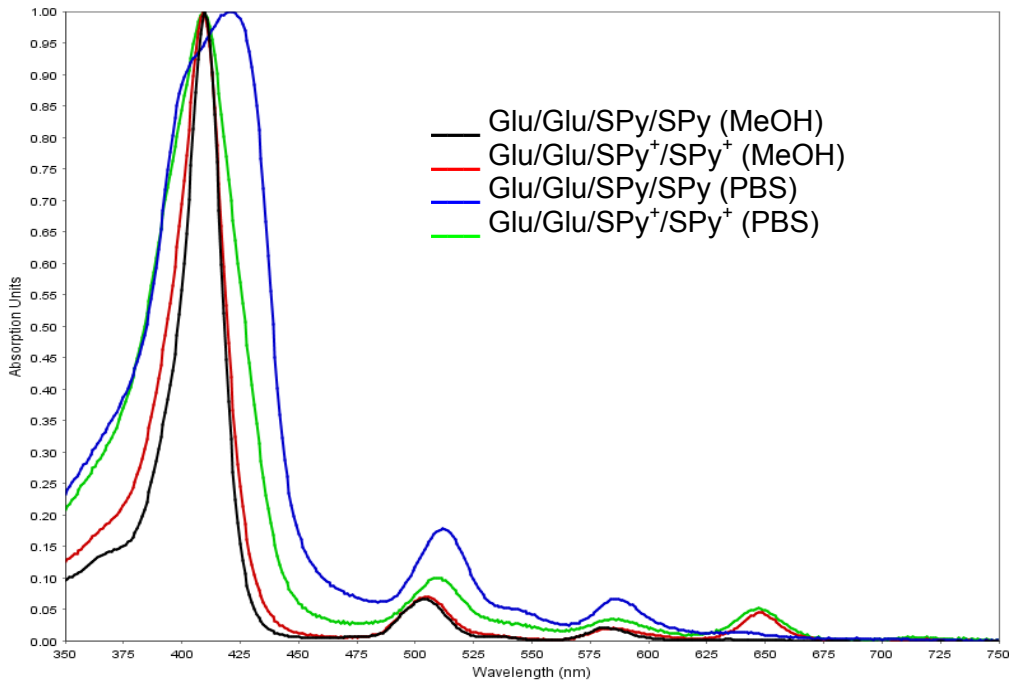

Figure 4.3: Normalized absorption spectra of Glu/Glu/SPy/SPy in methanol and PBS and of the charged Glu/Glu/SPy^+/SPy^+ in the same solvents.

a much brighter fluorescence (Figure 4.4, week 1), indicating that the porphyrins were indeed taken up by these cells. Since the cells were rinsed to remove unbound porphyrins, no further uptake of porphyrin is possible.

Comparison of fluorescence intensity by FLim program of 10 μM of porphyrins at day 1 shows that the charged Glu/Glu/SPy^+/SPy^+ and tetraGlu have similar intensities and are more intense than uncharged Glu/Glu/SPy/SPy by a factor of ca. 1.4. The 5,15 isomer, Glu/SPy/Glu/SPy, which was also a possible selection from the 21-membered library, shows the poorest uptake (data not shown). The 5,15 Glu/SPy^+/Glu/SPy^+ pyridinium derivative was not further evaluated, because the 5,15 pyridinium species are known to be poorly absorbed by many cell lines and similar cellular uptake results have been previously reported for 5,10- versus 5,15- isomers [4,9]. Re-examination of the same slides one week later reveals a substantial increase in fluorescence intensity of the 5,10 isomers and that the fluorescence of Glu/Glu/SPy/SPy porphyrin is still significantly less intense than the charged derivative Glu/Glu/SPy^+/SPy^+ (Figure 4.4, week 1). The increased fluorescence intensities indicate that the porphyrins in the cells are initially aggregated (quenching the fluorescence) and that it takes time for them to disaggregate (see chapter 3). It is noteworthy that even the tetraGlu derivative, which was shown to be highly active as a PDT agent [5], must have some degree of aggregation in the cells when used at this concentration, which is born out by the UV-visible spectra (Figure 4.5). This implies that this compound may be more active than initially reported if allowed time to disaggregate.

In order to further discern any differences between the compounds in terms of cell uptake, lower concentrations were also used. The FLim program was used to compare

the fluorescence intensity of MDA-MB-231 cells treated with 2.5 μM of the porphyrins as above Figure 4.4). On day 1 a weak fluorescence is observed for all porphyrins tested. However, imaging after one week, shows a drastic increase in fluorescence intensity for all porphyrins. Once again, the uncharged Glu/Glu/SPy/SPy shows the poorest uptake into the MDA-MB-231 cells. Note that at this lower concentration the tetraGlu shows a slightly better cellular uptake than the charged Glu/Glu/SPy^+/SPy^+ compound, but at 10 μM the uptake appeared to be similar.

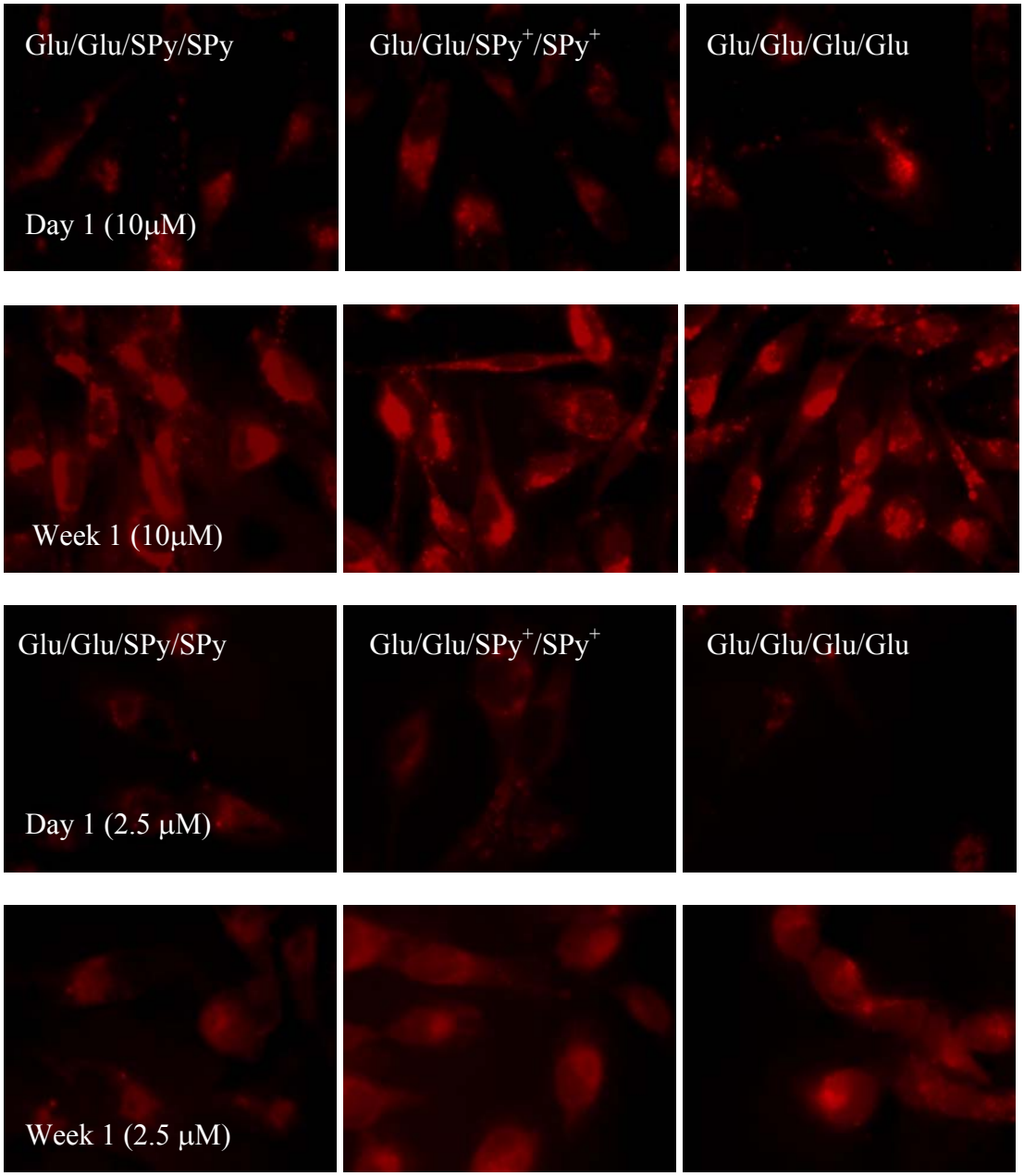

Figure 4.4: Comparison of fluorescence intensities of 10 μM and 2.5 μM Glu/Glu/SPy/SPy and the charged derivative Glu/Glu/SPy$^+$/SPy$^+$, compared to tetraGlu. Images are taken under identical instrumental conditions and are not manipulated.

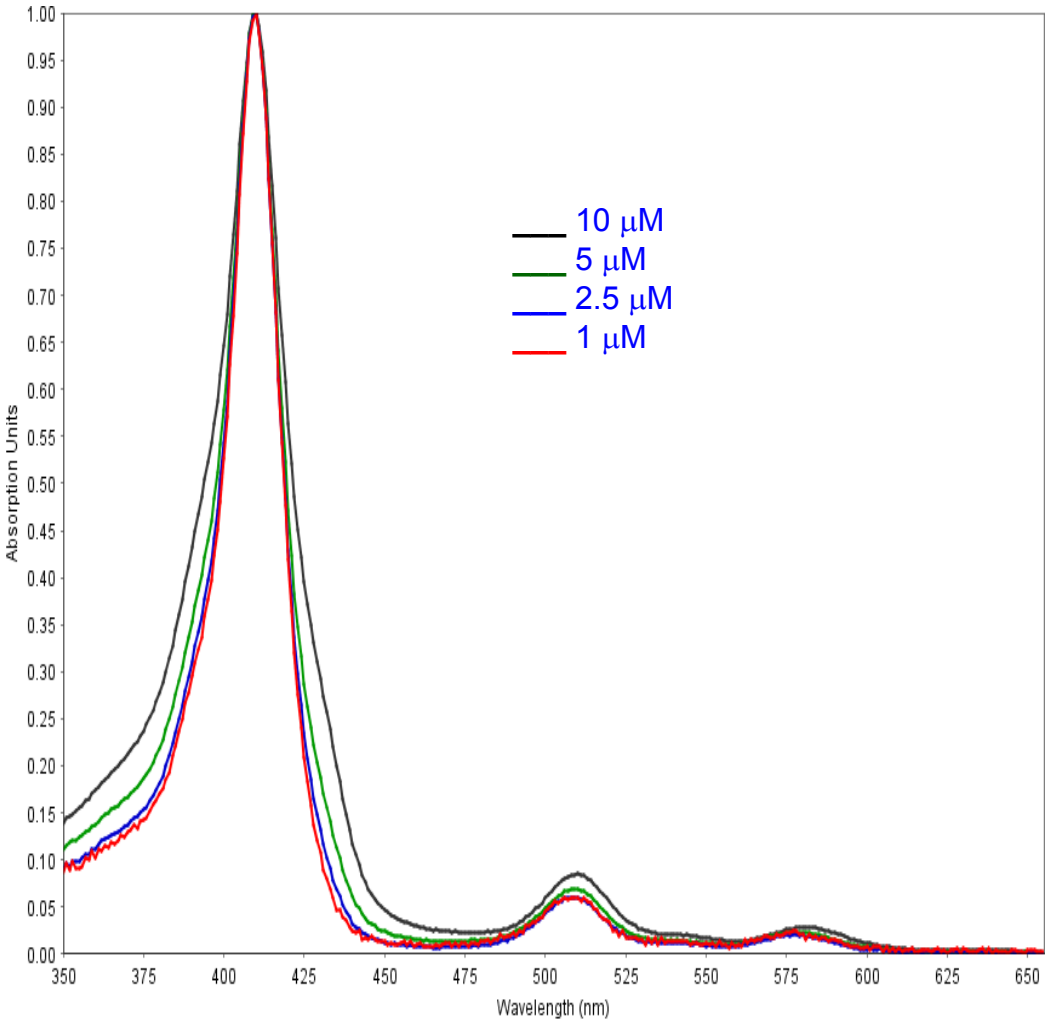

Figure 4.5: Normalized absorption spectra for varying concentrations of tetraGlu porphyrin in aqueous PBS.

These results suggest that the porphyrins bind and/or enter the cells as nanoscaled aggregates, which have significantly quenched fluorescence by well understood mechanisms including shading, energy transfer, and enhanced vibrational relaxation [7]. The UV-vis spectra of the compounds of interest in polar organic solvents (e.g. CH_3OH) are typical of porphyrin derivatives based on $TPPF_{20}$; however, the Soret bands in PBS

are significantly broadened and/or split, which is typical of aggregated porphyrins (see Figure 4.3 and 4.5) [32,33].

The PDT activity of the winning compounds from L-1 was evaluated using breast cancer cells, MDA-MB-231. Since the 5,15 isomer does not bind efficiently to these cells (via fluorescence), it was not evaluated. The uncharged 5,10- isomer Glu/Glu/SPy/SPy and its cationic derivative, Glu/Glu/SPy^+/SPy^+, were evaluated at 10 μM and 2.5 μM and compared to the Glu_4 compound. After incubation for 20 hours, the cells were washed 3-5 times to remove unbound porphyrin materials and irradiated for 20 minutes with white light from a 13 Watt fluorescent bulb (0.9 mW/cm^2). Cell death was monitored by trypan blue dye staining over 24 hr. Blue stained cells were counted using a hemacytometer as non-viable cells using light microscopy.

With all three compounds, more than 25% of the cells are necrotic immediately after PDT treatment under the specified conditions (Figure 4.6A). The assay also reveals that the percentage of non-viable cells for Glu/Glu/SPy^+/SPy^+ and tetraGlu, continues to increase with time to >80% after 24 hours. The cell density is observed to increase, during this time so some of the treated cells are able to divide. The persistent increase in the percentage of non-viable cells over 24 hours implies a secondary mechanism, i.e. cell death via apoptosis [34-36]. The uncharged Glu/Glu/SPy/SPy showed less than 60% cell death over 24 hr and was therefore not evaluated at the lower concentration. One may speculate that the uncharged Glu/Glu/SPy/SPy remains aggregated and so are poorly fluorescent and have significantly diminished triplet quantum yields (see Chapter 3 on porphyrin nanoparticles).

The cationic Glu/Glu/SPy^+/SPy^+ was evaluated at 2.5 μM and compared to the tetraGlu standard (Figure 4.6B). At this concentration ca. 40% of the cells are found to be necrotic just after exposure to the light. The percentage of non-viable cells continues to increase to >60% over a 24 hr period. When the cells are treated with a 4-fold lower concentration of tetraGlu, *more* cells were found to be necrotic immediately following the irradiating light (28 % vs 44 %). While for cells treated with Glu/Glu/SPy^+/SPy^+, there was a decrease in the necrotic cells just after light exposure (57 % vs 38 %) at the lower concentration. This can be explained through Figure 4.5, which shows the normalized absorption spectra for varying concentrations of the tetraGlu porphyrin in aqueous solution (PBS). Note the half width of the Soret band broadens with increasing concentrations, which is interpreted as indicating aggregation of the chromophores. Since dye aggregates are less efficient in forming excited state triplets, one expects reduced PDT activity, as observed. Chapter 3 discusses this in detail and present viable methods to allow disaggregation of the chromophores before light illumination.

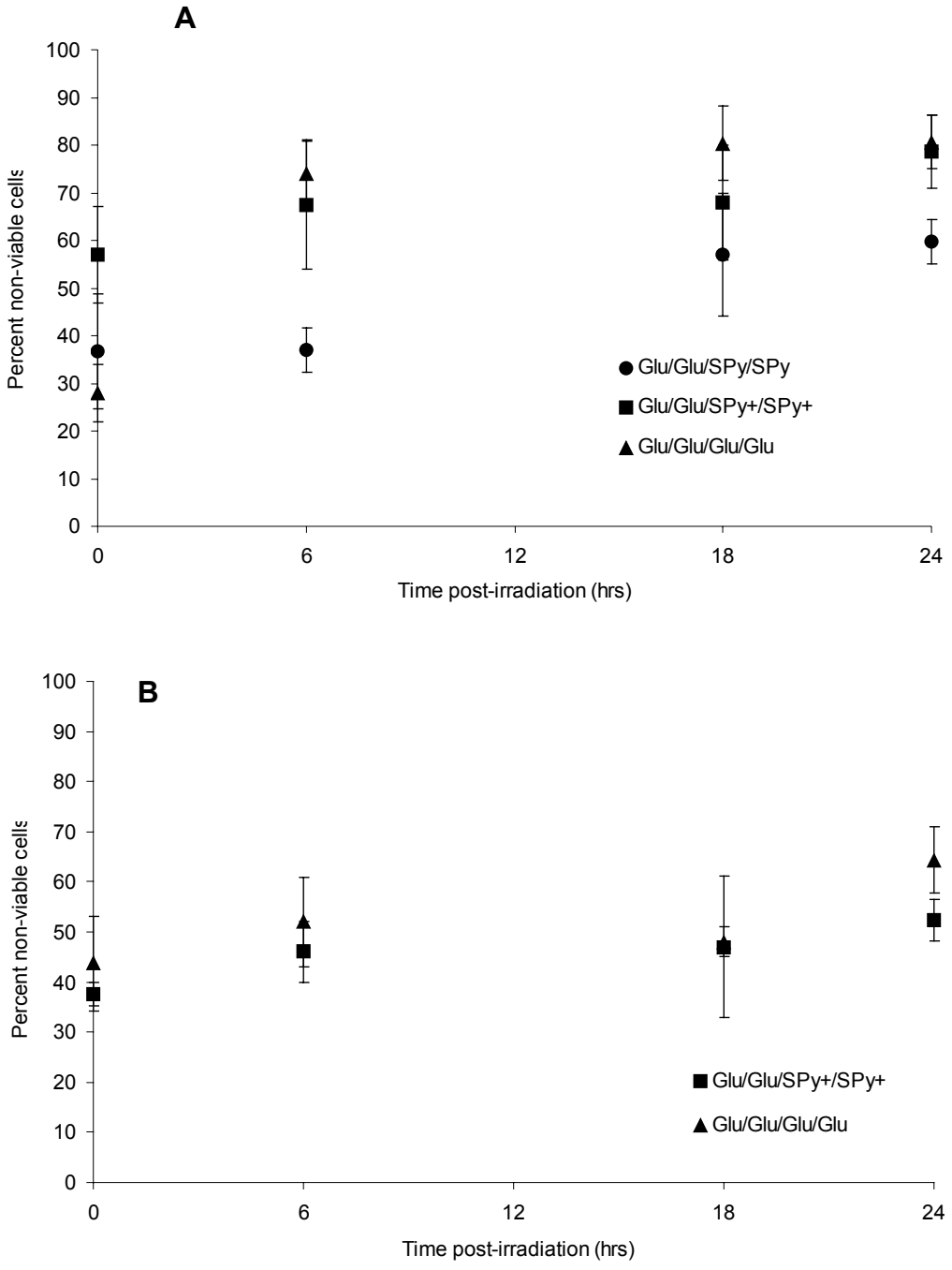

Figure 4.6: Photodynamic activity of **(A)** 10 μM Glu/Glu/Spy/SPy and its charged analogue Glu/Gly/SPy^+/SPy^+ compared to tetraGlu, and **(B)** 2.5 μM of the Glu/Gly/SPy^+/SPy and Glu porphyrin derivatives. MDA-MB-231 cell death over a 24 hr period was quantified by trypan blue staining. Cells were irradiated with white light form a 13 W fluorescent bulb for 20 min (0.9 mW/cm^2 =10.8 kJ/m^2). Results are average of three independent trials ± 1 S.D.

4.3.2 Mixed aryl porphyrin analogues of the porphyrins selected from L-1.

The identity of lead compounds selected from members of library L-1 by the MDA-MB-231 cells was made by MALDI-MS. The two possible isomeric forms (Figure 4.2 compound A and B) were prepared by the statistical synthesis of the winning compounds using only the thioglucose and the thiopyridine and $TPPF_{20}$ followed by chromatographic separation of the six compounds, methylation of the pyridyl nitrogen, and deprotection of the glucosyl groups to yield the target compounds.

The compounds studied in section **4.3A** have the pyridinium attached to the tetrafluorophenyl group on the macrocycle. Thus these compounds have different hydrophobic properties and polarities than porphyrins bearing the pyridinium directly on the meso position that we [9] and other groups [15,37] have studied. Secondly, the molecular dynamics of the pyridinium-S-tetrafluorophenyl bonds have an impact on the molecular properties of these compounds. Thus the molecular properties of the compounds in section **3.4A** that effect intermolecular interactions, especially the formation of aggregates in aqueous solution, may be significantly different than compounds with wherein the pyridinium moiety is directly attached to the porphyrin.

To investigate these differences in hydrophobicity and dynamics on aggregation and cell uptake, we made analogues of the selected compounds wherein the pyridinium is directly attached to the porphyrin. The reaction of pyrrole with pentafluorobenzaldehyde and 4-pyridinecarboxaldehyde (2:1:1) results in a statistical mixture of six porphyrins that are readily separated by flash chromatography. This facile, scalable reaction affords three of the desired porphyrin cores wherein the pentafluorophenyl and pyridyl groups can be separately and quantitatively modified (Figure 4.1 top).

The coupling reactions of thiols to the perfluorophenyl groups of these mixed aryl porphyrins proceeds with similar yields as the parent core $TPPF_{20}$. For example, the protected thioglucose is readily appended to 5,10-di-(pentafluorophenyl)-15,20-di-(pyridin-4-yl)porphyrin (compound g, F/F/Py/Py); and 5,15-di-(pentafluorophenyl)-

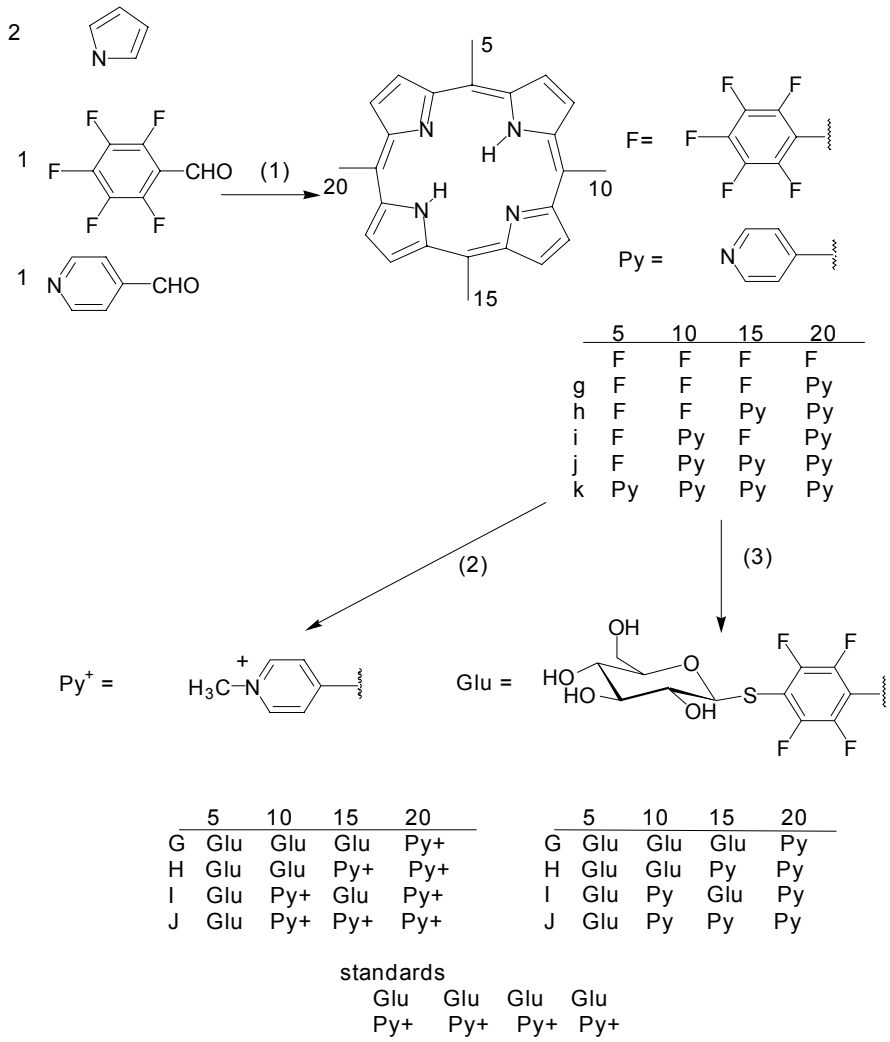

Figure 4.7: Top: general reaction scheme for a typical mixed aryl aldehyde porphyrin synthesis (1) uses a 2:1:1 ratio of pyrrole: pyridenecarboxaldehyde: pentafluorobenzaldehyde in refluxing propionic acid, which yields six isomers [9]. After chromatographic separation of the desired compounds (g-j) (2) the formation of the N-methyl pyridinium salt uses an excess of CH_3I in CH_2Cl_2 and, (3) the substitution of the 4-fluoro group uses the protected thioglucose in DMF at room temperature with diethylamine followed by deprotection with four equivalents of $NaOCH_3$ in CH_3OH.

10,20-di-(pyridine-4-yl)porphyrin (compound h, F/Py/F/Py), using 2 equivalents of the thioglucose in a 4:4:1 (v/v) mixture of DMF/chloroform/methanol as the solvent, while stirring at RT under N_2 to yield the sugar appended porphyrin (Figure 4.7).

Uptake by Breast Cancer Cells

Each of the compounds to be tested (Figure 4.7) were incubated with MDA-MB-231 cells at 5 μM for 20 hrs. Following this period, the cells were rinsed with PBS to remove unbound porphyrin and fixed with 4% paraformaldehyde. Using fluorescence microscopy, the fluorescence intensity and uptake/binding of each isomer was evaluated. Considering the fluorescence micrographs of cells treated with the analogues of the selected compounds from the combinatorial library, Glu/Glu/Glu/Py, $Py^+/Py^+/Py^+/Glu$, $Glu/Glu/Py^+/Py^+$ and the standards $Py^+/Py^+/Py^+/Py^+$, Glu/Glu/Glu/Glu the relative intensities are 1:1.2:1.4:1.2:1.4, respectively (Figure 4.8). The fluorescence intensities of $Glu/Py^+/Glu/Py^+$, Glu/Py/Glu/Py, Glu/Py/Py/Py, and $Glu/Glu/Glu/Py^+$ are negligible. Thus the tetraGlu and $Glu/Glu/Py^+/Py^+$ derivatives are the best binders to this cell line. Consistent with previous reports [4], this study also shows that cationic species bind better than uncharged species.

The uptake of these derivatives, as shown by fluorescence microscopy, can further be investigated by the absorption spectra in aqueous media. Figures 4.9-4.10 shows the overlay plots of both absorption and emission spectra in methanol and PBS.

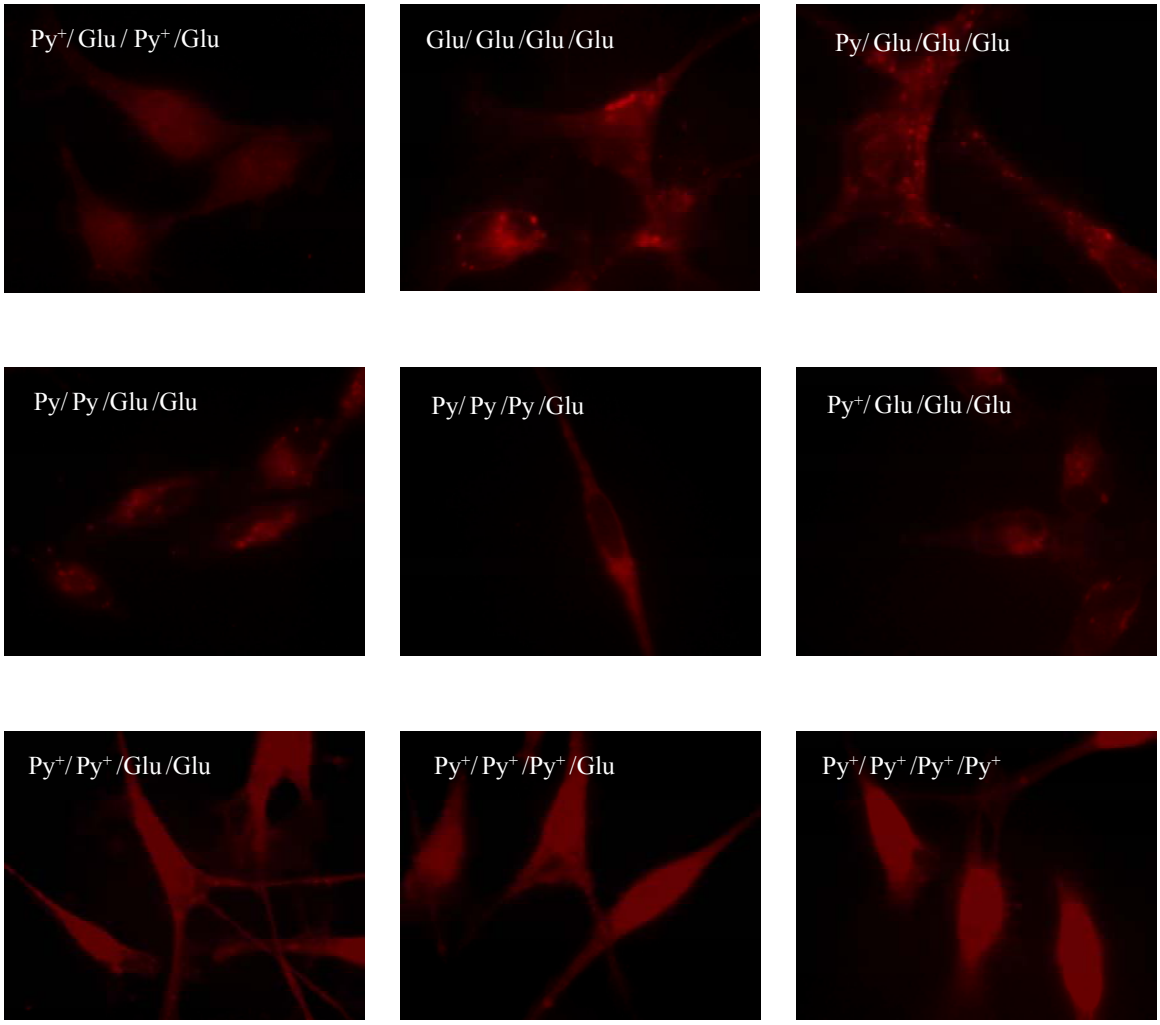

Figure 4.8: Fluorescence microscopy of the mixed aryl porphyrin derivatives (structures are represented in Figure 4.7) derived from the winners of library L-1. These directly link the pyridyl groups to the porphyrin. Each porphyrin is incubated at a 5 μM concentration for 20 hrs with MDA-MB-231 cells. Following removal of unbound porphyrin by rinsing with PBS, the cells are fixed and imaged under identical instrumental conditions. Images are not enhanced and represent magnification at 60X.

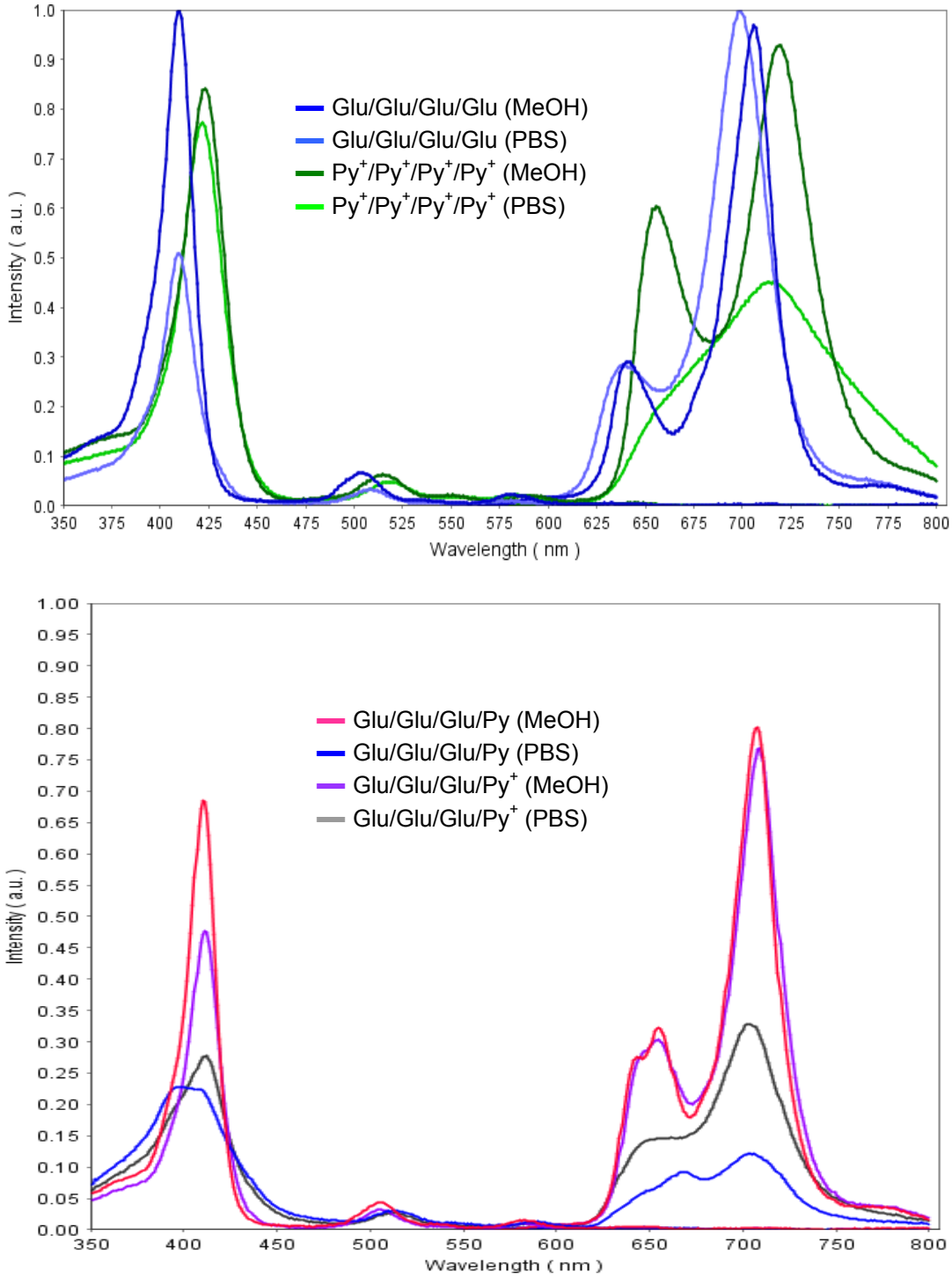

Figure 4.9: Overlay plots of absorption (left) and emission (right) spectra for the mixed aryl pyridyl porphyrins (structures in Figure 4.7) in methanol and aqueous PBS.

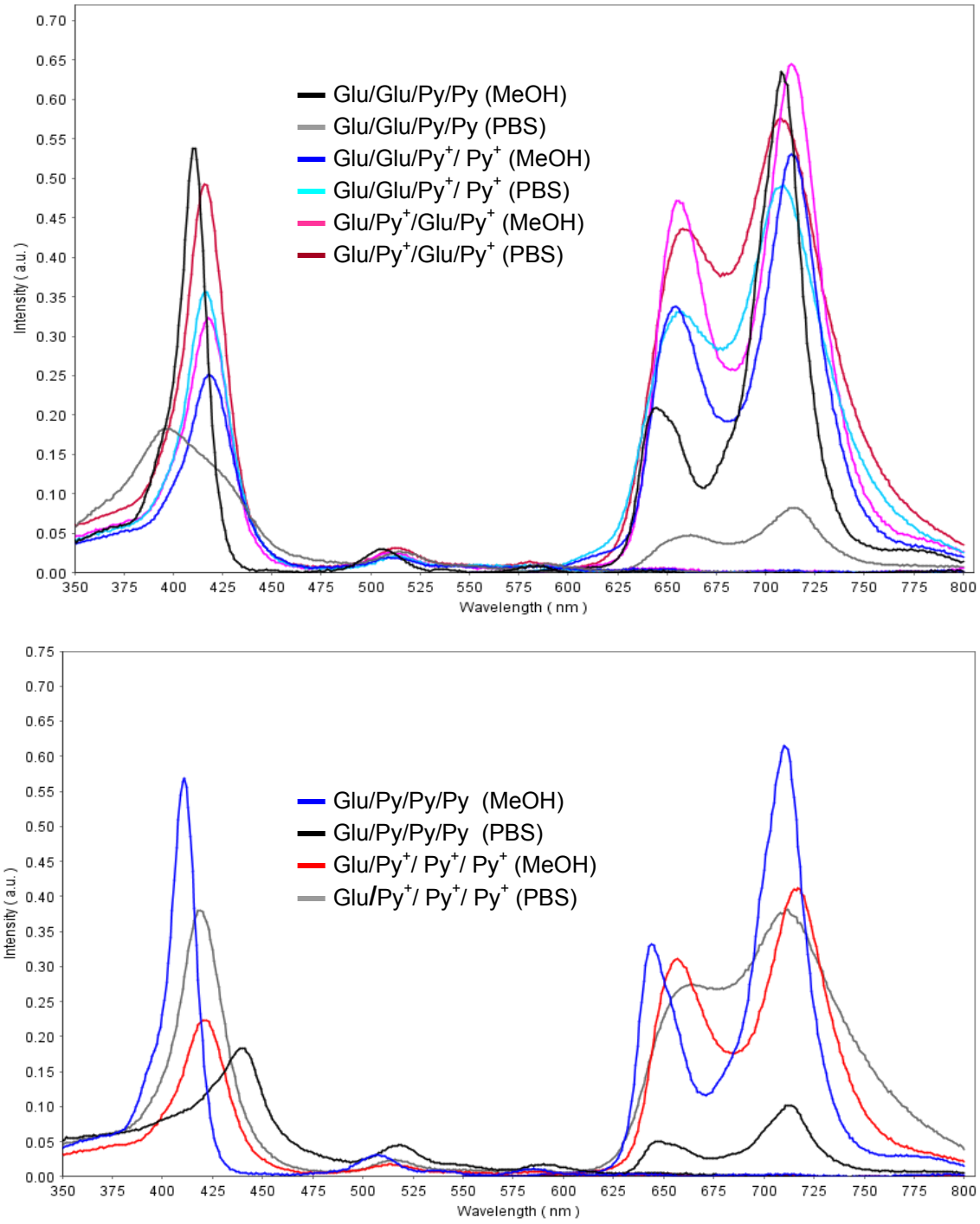

Figure 4.10: Overlay plots of absorption (left) and emission (right) spectra for the mixed aryl pyridyl porphyrins (structures in Figure 4.7) in methanol and aqueous PBS.

In aqueous solvents there is a broadening of the Soret bands and red or blue shifts of Q bands compared to the spectra in methanol or to compounds freely soluble in water such as the tetraPy$^+$ porphyrin. The UV-vis data suggests significant aggregation of especially the uncharged mixed aryl porphyrins, yet some degree of aggregation is indicated for the other macrocycles as well (see structures in Figure 4.7). Despite the peripheral hydrophilic moieties, the porphyrin core remains hydrophobic and pi-stacking is still possible. Additionally, hydrogen bonding and electrostatic interactions are weaker, but not eliminated in water. Since all of these intermolecular forces are in equilibrium, the relative concentrations largely dictate the degree of aggregation – as observed for the tetraGlu compound in Figure 4.5.

	Quantum Yield	
	MeOH	PBS
Cresyl Violet	54%	
Glu/Glu/Glu/Glu	7%	7%
Py/Glu/Glu/Glu	9%	3%
Py/Py/Glu/ Glu	9%	3%
Py/Py/Py/Glu	9%	3%
Py$^+$/Glu/Glu/Glu	10%	7%
Py$^+$/Py$^+$/Glu/Glu	10%	8%
Py$^+$/Glu/Py$^+$/Glu	10%	7%
Py$^+$/Py$^+$/Py$^+$/Glu	10%	7%
Py$^+$/Py$^+$/Py$^+$/Py$^+$	6%	4%

Table 4.1: Fluorescence quantum yield (Φ_F) determinations for the mixed aryl porphyrins 2.5 μM in methanol and aqueous PBS media. Reported literature values for TPP is 11% (in toluene). Cresyl violet is used as a standard.

The triplet quantum yield for TPP is 80% ± 10%, and for $TPPF_{20}$ is >80% [38]. The fluorescence quantum yields of these mixed aryl derivatives in methanol and PBS is shown in Table 4.1. Because these are measured indirectly using a known standard compound, it should be noted that these values may have some systematic error; however all experiments were performed on the same day and using identical concentrations to minimize any experimental errors. These calculations suggest that the tetraGlu, with a reduced fluorescence quantum yield of Φ_F = 7% in methanol and PBS, has a concomitantly greater triplet quantum yield than the parent $TPPF_{20}$. This effect is probably due to both the electronic differences and the "heavy atom effect" of replacing the fluorides with the sulfur atoms. The importance of triplet quantum yield is that it is the triplet state that sensitizes the formation of singlet oxygen, which as mentioned before, is the dominant pathway to cellular necrosis or induction of apoptosis. Thus the quantum yields of singlet oxygen (Φ_{ox}) are expected to be greater compared to nonfluorinated porphyrin derivatives such as tetraphenylporphryin. Although the fluorescence quantum yield of these porphyrins is 6-10% in methanol and 3-8% in PBS, the large extinction coefficient ($\sim 2\times10^5$ M/cm) and extended integration times permits the observation of nM concentration by fluorescence microscopy. It should be noted that the major porphyrin derivatives studied in this research have nearly equivalent fluorescence quantum yields in PBS media; therefore the relative intensities should be proportional to the quantities of porphyrins inside the cells. The exceptions to this are the macrocycles with neutral, pyridyl groups, which may be obfuscated by a small degree of aggregation that is not clearly visible in the UV-visible spectra.

4.4 Synthesis of a small solution phase combinatorial library using tetrakis(pentafluorophenyl)porphyrin and primary amines

Thiol substrates are not exclusive to substitution of the 4-fluoro groups on the $TPPF_{20}$ platform. As illustrated in Chapter 2, amines are efficiently substituted onto the porphyrin with microwave heating in NMP. This section presents a small solution phase combinatorial library using histamine and aminopentane as proof-of-principle reactions for $TPPF_{20}$ (Figure 4.11). A mixture of the three primary amines used in chapter 3 (protected derivatives of a polyethylene glycol, an ethylenediamine, and a lysine) in NMP and microwave heating did not result in the expected library of 21 compounds and was incomplete in since not all fluorines were replaced. The standard reaction of 20 equivalents of histamine and aminopentane, both of which are primary amines, with $TPPF_{20}$ (5 mg, 5.1 μmol) at room temperature in the dark, overnight, resulted in the disappearance of the starting porphyrin as visualized on thin layer chromatography.

For a two substituent reaction, a 6-membered library is expected. However if the reaction is stopped immediately after all starting $TPPF_{20}$ has reacted, there remains a mixture that contains the mono-, di-, and tri-fluoro -substituted products (e.g. it is more similar to a 21-member library wherein the F is one of the substituents. Since 5,10- and 5,15- isomers have the same molecular weights, their peaks overlap and are indistinguishable by mass spectrometry. The product distribution is observed in the ESI-MS of the histamine and aminopentane combinatorial library (Figure 4.11). Although, there is incomplete substitution, thus incomplete formation of all the expected products, longer reaction times may ameliorate this problem. Thus we observe in the ESI-MS more than the expected six compounds.

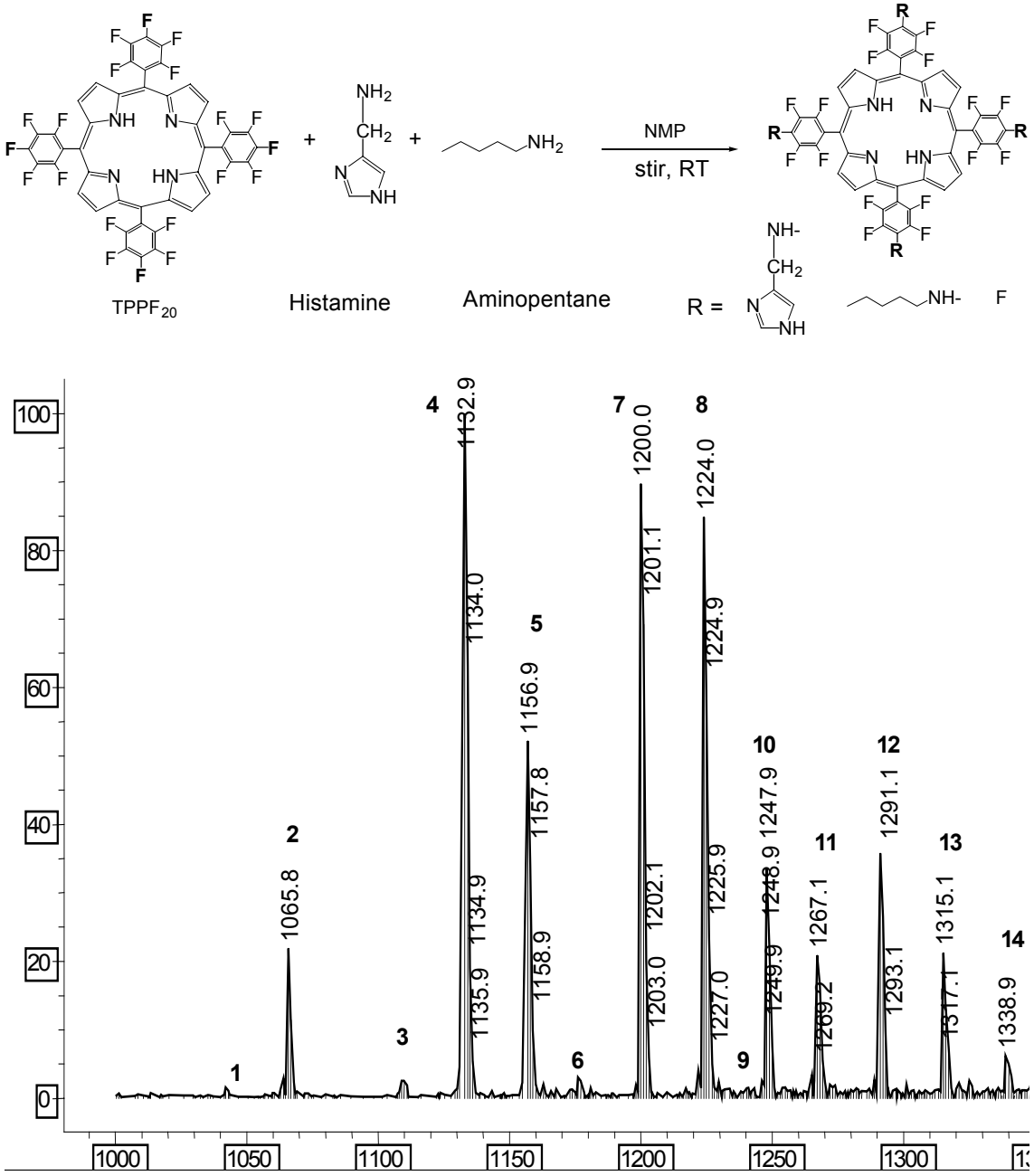

Figure 4.11: (Top) Reaction of $TPPF_{20}$ with the primary amines histamine and aminopentane at room temperature in NMP for 24 hours does not lead to complete substitution of the 4-fluoro groups, thus yields a library of up to 21 compounds. This library is characterized by ESI-MS (bottom).

Member	m/z	5	10	15	20
1	1041	F	F	F	Pen
2	1065	F	F	F	His
3	1108	F	F	Pen	Pen
	"	F	Pen	F	Pen
4	1132	F	F	Pen	His
	"	F	Pen	F	His
5	1156	F	F	His	His
	"	F	His	F	His
6	1175	F	Pen	Pen	Pen
7	1199	F	Pen	His	Pen
	"	F	Pen	Pen	His
8	1223	F	Pen	His	His
	"	F	His	Pen	His
9	1243	Pen	Pen	Pen	Pen
10	1247	F	His	His	His
11	1266	Pen	Pen	Pen	His
12	1290	Pen	Pen	His	His
	"	Pen	His	Pen	His
13	1314	Pen	His	His	His
14	1338	His	His	His	His

Table 4.2: Possible compounds for the $TPPF_{20}$ library using histamine (His) and aminopentane (Pen) primary amines.

4.5 Synthesis of a small solution phase combinatorial library using tri(pentafluorophenyl)corrole

Corroles are porphyrinoid macrocycles missing one of the porphyrin methylene bridges and are found in nature as compounds such as vitamin B-12. In general, free base corroles are found to have a greater fluorescence quantum yield than porphyrins because they have a direct pyrrole-pyrrole linkage [39-41]. Thus these macrocycles have been proposed a fluorescence sensors and fluorescence imagining agents. Because of the 3-charge of the free base, these compound stabilize high valent metal ions and/or metals that are suitable for contrast agents such as Ga(III). Since $TPPF_{20}$ porphyrin has been shown to react easily with a variety of substrates, we hypothesized that corroles bearing three pentafluorophenyl moieties ($triPCF_{15}$) could also be substituted by suitable nucleophiles such as the above thio reagents [5,25]. Since the fluorinated groups on $triPCF_{15}$ are orthogonal to the corrole macrocycle, as they are on $TPPF_{20}$, the reactivity is expected to be similar. The synthesis of a small combinatorial library based on the $triPCF_{15}$ core was attempted using the conditions developed for the 21-membered library using the protected thio sugar substitution (Figure 4.12).

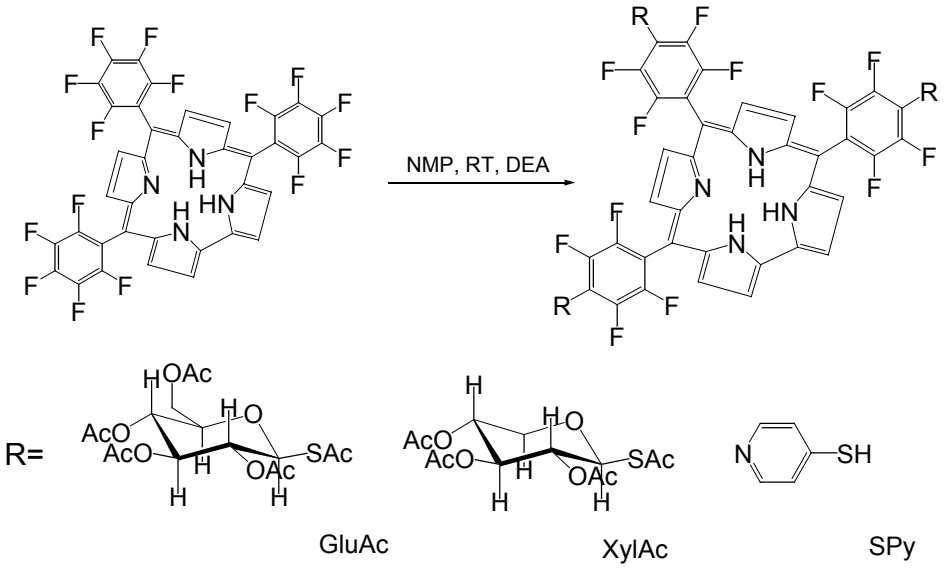

Figure 4.12: Solution phase combinatorial reaction scheme using tri(pentafluorophenyl)corrole. Protected glucose and xylose thioacetates, as well as thio pyridine are used as the nucleophiles. Three substituents would lead to a 16-member library (See Figure 4.2).

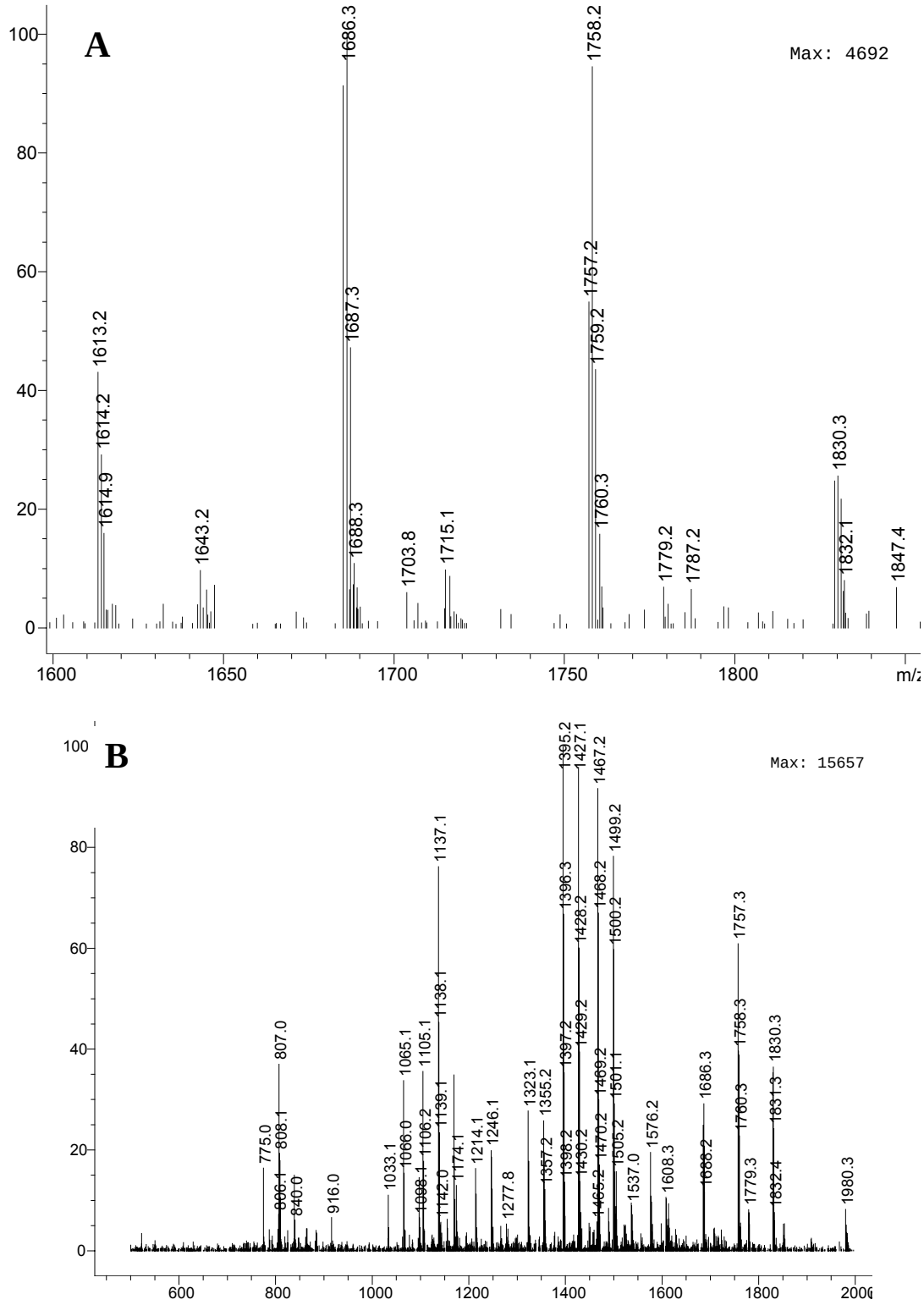

Figure 4.13: ESI-MS of the corrole library using **(A)** only glucose and xylose thioacetates where six compounds are expected, and **(B)** the two thiosugars as well as thio pyridine as the nucleophiles, where 16 compounds are expected. Since the isomers have the same molecular weights, the number of isobaric compounds for library A is four, and for library B is 10.

With triPCF$_{15}$ corrole a library with two substituents yields six compounds but there are two sets of isomers so there are only four isobaric peaks expected in the mass spectra with two representing isomeric forms. Similarly, in the case of three substituents, one expects 18 compounds, but only 10 have unique molar masses because of the various positional isomers. In the 21-membered library synthesis using the TPPF$_{20}$ platform, dimethyl formamide (DMF) was used, but the substitution chemistry works better for the corrole system using N-methylpyrrolidone (NMP). This indicates a solvent effect on the reactions of the corrole versus porphyrin, which may be a result of differences in the electron withdrawing effects of corroles in comparison to porphyrins. The acidity of the corrole may play an important role in these reactions and solvents [42].

Figure 4.13A shows the ESI-MS of the crude reaction mixture, where only the thiosugars where used in the substitution reaction. The reaction was complete (as judged by the expected product distributions and peak intensities in the ESI-MS) using three equivalents of the thioglucose and thioxylose acetate protected sugars in NMP stirring overnight in the dark. However, the attempt to create a 18-membered library on a corrole platform using thio pyridine in addition to the protected sugars proved unsuccessful. Evaluation of the ESI-MS spectra of the crude product mixture (Figure 4.13 B) showed only partially substitution of the 4-fluoro groups on the corrole systems. Neither an increase in the quantity of the thio derivatives nor an increase reaction times (from hrs to days) resulted in complete reactions. The ESI-MS showed a distribution of trisubstituted as well as disubstituted thiosugars appended corroles, but peaks corresponding to thio pyridine moieties coupled to the corrole were largely absent.

1	F/F/F	796
*2/3	F/F/Xyl	1068
*4/5	F/F/Glu	1140
*6/7	F/Xyl/Xyl	1340
8	Glu/F/Xyl	1412
9	F/Glu/Xyl	1412
10	F/Xyl/Glu	1412
*11/12	F/Glu/Glu	1484
13	Xyl/Xyl/Xyl	1612
*14/15	Glu/Xyl/Xyl	1684
*16/17	Glu/Glu/Xyl	1756
18	Glu/Glu/Glu	1828

1	F/F/F	796
*2/3	F/F/ThioPy	887
*4/5	F/ThioPy/ThioPy	978
*6/7	XylSAc/F/F	1068
8	ThioPy/ThioPy/ThioPy	1069
*9/10	GluSAc/F/F	1140
11	XylSAc/F/ThioPy	1159
12	GluSAc/F/ThioPy	1231
*13/14	XylSAc/ThioPy/ThioPy	1250
*15/16	GluSAc/ThioPy/ThioPy	1322
*17/18	XylSAc/XylSAc/F	1340
19	GluSAc/XylSAc/F	1412
*20/21	XylSAc/XylSAc/ThioPy	1431
*22/23	GluSAc/GluSAc/F	1484
24	GluSAc/XylSAc/ThioPy	1503
*25/26	GluSAc/GluSAc/ThioPy	1575
27	XylSAc/XylSAc/XylSAc	1612
*28/29	GluSAc/XylSAc/XylSAc	1684
*30/31	GluSAc/GluSAc/XylSAc	1756
32	GluSAc/GluSAc/GluSAc	1828

Table 4.3: Possible compounds for the corrole libraries
* indicates an isomer for this compound exist

4.6 Conclusion

A simple, one-step reaction to functionalize the $TPPF_{20}$ platform with different primary thio reagents results in solution phase combinatorial libraries. This high yield reaction increases the repertoire of 'click' reactions [43]. These porphyrin libraries bearing carbohydrate, polar pyridyl, and alkane moieties were synthesized and characterized by mass spectrometry. A proof-of-principle method based on mass spectral identification of winning compounds selected by human breast cancer MDA-MB-231 cells indicates that two pyridyl and two sugar motifs are important for binding. Synthesis and evaluation of the two possible isomers containing two pyridyls and two glucosyl moieties reveals that the isomer with the sugars on one side and the polar groups on the other side of the macrocycle binds this cell line better than the arrangement with the sugars on opposite sides.

In addition, although nucleophilic thio and amine reagents can substitute para fluorine atoms of the perfluorophenyl groups, the reactivity of these nucleophiles are not uniform towards the $triPCF_{15}$ system and thus at present the corrole is not as efficient as a core for the formation of solution phase combinatorial libraries at the $TPPF_{20}$.

4.7 References

(1) Drain, C. M.; Bazzan, G.; Milic, T.; Vinodu, M.; Goeltz, J. C. *Israel J. Chem.* **2005**, *45*, 255-269.

(2) Drain, C. M.; Chen., X. In *Encyclopedia of Nanoscience & Nanotechnology*; Nalwa, H. S., Ed.; American Scientific Press: New York, 2004; Vol. 9.

(3) Milic, T. N.; Chi, N.; Yablon, D. G.; Flynn, G. W.; Batteas, J. D.; Drain, C. M. *Angew. Chem., Int. Ed.* **2002**, *41*, 2117-2119.

(4) Chen, X.; Drain, C. M. *Drug Design Rev.* **2004**, *1*, 215-234.

(5) Chen, X.; Hui, L.; Foster, D. A.; Drain, C. M. *Biochemistry* **2004**, *43*, 10918-10929.

(6) Retsek, J. L.; Drain, C. M.; Kirmaier, C.; Nurco, D. J.; Medforth, C. J.; Smith, K. M.; Sazanovich, I. V.; Chirvony, V. S.; Fajer, J.; Holten., D. *J. Am. Chem. Soc.* **2003**, *125*, 9787-9800.

(7) Drain, C. M.; Gentemann, S.; Roberts, J. A.; Nelson, N. Y.; Medforth, C. J.; Jia, S.; Simpson, M. C.; Smith, K. M.; Fajer, J.; Shelnutt, J. A.; Holten, D. *J. Am. Chem. Soc.* **1998**, *120*, 3781-3791.

(8) Lehn, J.-M. *Proc. Natl. Acad. Sci., USA* **2002**, *99*, 4763-4768.

(9) Drain, C. M.; Gong, X.; Ruta, V.; Soll, C. E.; Chicoineau, P. F. *J. Comb. Chem.* **1999**, *1*, 286-290.

(10) Mansuy, D. *Coord. Chem. Rev.* **1993**, *125*, 129-141.

(11) Merlau, M. L.; Mejia, M. d. P.; Nguyen, S. T.; Hupp, J. T. *Angew. Chem. Int. Ed.* **2001**, *40*, 4239-4242.

(12) Suslick, K. S. In *The Porphyrin Handbook*; Kadish, K. M., Smith, K. M., Guilard, R., Eds.; Academic Press, New York, 2000.

(13) Drain, C. M.; Hupp, J. T.; Suslick, K. S.; Wasielewski, M. R.; Chen, X. *J. Porphyrins Phthalocyanines* **2002**, *6*, 243-258.

(14) Suslick, K. S.; Rakow, N. A. *Artificial Chemical Sensing* **2001**, 8-14.

(15) Bonnett, R. *Chem. Soc. Rev.* **1995**, 19-33.

(16) Liu, M. O.; Tai, C.-H.; Sain, M.-Z.; Hu, A. T.; Chou, F.-I. *J. Photochem. Photobiol., A: Chem* **2004**, *165*, 131-136.

(17) Schneider, R.; Schmitt, R.; Frochot, C.; Fort, Y.; Lourette, N.; Guillemin, F.; Muller, J.-F.; Barberi-Heyob, M. *Bioorg. Med. Chem.* **2005**, *13*, 2799-2808.

(18) Sternberg, E. D.; Dolphin, D.; Bruckner, C. *Tetrahedron* **1998**, *54*, 4151--4202.

(19) Kocisko, D. A.; Caughey, W. S.; Race, R. E.; Roper, G.; Caughey, B.; Morrey, J. D. *Antimicrob. Agents Chemother.* **2006**, *50*, 759-761.

(20) Kocisko, D. A.; Engel, A. L.; Harbuck, K.; Arnold, K. M.; Olsen, E. A.; Raymond, L. D.; Vilette, D.; Caughey, B. *Neuroscience Letters* **2005**, *388*, 106-111.

(21) Priola, S. A.; Raines, A.; Caughey, W. S. *Science* **2000**, *287*, 1503-1506.

(22) Caughey, W. S.; Raymond, L. D.; Horiuchi, M.; Caughey, B. *Proc. Natl. Acad. Sci.* **1998**, *95*, 12117-12122.

(23) Priola, S. A.; Caughey, B.; Caughey, W. S. *Curr. Opin. Microbiol.* **1999**, *2*, 563-566.

(24) Pasetto, P.; Chen, X.; Drain, C. M.; Franck, R. W. *Chem. Commun.* **2001**, 81-82.

(25) Samaroo, D.; Soll, C. E.; Todaro, L. J.; Drain, C. M. *Org. Lett.* **2006**, *8*, 4985-4988.

(26) Kamat, P. V.; Das, S.; Thomas, K. G.; George, M. V. *J. Phys. Chem.* **1992**, *96*, 195-199.

(27) Bonnett, R.; Martinez, G. *Tetrahedron* **2001**, *57*, 9513-9547.

(28) Battioni, P.; Brigaud, O.; Desvaux, H.; Mansuy, D.; Traylor, T. G. *Tetrahedron Lett.* **1991**, *32*, 2893-2896.

(29) Chen, X., Carbohydrate conjugated porphyrins targeting photodynamic therapy (PDT): potent inducers of cancer cell death both by necrosis and apoptosis; solution-phase combinatorial libraries with whole cell selection method, The Graduate School and University Center of the City of New York, 2004.

(30) Guliaev, A. B.; Leontis, N. B., 1999; Vol. 38.

(31) Pasternack, R. F.; Goldsmith, J. I.; Szep, S.; Gibbs, E. J., 1998; Vol. 75.

(32) Castriciano, M. A.; Romeo, A.; Scolaro, L. M. *J. Porphyrins Phthalocyanines* **2002**, *6*, 431-438.

(33) Hirohara, S.; Obata, M.; Ogata, S.; Kajiwara, K.; Ohtsuki, C.; Tanihara, M.; Yano, S. *J. Photochem. Photobiol. B: Biol.* **2006**, *84*, 56-63.

(34) Yu, S.-W.; Wang, H.; Poitras, M. F.; Coombs, C.; Bowers, W. J.; Federoff, H. J.; Poirier, G. G.; Dawson, T. M.; Dawson, V. L. *Science* **2002**, *297*, 259-263.

(35) Lam, M.; Oleinick, N. L.; Nieminen, A.-L. *J. Biol. Chem.* **2001**, *276*, 47379-47386.

(36) Oleinick, N. L.; Morris, R. L.; Belichenko, I. *Photochem. Photobiol. Sci.* **2002**, *1*, 1-21.

(37) Sternberg, E. D.; Dolphin, D.; Bruckner, C. *Tetrahedron* **1998**, *54*, 4151-4202.

(38) Yang, S. I.; Seth, J.; Strachan, J.-P.; Gentlemann, S.; Kim, D.; Holten, D.; Lindsey, J. S.; Bocian, D. F. *J. Porphyrins Phthalocyanines* **1999**, *3*, 117-147.

(39) Gross, Z.; Galili, N.; Saltsman, I. *Angew. Chem. Int. Ed. Engl.* **1999**, *38*, 1427-1429.

(40) Gross, Z.; Mahammed, A. *J. Porphyrins Phthalocyanines* **2002**, *6*, 553-555.

(41) Gross, Z.; Galili, N.; Simkhovich, L.; Saltsman, I.; Botoshansky, M.; Blaser, D.; Boese, R.; Goldberg, I. *Org. Lett.* **1999**, *1*, 599-602.

(42) Mahammed, A.; Weaver, J. J.; Gray, H. B.; Abdelas, M.; Gross, Z. *Tetrahedron Lett.* **2003**, *44*, 2077-2079.

(43) Kolb, H. C.; Finn, M. G.; Sharpless, K. B. *Angew. Chem. Int. Ed.* **2001**, *40*, 2004-2021.

Chapter 5: Future Directions to this Research

5.1 A Study of Several Glycosylated Porphyrins across Several Cancer Cell Lines and Tissue Types

In Chapter 4, the synthesis and PDT effect of several glycosylated porphyrin-based photosensitizers was studied [1,2]. In Chapter 2 the preparation and chapter 3 the PDT effect, of porphyrins appended with polyethyleneglycol (PEG) units, ethylene diamines (EDA) and polylysines (Lys) were examined. Each class of chemical entity was attached to the core porphyrin, tetrakis(pentafluorophenyl) porphyrin ($TPPF_{20}$) – since the reactivity of the *para* fluorine group often affords products in 90 + % yields. Earlier studies showed that MDA-MB-231 breast cancer cells preferred the tetraglucose rather than the tetragalactose derivatives of $TPPF_{20}$ [1]. It was also demonstrated that the tetraglucose porphyrin was selective for cancer cells over normal cells by a factor of 5 – 10, using 3Y1 mouse fibroblast. In addition to glucose, it was also demonstrated that the substitution pattern of cationic pyridyl moieties on the porphyrin macrocycle is important [2].

Porphyrins appended with four amphipathic amines form stable porphyrin nanoparticles that were shown to be taken up selectively in MDA-MB-231 cancer cells over 3Y1 normal mouse fibroblast (Chapter 3). In addition, these porphyrin nanoparticles elicited cell death with a two-dose light irradiation or by allowing the nanoparticle to disaggregate with time. An important finding is that for each porphyrin derivative, it is necessary to examine the degree of aggregation of the porphyrin in aqueous cell culture solutions (e.g. PBS) by absorption and emission spectra. The optical

spectra easily revealed the degree of aggregation by the extent of broadening and red/blue shifts in the absorption bands.

For PDT, an agent that strongly absorbs in the 650 – 750 nm red region is preferred, because this allows for better tissue penetration. *Since there are numerous cancer cell lines, each with specific targeting and uptake issues, it is likely that one PDT agent will NOT be suitable for all types of cancer.* Thus in this section, the uptake and selectivity of several porphyrin derivatives bearing functionalities known to impart selectivity to cancer and other types of cells are rapidly screened using a method based on fluorescence microscopy.

5.1.1 Experimental Procedures

Cell Culture

MDA-MB-231 cells maintained in DMEM, 10% BCS, 1% antimycotic at 37ºC and in 5% CO_2 atmosphere were plated onto coverslips in cell culture dishes. N18 were maintained in DMEM, 5% FBS and 1% Penn/Strep. B16-F10 were maintained in DMEM, 10% FBS and 1% Penn/Strep. Porphyrins (dissolved in methanol) were added to the cultures to a final concentration of 2 μM such that there was never more than 0.5% methanol in the solution. After 20 h incubation, cells were washed with PBS 3 – 5 times and fixed in 4% paraformaldehyde solution for 10 min at RT. The cells were then washed with PBS 3 times. The coverslips were mounted onto glass slides in Dako fluorescent mounting medium, and then visualized using a Nikon Optiphot 2 fluorescence microscope. Images were captured as JPEG files at 60X magnification, with excitation: 505 – 565 nm and emission at 565 – 685 nm. For each set of experiments, cells were cultured and the fluorescence images were taken under identical culture and microscopic

conditions. For quantitative studies, the image intensities of the cells in the fluorescence micrographs were calculated by FLim program (coded by Nathan Stevens, see Chapter 3).

5.1.2 Results and Discussion

The cancer cell lineages used in these studies were MDA-MB-231 (human breast cancer), B16-F10 (mouse melanoma) and N18 (mouse neuroblastoma) [3]. The MDA-MB-231 cells have an up-regulation of glucose receptors on the cell membrane [1], which leads to the uptake of a tetraglucose $TPPF_{20}$ derivative and its activity in inducing necrosis and apoptosis [1]. As noted above, it is not expected that the tetraglucose porphyrin will impart selectivity to all other cell lines and types. Because each cell type has different cell walls composed of cadre of different lipids that are imbedded with a variety of structural and functional proteins (e.g. channels, pores, transporters, receptors, glycoproteins, etc.), small molecules, and other structures, the affinity of exogenous agents such as the porphyrin derivatives to each cell line is expected to be different. N18 cell line has glutamate receptors on its membrane [4], whereas B16-F10 has up-regulation of integrin [5] receptors. This leads to the conclusion that all cancer types cannot be treated by one universal agent/drug – in most cases they are tissue or cell-type dependent.

Exploiting the fluorescent properties of porphyrins affords a rapid screening assay for the binding/uptake of these compound using fluorescence microscopy and a quantitative analysis of the resulting micrographs. By these means several porphyrins can be evaluated simultaneously. The culturing of each individual cell line is relatively easy and follows standard cell culture protocol. Briefly, all cell lines require incubation

at 37°C, 5% CO_2 in the dark, in Dulbecco's modified eagle medium supplemented with either 10% bovine calf serum or 5% fetal bovine serum. The fluorescence assays require, in most cases, an overnight incubation of a specific concentration of the porphyrin with the cells. After removing any unbound porphyrin, the cells are fixed to glass slides and observed under the optical and fluorescence microscope. Depending on the intensities of the fluorescence output, conclusions can be formed as to the degree of uptake and binding affinities of the porphyrins to the cell lines/tissue types.

Four glycosylated porphyrins (synthesis reported in Chapter 4) were tested across the various cell lines at a 2 μM concentration. The structures of the porphyrins and the cellular uptake are presented in Figure 5.1. From the fluorescence micrographs it is apparent that the tetracationic pyridinium porphyrin (tetraPy^{4+}) is bound to the cells better than any of the other derivatives for each tissue type. It should be noted that tetraPyr^{4+} has been studied for over 40 years and is known to be a poor PDT agent largely because it does not inter into the cells/tissues but binds to the cell surface [6]. When comparing 5,15- versus the 5,10- glycosylated porphyrins, clearly the 5,10- isomer is preferentially taken up across MDA-MB-231 and N18 cells; however each is taken up to a similar extent in B16-F10 cells.

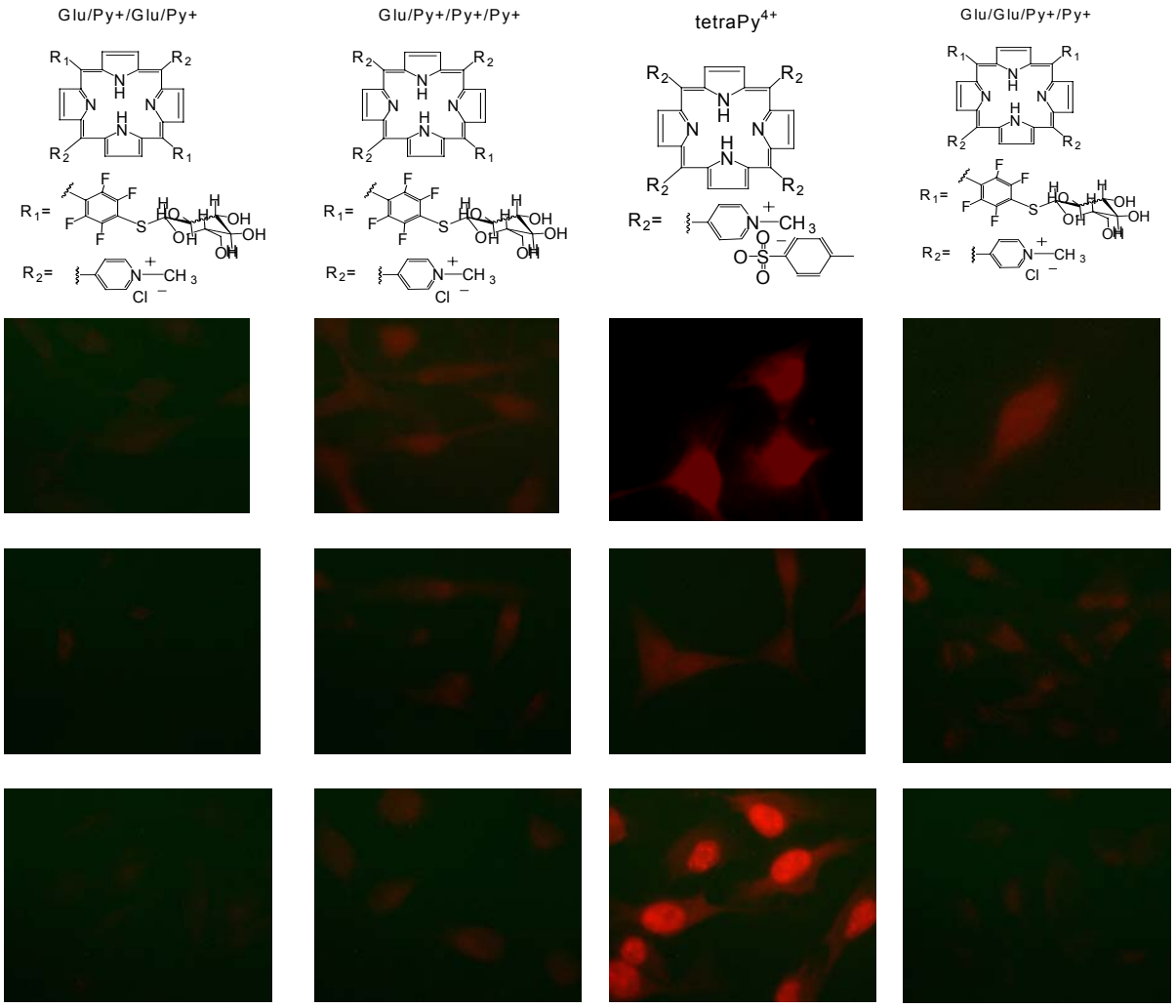

Figure 5.1: Comparison of thioglycosylated porphyrins across different cell lines at a concentration of 2 μM. Row 1: MDA-MB-231 cells (breast cancer), Row 2: N18 cells (mouse neuroblastoma), Row 3: B16-F10 cells (mouse melanoma). Cells were incubated with the porphyrin derivative for 24 hours, rinsed three times with PBS, and fixed onto glass slides. Fluorescence images were taken under identical conditions and the images are the raw data (not contrast enhanced).

The 5,15- glycosylated porphyrin shows the poorest uptake across all cell lines, reaffirming that the position of the charges on a porphyrin is important. The number of cationic charges is also of importance, since the Glu/Py^+/Py^+/Py^+ shows greater binding than Glu/Glu/Py^+/Py^+ dicationic porphyrin.

5.1.3 Conclusion

In summary, saccharide functional groups were appended onto the $TPPF_{20}$ (Chapter 3); these derivatives were tested across a variety of cancer cell types, with the intention of discovering new motifs and strategies for development of new PDT agents. This study yielded several relevant outcomes based on the specificity of the type of cancer cell line to one or more of the porphyrin species tested. Although, most of the derivatives were similar in structure or contained the same number of cationic charges, the uptake across the various tissue types differed. In addition, the degree of uptake (relative fluorescence intensity) for a particular porphyrin across the tissue type varied as well.

It is important to note that the fluorescence micrographs used in this assay do not readily differentiate between binding to the cell walls and uptake into the cell, thus these results do not a priori correlate to effectiveness as PDT agents (e.g. the $tetraPy^{4+}$). Therefore, the next step of these studies should look at the PDT effect against these cell lines, rather than the much used MDA-MB-231.

5.2 Porphyrins are anti-HIV agents

PDT agents such as porphyrins and phthalocyanines preferentially accumulate in tumors due to an increased cellular proliferation rate, phagocytosis, or receptor-mediated uptake [7-9]. The photosensitizing agents are used according to their efficiency in producing singlet oxygen, which is very reactive and damages lipids, nucleic acids and proteins. Therefore, it is presumed that membrane damage (cell, nuclear, organelle) may be a principle mechanism for cell death. The potential applications of porphyrins go well beyond their current use as anti-cancer agents, as several labs have reported that they may be effective for anti-bacterial and anti-viral applications, i.e. against human immunodeficiency virus (HIV) [10-16].

AIDS is a global problem, one that affects millions of people across all continents. The entry of HIV – the virus that causes AIDS – into cells is a complex process that is mediated by the viral envelope glycoproteins and receptors present on the host cell membrane. This glycoprotein, gp120, is the first step in viral entry. By targeting its binding to the CD4 receptor, HIV entry into cells can possibly be prevented. The goal of this mini-project was to identify modified porphyrins that could potentially be used as microbicides to provide a defense against infection by the sexually transmitted virus. An extensive introduction of the use of porphyrins as anti-HIV agents was presented in Chapter 1. Briefly, the literature hypothesizes that this inhibition occurs because porphyrins bind to the V3 loop of gp120, which is a positively charged structure. This binding may disrupt and interfere with the initial gp120-CD4 binding or the subsequent gp120-coreceptor interaction, which would lead to the failure of membrane fusion and

viral entry into the cell [17-19]. The study evaluated porphyrins that can be used as inhibitors of CD4-gp120 complex formation.

5.2.1 Experimental Procedures

General

Porphyrins were commercially available from Sigma-Aldrich, Frontier Scientific, or Kava Technology.

ELISAs

(A) Inhibition assay of CD4-gp120 binding

ELISA wells were coated overnight at 4 °C with 100 μl of sCD4 (Progenics, 10 μg/ml in coating buffer, pH 9.6), washed 4 - 5 times with 0.05 % Tween 20/1X PBS washing buffer (WB), and blocked in 100 μl blocking buffer (1.5 % FBS/RPMI) at 37 °C for 1-2 h. Simultaneously, porphyrins (100 μg/mL, 1:2 dilution) were preincubated with 150 μl of HIV-1 gp120IIIB (Progenics, 5 μg/ml) for 1 h at 37 °C. After five washes with WB, wells were incubated with 100 μL of the preincubated gp120/porphyrin mixture for 1 h at 37 °C. After six washes with WB, 100 μL of a 1:1000 dilution of alkaline phosphatase-conjugated streptavidin (Life Technologies) was added and incubated for 1 h at 37 °C. Bound gp120 was detected by anti-gp120 biotin-conjugated antibodies. Following six washes with WB, the assay was developed at room temperature in the dark until color development (5 - 10 min) with *p*-nitrophenyl phosphate substrate (Sigma) and monitored at 405 nm.

(B) Competition assay of V3 loop of gp120

ELISA wells were coated overnight at 4 °C with 100 μL of sheep anti-C (α-C5) terminus of gp120 (1 μg/mL in coating buffer, pH 9.6), washed 4 - 5 times with WB, and

blocked in 100 μL blocking buffer (1.5 % FBS/RPMI) at 37 °C for 1 - 2 h. Simultaneously, 120 μl porphyrins (100 μg/mL, 1:2 dilution) and 120 μl mAbs (1 μg/mL 694, 447, 1418 (1:10 dilution)), respectively were preincubated with 120 μL of HIV-1 gp120IIIB (Progenics, 1ug/mL) for 1 h at 37 °C. After five washes with WB, wells were incubated with 100 μL of the preincubated gp120/porphyrin and gp120/mAbs mixtures for 1 h at 37 °C. After six washes with WB, 100 μL of monoclonal antibody against V3 loop, 694-Biotin antibody (1 μg/mL) or 100 μL of 447-Biotin antibody (1 μg/mL) was added and incubated for 1 h at 37 °C. After six washes, 100 μL of a 1:1000 dilution of alkaline phosphatase-conjugated streptavidin or alkaline-phosphatase conjugated human IgG-Fc was added and incubated for 1 h at 37 °C. Following six washes with WB, the assay was developed at room temperature in the dark until color development (5 - 10 min) with *p*-nitrophenyl phosphate substrate and monitored at 405nm.

5.2.2 Results & Discussion

By testing anionic and cationic water-soluble porphyrins, this will determine which inhibits the binding of antibodies to the V3 loop of gp120. To test for antiviral activity, enzyme-linked immunosorbent assays (ELISA) were used to test for binding and

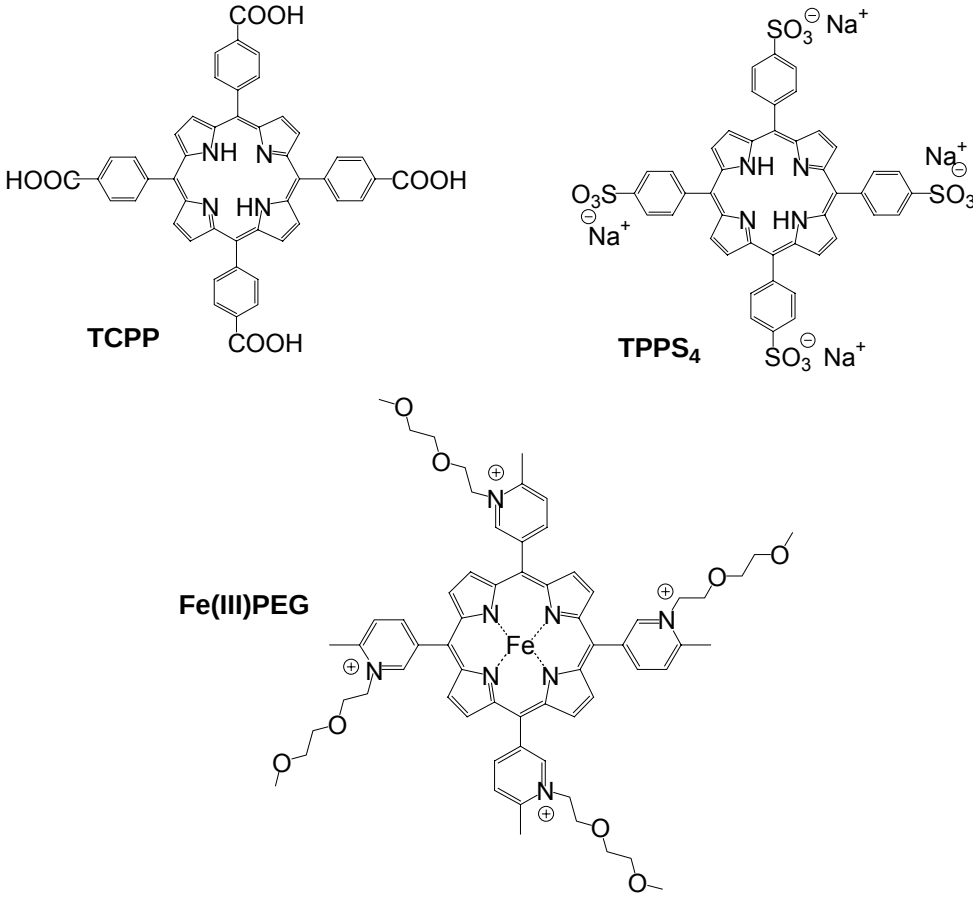

Figure 5.2: Structures of porphyrins tested against gp120 and V3 loop

competition of porphyrins against HIV-1 proteins. The modality of using porphyrin as anti-viral agents is new to this lab. Therefore the porphyrins tested (Figure 5.2) are commercially available and were used to lay the groundwork for future studies. Among the porphyrins evaluated is cationic Fe(III)PEG, anionic $TPPS_4$ and uncharged TCPP.

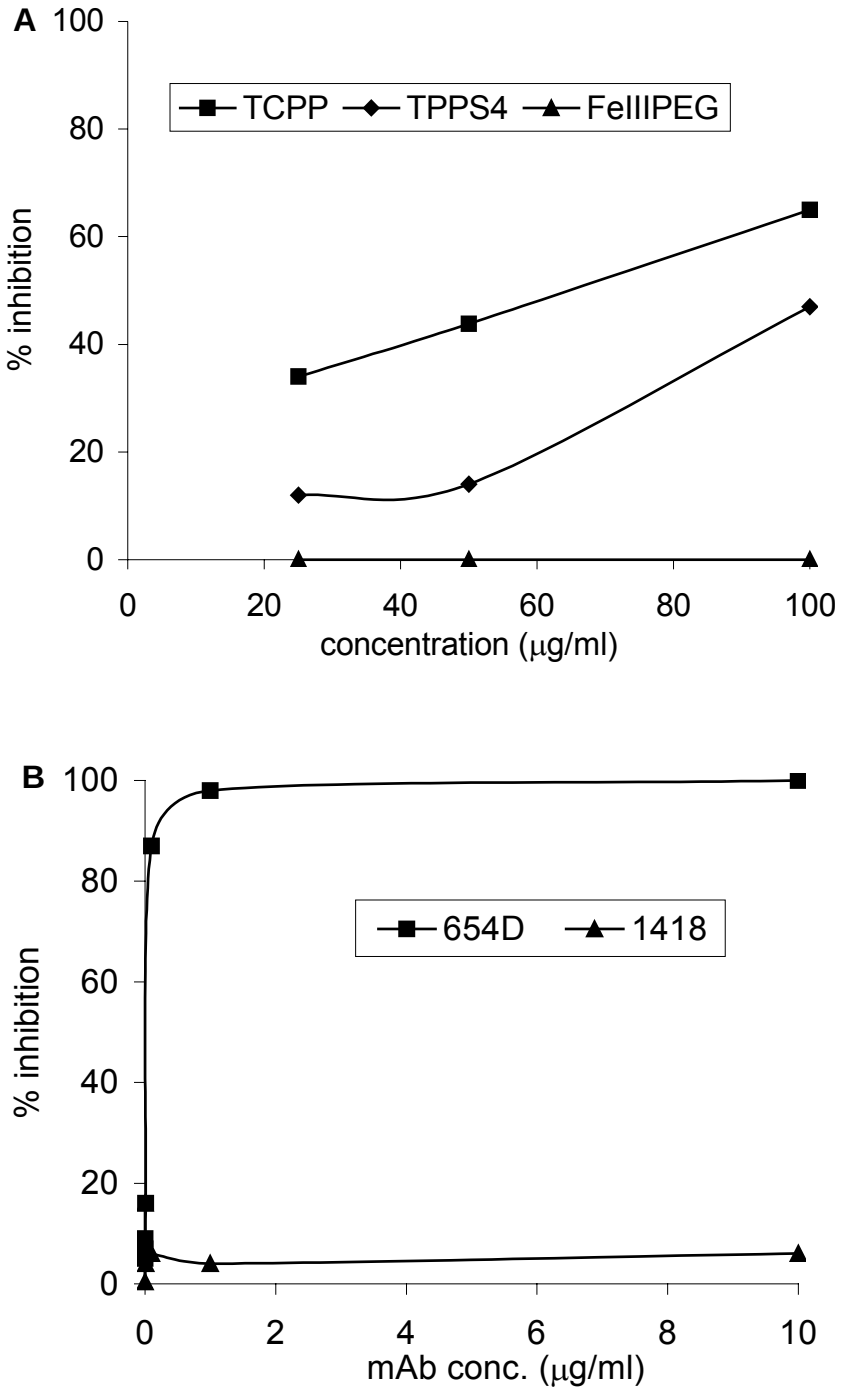

Figure 5.3: Inhibition of CD4-gp120 binding. Results represent percentages of CD4-gp120 inhibition compared to that of antibodies raised against gp120IIIB (100% inhibition, 654D). (A) assay, (B) controls.

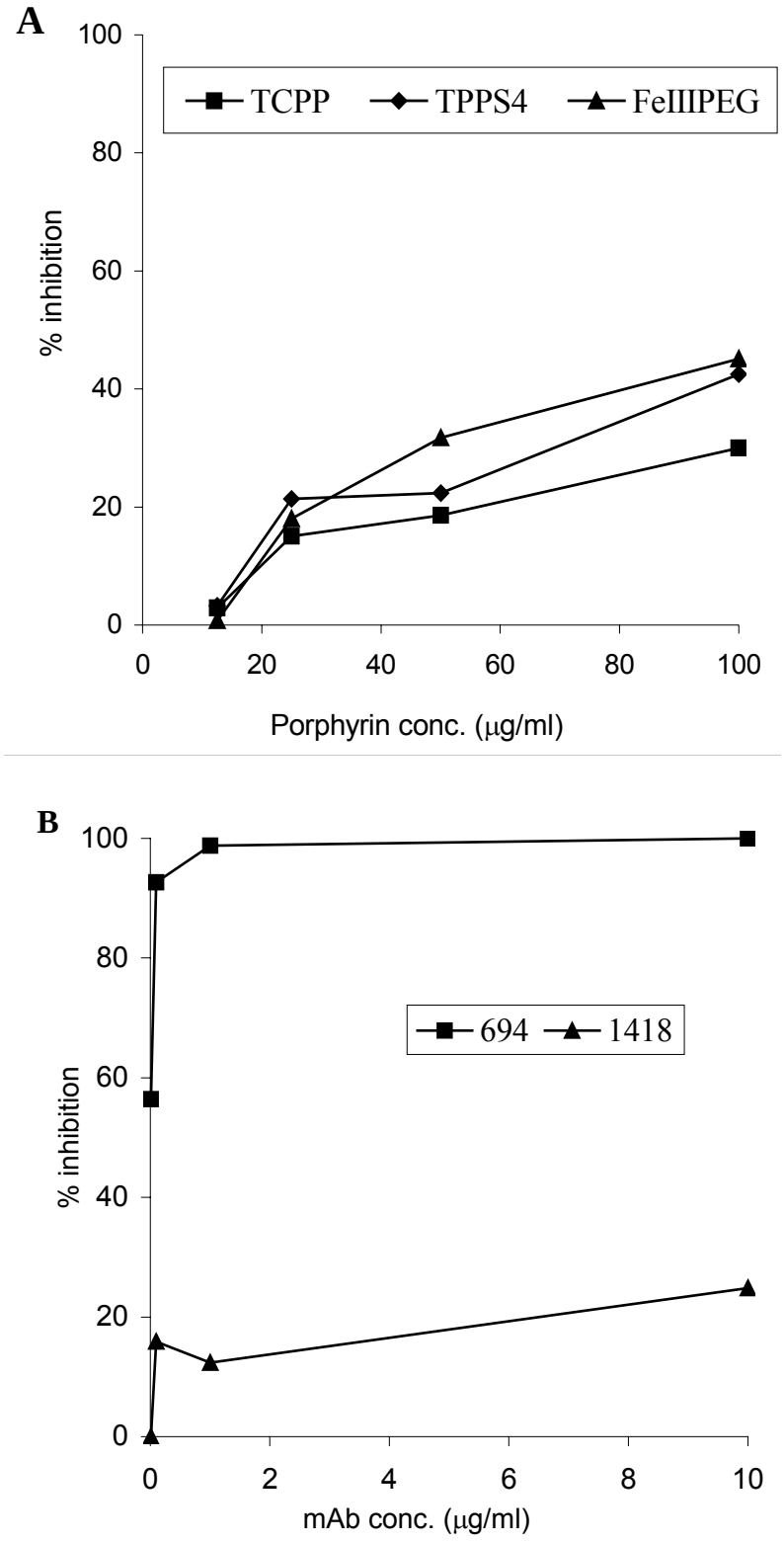

Figure 5.4: Competition for binding to V3 loop. Results represent competition of porphyrin binding to V3 loop with 694Ab raised against V3 loop. 1418 Parvovirus is negative control. 694 show optimal binding. (A) assay, (B) controls. 100 μg/mL Fe(III)PEG porphyrin corresponds to 8.76 μM.

Previous reports propose that anionic porphyrins bind to gp120, specifically the V3 loop, because of ionic interactions [17,20]. However, the conclusions that can be drawn from Figure 5.3A and Figure 5.4A is that the tetrasulfonated ($TPPS_4$), and the tetracarboxylate (TCPP) porphyrin derivative show only moderate inhibition of CD4 binding to gp120 and similar efficiencies in binding to the octacationic V3 loop of monomeric gp120IIIB. However, the tetracationic Fe(III)PEG fails to inhibit CD4 binding to gp120 but appears to compete for binding for the V3 loop of gp120IIIB. This shows that there may be more to the binding than just charges/electrostatic interactions. The positive controls, represent antibodies raised against the V3 loop and gp120IIIB, are shown in Figures 5.3B and 5.4B, which strongly bind to the HIV-1 proteins.

5.2.3 Conclusion

In addition to an anti-cancer agent, porphyrins are extremely versatile chromophores. Their properties can be exploited chemically (as catalysts, sensors, solar cells, in imaging, etc.) and biologically (anti-bacterial, anti-fungal and anti-viral agents). A database search at http://chembank.med.harvard.edu on HIV-inhibitors revealed a series of compounds that were uracil analogs. This information can serve as a guide for creating new compounds, based on porphyrin-uracil appendages that can be evaluated as a new class of anti-viral agents against the HIV-1 proteins used in the above studies.

It should be noted that open-shell metalloporphyrins such as Fe(III)PEG can act as anti-cancer, anti-viral, anti-bacterial agents be a different mechanism than the sensitization of the formation of singlet oxygen, Specifically, some metalloporphyrins are catalysts for the activation of oxygen in the direct oxidation of substrates via a mechanism that is proposed to be similar to that of cytochrome P450. [21,22].

Metalloporphyrins can catalyze a variety of oxidations – notably including the hydroxylation of un-activated alkanes. Unlike photodynamic applications wherein the specificity can be accomplished or augmented by selective irradiation with light, porphyrinic systems that catalyze oxidations would need to be highly specific to the target substrate, cell or tissue.

5.3 Chlorins

Chlorins represent a class of porphyrinoid with one pyrrole double bond missing, often times reduced. In comparison to porphyrins, chlorins offer stronger absorption bands in the red region, which allows greater penetration into tissues in PDT applications. Some chlorins have significantly greater fluorescence quantum yields, making them good

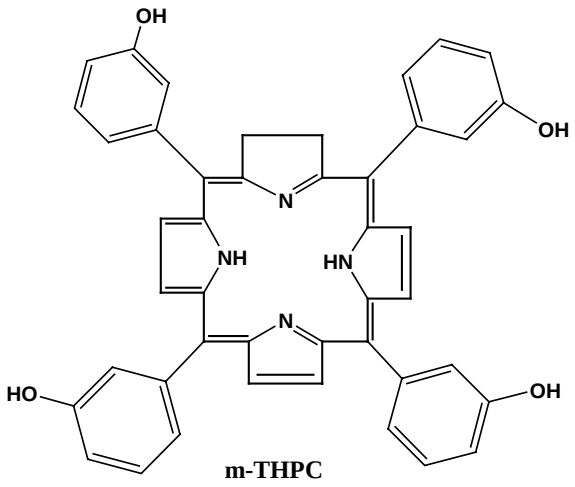

Figure 5.5: tetra(meta-hydroxyphenyl)chlorin (THPC) chlorin currently in clinical trials. Note reduced double bond on top pyrrole.

fluorescent tags [23,24]. One of several promising second-generation photosensitizers for PDT currently in clinical trials is meso-tetrakis(m-hydroxyphenyl) chlorin (m-THPC), a chlorin-based derivative (Figure 5.5) [24].

In the previous chapters, data has been presented using thioglycosylated porphyrins as a PDT agent. With this in mind, and the knowledge that chlorins have increased absorption at longer wavelengths, we have synthesized two chlorins analogues of the glycosylated $TPPF_{20}$ compound that was shown to be taken up and active against the MDA-MB-231 breast cancer cells.

5.3.1 Experimental Procedures

General

UV-vis spectra were collected on a Varian Bio3 spectrophotometer. Steady-state fluorescence spectra were taken on chlorins in methanol and in PBS, with excitation at an optical density where the UV-vis absorbance is the same and recorded on a Fluorolog τ3, Jobin-SPEX Instruments S. A., Inc. All chemicals were purchased from Sigma-Aldrich. Dulbecco's Modified Eagle Medium (DMEM), trypsin-EDTA and antimycotic for cell culture were obtained from GibcoBRL. Hanks' balanced salt solution was obtained from Cellgro (Mediatech). Bovine calf serum was obtained from HyClone. PBS was purchased from Invitrogen.

Synthesis

tetrakis-(4-1'-thioglucosyl-2,3,5,6-tetrafluorophenyl)-2,3-cis-dihydroxy-2,3-chlorin (Glu_4TPCF_{16} diol)

Synthesis of Glu_4TPCF_{16} diol chlorin is accomplished by coupling the acetate protected thioglucose to 5,10,15,20-tetrakis-1,2,3,4,5-(pentafluorophenyl)-2,3-cis-dihydroxy-2,3-chlorin. 5,10,15,20-tetrakis(pentafluorophenyl)porphyrin ($TPPF_{20}$) (200 mg, 0.21 mmol) was dissolved in freshly distilled, ethanol stabilized chloroform/10% pyridine (45 mL) and was treated with OsO_4 (70 mg, 1.3 equiv). The reaction flask was sealed and stirred at ambient temperature for 2 days and was shielded from light. Purging with gaseous H_2S for 5 min quenched the reaction. Following the addition of methanol (10 mL), the precipitated black OsS was filtered off. The filtrate was evaporated to dryness in vacuo. The resulting residue was loaded onto a silica gel column and eluted

with chloroform (to elute out unreacted porphyrin) followed by chloroform /methanol (1.5%). The resulting greenish colored fraction was collected and purified by column chromatography an additional time. Yield 134 mg (65%). ^{1}H NMR (500MHz, $CDCl_3$): δ = 8.80 (d, J = 5.0 Hz, 2H), 8.56 (m, 4H), 6.25 (d, J = 4.8, 2H), 3.2 (s, 2H) and –1.96 (s, 2H). UV-vis ($CHCl_3$) λ_{max} (ε in 10^{-5} x $M^{-1}cm^{-1}$): 403 (1.72), 493(sh), 503, 529, 594, 648 (0.44). Emission: (CH_2Cl_2) at 640 nm and 706 nm (excited at 410 nm). ESI-MS: 1009 (MH^+).

A mixture of the above chlorin (10 mg 9.92 μmol), 2,3,4,6-tetra-O-acetyl-glucosylthioacetate (32.5 mg, 8 equiv) and diethyl amine (26 μL, 250 μmol) was stirred in DMF (2.5 mL) at room temperature under nitrogen for 2 days. When TLC showed absence of starting compound, the solvent was removed under vacuum and the product was purified by flash column chromatography using hexane/ethyl acetate solvent system. A 50:50 (v/v) hexane/ethyl acetate eluted the tri substituted glucose chlorin, followed by a solvent ratio of 40:60 (hexane/ethyl acetate) that eluted the intended compound, protected Glu_4TPCF_{16} diol chlorin. The product was purified twice by precipitation using chloroform/hexane. Yield >70%. ^{1}H NMR (500MHz, $CDCl_3$): δ = 8.91 (m, 2H), 8.63 (m, 4H), 7.07-6.22 (m, 2H), 5.23 (m, 16H), 4.32 (m, 8H), 3.89 (m, 4H), 2.23 (m, 12H), 2.10 (s, 36H) and –1.93 (m, 2H). UV-vis ($CHCl_3$) λ_{max}: 403, 493(sh), 503, 529, 594, 648. Fluorescence (CH_2Cl_2) at 651 nm and 715 nm (excited at 404nm). ESI-MS: 2386 (MH^+). Deprotection of the glucose moieties on the $Glu_4AcTPCF_{16}$ diol chlorin are done by dissolving the resulting protected thioglucose chlorin (8.9 mg) in 9:1 CH_2Cl_2/ methanol (4 mL) and adding stoichiometric amount of sodium methoxide (119.0 μL of 0.5 M solution in methanol, 16 equiv). It was stirred at room temperature under dark for 1 h

and then neutralized by ammonium acetate buffer (pH = 7.2). The precipitated product was collected and redissolved in methanol. Three precipitations from diethyl ether ensued. Yield 6.1 mg (> 90%). MALDI –MS: 1714 (M+2H), 1736 (M+ Na). UV-vis (MeOH) $\lambda_{max:}$ 403, 502, 528, 593, 646. Fluorescence (MeOH) at 651 nm and 720 nm (excited at 418 nm).

Synthesis and coupling of thioglucose to yield Glu_4TPCF_{16} NCH_3 chlorin

A toluene (5ml) solution of *meso*-5,10,15,20-tetrakis(pentafluorophenyl) porphyrin (22 mg), N-methylglycine (8 mg, 2 equiv) and paraformaldehyde (6.8 mg) was heated at reflux for 5 h under a nitrogen atmosphere. Further portions of N-methylglycine (8 mg) and paraformaldehyde (6.8 mg) were then added and the resulting mixture was refluxed for another 5 h. It was then kept at 50°C overnight. The solvent was evaporated and the compound was separated by column chromatography. Hexane/chloroform (50:50 v/v) eluted the negligible amount of unreacted porphyrins. Use of hexane/ethyl acetate (50:50 v/v) then eluted chlorin followed by a small amount of the bacteriochlorin (wherein two double bonds are missing from opposite pyrrole beta positions). The $TPCF_{20}NCH_3$ chlorin collected was subjected to column chromatography using the same solvent ratio. Yield: 34.8 mg (74%). ^{1}H NMR (500MHz, $CDCl_3$): δ = 8.71 (d, J = 5.0 Hz, 2H), 8.48 (s, 2H), 8.40 (d, J = 4.9, 2H), 5.26 (m, 2H), 3.14 (m, 2H), 2.54 (m, 2H), 2.21 (s, 3H) and –1.80 (s, 2H). UV-vis ($CHCl_3$) λ_{max} (ε in 10^{-5} x $M^{-1}cm^{-1}$): 404 (1.82), 495(sh), 504, 528, 598, 651 (0.52). Fluorescence (CH_2Cl_2) at 655 nm and 723 nm (excited at 410nm) ESI-MS: 1032 (MH^+).

A mixture of the resulting $TPCF_{20}NCH_3$ chlorin (10.2 mg, 9.90 μmol), 2,3,4,6-tetra-O-acetyl-glucosylthioacetate (32.5 mg, 8 equiv), diethyl amine (26 μL, 250 μmol)

was stirred in DMF (2.5 mL) at room temperature under nitrogen for 1 day. When TLC showed absence of starting compound, the solvent was removed under vacuum and the product was purified two times by flash silica column chromatography using chloroform/methanol (3%) solvent system. The product was further purified by precipitation using chloroform/hexane two times. Yield of $Glu_4AcTPCF_{16}NCH_3$ > 80%. ^1H NMR (500MHz, $CDCl_3$): δ = 8.83 (t, 2H), 8.57 (s, 2H), 8.55-8.48 (dd, J = 5.0, 4.9, 2H), 5.38 (m, 6H), 5.25 (m, 12H), 4.32 (m, 8H), 3.90 (m, 4H), 3.16 (t, 2H), 2,59 (t, 2H), 2.25 (m, 15H), 2.10 (m, 36H) and –1.71 (s, 2H). UV-vis ($CHCl_3$) $\lambda_{max:}$ 404, 495(sh), 504, 528, 598, 651. Fluorescence (CH_2Cl_2) at 658 nm and 723 nm (excited at 410 nm) ESI-MS: 2409 (MH^+).

Deprotection of the glucose moieties on are done by dissolving the resulting protected thioglucose $Glu_4AcTPCF_{16}NCH_3$ chlorin (10.6 mg) in 9:1 CH_2Cl_2/methanol (4 mL) and adding stoichiometric amount of sodium methoxide (144.0 μL of 0.5 M solution in methanol, 16 equiv). It was stirred at room temperature in the dark for 1 h and then neutralized by ammonium acetate buffer (pH = 7.2). The precipitated product was collected and redissolved in methanol. Three precipitations from diethyl ether ensued. Yield 7.2 mg (> 90%). UV-vis (MeOH) $\lambda_{max:}$ 403, 503, 528, 596, 650. Fluorescence (MeOH) at 655 nm and 722 nm (excited at 418 nm).

Quantum Yield Calculations

From the normalized absorption and corrected emission spectra, the quantum yield for radiative decay can be obtained using the following equation from George et al [25]:

$$Q = Q_R \frac{I}{I_R} \frac{OD_R}{OD} \frac{n^2}{n_R^2}$$

In this equation, Q is the quantum yield of the unknown sample; Q_R is the quantum yield of the standard sample, I_R and I are the integrated intensity for the standard and unknown samples, respectively. OD represents the optical density and η is the refractive index of the solvent used. The standard or reference sample used for the quantum yield determination was cresyl violet dissolved in methanol. This dye has a quantum yield of 0.54 in the spectral range 600 nm – 650 nm [26].

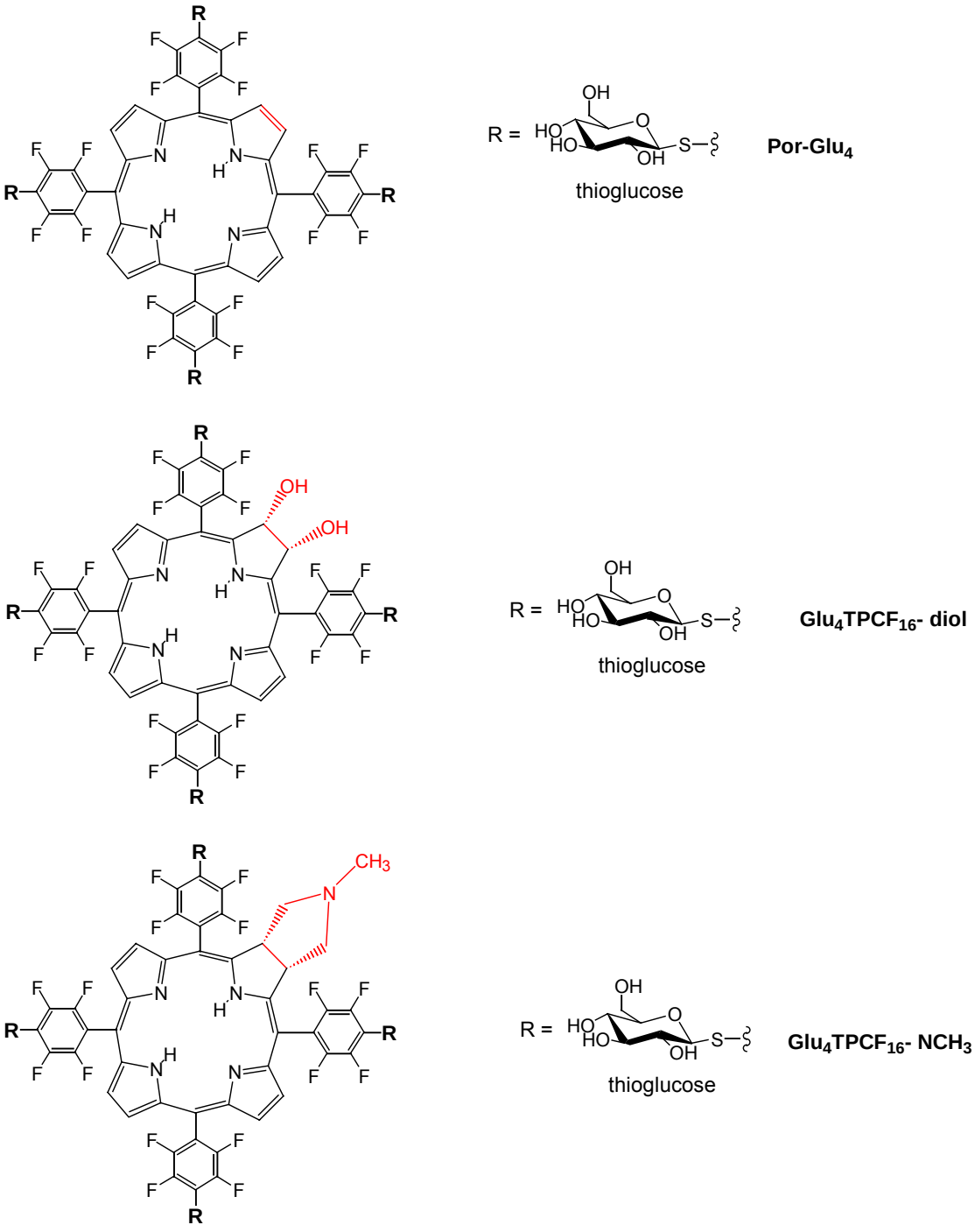

Figure 5.6: Structures of chlorins evaluated for binding to MDA-MB-231

5.3.2 Results and Discussion

The nucleophilic coupling of the thioglucose to the position of the pentafluorophenyl moieties of both chlorins was carried out by the reported procedure (DMF, room temperature, basic pH) [1]. Compared to Por-Glu_4, the coupling reaction is not complete within 24 h, but more than 90 % product formation is detected after 48 h. Since only the deprotected glycosylated chlorins (Figure 5.6) were evaluated for binding to cancer cells, their spectral properties in methanol and PBS are shown in Figures 5.7 and 5.8, respectively. The absorption and fluorescent emission properties of the parent $TPCF_{20}$ diol and $TPCF_{20}$ NCH_3 chlorins and the acetate protected Glu_4AcF_{16} chlorins are listed in the experimental section and do not differ much from the deprotected thioglycosylated chlorins. From Figure 5.7, the spectral properties of both deprotected Glu_4TPCF_{16} diol and Glu_4TPCF_{16} NCH_3 chlorins are almost identical but differ much from Por-Glu_4. Both chlorins exhibited an intense absorption peak around 650 nm in methanol. This peak blue shifted to around 642 nm – 646 nm in an aqueous solution. Their emission spectra in methanol have two bands, with λ_{max} around 651 nm – 655 nm and a satellite peak at 720 nm – 722 nm (for Por-Glu_4 the peaks are 651 nm and 720 nm). However, the intensity of the peaks differs. As expected the fluorescence quantum yield of these chlorins [27] are about 5 – 6 times greater than that of Por-Glu_4 in methanol and about 4 – 5 times greater in aqueous solutions (Table 5.1). The fluorescence quantum yield for chlorins may be greater due to either reduced internal conversion or reduced intersystem crossing to the triplet state [24].

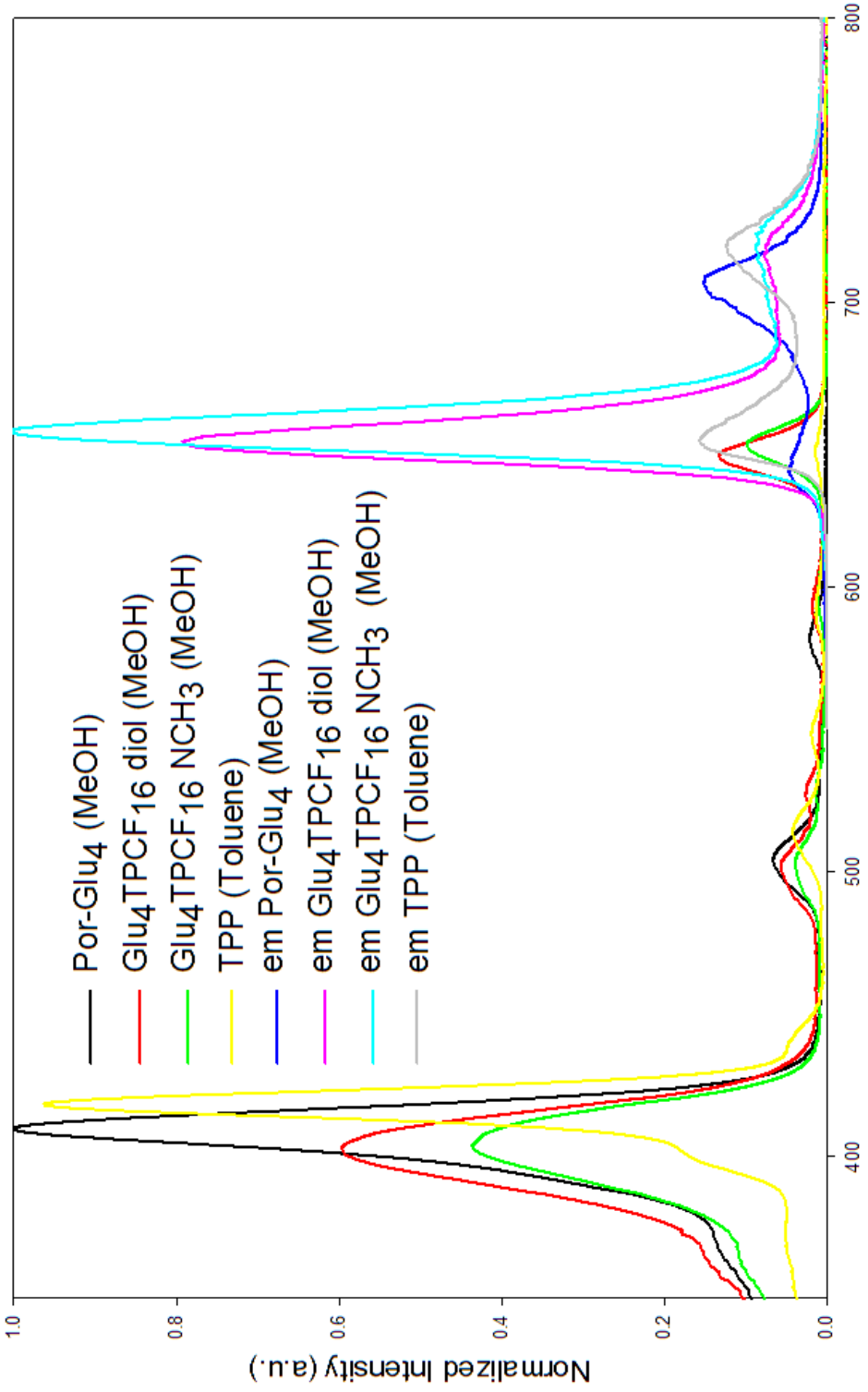

Figure 5.7: Absorption and emission of chlorins in methanol.

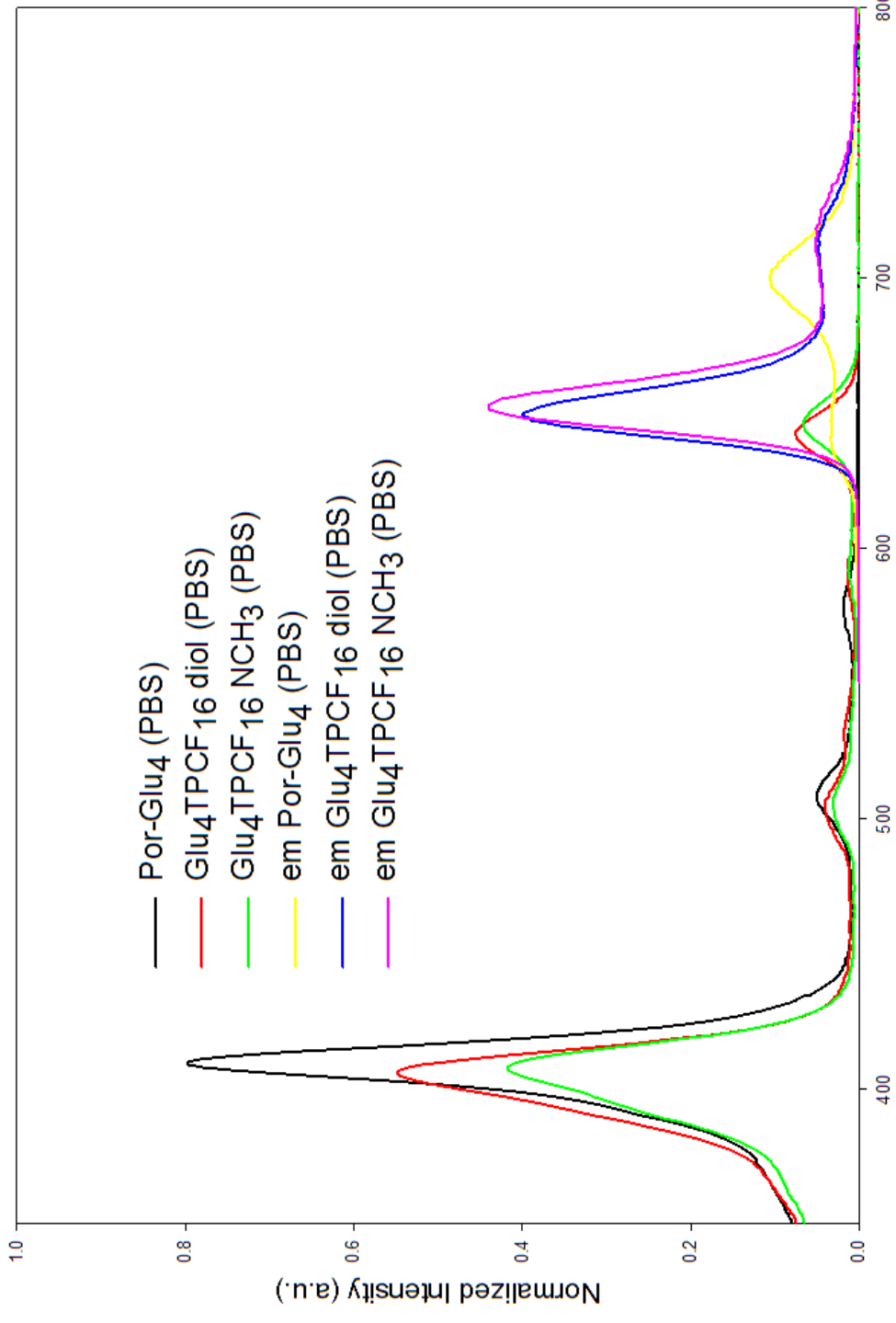

Figure S2: Absorption and emission of chlorins in aqueous PBS.

MDA-MB-231 cells were selected to evaluate these chlorins, because the thioglycosylated porphyrin (Por-Glu_4) showed great selectivity, uptake and photodynamic effects on this breast cancer cell line. Cells were incubated with 1 or 2 μM concentrations of the two chlorins as well as Por-Glu_4 for comparison. At 5 μM and 10 μM concentrations of the chlorins, the detector coupled to the fluorescence microscope becomes saturated by the emission intensity because of the significantly increase fluorescence quantum yield. When this occurs, the relative fluorescence intensity calculations are misleading. To acquire a more accurate relative intensity calculation, the

Porphyrin or Chlorin	Quantum Yield
TPP (Toluene)	13%
Por-Glu_4 (MeOH)	7%
Glu_4TPCF_{16} diol (MeOH)	34%
$Glu_4TPCF_{16}NCH_3$ (MeOH)	49%
Por-Glu_4 (PBS)	7%
Glu_4TPCF_{16} diol (PBS)	28%
$Glu_4TPCF_{16}NCH_3$ (PBS)	32%

Table 5.1: Fluorescence quantum yield calculations of chlorins in methanol and aqueous solutions. The relative quantum yields for Por-Glu_4 : Glu_4TPCF_{16} diol : $Glu_4TPCF_{16}NCH_3$ in PBS are 1: 4 : 4.5. Reported literature values for φ_F for TPP standard is 11%.

concentrations were reduced to 1 – 3 μM. At 2.5 μM, the relative fluorescence intensities for Por-Glu_4, Glu_4TPCF_{16} diol and $Glu_4TPCF_{16}NCH_3$ chlorin (Figure 5.9) are 1:3:6, whereas at the 1 μM the relative intensities are 1:2:7, respectively. Since the relative fluorescence quantum yields are 1:4:4.5 in aqueous media, if the compounds

were taken up equivalently these ratios would be reflected in the fluorescence intensities in the micrographs (assuming they aggregate similarly, see chapter 3 and 4). Thus it appears that the chlorin diol is not taken up as well as the chlorin NCH_3 derivative, and that the latter is taken up better than the parent Por-Glu_4 compound even though the compounds are structurally similar. However, due to the high fluorescence quantum yield for these chlorins, they may not be as efficient PDT agents, as in the case of m-THPC [24]. For PDT applications the optical cross section of the chlorin dyes in the red region is significantly larger than the porphyrin analogues, thus if only red light is used to activate the chlorins, the increased absorbtivity somewhat ameliorates the reduced triplet quantum yield. These compounds and the photo-physics in biological systems will be the subject of future studies.

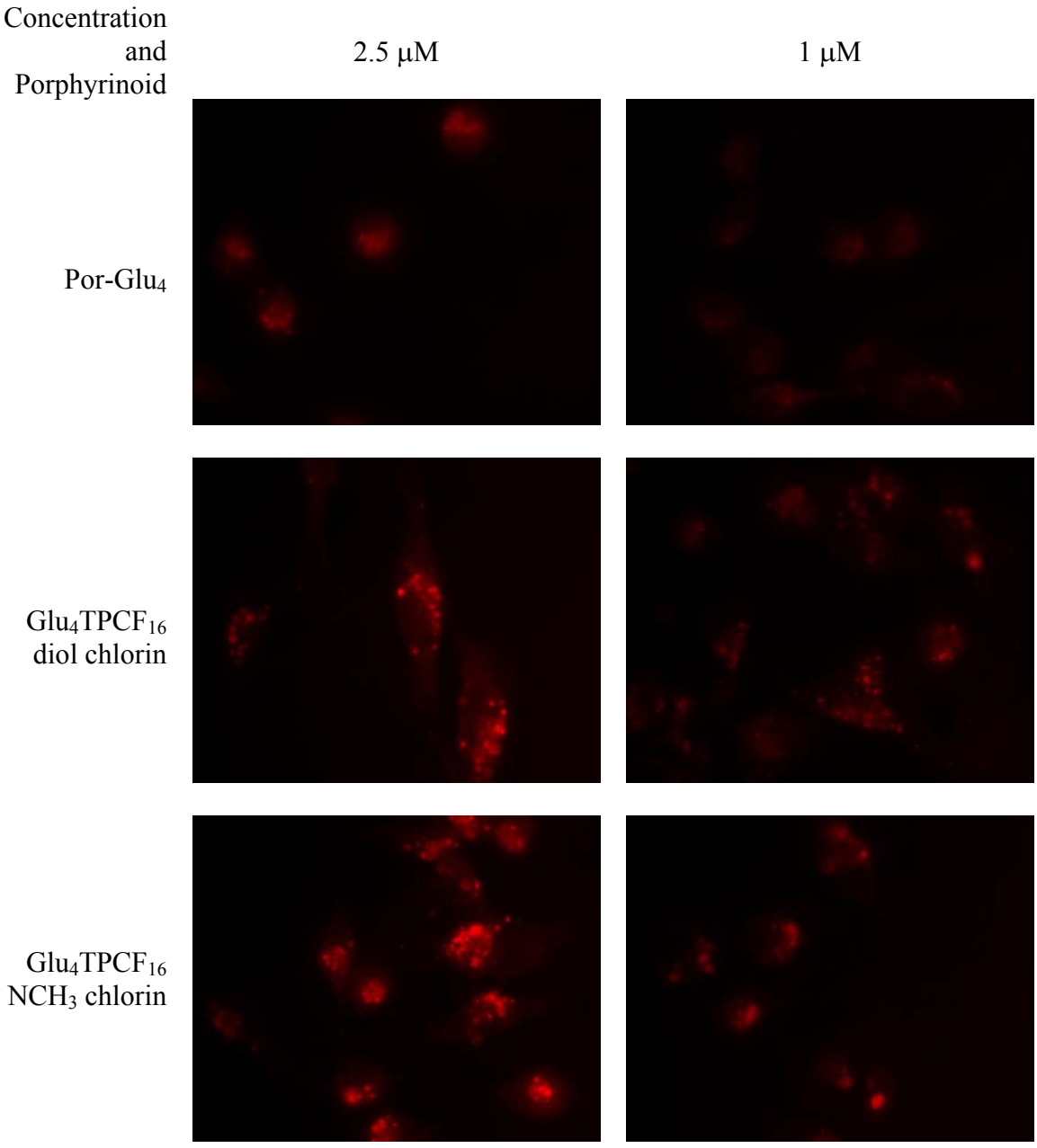

Figure 5.9: Fluorescence microscopy of chlorin compared to Glu_4 porphyrin at two different concentrations. The porphyrinoid is incubated at a 2.5 or 1 μM concentration for 20 hrs with MDA-MB-231 cells. Following removal of unbound porphyrinoid, the cells are fixed and imaged. At the 2.5 μM, the relative fluorescence intensities for Por-Glu_4, Glu_4TPCF_{16} diol and Glu_4TPCF_{16} NCH_3 chlorin are 1:3:6, whereas at the 1 μM the relative intensities are 1:2:7, respectively. Images are not enhanced and represent magnification at 60X.

5.3.3 Conclusion

The higher fluorescence quantum yield of the thioglycosylated chlorin compounds compared to porphyrin may pose a disadvantage in terms of PDT. The reason is that for porphyrins about ~ 80 % undergo intersystem crossing to the excited triplet state (Chapter 1). This number may be substantial reduced in the case of the chlorins. An effective PDT agent needs to cross to this excited triplet state in order to generate the reactive oxygen species responsible for cellular damage. One way to solve this problem for the chlorins could be to use the metallated derivatives with an element that increases the rate of intersystem crossing to the triplet state, such as using Zn(II), Pd(II), or Pt(II). Derivatives of chlorins with Zn(II) should have a reduced fluorescence quantum yield and increase triplet, yet retain the intense red region absorption band necessary for better tissue penetration. As such, these derivatives should be evaluated for binding and the photodynamic effect to cancer cells. The metallochlorin derivatives are currently under investigation.

5.4 References

(1) Chen, X.; Hui, L.; Foster, D. A.; Drain, C. M. *Biochemistry* **2004**, *43*, 10918-10929.

(2) Drain, C. M.; Gong, X.; Ruta, V.; Soll, C. E.; Chicoineau, P. F. *J. Comb. Chem.* **1999**, *1*, 286-290.

(3) N18 and B16-F10 cell lines were a gift from Prof. Probal Banerjee's lab (College of Staten Island). MDA-MB-231 were obtained from Prof. David Foster's lab (Hunter College).

(4) Malouf, A. T.; Schnaar, R. L.; Coyle, J. T. *J. Biol. Chem.* **1984**, *259*, 12756-12762.

(5) Sengupta, S.; Ray, S.; Chattopadhyay, N.; Biswas, N.; Chatterjee, A. *J. Exp. Clin. Cancer Res.* **2000**, *19*, 81-7.

(6) Ohyama, T.; Sasagawa, A.; Terui, N.; Mita, H.; Yamamoto, Y. *Nucleic Acids Symp. Ser.* **2003**, *3*, 189-190.

(7) Lamarche, F.; Sol, V.; Huang, Y. M.; Granet, R.; Guilloton, M.; Krausz, P. *J. Porphyrins Phthalocyanines* **2002**, *6*, 130-134.

(8) Osterloh, J.; Vicente, M. G. H. *J. Porphyrins Phthalocyanines* **2002**, *6*, 305-324.

(9) MacDonald, I. J.; Dougherty, T. J. *J. Porphyrins Phthalocyanines* **2001**, *5*, 105-126.

(10) Malik, Z.; Ladan, H.; Nitzan, Y.; Smetana, Z. Photodynamic therapy of cancer, Budapest, Hungary, 1994; p 305-312.

(11) Nitzan, Y.; Dror, R.; Ladan, H.; Malik, Z.; Kimel, S.; Gottfried, V. *Photochem. Photobiol.* **1995**, *62*, 342-347.

(12) Nitzan, Y.; Gutterman, M.; Malik, Z.; Ehrenberg, B. *Photochem. Photobiol.* **1992**, *55*, 89-96.

(13) Orenstein, A.; Klein, D.; Kopolovic, J.; Winkler, E.; Malik, Z.; Keller, N.; Nitzan, Y. *FEMS Immun. Med. Microbiol.* **1998**, *19*, 307-314.

(14) Valduga, G.; Breda, B.; Giacometti, G. M.; Jori, G.; Reddi, E. *Biochem. Biophys. Res. Commun.* **1999**, *256*, 84-88.

(15) Tome, J. P. C.; Neves, M. G. P. M. S.; Tome, A. C.; Cavaleiro, J. A. S.; Soncin, M.; Magaraggia, M.; Ferro, S.; Jori, G. *J. Med. Chem.* **2004**, *47*, 6649-6652.

(16) Vzorov, A. N.; Marzilli, L. G.; Compans, R. W.; Dixon, D. W. *Antivir. Res.* **2003**, *59*, 99-109.

(17) Neurath, A. R.; Strick, N.; Haberfield, P.; Jiang, S. *Antivir. Chem. Chemother.* **1992**, *3*, 55-63.

(18) Neurath, A. R.; Haberfield, P.; Joshi, B.; Hewlett, I. K.; Strick, N.; Jiang, S. *Antivir. Chem. Chemother.* **1991**, *2*, 303-312.

(19) Debnath, A. K.; Jiang, S.; Strick, N.; Lin, K.; Haberfield, P.; Neurath, A. R. *J. Med. Chem.* **1994**, *37*, 1099-1108.

(20) Dixon, D. W.; Gill, A. F.; Giribabu, L.; Vzorov, A. N.; Alam, A. B.; Compans, R. W. *J. Inorg. Biochem.* **2005**, *99*, 813-821.

(21) Mansuy, D.; Battioni, P. In *Metalloporphyrins in Catalytic Oxidations*; Sheldon, R. A., Ed.; Marcel Dekker, Inc., New York,, 1994.

(22) Groves, J. T. In *Advances in Inorganic Biochemistry, vol. 1*; Eichhorn, G. L. a. M., L.G., Ed.; Elsevier North Holland, New York, 1979.

(23) McCarthy, J. R.; Perez, J. M.; Bruckner, C.; Weissleder, R. *Nano Lett.* **2005**, *5*, 2552-2556.

(24) Bonnett, R.; Charlesworth, P.; Djelal, B. D.; Foley, S.; McGarvey, D. J.; Truscott, T. G. *J. Chem. Soc., Perkin Trans. 2* **1999**, 325-328.

(25) Kamat, P. V.; Das, S.; Thomas, K. G.; George, M. V. *J. Phys. Chem.* **1992**, *96*, 195-199.

(26) Bonnett, R.; Martinez, G. *Tetrahedron* **2001**, *57*, 9513-9547.

(27) Maestrin, A. P. J.; Ribeiro, A. O.; Tedesco, A. C.; Neri, C. R.; Vinhado, F. S.; Serra, O. A.; Martins, P. R.; Iamamoto, Y.; Silva, A. M. G.; Tome, A. C.; Neves, M. G. P. M. S.; Cavaleiro, J. A. S. *J. Braz. Chem. Soc.* **2004**, *15*, 923-930.

Chapter 6: Bibliography

Chapter 1

(1) Lane, N. *Scientific American* **2003**, *288*, 38-44.

(2) Rosenkranz, A. A.; Jans, D. A.; Sobolev, A. S. *Immunol. Cell Biol.* **2000**, *78*, 452-464.

(3) Hasan, T.; Moor, A. C. E.; Ortel, B. In *Cancer Medicine*; 5th ed.; Holland, J. F., Frei III, E., Bast Jr., R. C., Kufe, D. W., Morton, D. L., Weichselbaum, R. R., Eds.; B.C. Decker Inc.: Hamilton, Ontario (Canada), 2000.

(4) Ahmad, K. *The Lancet: Oncology* **2002**, *3*, 451.

(5) Konan, Y. N.; Berton, M.; Gurny, R.; Allemann, E. *Eur. J. Pharmaceutical Sciences* **2003**, *18*, 241-249.

(6) Osterloh, J.; Vicente, M. G. H. *J. Porphyrins Phthalocyanines* **2002**, *6*, 305-324.

(7) Morgan, A. R.; Petousis, N. H.; van Lier, J. E. *Eur. J. Med. Chem.* **1997**, *32*, 21-26.

(8) Henderson, B. W.; Dougherty, T. J. *Photochem. Photobiol.* **1992**, *55*, 145-157.

(9) Noodt, B. B.; Berg, K.; Stokke, T.; Peng, Q.; Nesland, J. M. *British J. Cancer* **1999**, *79*, 72-81.

(10) MacDonald, I. J.; Dougherty, T. J. *J. Porphyrins Phthalocyanines* **2001**, *5*, 105-126.

(11) Lam, M.; Oleinick, N. L.; Nieminen, A.-L. *J. Biol. Chem.* **2001**, *276*, 47379-47386.

(12) Rouhi, A. M. *C&E News* **1998**, *76*, 22-27.

(13) Aviezer, D.; Cotton, S.; David, M.; Segev, A.; Khaselev, N.; Galili, N.; Gross, Z.; Yayon, A. *Cancer Res.* **2000**, *60*, 2973-2980.

(14) Hornung, R.; Fehr, M. K.; Monti-Frayne, J.; Krasieva, T. B.; Tromberg, B. J.; Berns, M. W.; Tadir, Y. *Photochem. Photobiol.* **1999**, *70*, 624-629.

(15) Kessel, D.; Luo, Y. *J. Porphyrins Phthalocyanines* **2001**, *5*, 181-184.

(16) Yslas, I.; Alvarez, M. G.; Marty, C.; Mori, G.; Durantini, E. N.; Rivarola, V. *Toxicology* **2000**, *149*, 69-74.

(17) Shibata, Y.; Matsumura, A.; Yoshida, F.; Yamamoto, T.; Nakai, K.; Nose, T.; Sakata, I.; Nakajima, S. *Cancer Lett.* **1998**, *129*, 77-85.

(18) Friberg, E. G.; Cunderlikova, B.; Pettersen, E. O.; Moan, J. *Cancer Lett.* **2003**, *195*, 73-80.

(19) Chen, X.; Drain, C. M. *Drug Design Rev.* **2004**, *1*, 215-234.

(20) Woodburn, K.; Fan, Q.; Kessel, D.; Luo, Y.; Young, S. *J. Invest. Dermatol.* **1998**, *110*, 746-751.

(21) Taber, S.; Fingar, V.; Coots, C.; Wieman, T. *Clin Cancer Res* **1998**, *4*, 2741-2746.

(22) Razum, N.; Snyder, A.; Doiron, D. *Proceedings of SPIE (Society for Photo-optical International Engineering),* **1996**, *2675*, 43-46.

(23) Berlin, K.; Jain, R. K.; Richert, C. *Biotechnol. Bioeng. Comb. Chem.* **1998**, *61*, 107-118.

(24) Drain, C. M.; Gong, X.; Ruta, V.; Soll, C. E.; Chicoineau, P. F. *J. Comb. Chem.* **1999**, *1*, 286-290.

(25) Kwong, P. D.; Wyatt, R.; Majeed, S.; Robinson, J.; Sweet, R. W.; Sodroski, J.; Hendrickson, W. A. *Structure* **2000**, *8*, 1329-1339.

(26) Moulard, M.; Phogat, S. K.; Shu, Y.; Labrijn, A. F.; Xiao, X.; Binley, J. M.; Zhang, M.-Y.; Sidorov, I. A.; Broder, C. C.; Robinson, J.; Parren, P. W. H. I.; Burton, D. R.; Dimitrov, D. S. *Proc. Natl. Acad. Sci.* **2002**, *99*, 6913-6918.

(27) Kwong, P. D.; Wyatt, R.; Robinson, J.; Sweet, R. W.; Sodroski, J.; Hendrickson, W. A. *Nature* **1998**, *393*, 648-659.

(28) Labrijn, A. F.; Parren, P. W. H. I. **1999**.

(29) Clapham, P. R.; McKnight, A. *J. Gen. Virol.* **2002**, *83*, 1809-1829.

(30) Zwick, M. B.; Kelleher, R.; Jensen, R.; Labrijn, A. F.; Wang, M.; Quinnan, G. V.; Parren, P. W. H. I.; Burton, D. R. *J. Virol.* **2003**, *77*, 6965-6978.

(31) Sharon, M.; Kessler, N.; Levy, R.; Zolla-Pazner, S.; Gorlach, M.; Anglister, J. *Structure* **2003**, *11*, 225-236.

(32) Pantophlet, R.; Wilson, I. A.; Burton, D. R. *J. Virol.* **2003**, *77*, 5889-5901.

(33) Myszka, D. G.; Sweet, R. W.; Hensley, P.; Brigham-Burke, M.; Kwong, P. D.; Hendrickson, W. A.; Wyatt, R.; Sodroski, J.; Doyle, M. L. *Proc. Natl. Acad. Sci.* **2000**, *97*, 9026-9031.

(34) Gallo, S. A.; Finnegan, C. M.; Viard, M.; Raviv, Y.; Dimitrov, A.; Rawat, S. S.; Puri, A.; Durell, S.; Blumenthal, R. *Biochim. Biophys. Acta - Biomembranes* **2003**, *1614*, 36-50.

(35) Neurath, A. R.; Strick, N.; Haberfield, P.; Jiang, S. *Antivir. Chem. Chemother.* **1992**, *3*, 55-63.

(36) Debnath, A. K.; Jiang, S.; Strick, N.; Lin, K.; Kahl, S. B.; Neurath, A. R. *Med. Chem. Res.* **1999**, *9*, 267-275.

(37) Song, R.; Witvrouw, M.; Schols, D.; Robert, A.; Balzarini, J.; De Clercq, E.; Bernadou, J.; Meunier, B. *Antivir. Chem. Chemother.* **1997**, *8*, 85-97.

(38) Vzorov, A. N.; Dixon, D. W.; Trommel, J. S.; Marzilli, L. G.; Compans, R. W. *Antimicrob. Agents Chemother.* **2002**, *46*, 3917-3925.

(39) Valduga, G.; Breda, B.; Giacometti, G. M.; Jori, G.; Reddi, E. *Biochem. Biophys. Res. Commun.* **1999**, *256*, 84-88.

(40) Malik, Z.; Ladan, H.; Nitzan, Y.; Smetana, Z. Photodynamic therapy of cancer, Budapest, Hungary, 1994; p 305-312.

(41) Nitzan, Y.; Gutterman, M.; Malik, Z.; Ehrenberg, B. *Photochem. Photobiol.* **1992**, *55*, 89-96.

(42) Nitzan, Y.; Dror, R.; Ladan, H.; Malik, Z.; Kimel, S.; Gottfried, V. *Photochem. Photobiol.* **1995**, *62*, 342-347.

(43) Tome, J. P. C.; Neves, M. G. P. M. S.; Tome, A. C.; Cavaleiro, J. A. S.; Soncin, M.; Magaraggia, M.; Ferro, S.; Jori, G. *J. Med. Chem.* **2004**, *47*, 6649-6652.

(44) Mizutani, T.; Wada, K.; Kitagawa, S. *J. Am. Chem. Soc.* **1999**, *121*, 11425-11431.

(45) Bouy-Debec, D.; Brigaud, O.; Leduc, P.; Battioni, P.; Mansuy, D. *Gazz. Chim. Ital.* **1996**, *126*, 233-237.

(46) Samaroo, D.; Soll, C. E.; Todaro, L. J.; Drain, C. M. *Org. Lett.* **2006**, *8*, 4985-4988.

(47) Greenwald, R. B.; Choe, Y. H.; McGuire, J.; Conover, C. D. *Adv. Drug Delivery Rev.* **2003**, *55*, 217-250.

(48) Molineux, G. *Pharmacotherapy* **2003**, *23*, 3S-8S.

(49) Blagbrough, I. S.; Geall, A. J.; Neal, A. P. *Biochem. Soc. Trans.* **2003**, *31*, 397-406.

(50) Frydman, B.; Valasinas, A. *Exp. Opin. Ther. Patents* **1999**, *9*, 1055-1068.

(51) Venkatesh, B.; Jayakumar, R.; Pandian, R. P.; Manoharan, P. T. *Biochem. Biophys. Res. Commun.* **1996**, *223*, 390-396.

(52) Hamblin, M. R.; Miller, J. L.; Rizvi, I.; Ortel, B.; Maytin, E. V.; Hasan, T. *Cancer Res.* **2001**, *61*, 7155-62.

(53) Hamblin, M. R.; Miller, J. L.; Loew, H. G.; Hasan, T. *British J. Cancer* **2003**, *89*, 937-943.

(54) Barrett, G. C.; Elmore, D. T. In *Amino acids and peptides*; Cambridge University Press: Cambridge, UK, 1998.

(55) Biron, E.; Voyer, N. *Chem. Commun.* **2005**, 4652-4654.

(56) Dixon, D. W.; Kim, M. S.; Kumar, V.; Obara, G.; Marzilli, L. G.; Schinazi, R. F. *Antivir. Chem. Chemother.* **1992**, *3*, 279-282.

(57) Mizutani, T.; Wada, K.; Kitagawa, S. *J. Org. Chem.* **2000**, *65*, 6097-6106.

(58) Blagbrough, I. S.; Geall, A. J. *Tet. Lett.* **1998**, *39*, 439-442.

(59) Lamarche, F.; Sol, V.; Huang, Y. M.; Granet, R.; Guilloton, M.; Krausz, P. *J. Porphyrins Phthalocyanines* **2002**, *6*, 130-134.

(60) Valasinas, A.; Reddy, V. K.; Blokhin, A. V.; Basu, H. S.; Bhattacharya, S.; Sarkar, A.; Marton, L. J.; Frydman, B. *Bioorg. Med. Chem.* **2003**, *11*, 4121-4131.

(61) Rovers, J. P.; Saarnak, A. E.; de Jode, M.; Sterenborg, H. J. C. M.; Terpstra, O. T.; Grahn, M. F. *Photochem. Photobiol.* **2000**, *71*, 210-217.

(62) Hornung, R.; Fehr, M. K.; Walt, H.; Wyss, P.; Berns, M. W.; Tadir, Y. *Photochem. Photobiol.* **2000**, *72*, 696-700.

(63) Laville, I.; Pigaglio, S.; Blais, J.-C.; Doz, F.; Loock, B.; Maillard, P.; Grierson, D. S.; Blais, J. *J. Med. Chem.* **2006**, *49*, 2558-2567.

(64) Lottner, C.; Knuechel, R.; Bernhardt, G.; Brunner, H. *Cancer Lett.* **2004**, *215*, 167-177.

(65) Lottner, C.; Knuechel, R.; Bernhardt, G.; Brunner, H. *Cancer Lett.* **2004**, *203*, 171-180.

(66) Rietveld, I. B.; Kim, E.; Vinogradov, S. A. *Tet.* **2003**, *59*, 3821-3831.

(67) Sol, V.; Blais, J. C.; Granet, R.; Guilloton, M.; Spiro, M.; Krausz, P. *J. Org. Chem.* **1999**, *64*, 4431-4444.

(68) Sol, V.; Blais, J. C.; Bolbach, G.; Carre, V.; Granet, R.; Guilloton, M.; Spiro, M.; Krausz, P. *Tet. Lett.* **1997**, *38*, 6391-6394.

(69) Sol, V.; Branland, P.; Granet, R.; Kaldapa, C.; Verneuil, B.; Krausz, P. *Bioorg. Med. Chem. Lett.* **1998**, *8*, 3007-3010.

(70) Flessner, M. F.; Dedrick, R. L. *Cancer Res* **1994**, *54*, 4376-4384.

(71) Schneider, R.; Schmitt, R.; Frochot, C.; Fort, Y.; Lourette, N.; Guillemin, F.; Muller, J.-F.; Barberi-Heyob, M. *Bioorg. Med. Chem.* **2005**, *13*, 2799-2808.

(72) Hifumi, E.; Sakata, H.; Nango, M.; Uda, T. *J. Mol. Cat. A: Chem.* **2000**, *155*, 209-218.

(73) Chaleix, V.; Sol, V.; Huang, Y.-M.; Guilloton, M.; Granet, R.; Blais, J. C.; Krausz, P. *Eur. J. Org. Chem.* **2003**, 1486-1493.

(74) Dombi, K. L.; Richert, C. *Molecules* **2000**, *5*, 1265–1280.

(75) Boitrel, B.; Baveux-Chambenoit, V.; Richard, P. *Eur. J. Org. Chem.* **2001**, 4213-4221.

(76) Li, H.; Czuchajowski, L. *Heterocyclic Chem.* **1999**, *6*, 57-77.

(77) Garcia, G.; Sol, V.; Lamarche, F.; Granet, R.; Guilloton, M.; Champavier, Y.; Krausz, P. *Bioorganic & Medicinal Chemistry Letters* **2006**, *16*, 3188-3192.

(78) Hirohara, S.; Obata, M.; Saito, A.; Ogata, S.; Ohtsuki, C.; Higashida, S.; Ogura, S.; Okura, I.; Sugai, Y.; Mikata, Y.; Tanihara, M.; Yano, S. *Photochem. Photobiol.* **2004**, *80*, 301-308.

(79) Tome, J. P. C.; Neves, M. G. P. M. S.; Tome, A. C.; Cavaleiro, J. A. S.; Mendonca, A. F.; Pegado, I. N.; Duarte, R.; Valdeira, M. L. *Bioorg. Med. Chem.* **2005**, *13*, 3878-3888.

(80) Haylett, A. K.; Forbes, E.; MacLennan, A.; Truscott, T. G.; Moore, J. V. *Cancer Lett.* **1996**, *105*, 187-193.

(81) Lakowicz, J. R. *Principles of fluorescence spectroscopy; 2nd Ed.* Kluwer Academic/Plenum Publishers: New York, 1999.

Chapter 2

(1) (a) Benaglia, M.; Danelli, T.; Fabris, F.; Sperandio, D.; Pozzi, G. *Org. Lett.* **2002**, *4*, 4229. (b) Yang, J.; Weinberg, R.; Breslow, R. *Chem. Commun.* **2000**, 531.

(2) Drain, C. M.; Hupp, J. T.; Suslick, K. S.; Wasielewski, M. R.; Chen, X. *J. Porphyrins Phthalocyanines* **2002**, *6*, 243.

(3) (a) Chen, X.; Hui, L.; Foster, D. A.; Drain, C. M. *Biochemistry* **2004**, *43*, 10918. (b) Sylvain, I.; Zerrouki, R.; Granet, R.; Huang, Y. M.; Lagorce, J.-F.; Guilloton, M.;

Blais, J.-C.; Krausz, P. *Bioorg. Med. Chem.* **2002**, *10*, 57. (c) Pasetto, P.; Chen, X.; Drain, C. M.; Franck, R. W. *Chem. Commun.* **2001**, 82. (d) Chen, X.; Drain, C. M. *Drug Design Rev.* **2004**, *1*, 215.

(4) Sauer, D. R.; Kalvin, D.; Phelan, K. M. *Org. Lett.* **2003**, *5*, 4721.

(5) Yoon, D. S.; Han, Y.; Stark, T. M.; Haber, J. C.; Gregg, B. T.; Stankovich, S. B. *Org. Lett.* **2004**, *6*, 4775.

(6) (a) Liu, M. O.; Tai, C.-H.; Wang, W.-Y.; Chen, J.-R.; Hu, A. T.; Wei, T.-H. *J. Organomet. Chem.* **2004**, *689*, 1078. (b) Liu, M. O.; Hu, A. T. *J. Organomet. Chem.* **2004**, *689*, 2450. (c) Boufatah, N.; Gellis, A.; Maldonado, J.; Vanelle, P. *Tetrahedon* **2004**, *60*, 9131.

(7) Drain, C. M.; Gong, X. *Chem. Commun.* **1997**, 2117.

(8) (a) Chaouchi, M.; Loupy, A.; Marque, S.; Petit, A. *Eur. J. Org. Chem.* **2002**, 1278. (b) Mojtahedi, M. M.; Saidi, M. R.; Shirzi, J. S.; Bolourtchian, M. *Synth. Commun.* **2002**, *32*, 851.

(9) (a) Shaw, S. J.; Elgie, K. J.; Edwards, C.; Boyle, R. W. *Tetrahedron Lett.* **1999**, *40*, 1595. (b) Suzuki, M.; Shimizu, S.; Shin, J.-Y.; Osuka, A. *Tetrahedron Lett.* **2003**, *44*, 4597. (c) Battioni, P.; Brigaud, O.; Desvaux, H.; Mansuy, D.; Traylor, T. G. *Tetrahedron Lett.* **1991**, *32*, 2893.

(10) (a) Molineux, G. *Pharmacotherapy* **2003**, *23*, 3S. (b) Hamblin, M. R.; Miller, J. L.; Rizvi, I.; Ortel, B.; Maytin, E. V.; Hasan, T. *Cancer Res.* **2001**, *61*, 7155.

(11) (a) Castriciano, M. A.; Romeo, A.; Scolaro, L. M. *J. Porphyrins Phthalocyanines* **2002**, *6*, 431. (b) Gandini, S. C. M.; Borissevitch, I. E.; Perussi, J. R.; Imasato, H.; Tabak, M. J. *Luminescence* **1998**, *78*, 53.

Chapter 3

(1) Chen, X.; Hui, L.; Foster, D. A.; Drain, C. M. *Biochem.* **2004**, *43*, 10918-10929.

(2) Gong, X.; Milic, T.; Xu, C.; Batteas, J. D.; Drain, C. M. *J. Am. Chem. Soc.* **2002**, *124*, 14290-14291.

(3) Kneuer, C.; Sameti, M.; Haltner, E. G.; Schiestel, T.; Schirra, H.; Schmidt, H.; Lehr, C.-M. *Int. J. Pharm.* **2000**, *196*, 257-261.

(4) Chithrani, B. D.; Ghazani, A. A.; Chan, W. C. W. *Nano Lett.* **2006**, *6*, 662-668.

(5) Pegaz, B.; Debefve, E.; Borle, F.; Ballini, J.-P.; van de Bergh, H.; Konan-Kouakou, Y. N. *J. Photochem. Photobiol. B: Biol.* **2005**, *80*, 19-27.

(6) Hussain, S. M.; Hess, K. L.; Gearhart, J. M.; Geiss, K. T.; Schlager, J. J. *Toxicology in Vitro*

Thirteenth International Workshop on In Vitro Toxicology **2005**, *19*, 975-983.

(7) Popielarski, S. R.; Hu-Lieskovan, S.; French, S. W.; Triche, T. J.; Davis, M. E. *Bioconjugate Chem.* **2005**, *16*, 1071-1080.

(8) Cui, Z.; Mumper, R. J. *Bioconjugate Chem.* **2002**, *13*, 1319-1327.

(9) Berry, C. C.; Curtis, A. S. G. *J. Phys. D: Appl. Phys.* **2003**, *36*, R198-R206.

(10) Berry, C. C. *J. Mater. Chem.* **2005**, *15*, 543-547.

(11) Hone, D. C.; Walker, P. I.; Evans-Gowing, R.; FitzGerald, S.; Beeby, A.; Chambrier, I.; Cook, M. J.; Russell, D. A. *Langmuir* **2002**, *18*, 2985-2987.

(12) Mauzerall, D.; Drain, C. M. *Biophys. J.* **1992**, *63*, 1544-1555.

(13) Drain, C. M.; Mauzerall, D. *Biophys. J.* **1992**, *63*, 1556-1563.

(14) Vargas, A.; Pegaz, B.; Debefve, E.; Konan-Kouakou, Y.; Lange, N.; Ballini, J.-P.; van de Bergh, H.; Gurny, R.; Delie, F. *Int. J. Pharm.* **2004**, *286*, 131-145.

(15) Konan, Y. N.; Berton, M.; Gurny, R.; Allemann, E. *Eur. J. Pharmaceutical Sciences* **2003**, *18*, 241-249.

(16) Konan, Y. N.; Cerny, R.; Favet, J.; Berton, M.; Gurny, R.; Allemann, E. *Eur. J. Pharmaceutics Biopharmaceutics* **2003**, *55*, 115-124.

(17) Wieder, M. E.; Hone, D. C.; Cook, M. J.; Handsley, M. M.; Gavrilovic, J.; Russell, D. A. *Photochem. Photobiol. Sci.* **2006**, *5*, 727-734.

(18) McCarthy, J. R.; Perez, J. M.; Bruckner, C.; Weissleder, R. *Nano Lett.* **2005**, *5*, 2552-2556.

(19) Gu, H.; Xu, K.; Yang, Z.; Chang, C. K.; Xu, B. *Chem. Commun.* **2005**, *34*, 4270 - 4272.

(20) Roy, I.; Ohulchanskyy, T. Y.; Pudavar, H. E.; Bergey, E. J.; Oseroff, A. R.; Morgan, J.; Dougherty, T. J.; Prasad, P. N. *J. Am. Chem. Soc.* **2003**, *125*, 7860-7865.

(21) Yan, F.; Kopelman, R. *Photochem. Photobiol.* **2003**, *78*, 587–591.

(22) Brasseur, N.; Ouellet, R.; La Madeleine, C.; van Lier, J. E. *British J. Cancer* **1999**, *80*, 1533-1541.

(23) Fu, J.; Li, X.; Ng, D. K. P.; Wu, C. *Langmuir* **2002**, *18*, 3843-3847.

(24) Drain, C. M.; Smeureanu, G.; Patel, S.; Gong, X.; Garno, J.; Arijeloye, J. *New J. Chem.* **2006**, *12*, 1834-1843.

(25) Samaroo, D.; Soll, C. E.; Todaro, L. J.; Drain, C. M. *Org. Lett.* **2006**, *8*, 4985-4988.

(26) Battioni, P.; Brigaud, O.; Desvaux, H.; Mansuy, D.; Traylor, T. G. *Tet. Lett.* **1991**, *32*, 2893-2896.

(27) Greenwald, R. B.; Choe, Y. H.; McGuire, J.; Conover, C. D. *Adv. Drug Delivery Rev.* **2003**, *55*, 217-250.

(28) Hamblin, M. R.; Miller, J. L.; Rizvi, I.; Ortel, B.; Maytin, E. V.; Hasan, T. *Cancer Res.* **2001**, *61*, 7155-62.

(29) Hamblin, M. R.; Miller, J. L.; Loew, H. G.; Hasan, T. *British J. Cancer* **2003**, *89*, 937-943.

(30) Hornung, R.; Fehr, M. K.; Monti-Frayne, J.; Krasieva, T. B.; Tromberg, B. J.; Berns, M. W.; Tadir, Y. *Photochem. Photobiol.* **1999**, *70*, 624-629.

(31) Hornung, R.; Fehr, M. K.; Walt, H.; Wyss, P.; Berns, M. W.; Tadir, Y. *Photochem. Photobiol.* **2000**, *72*, 696-700.

(32) Ris, H.-B.; Krueger, T.; Giger, A.; Lim, C. K.; Stewart, J. C. M.; Althaus, U.; Altermatt, H. J. *British J. Cancer* **1999**, *79*, 1061-1066.

(33) Rovers, J. P.; Saarnak, A. E.; de Jode, M.; Sterenborg, H. J. C. M.; Terpstra, O. T.; Grahn, M. F. *Photochem. Photobiol.* **2000**, *71*, 210-217.

(34) Benaglia, M.; Danelli, T.; Fabris, F.; Sperandio, D.; Pozzi, G. *Org. Lett.* **2002**, *4*, 4229-4232.

(35) Benaglia, M.; Danelli, T.; Pozzi, G. *Org. Biomol. Chem.* **2003**, *1*, 454-456.

(36) Gao, H.; Shi, W.; Freund, L. B. *Proc. Natl. Acad. Sci.* **2005**, *102*, 9469-9474.

(37) Lamarche, F.; Sol, V.; Huang, Y. M.; Granet, R.; Guilloton, M.; Krausz, P. *J. Porphyrins Phthalocyanines* **2002**, *6*, 130-134.

(38) Molineux, G. *Pharmacotherapy* **2003**, *23*, 3S-8S.

(39) Kim, Y. K.; Jeong, D. H.; Kim, D.; Jeoung, S. C.; Cho, H. S.; Kim, S. K.; Aratani, N.; Osuka, A. *J. Am. Chem. Soc.* **2001**, *123*, 76-86.

(40) Lakowicz, J. R. *Principles of fluorescence spectroscopy*; 2nd. ed.; Kluwer Academic/Plenum Publishers: New York, 1999.

(41) Aoyama, Y.; Kanamori, T.; Nakai, T.; Sasaki, T.; Horiuchi, S.; Sando, S.; Niidome, T. *J. Am. Chem. Soc.* **2003**, *125*, 3455-3457.

(42) Mao, H.-Q.; Roy, K.; Troung-Le, V. L.; Janes, K. A.; Lin, K. Y.; Wang, Y.; August, J. T.; Leong, K. W. *Journal of Controlled Release* **2001**, *70*, 399-421.

(43) Nakai, T.; Kanamori, T.; Sando, S.; Aoyama, Y. *J. Am. Chem. Soc.* **2003**, *125*, 8465-8475.

(44) Zhong, M.; Shen, Y.; Zheng, Y.; Joseph, T.; Jackson, D.; Foster, D. A. *Biochem. Biophys. Res. Commun.* **2003**, *302*, 615-619.

(45) Zhong, M.; Lu, Z.; Foster, D. A. *Oncogene* **2002**, *21*, 1071-1078.

(46) Ame, J.-C.; Spenlehauer, C.; de Murcia, G. *BioEssays* **2004**, *26*, 882-893.

(47) Yu, S.-W.; Wang, H.; Poitras, M. F.; Coombs, C.; Bowers, W. J.; Federoff, H. J.; Poirier, G. G.; Dawson, T. M.; Dawson, V. L. *Science* **2002**, *297*, 259-263.

(48) Lam, M.; Oleinick, N. L.; Nieminen, A.-L. *J. Biol. Chem.* **2001**, *276*, 47379-47386.

(49) Oleinick, N. L.; Morris, R. L.; Belichenko, I. *Photochem. Photobiol. Sci.* **2002**, *1*, 1-21.

(50) de Murcia, G.; de Murcia, J. M. *Trends Biochem. Sci.* **1994**, *19*, 172-173.

(51) Noodt, B. B.; Berg, K.; Stokke, T.; Peng, Q.; Nesland, J. M. *British J. Cancer* **1999**, *79*, 72-81.

(52) Sharoni, Y.; Bosin, E.; Miinster, A.; Levy, J.; Schally, A. V. *Proc. Natl. Acad. Sci.* **1989**, *86*, 1648-1651.

(53) Jessani, N.; Niessen, S.; Mueller, B. M.; Cravatt, B. F. *Cell Cycle* **2005**, *4*, 253-255.

Chapter 4

(1) Drain, C. M.; Bazzan, G.; Milic, T.; Vinodu, M.; Goeltz, J. C. *Israel J. Chem.* **2005**, *45*, 255-269.

(2) Drain, C. M.; Chen., X. In *Encyclopedia of Nanoscience & Nanotechnology*; Nalwa, H. S., Ed.; American Scientific Press: New York, 2004; Vol. 9.

(3) Milic, T. N.; Chi, N.; Yablon, D. G.; Flynn, G. W.; Batteas, J. D.; Drain, C. M. *Angew. Chem., Int. Ed.* **2002**, *41*, 2117-2119.

(4) Chen, X.; Drain, C. M. *Drug Design Rev.* **2004**, *1*, 215-234.

(5) Chen, X.; Hui, L.; Foster, D. A.; Drain, C. M. *Biochemistry* **2004**, *43*, 10918-10929.

(6) Retsek, J. L.; Drain, C. M.; Kirmaier, C.; Nurco, D. J.; Medforth, C. J.; Smith, K. M.; Sazanovich, I. V.; Chirvony, V. S.; Fajer, J.; Holten., D. *J. Am. Chem. Soc.* **2003**, *125*, 9787-9800.

(7) Drain, C. M.; Gentemann, S.; Roberts, J. A.; Nelson, N. Y.; Medforth, C. J.; Jia, S.; Simpson, M. C.; Smith, K. M.; Fajer, J.; Shelnutt, J. A.; Holten, D. *J. Am. Chem. Soc.* **1998**, *120*, 3781-3791.

(8) Lehn, J.-M. *Proc. Natl. Acad. Sci., USA* **2002**, *99*, 4763-4768.

(9) Drain, C. M.; Gong, X.; Ruta, V.; Soll, C. E.; Chicoineau, P. F. *J. Comb. Chem.* **1999**, *1*, 286-290.

(10) Mansuy, D. *Coord. Chem. Rev.* **1993**, *125*, 129-141.

(11) Merlau, M. L.; Mejia, M. d. P.; Nguyen, S. T.; Hupp, J. T. *Angew. Chem. Int. Ed.* **2001**, *40*, 4239-4242.

(12) Suslick, K. S. In *The Porphyrin Handbook*; Kadish, K. M., Smith, K. M., Guilard, R., Eds.; Academic Press, New York, 2000.

(13) Drain, C. M.; Hupp, J. T.; Suslick, K. S.; Wasielewski, M. R.; Chen, X. *J. Porphyrins Phthalocyanines* **2002**, *6*, 243-258.

(14) Suslick, K. S.; Rakow, N. A. *Artificial Chemical Sensing* **2001**, 8-14.

(15) Bonnett, R. *Chem. Soc. Rev.* **1995**, 19-33.

(16) Liu, M. O.; Tai, C.-H.; Sain, M.-Z.; Hu, A. T.; Chou, F.-I. *J. Photochem. Photobiol., A: Chem* **2004**, *165*, 131-136.

(17) Schneider, R.; Schmitt, R.; Frochot, C.; Fort, Y.; Lourette, N.; Guillemin, F.; Muller, J.-F.; Barberi-Heyob, M. *Bioorg. Med. Chem.* **2005**, *13*, 2799-2808.

(18) Sternberg, E. D.; Dolphin, D.; Bruckner, C. *Tetrahedron* **1998**, *54*, 4151--4202.

(19) Kocisko, D. A.; Caughey, W. S.; Race, R. E.; Roper, G.; Caughey, B.; Morrey, J. D. *Antimicrob. Agents Chemother.* **2006**, *50*, 759-761.

(20) Kocisko, D. A.; Engel, A. L.; Harbuck, K.; Arnold, K. M.; Olsen, E. A.; Raymond, L. D.; Vilette, D.; Caughey, B. *Neuroscience Letters* **2005**, *388*, 106-111.

(21) Priola, S. A.; Raines, A.; Caughey, W. S. *Science* **2000**, *287*, 1503-1506.

(22) Caughey, W. S.; Raymond, L. D.; Horiuchi, M.; Caughey, B. *Proc. Natl. Acad. Sci.* **1998**, *95*, 12117-12122.

(23) Priola, S. A.; Caughey, B.; Caughey, W. S. *Curr. Opin. Microbiol.* **1999**, *2*, 563-566.

(24) Pasetto, P.; Chen, X.; Drain, C. M.; Franck, R. W. *Chem. Commun.* **2001**, 81-82.

(25) Samaroo, D.; Soll, C. E.; Todaro, L. J.; Drain, C. M. *Org. Lett.* **2006**, *8*, 4985-4988.

(26) Kamat, P. V.; Das, S.; Thomas, K. G.; George, M. V. *J. Phys. Chem.* **1992**, *96*, 195-199.

(27) Bonnett, R.; Martinez, G. *Tetrahedron* **2001**, *57*, 9513-9547.

(28) Battioni, P.; Brigaud, O.; Desvaux, H.; Mansuy, D.; Traylor, T. G. *Tetrahedron Lett.* **1991**, *32*, 2893-2896.

(29) Chen, X., Carbohydrate conjugated porphyrins targeting photodynamic therapy (PDT): potent inducers of cancer cell death both by necrosis and apoptosis; solution-phase combinatorial libraries with whole cell selection method, The Graduate School and University Center of the City of New York, 2004.

(30) Guliaev, A. B.; Leontis, N. B., 1999; Vol. 38.

(31) Pasternack, R. F.; Goldsmith, J. I.; Szep, S.; Gibbs, E. J., 1998; Vol. 75.

(32) Castriciano, M. A.; Romeo, A.; Scolaro, L. M. *J. Porphyrins Phthalocyanines* **2002**, *6*, 431-438.

(33) Hirohara, S.; Obata, M.; Ogata, S.; Kajiwara, K.; Ohtsuki, C.; Tanihara, M.; Yano, S. *J. Photochem. Photobiol. B: Biol.* **2006**, *84*, 56-63.

(34) Yu, S.-W.; Wang, H.; Poitras, M. F.; Coombs, C.; Bowers, W. J.; Federoff, H. J.; Poirier, G. G.; Dawson, T. M.; Dawson, V. L. *Science* **2002**, *297*, 259-263.

(35) Lam, M.; Oleinick, N. L.; Nieminen, A.-L. *J. Biol. Chem.* **2001**, *276*, 47379-47386.

(36) Oleinick, N. L.; Morris, R. L.; Belichenko, I. *Photochem. Photobiol. Sci.* **2002**, *1*, 1-21.

(37) Sternberg, E. D.; Dolphin, D.; Bruckner, C. *Tetrahedron* **1998**, *54*, 4151-4202.

(38) Yang, S. I.; Seth, J.; Strachan, J.-P.; Gentlemann, S.; Kim, D.; Holten, D.; Lindsey, J. S.; Bocian, D. F. *J. Porphyrins Phthalocyanines* **1999**, *3*, 117-147.

(39) Gross, Z.; Galili, N.; Saltsman, I. *Angew. Chem. Int. Ed. Engl.* **1999**, *38*, 1427-1429.

(40) Gross, Z.; Mahammed, A. *J. Porphyrins Phthalocyanines* **2002**, *6*, 553-555.

(41) Gross, Z.; Galili, N.; Simkhovich, L.; Saltsman, I.; Botoshansky, M.; Blaser, D.; Boese, R.; Goldberg, I. *Org. Lett.* **1999**, *1*, 599-602.

(42) Mahammed, A.; Weaver, J. J.; Gray, H. B.; Abdelas, M.; Gross, Z. *Tetrahedron Lett.* **2003**, *44*, 2077-2079.

(43) Kolb, H. C.; Finn, M. G.; Sharpless, K. B. *Angew. Chem. Int. Ed.* **2001**, *40*, 2004-2021.

Chapter 5

(1) Chen, X.; Hui, L.; Foster, D. A.; Drain, C. M. *Biochemistry* **2004**, *43*, 10918-10929.

(2) Drain, C. M.; Gong, X.; Ruta, V.; Soll, C. E.; Chicoineau, P. F. *J. Comb. Chem.* **1999**, *1*, 286-290.

(3) N18 and B16-F10 cell lines were a gift from Prof. Probal Banerjee's lab (College of Staten Island). MDA-MB-231 were obtained from Prof. David Foster's lab (Hunter College).

(4) Malouf, A. T.; Schnaar, R. L.; Coyle, J. T. *J. Biol. Chem.* **1984**, *259*, 12756-12762.

(5) Sengupta, S.; Ray, S.; Chattopadhyay, N.; Biswas, N.; Chatterjee, A. *J. Exp. Clin. Cancer Res.* **2000**, *19*, 81-7.

(6) Ohyama, T.; Sasagawa, A.; Terui, N.; Mita, H.; Yamamoto, Y. *Nucleic Acids Symp. Ser.* **2003**, *3*, 189-190.

(7) Lamarche, F.; Sol, V.; Huang, Y. M.; Granet, R.; Guilloton, M.; Krausz, P. *J. Porphyrins Phthalocyanines* **2002**, *6*, 130-134.

(8) Osterloh, J.; Vicente, M. G. H. *J. Porphyrins Phthalocyanines* **2002**, *6*, 305-324.

(9) MacDonald, I. J.; Dougherty, T. J. *J. Porphyrins Phthalocyanines* **2001**, *5*, 105-126.

(10) Malik, Z.; Ladan, H.; Nitzan, Y.; Smetana, Z. Photodynamic therapy of cancer, Budapest, Hungary, 1994; p 305-312.

(11) Nitzan, Y.; Dror, R.; Ladan, H.; Malik, Z.; Kimel, S.; Gottfried, V. *Photochem. Photobiol.* **1995**, *62*, 342-347.

(12) Nitzan, Y.; Gutterman, M.; Malik, Z.; Ehrenberg, B. *Photochem. Photobiol.* **1992**, *55*, 89-96.

(13) Orenstein, A.; Klein, D.; Kopolovic, J.; Winkler, E.; Malik, Z.; Keller, N.; Nitzan, Y. *FEMS Immun. Med. Microbiol.* **1998**, *19*, 307-314.

(14) Valduga, G.; Breda, B.; Giacometti, G. M.; Jori, G.; Reddi, E. *Biochem. Biophys. Res. Commun.* **1999**, *256*, 84-88.

(15) Tome, J. P. C.; Neves, M. G. P. M. S.; Tome, A. C.; Cavaleiro, J. A. S.; Soncin, M.; Magaraggia, M.; Ferro, S.; Jori, G. *J. Med. Chem.* **2004**, *47*, 6649-6652.

(16) Vzorov, A. N.; Marzilli, L. G.; Compans, R. W.; Dixon, D. W. *Antivir. Res.* **2003**, *59*, 99-109.

(17) Neurath, A. R.; Strick, N.; Haberfield, P.; Jiang, S. *Antivir. Chem. Chemother.* **1992**, *3*, 55-63.

(18) Neurath, A. R.; Haberfield, P.; Joshi, B.; Hewlett, I. K.; Strick, N.; Jiang, S. *Antivir. Chem. Chemother.* **1991**, *2*, 303-312.

(19) Debnath, A. K.; Jiang, S.; Strick, N.; Lin, K.; Haberfield, P.; Neurath, A. R. *J. Med. Chem.* **1994**, *37*, 1099-1108.

(20) Dixon, D. W.; Gill, A. F.; Giribabu, L.; Vzorov, A. N.; Alam, A. B.; Compans, R. W. *J. Inorg. Biochem.* **2005**, *99*, 813-821.

(21) Mansuy, D.; Battioni, P. In *Metalloporphyrins in Catalytic Oxidations*; Sheldon, R. A., Ed.; Marcel Dekker, Inc., New York,, 1994.

(22) Groves, J. T. In *Advances in Inorganic Biochemistry, vol. 1*; Eichhorn, G. L. a. M., L.G., Ed.; Elsevier North Holland, New York, 1979.

(23) McCarthy, J. R.; Perez, J. M.; Bruckner, C.; Weissleder, R. *Nano Lett.* **2005**, *5*, 2552-2556.

(24) Bonnett, R.; Charlesworth, P.; Djelal, B. D.; Foley, S.; McGarvey, D. J.; Truscott, T. G. *J. Chem. Soc., Perkin Trans. 2* **1999**, 325-328.

(25) Kamat, P. V.; Das, S.; Thomas, K. G.; George, M. V. *J. Phys. Chem.* **1992**, *96*, 195-199.

(26) Bonnett, R.; Martinez, G. *Tetrahedron* **2001**, *57*, 9513-9547.